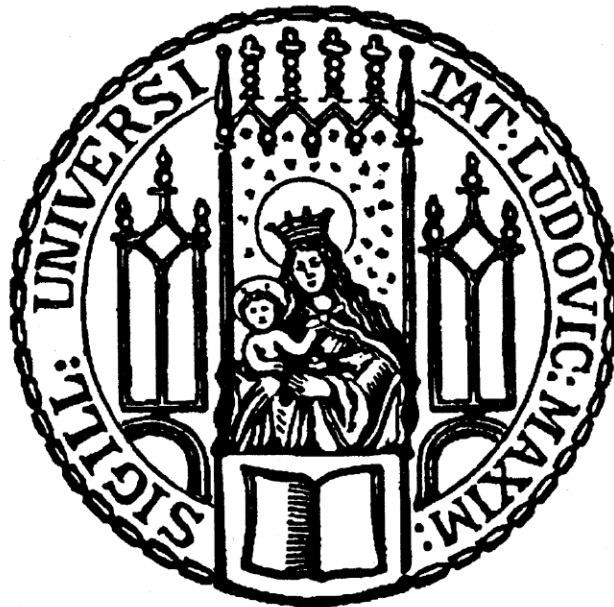Dissertation zur Erlangung des Doktorgrades

der Fakultät für Chemie und Pharmazie

der Ludwig-Maximilians-Universität München

Protein Aggregation Induced by Pumping of Biopharmaceutics

Natalie Maria Deiringer

aus

Altötting, Deutschland

2022

II

Erklärung

Diese Dissertation wurde im Sinne von § 7 der Promotionsordnung vom 28. November 2011 von Herrn Prof. Dr. Wolfgang Frieß betreut.

Eidesstattliche Versicherung

Diese Dissertation wurde selbstständig und ohne unerlaubte Hilfe erarbeitet.

München, den 24.10.2022 _____

Natalie Maria Deiringer

Dissertation eingereicht am: 24.10.2022

1. Gutachter: Prof. Dr. Wolfgang Frieß

2. Gutachter: Prof. Dr. Olivia Merkel

Mündliche Prüfung am: 29.11.2022

IV

'The important thing is not to stop questioning. Curiosity has its own reason for existing. One cannot help but be in awe when he contemplates the mysteries of eternity, of life, of the marvellous structure of reality. It is enough if one tries merely to comprehend a little of this mystery every day.'

Albert Einstein, *Life Magazine, May 2, 1955*

Acknowledgements

Table of Contents

X

CHAPTER IV PROTEINS ON THE RACK: MECHANISTIC STUDIES ON PROTEIN PARTICLE FORMATION DURING PERISTALTIC PUMPING 46

CHAPTER V CATCHING SPEEDY GONZALES: DRIVING FORCES FOR PROTEIN FILM FORMATION ON SILICONE RUBBER TUBING DURING PUMPING..................................74

CHAPTER VIII MODIFICATION OF TUBINGS FOR PERISTALTIC PUMPING OF BIOPHARMACEUTICS...158

CHAPTER IX EFFECT OF THE TUBING MATERIAL USED IN PERISTALTIC PUMPING IN TANGENTIAL FLOW FILTRATION PROCESSES OF BIOPHARMACEUTICS ON PARTICLE FORMATION AND FLUX

Chapter I General Introduction

1. Challenges during Manufacturing of Biopharmaceuticals

Biopharmaceuticals are leading amongst the drugs with the highest worldwide sales. Within the biopharmaceuticals, the monoclonal antibody segment dominated the global pharmaceutical market in 2017 and is expected to hold a leading position in the near future.[1,2] Quality standards are high to guarantee the protein drug product safety. Besides protein and activity loss, protein aggregation is a major issue during manufacturing. Protein aggregates are higher molecular weight species of the desired species formed by covalent bonds or noncovalent interactions.[3] Protein aggregates have been indicated as potential cause for immunogenic reactions in patients and reduced therapy efficiency.[4–6] Their presence in the drug product, can also serve as seed for further aggregation upon storage.[7] Therefore, protein aggregate levels must be well controlled.[8,9] From a technical point of view, protein aggregates can greatly impact process steps filtration.[10] Consequently, strategies to avoid and remove protein aggregates are essential.

2. Protein aggregation pathways

Reasons for protein aggregation are manifold and depend on physicochemical properties of the protein molecules and on the environmental conditions. Protein aggregates are classified based on bound type (covalent vs. noncovalent), reversibility (reversible vs. irreversible), size and protein conformation (native vs. nonnative).[3] Specifically, size of protein aggregates can range from soluble oligomers like dimers, trimers, etc. of around 20 nm to larger insoluble submicron particles up to 1 μm, subvisible particles from 1 - 100 μm and larger visible particles.[11] Various detection methods are available for each size range including size exclusion chromatography, resonant mass measurement, nanoparticle tracking analysis, flow imaging techniques and several new emerging techniques like imaging flow cytometry and tunable resistive pulse sensing.[12]

Protein aggregation can be based on a single or an interplay of different pathways. According to Philo and Arakawa[7], five pathways are seen as the most important ones (Figure 1).

Mechanism 1 and 2 are based on the assembly of native, partially, or completely unfolded monomer. The aggregates are either formed based on a buildup of monomers driven by the self-interaction of the native monomer or conformationally altered monomers. While the

propensity of self-interaction of the protein depends on local charge and hydrophobicity properties, conformational changes e. g. due to heat depend on the sensitive of the proteins' higher order structure. Whereas the amino acid sequence is unaltered in case of mechanism 2, chemical variants caused e. g. by oxidation of methionine or tryptophane serve as initiator for aggregation in mechanism 3. Chemical changes can increase the potential for self-interaction and conformational instability.[13] Thus, mechanism 3 not only leads to covalent aggregates but also non-covalent.

Mechanism 4 - 'Nucleation-controlled aggregation' - involves a critical nucleus which can be an external contaminant or a product aggregate. Interaction of monomers with the critical nucleus fosters the formation of much larger species. Examples for external contaminants triggering the mechanism are steel particles shed from a piston pump[14,15] or silicone oil used for lubrication of syringes.[16]

Finally, surface - induced aggregation is linked to the enrichment of protein on solid, liquid or air interfaces (Mechanism 5). The adsorption to the interface can thereby be driven by hydrophobic and/or electrostatic interactions. Upon adsorption, conformation might be altered, and the partially unfolded monomer is released into the bulk. Altered monomer from the surface might result in a pathway similar to mechanism 2. Mechanism 4 is related to mechanism 5 as the nucleus surface may act in the sense of mechanism 5. Under dynamic conditions like agitation, aggregates are released from the interface as the film of high local protein concentration is ruptured.[17,18]
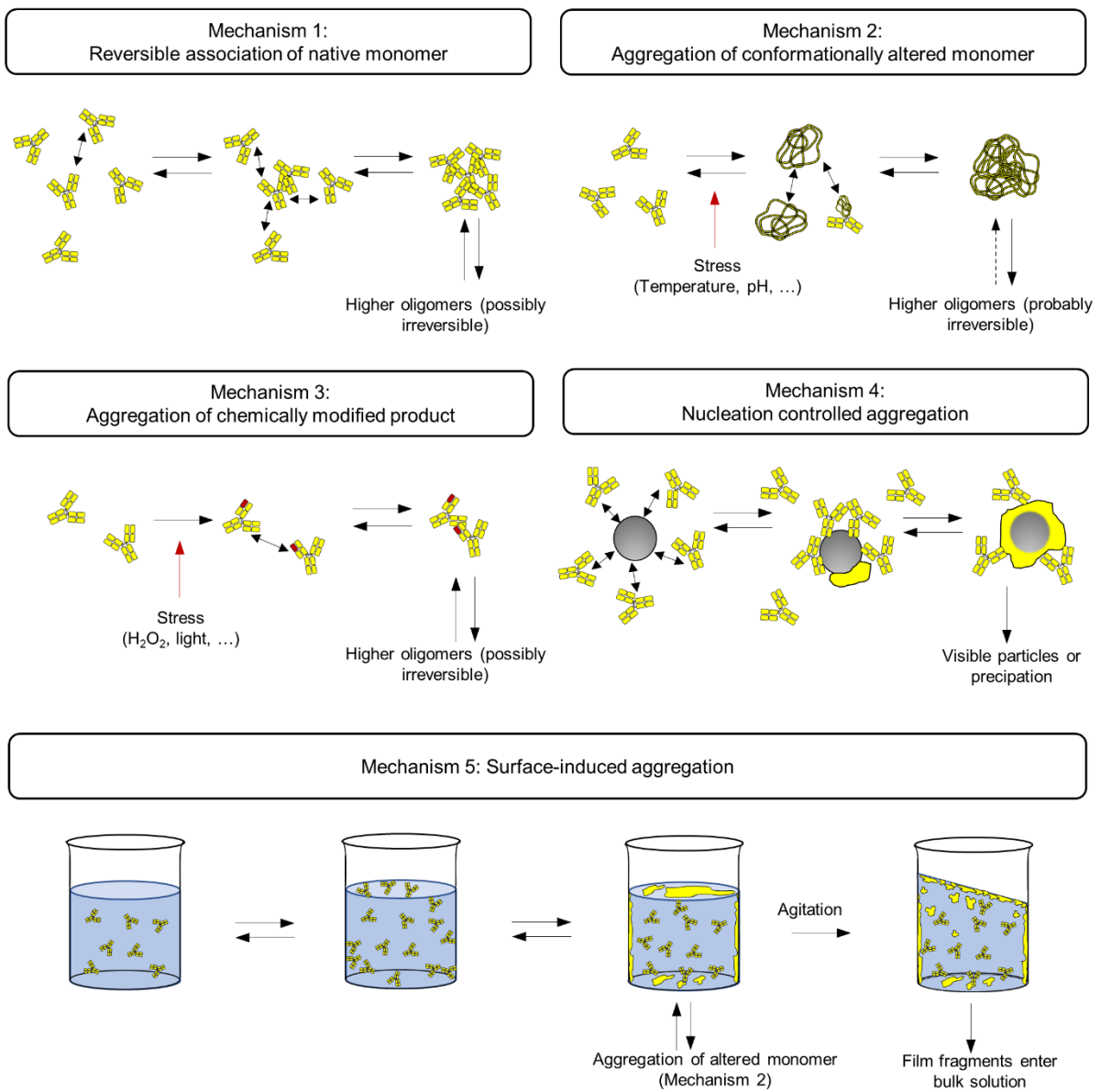
Figure 1 Schematic illustration of aggregation pathways. Inspired by Philo and Arakawa.[7]

3. Strategies to reduce protein aggregation during manufacturing and storage

At nearly every stage of manufacturing protein aggregation has been reported. Exemplarily, during purification, the protein is exposed to drastic changes in pH, ionic strength, buffer system, or protein concentrations, as well as mechanical stress and contact materials.[19] Also exposure to the liquid/air interface during homogenisation by shaking or stirring led to aggregate formation.[20]

Depending on the underlying mechanism, aggregation can be tackled by avoiding triggers like environmental stress and the formulation. First and foremost, the pH value is important as it affects the protein charge which is key in self-interaction and chemical reactions like deamidation, oxidation and fragmentation.[21,22] Buffering agents like acetate, histidine, citrate and phosphate ensure a stable pH during handling and storage. Specific ion effects of the buffer ions impact the protein´s conformational and chemical stability. Zheng and Janis[21] observed that asparagine deamidation of a monoclonal antibody was dependent on buffer type. Salts are also known to affect conformational stability, protein self-interaction, and solubility. Franz Hofmeister[23] discovered an ion specific relationship between salts and the propensity to induce protein precipitation. Ions were ranked based on their ability of preserving (kosmotropic) to breaking (chaotropic) the structure of water. Kosmotropic salts tend to stabilize intramolecular interaction within protein and decrease protein solubility (salting out), while chaotropic salts lead to a decrease in protein stability and increase in protein solubility (salting in).[24] Strong charge shielding by salts has been shown to increase aggregation propensity.[25,26] Sugars such as sucrose and trehalose stabilize proteins by preferential hydration in liquid state.[27,28] But nanoparticulate impurities present in sugars may induce aggregation by mechanism 4.[29] Non-ionic surfactants like polysorbate 20, polysorbate 80 and poloxamer 188 drastically reduce protein aggregation triggered by interfaces. The surfactants enrich at surfaces and keep the protein away from adsorption.[30] A drawback of polysorbates is their potential to initiate protein oxidation via peroxides (mechanism 3)[31] and free fatty acid particle formation (mechanism 4).[32] Antioxidants like methionine and n-acetyl-tryptophan scavenger radicals and thereby reduce an oxidation driven aggregation by mechanism 3.[33] For a complete list of excipients with drawbacks and benefits please see Kamerzell et al.[34]

Various screening techniques are available to probe formulation dependent protein stability. Exemplary, characteristics of the thermal or chemical unfolding, the diffusion interaction parameter and computational modelling are valuable methods for formulation development.[34–36] Typically, formulation development targets the identification of a 'sweet spot' balancing colloidal, conformational, chemical, and interfacial stability.

Protein particles may be removed by filtration later in the process.[19] But smaller aggregates will sustain as they could only be caught by chromatography. Furthermore, aggregates and particles generated during final filling enter the drug product and the pumping involved in the filling step has been identified as a contributor to protein aggregation.[37,38]

4. Pumping of Biopharmaceuticals

Pumps are frequently used for transferring proteins during downstream processing operations like chromatography, filtration, tank transfer and filling.[19] Pumps must have high reliability, low risk of contamination and low maintenance. Pump types commonly used in pharmaceutical industries are piston pumps, rotary lobe pumps, quaternary diaphragm pumps and peristaltic pumps.[39,40] These pumps are positive displacement pumps which means that the fluid is moved by entrapment of a fixed amount and subsequent displacement into the discharge line. Depending on process requirements, the pumps used are associated with benefits and drawbacks based on their design (Table 1).

Table 1 Overview of characteristics of pumps used in biopharmaceutical manufacturing. Adapted from Hill.[41]

	Rotary Pump		Reciprocating Pump	
	Peristaltic	Lobe	Quaternary Diaphragm	Piston
Operating principle	Fluid is moved through a tube which is repeatedly compressed and decompressed by a moving rotor.	Fluid is moved by counterrotation of two lobes.	Fluid is moved by reciprocating movement of a flexible diaphragm within the pump chamber.	Fluid is moved by the reciprocating movement of a piston causing suction of the fluid.
Scale up with same equipment	Yes	Yes	Yes	No
Single-use options	Yes	No	Yes	No
Clean in place	not applicable	Yes	Yes	Yes
Sterilization in place	not applicable	Yes	Yes	No
Self-priming	Yes	No	Yes	Yes
Shear	Low	Low	Low	High
Particle shedding from equipment	High	Unlikely	Unlikely	Low

Scalability allows easy adaption to changing production conditions. Systems with single-use equipment are less prone for cross-contamination, require less instrumentation and demand less utility but come with the running costs for consumables and require waste management.[42,43] Like pumps with single-use options, easy to clean and sterilizable equipment is beneficial for multi-purpose use. Specifically, self-priming pumps are favoured as they evacuate air and thereby reduce the risk of overheating and pump failure and reduce maintenance. High shear may negatively impact shear sensitive proteins like enzymes.[44] Peristaltic pumps are known for rubber particle shedding from the tubing by abrasion during roller movement. Shed silicone particles are expected to be below any detection limit during

production conditions, and do not trigger protein aggregation during storage.[45,46] In contrast, stainless steel particles shed from the surface of a piston pump might interfere with protein stability.[14] Protein particles formed upon pumping impact product quality and safety as well as processability. Exemplary, membrane fouling during tangential flow filtration is associated with flux decrease, longer process times and potential process failure. One potential contributor for membrane clogging are protein particles induced by pumping which block pores by deposition on the membrane.[10,47] While various studies focused on the aggregation pathways in piston[48,49] and lobe pumps,[50] peristaltic pumps have not been analysed in detail.[51,52] Due to the benefits of single use equipment, high scalability, low shear and low maintenance, peristaltic pumps are versatile components in manufacturing of biopharmaceuticals. An understanding of driving forces of protein aggregation upon peristaltic pumping would support pump selection, tubing selection and formulation development.

5. References

1. Biopharmaceuticals Market Size, Share and Industry Analysis | 2025. Accessed February 20, 2022. https://www.alliedmarketresearch.com/biopharmaceutical-market

2. Biopharmaceuticals Industry | 2022 - 27 | Market Growth, Overview, Size. Accessed February 20, 2022. https://www.mordorintelligence.com/industry-reports/global-biopharmaceuticals-market-industry

3. Mahler HC, Friess W, Grauschopf U, Kiese S. Protein Aggregation: Pathways, Induction Factors and Analysis. J Pharm Sci. 2009;98(9):2909-2934. doi:10.1002/jps.21566

4. Rosenberg AS. Effects of Protein Aggregates: An Immunologic Perspective. AAPS J. 2006;8(3):E501-E507. doi:10.1208/aapsj080359

5. Moussa EM, Panchal JP, Moorthy BS, et al. Immunogenicity of Therapeutic Protein Aggregates. J Pharm Sci. 2016;105(2):417-430. doi:10.1016/j.xphs.2015.11.002

6. Schellekens H. Immunogenicity of Therapeutic Proteins: Clinical Implications and Future Prospects. Clin Ther. 2002;24(11):1720-1740. doi:10.1016/s0149-2918(02)80075-3

7. Philo JS, Arakawa T. Mechanisms of Protein Aggregation. Curr Pharm Biotechnol. 2009;10(4):348-351. doi:10.2174/138920109788488932

8. USP <788> Particulate matter in injections. In: United States Pharmacopeia. United States Pharmacopeial Convention; 2014.

9. EP <2.9.19>. Particulate Contamination: Sub-Visible Particles. In: European Pharmacopoeia. 6th ed. European Directorate For The Quality Of Medicine; 2008.

10. Chandavarkar AS. Dynamics of Fouling of Microporous Membranes by Proteins. Massachusetts Institute of Technology; 1990.

11. Narhi LO, Schmit J, Bechtold-Peters K, Sharma D. Classification of Protein Aggregates. J Pharm Sci. 2011;101(2):493-498. doi:10.1002/jps.22790

12. Roesch A, Stadler D, Helbig C, et al. Particles in Biopharmaceutical Formulations, Part 2: An Update on Analytical Techniques and Applications for Therapeutic Proteins, Viruses, Vaccines and Cells. J Pharm Sci. 2022;111(4):933-950. doi:10.1016/j.xphs.2021.12.011

13. Alam ME, Slaney TR, Wu L, et al. Unique Impacts of Methionine Oxidation, Tryptophan Oxidation, and Asparagine Deamidation on Antibody Stability and Aggregation. J Pharm Sci. 2020;109(1):656-669. doi:10.1016/J.XPHS.2019.10.051

14.   Bee JS, Davis M, Freund E, Carpenter JF, Randolph TW. Aggregation of a Monoclonal Antibody Induced by Adsorption to Stainless Steel. Biotechnol Bioeng. 2010;105(1):121-129. doi:10.1002/bit.22525

15.   Tyagi AK, Randolph TW, Dong A, Maloney KM, Hitscherich C, Carpenter JF. IgG particle formation during filling pump operation: A case study of heterogeneous nucleation on stainless steel nanoparticles. J Pharm Sci. 2009;98(1):94-104. doi:10.1002/jps.21419

16.   Jones LS, Kaufmann A, Middaugh CR. Silicone oil induced aggregation of proteins. J Pharm Sci. 2005;94(4):918-927. doi:10.1002/jps.20321

17.   Koepf E, Eisele S, Schroeder R, Brezesinski G, Friess W. Notorious but not understood: How liquid-air interfacial stress triggers protein aggregation. Int J Pharm. 2018;537(1-2):202-212. doi:10.1016/j.ijpharm.2017.12.043

18.   Bee JS, Schwartz DK, Trabelsi S, et al. Production of particles of therapeutic proteins at the air-water interface during compression/dilation cycles. Soft Matter. 2012;8:10329-10335. doi:10.1039/c2sm26184g

19.   Vázquez-Rey M, Lang DA. Aggregates in monoclonal antibody manufacturing processes. Biotechnol Bioeng. 2011;108(7):1494-1508. doi:10.1002/bit.23155

20.   Kiese S, Papppenberger A, Friess W, Mahler HC. Shaken, not stirred: Mechanical stress testing of an IgG1 antibody. J Pharm Sci. 2008;97(10):4347-4366. doi:10.1002/jps.21328

21.   Zheng JY, Janis LJ. Influence of pH, buffer species, and storage temperature on physicochemical stability of a humanized monoclonal antibody LA298. Int J Pharm. 2006;308(1-2):46-51. doi:10.1016/j.ijpharm.2005.10.024

22.   Wang W, Ohtake S. Science and art of protein formulation development. Int J Pharm. 2019;568:118505. doi:10.1016/j.ijpharm.2019.118505

23.   Hofmeister F. Zur Lehre von der Wirkung der Salze. Archiv für experimentelle Pathologie und Pharmakologie. 1888;24:247-260. doi:10.1007/BF01918191

24.   Okur HI, Hladílková J, Rembert KB, et al. Beyond the Hofmeister Series: Ion-Specific Effects on Proteins and Their Biological Functions. Journal of Physical Chemistry B. 2017;121(9):1997-2014. doi:10.1021/acs.jpcb.6b10797

25.   Ye Y, Huo X, Yin Z. Protein-protein interactions at high concentrations: Effects of ArgHCl and NaCl on the stability, viscosity and aggregation mechanisms of protein solution. Int J Pharm. 2021;601:120535. doi:10.1016/j.ijpharm.2021.120535

26.   Rubin J, Linden L, Coco WM, Bommarius AS, Behrens SH. Salt-induced aggregation of a monoclonal human immunoglobulin G1. J Pharm Sci. 2013;102(2):377-386. doi:10.1002/jps.23363

27.   Kim YS, Jones LS, Dong A, et al. Effects of sucrose on conformational equilibria and fluctuations within the native-state ensemble of proteins. Protein Science. 2003;12(6):1252-1261. doi:10.1110/ps.0242603

28.   Kaushik JK, Bhat R. Why Is Trehalose an Exceptional Protein Stabilizer? An Analysis of the Thermal Stability of Proteins in the Presence of the compatible Osmolyte Trehalose. J Biol Chem. 2003;278(29):26458-26465. doi:10.1074/jbc.M300815200

29.   Banks DD, Hambly DM, Scavezze JL, Siska CC, Stackhouse NL, Gadgil HS. The Effect of Sucrose Hydrolysis on the Stability of Protein Therapeutics during Accelerated Formulation Studies. J Pharm Sci. 2009;98(12):4501-4510. doi:10.1002/jps.21749

30.   Kanthe AD, Krause M, Zheng S, et al. Armoring the Interface with Surfactants to Prevent the Adsorption of Monoclonal Antibodies. ACS Appl Mater Interfaces. 2020;12(8):9977-9988. doi:10.1021/acsami.9b21979

31.   Wang W, Wang YJ, Wang DQ. Dual effects of Tween 80 on protein stability. Int J Pharm. 2008;347(1-2):31-38. doi:10.1016/j.ijpharm.2007.06.042

32.   Larson NR, Wei Y, Prajapati I, et al. Comparison of Polysorbate 80 Hydrolysis and Oxidation on the Aggregation of a Monoclonal Antibody. J Pharm Sci. 2020;109(1):633-639. doi:10.1016/j.xphs.2019.10.069

33.   Dion MZ, Leiske D, Sharma VK, Zuch de Zafra CL, Salisbury CM. Mitigation of Oxidation in Therapeutic Antibody Formulations: A Biochemical Efficacy and Safety Evaluation of N-Acetyl-Tryptophan and L-Methionine. Pharm Res. 2018;35(11):222. doi:10.1007/s11095-018-2467-5

34.   Kamerzell TJ, Esfandiary R, Joshi SB, Middaugh CR, Volkin DB. Protein-excipient interactions: Mechanisms and biophysical characterization applied to protein formulation development. Adv Drug Deliv Rev. 2011;63(13):1118-1159. doi:10.1016/j.addr.2011.07.006

35.   Capelle MAH, Gurny R, Arvinte T. High throughput screening of protein formulation stability: Practical considerations. European Journal of Pharmaceutics and Biopharmaceutics. 2007;65(2):131-148. doi:10.1016/j.ejpb.2006.09.009

36.   Mehta CH, Narayan R, Nayak UY. Computational modeling for formulation design. Drug Discov Today. 2019;24(3):781-788. doi:10.1016/j.drudis.2018.11.018

37.   Roffi K, Li L, Pantazis J. Adsorbed protein film on pump surfaces leads to particle formation during fill-finish manufacturing. Biotechnol Bioeng. 2021;118(8):2947-2957. doi:10.1002/bit.27801

38.   Nayak A, Colandene J, Bradford V, Perkins M. Characterization of subvisible particle formation during the filling pump operation of a monoclonal antibody solution. J Pharm Sci. 2011;100(10):4198-4204. doi:10.1002/jps.22676

39.   Thomas CR, Geer D. Effects of shear on proteins in solution. Biotechnol Lett. 2011;33(3):443-456. doi:10.1007/s10529-010-0469-4

40.   Fernandez-Cerezo L, Rayat ACME, Chatel A, Pollard JM, Lye GJ, Hoare M. The prediction of the operating conditions on the permeate flux and on protein aggregation during membrane processing of monoclonal antibodies. J Memb Sci. 2020;596:117606. doi:10.1016/j.memsci.2019.117606

41.   Hill C. Quick Reference Guide-An Overview of Pharmaceutical Pump Types, Capabilities and Differentiators. Accessed February 20, 2022. https://www.contractpharma.com/issues/2018-01-01/view_features/pharma-industry-outlook

42.   Jacquemart R, Vandersluis M, Zhao M, Sukhija K, Sidhu N, Stout J. A Single-use Strategy to Enable Manufacturing of Affordable Biologics. Comput Struct Biotechnol J. 2016;14:309-318. doi:10.1016/j.csbj.2016.06.007

43.   Rawlings B, Pora H. A Prescriptive Approach to Management of Solid Waste from Single-Use Systems. Bioprocess Int. 2009;7:40-46.

44.   Charm SE, Wong BL. Shear effects on enzymes. Enzyme Microb Technol. 1981;3(2):111-118. doi:10.1016/0141-0229(81)90068-5

45.   Saller V, Hediger C, Matilainen J, et al. Influence of particle shedding from silicone tubing on antibody stability. Journal of Pharmacy and Pharmacology. 2018;70(5):675-685. doi:10.1111/jphp.12603

46.   Saller V, Matilainen J, Grauschopf U, Bechtold-Peters K, Mahler HC, Friess W. Particle Shedding from Peristaltic Pump Tubing in Biopharmaceutical Drug Product Manufacturing. J Pharm Sci. 2015;104(4):1440-1450. doi:10.1002/jps.24357

47.   Callahan DJ, Stanley B, Li Y. Control of Protein Particle Formation During Ultrafiltration/Diafiltration Through Interfacial Protection. J Pharm Sci. 2014;103(3):862-869. doi:10.1002/jps.23861

48.   Kalonia CK, Heinrich F, Curtis JE, Raman S, Miller MA, Hudson SD. Protein Adsorption and Layer Formation at the Stainless Steel− Solution Interface Mediates Shear-Induced

Particle Formation for an IgG1 Monoclonal Antibody. Mol Pharmaceutics. 2018;15(3):1319-1331. doi:10.1021/acs.molpharmaceut.7b01127

49.   Wu H, Randolph TW. Aggregation and Particle Formation During Pumping of an Antibody Formulation Are Controlled by Electrostatic Interactions Between Pump Surfaces and Protein Molecules. J Pharm Sci. 2020;109(4):1473-1482. doi:10.1016/j.xphs.2020.01.023

50.   Gomme PT, Hunt BM, Tatford OC, Johnston A, Bertolini J. Effect of lobe pumping on human albumin: investigating the underlying mechanisms of aggregate formation. Biotechnol Appl Biochem. 2006;43(2):103-111. doi:10.1042/ba20050147

51.   Her C, Carpenter JF. Effects of Tubing Type, Formulation, and Postpumping Agitation on Nanoparticle and Microparticle Formation in Intravenous Immunoglobulin Solutions Processed With a Peristaltic Filling Pump. J Pharm Sci. 2020;109(1):739-749. doi:10.1016/j.xphs.2019.05.013

52.   Her C, Tanenbaum LM, Bandi S, et al. Effects of Tubing Type, Operating Parameters, and Surfactants on Particle Formation During Peristaltic Filling Pump Processing of a mAb Formulation. J Pharm Sci. 2020;109(4):1439-1448. doi:10.1016/j.xphs.2020.01.009

Chapter II Objectives and Outline of the Thesis

The aim of the thesis is to contribute to a deeper understanding of protein aggregation during peristaltic pumping and provide options for reduction. Peristaltic pumping plays an important role for transfer, filtration, and filling of biopharmaceuticals. Protein aggregates formed upon pumping can impact process functionality as well as safety and quality of the final product. The thesis consists of three main projects: Several studies focused on the pathways of protein aggregation during peristaltic pumping (**Chapter III-VII**). Based on the outcome of these mechanistic studies, a new approach for novel tubing modification to reduce protein aggregation was developed (**Chapter VIII**). Finally, this novel tubing was employed in pump studies including tangential flow filtration (**Chapter IX**).

As a first step, the potential pathways for aggregate formation were investigated. The effect of plastic particles shed from silicone tubing was analyzed in detail and new methods to identify the nanometer sized silicone particles in protein aggregates were developed (**Chapter III**). Further potential causes for protein particle formation upon peristaltic pumping are cavitation, heat, protein adsorption, and mechanical stretching of the tubing. By linking results from pumping studies to findings in experiments simulating each single cause (**Chapter IV**), protein film formation on the tubing surface and its rupture during roller movement was identified as the key mechanism. To get a better understanding, adsorption kinetics and their effect on film morphology were monitored using high-speed techniques (**Chapter V**) considering protein characteristics, formulation composition, and surface characteristics. With this understanding five different tubing materials were compared, and particle formation propensity could be linked to surface hydrophobicity and hardness (**Chapter VI**). Finally, particle formation propensity of six different monoclonal antibodies upon pumping with silicone tubing was linked to characteristics like hydrophobicity, conformational stability, or surface activity (**Chapter VII**).

In **Chapter VIII**, tubings were modified by the incorporation of amphiphilic block copolymers. The modified tubings were to be tested on reduction of protein adsorption, protein particle formation propensity and sustainability of the effect compared to unmodified materials.

Finally, the modified tubing was employed in tangential flow filtration studies which come with more intense pumping compared to filling (**Chapter IX**). Not only product quality is impacted by protein particle formation, but also aggregate deposition on the membrane decreases flux, prolongs process time and can even lead to process failure. The effect of protein particle concentration on flux decrease was studied in low and high viscosity environment depending on tubing choice.

Overall, this thesis highlights the complexity of protein aggregation during peristaltic pumping. The outcome of the studies should resolve the underlying aggregation mechanism to give guidance on optimization of tubing choice and formulation development.

Chapter III Finding the Needle in the Haystack: High-Resolution Techniques for Characterization of Mixed Protein Particles Containing Shed Silicone Rubber Particles Generated During Pumping

This chapter is published as:

[1]Department of Pharmacy, Pharmaceutical Technology and Biopharmaceutics, Ludwig-Maximilians-Universität München, Munich, Germany

[2]Chair for Analytical Chemistry, Technische Universität München, Munich, Germany

[3]Department of Pharmacy, Pharmaceutical Biology, Ludwig-Maximilians-Universität München, Munich, Germany

* Authors contributed equally

Author contributions:

N.D., W.F., C.Haa. and C.Hai. conceived and designed the study. N.D. performed pumping and adsorption studies and prepared all samples for further analysis. N.D. and S.Z. conducted CLSM measurements. C.Haa. and K.W. performed Raman microscopy measurements and VCA analysis. N.D. and C.Haa. analyzed data and wrote the original draft. W.F., C.Hai., S.Z. and K.W. revised and edited the manuscript. W.F., S.Z. and C.Hai. supervised the study.

Note from the authors:

The version included in this thesis is identical with the published article apart from minor changes.

1. Abstract

During the manufacturing process of biopharmaceuticals, peristaltic pumps are employed at different stages for transferring and dosing of the final product. Commonly used silicone tubings are known for particle shedding from the inner tubing surface due to friction in the pump head. These nanometer sized silicone rubber particles could interfere with proteins. Until now, only mixed protein particles containing micrometer-sized contaminations such as silicone oil have been characterized, detected, and quantified. To overcome the detection limits in particle sizes of contaminants, this study aimed for the definite identification of protein particles containing nanometer sized silicone particles in qualitative and quantitative manner. The mixed particles consisted of silicone rubber particles either coated with a protein monolayer or embedded into protein aggregates. Confocal Raman microscopy allows label free chemical identification of components and 3D particle imaging. Labeling the tubing enables high-resolution imaging via confocal laser scanning microscopy and counting of mixed particles via Imaging Flow Cytometry. Overall, these methods allow the detection and identification of particles of unknown origin and composition and could be a forensic tool for solving problems with contaminations during processing of biopharmaceuticals.

Keywords: antibody, protein aggregation, mixed protein particles, pumping, silicone, tubing, Raman microscopy, fluorescence, confocal microscopy, imaging flow cytometry

Abbreviations: 3D-LSM - 3D laser scanning microscope; BET - Brunauer-Emmet-Teller; Bodipy - [[(3,5-dimethyl-1H-pyrrol-2-yl)(3,5-dimethyl-2H-pyrrol-2-ylidene)methyl]methane] (difluoroborane); CLSM - confocal laser scanning microscopy; FNU - formazine nephelometric units; IFC - Imaging Flow Cytometry; mAb - monoclonal antibody; PS20 - polysorbate 20; qLD - quantitative laser diffraction; ROI - region of interest; S_A - arithmetical mean height of the surface; SD – standard deviation; SEM - Scanning Electron Microscopy; S_Z - maximum height of the surface; VCA - vertex component analysis

2. Introduction

Biopharmaceuticals are experiencing a rapid growth in pharmaceutical industry with a total of 316 active licenses in 2018. Currently, 40% of the 6 000 or more products in global clinical development are biopharmaceuticals - mostly proteins - due to their high target specificity.[1] Because of their complex structure, proteins are sensitive to different kinds of stress like shear, oxidation or interfacial adsorption. This may lead to aggregate formation, which can potentially trigger immune responses.[2–4] In addition, regulatory guidelines for particle limitations from the European Pharmacopeia[5] and the USP[6] need to be fulfilled for product approval. To ensure product safety and quality, particle levels should be kept low.[2,3,7]

Particles in biopharmaceutical products can be of protein origin, may derive from excipients[8] or from a foreign source during processing or storage such as rubber from stoppers, glass from vials, fibers from filters, or silicone oil droplets from syringes.[9–11] Interactions between protein molecules and external particles can lead to protein aggregation,[12] e. g. shed stainless steel particles from the piston pumps serve as aggregation nuclei via adsorption and structural change of protein molecules at the surface.[13,14]

Pumps are essential during the downstream and fill&finish processes. The generated protein particles depend on the applied pumping parameters and the type of pump.[15] By now, the most used pumps are rotary piston pumps, time-pressure fillers, and peristaltic pumps. Particularly rotary piston pumps can quickly generate high amounts of protein particles[16,17] by disruption of the protein film built on the stainless steel surface.[18] In comparison, peristaltic pumps generate significantly less protein aggregates.[17,19,20] Often peristaltic pumps are preferred for filling lines because of their complete disposable flow path that helps to avoid cross contamination. Her and Carpenter showed that protein aggregation in peristaltic pumps depends on tubing type and formulation.[21] It is assumed that the aggregation is more likely driven by interfacial stress[20,22] than by shear stress.[23] Peristaltic pumps are mostly equipped with silicone tubings due to cost and availability, but these tubings shed particles. If used in medical devices they lead to inflammation and fibrosis due to accumulation in lysosomes of macrophages.[24–26] Saller et al.[27] showed that different amounts of nanometer-sized silicone rubber particles abrade from the inner tubing wall depending on surface roughness. These particles can enter the final product and potentially interact with proteins leading to immune responses in patients.

While intensive studies have already focused on the silicone oil composite protein particles and their immunogenicity[28–30], silicone rubber also has a potential for triggering immune responses. An early study of Anderson et al., reports on protein adsorption to silicone rubber followed by macrophage activation and leading to cytokine expression.[31] For the differentiation between protein particles and contaminations, a variety of methods have been established e.g.

silicone oil droplets can be distinguished from protein particles by flow imaging, resonant mass measurements[32–34] or flow cytometry[35]. However, contaminations in protein particles can be detected only in the micrometer size range.[35,36] Identifying the formation of heterogeneous particles upon peristaltic pumping is associated with two main burdens. First, the nanometer size of the contaminant makes its identification by light microscopy-based techniques such as micro flow imaging impossible. Second, the rubber particles do not show spectral features like auto fluorescence or deep color, which could enable identification. Methods combining optical information with chemical identification at high resolution may enable to overcome this problem. In the past, Raman microscopy[37] and Imaging Flow Cytometry (IFC)[36] showed great potential to resolve the mixed particles of micrometer sized silicone oil droplets and micrometer sized protein particles. While Raman microscopy is able to analyze native particles in a label free way through the spectral differences of the two species, fluorescence labelling of at least one component after particle formation allows counting by IFC and high-resolution images by confocal laser scanning microscopy (CLSM). CLSM can provide sharp images by collecting the emitted photons from the sample's fluorophore utilizing a spatial pinhole which reduces out of focus light. Refining these methods could allow analysis of nanosized contaminants in larger protein aggregates.

In this study, we demonstrate the detection and chemical resolution of heterogeneous particles consisting of aggregated protein and nanometer sized silicone rubber particles. Protein particles generated through peristaltic pumping through two silicone tubings of different surface characteristics and shedding propensity were characterized by turbidity, flow imaging, and quantitative laser diffraction (qLD). Raman microscopy, CLSM, and imaging flow cytometry methods were developed to identify and classify mixed particles and to resolve the distribution of the small non-proteinaceous contaminants within the larger protein particles. Adsorption of mAb to silicone particles was evaluated to gain insight into the mixed protein particle formation. The newly developed methods possess great potential for solving scientific problems on micro- and nanometer-based contaminations of protein aggregates to ensure quality and safety of biopharmaceuticals.

3. Materials and Methods

3.1. Materials

33.4 mg/mL monoclonal IgG1 antibody (Isoelectric point: 8.0-8.3) in 20 mM histidine buffer pH 5.4 served as model monoclonal antibody (mAb). Buffers were prepared using highly purified water (HPW) from an Arium pro DI Ultrapure Water System (Sartorius Stedim Biotech GmbH, Goettingen, Germany). Histidine (Applichem, Darmstadt, Germany) or potassium dihydrogen phosphate (Grüssing GmbH, Filsum, Germany) were dissolved, and pH was adjusted either with hydrochloric acid (VWR, Darmstadt, Germany) or potassium hydroxide (Bernd Kraft GmbH, Duisburg, Germany). Buffers were filtered through 0.2 µm cellulose acetate filters (47 mm ø, Sartorius Stedim Biotech GmbH) and mAb formulations through 0.2 µm polyethersulfone membrane syringe filters (VWR).

The employed Pt-cured silicone tubings Accusil (Watson-Marlow, Falmouth, United Kingdom) and Versilic (Saint-Gobain, Taunton, MA, USA) had an inner diameter of 6.0 mm and a wall thickness of 2.1 mm. Tubing sets were assembled by connecting two 20 cm long pieces for the area in the pump head to 35 cm long tubing pieces via polypropylene Y-connectors (Kartell, VWR). To mimic production conditions tubing sets were rinsed with 5 L HPW at 80 °C and steam sterilized (121 °C, 15 min, 2 bar).

Silicone rubber microparticles KMP-594 (average particle size of 4.6 µm) were kindly donated by Shin-Etsu Chemical Co. Ltd, Tokyo, Japan. Chemicals were obtained as follows: [[(3,5-dimethyl-1H-pyrrol-2-yl)(3,5-dimethyl-2H-pyrrol-2-ylidene)methyl]methane] (difluoroborane) (Bodipy) from ABCR (Karlsruhe, Germany), chloroform and ethanol from VWR; polysorbate 20 (PS20) from Merck (Darmstadt, Germany), and sodium azide from Acros Organics (Geel, Belgium).

3.2. Fluorescent labeling of tubing and silicone rubber particles

Autoclaved tubing was filled with either 1 mg/mL Bodipy in EtOH for IFC or 2 mg/mL Bodipy in 20:80 (v/v) chloroform:EtOH for CLSM. After 24 h incubation, solvent residues were removed using a vacuum oven (Memmert, Büchenbach, Germany) for 3 h at 300 mbar and for 21 h at 10 mbar at 25 °C. For IFC measurements, 100 mg silicone rubber microparticles were suspended in 1 mL of 1mg/mL Bodipy solution in EtOH and processed as described above. After drying, the particles were resuspended in histidine buffer and centrifuged once at 12,800 g for 10 min for washing. The labeled silicone beads were collected and resuspended in 20 mM histidine pH 5.4 with 0.1% PS20 at a concentration of 4 mg/mL.

3.3. Sample preparation

All pumping experiments were conducted in a laminar flow hood to avoid external particle contamination. Tubing sets were pre-rinsed by pumping 20 L HPW with a Flexicon PD12 peristaltic pump (Watson-Marlow Flexicon, Ringsted, Denmark) in continuous mode at 180 rpm. These settings resulted in a flow rate of 23 mL/s at an occlusion pressure of approximately 1.3 bar upon operation in air (manometer from WIKA Alexander Wiegand SE & Co. KG, Klingenberg, Germany, accuracy class 2.5). For sample preparation, 45 mL of formulation buffer followed by 45 mL of 1 mg/mL antibody solution were circulated 20 times at 180 rpm. Protein concentration was verified by UV absorption at 280 nm using a Nanodrop Micro-Volume UV-Vis spectrometer (Nano Drop 2000, Thermo Scientific, Wilmington, USA) and an extinction coefficient of 1.51 cm^2/mg. As a reference for silicone free protein particles, 1 mL of a 1 mg/mL antibody solution was shaken for 2 min in a CapMix device (3M Espe, Neuss, Germany) or stirred for 1 h at 300 rpm with a Variomag Poly 15 (H + P LABORTECHNIK, Oberschleißheim, Germany). As bacteriostatic agent, 0.01% sodium azide was added to the samples for the IFC measurements.

3.4. 3D laser scanning microscopy

Surface roughness of the inner tubing walls was visualized using a 3D laser scanning microscope (3D-LSM) Keyence VK-X200 equipped with a CF Plan ELWD 50x objective (Keyence GmbH, Neu-Isenburg, Germany). Micrographs of small tubing pieces were captured with the VK Viewer software in 'Expert Mode' at the standard settings. Two pictures were stitched and three representative regions of 100 x 100 µm^2 were used for surface roughness calculations using the MultiFileAnalyzer version 1.3.1.120. Tubing curvature was corrected for via the correct tilt – sec curved surface function and artefacts were eliminated by a medium height cut level.

3.5. Scanning Electron Microscopy (SEM)

Silicone particles fixed on an aluminum sample grid were carbon sputtered under vacuum and analyzed by a Helios NanoLab G3 UC scanning electron microscope (FEI, Hillsboro, Oregon, USA) at 2.0 kV and a working distance of approximately 10.5 mm.

3.6. Specific surface area

The specific surface area of the silicone particles was determined by an Autosorb 1 (Quantachrome, Odelzhausen, Germany) equipped with a liquid nitrogen bath at -196 °C using krypton gas adsorption and Brunauer-Emmet-Teller (BET) isotherm analysis. Approximately 1.5 g were outgassed for at least 2 h at 150 °C. An 11-point gas adsorption curve was measured (p/p_0 ratio of approximately 0.05-0.3). A multipoint Brunauer-Emmet-Teller fit was performed with the Autosorb 1 software.

3.7. Turbidity

A sample volume of 1.8 mL was analyzed using a Nephla turbidimeter (Dr. Lange, Duesseldorf, Germany). Data is presented in formazine nephelometric units (FNU).

3.8. Detection of subvisible particles

For an estimation of the particle size distribution and the total particle amount, the samples were analyzed by quantitative laser diffraction (qLD) using the Aggregates Sizer with WingSALD bio software version 3.2.2 (Shimadzu Corporation, Kyoto, Japan) in a batch cell with 5 mL sample volume. The calculations were based on a material specific refractive index of 1.46, an imaginary index of 0.1, and a protein particle density of 1.32 g/cm^3.[38] The cut-off level of noise was set to 500.

Samples were also analyzed with a FlowCAM® 8100 (Fluid Imaging Technologies, Inc., Scarborough, ME, USA) equipped with a 10x magnification cell (81 µm × 700 µm). A sample volume of 150 µl was used and images were collected at a flow rate of 0.15 mL/min, an auto image frame rate of 28 frames/s and a sampling time of 60 s, which resulted in an efficiency value higher than 70%. Particles were identified using the following settings: 3 µm distance to the nearest neighbor, particle segmentation thresholds of 13 and 10 for the dark and light pixels, respectively. Particle size was reported as the equivalent spherical diameter using the VisualSpreadsheet® 4.7.6 software.

3.9. Raman microscopy

3 µl samples were transferred to a self-constructed microfluidic channel with a width of 50 µm and a depth of 160 µm. Vibrational spectra were collected by a WITec alpha 300R microscope (WITec GmbH, Ulm, Germany), equipped with a 532 nm DPL laser (Cobolt AB, Solna, Sweden). The laser was focused through a 63× oil immersion objective (Zeiss Plan-

Apochromat SF25 63x/1.4; Carl Zeiss AG, Germany) into the static liquid. The true-power module ensured stable laser output, which was set between 40 and 50 mW. Large area map configurations were performed by collecting single point Raman spectra with a pixel size of 0.25 – 0.5 µm (x / y axis) and 1 µm (x / z axis) using a high-performance CCD camera with a spectral resolution of 4 cm^{-1}. Dependent on particle morphology and map configuration, exposure times were set between 0.2 s and 4 s to minimize sample damage.

Raman spectral maps were processed by spike removal, baseline correction (penalized spline), and normalized to the area under the curve. Hyperspectral data was unmixed via vertex component analysis (VCA)[39] using the software package Imagelab (Epina GmbH, Austria). A resampling factor of three was used and the spectral range above 3041 cm^{-1} was excluded to speed up calculation time. Concentration maps of the three main components (endmembers) show the lateral distribution of each component within the investigated area.

3.10.   Confocal laser scanning microscopy

Samples were fixed on glass slides by mixing 100 µl of sample with one drop of FluorSave™ Reagent (Merck Millipore Calbiochem, Darmstadt, Germany). Confocal images and z-stacks were acquired using a Leica TCS SP8 SMD microscope (Leica Microsystems, Wetzlar, Germany) equipped with a Leica PL APO 63x/1.20 water immersion objective at the 496 nm laser line for excitation. Images were analyzed using ImageJ. Images of pumped protein particles were composed z-stacks for better solution.

3.11.   Imaging Flow Cytometry

Samples were run either in native form, stained with ProteoStat, or with ProteoStat and Bodipy (Amnis® Protein Aggregate & Silicone Oil Detection Kit, Luminex Corp, Seattle, US). Fluorescent labeling was performed by mixing 2 µl 50x dye cocktail containing ProteoStat or ProteoStat and Bodipy in 1x Assay Buffer with 98 µl sample. Final concentrations for ProteoStat and Bodipy were 0.75 µmol/l and 94 nmol/l, respectively. After at least 10 minutes incubation, samples were analyzed with an Amnis FlowSight® imaging flow cytometer (Luminex, Austin, USA) equipped with a 20× magnification objective allowing 1 µm pixel resolution and a 60 µm wide field-of-view. The assay was based on the method developed by Probst.[36] The 785 nm side scatter (SSC) excitation laser was set to 70 mW and the 488 nm fluorescence excitation laser to 60 mW. BF in Ch01 (457/45, center wavelength/band width) and Ch09 (582/25) intensity is set automatically by the instrument software to achieve consistent background. Images were collected as followed: SSC in Ch06 (emission 762/35);

Bodipy in Ch02 (528/65); ProteoStat in Ch04 (610/30); Bodipy precipitates in Ch05 (702/85). All events detected were recorded in high sensitivity mode without user threshold for 120 seconds, equal to 2.52 µl sample volume. All data was analyzed using IDEAS® 6.2 (Luminex, Seattle, USA) image analysis software.

3.12.   Adsorption of protein to silicone particles

Identification of interfacial induced protein aggregation and quantification of adsorbed protein on silicone particles was evaluated by mixing 400 mg silicone particles with 1.5 mL protein stock solution (c=0.5; 1.0; 5.0 mg/mL) and rotating up to 48 h (SU1100, Sunlab Sustainable Lab Instruments, Mannheim, Germany) at 25 rpm at room temperature. Samples were centrifuged at 12,800 g for 10 min and analyzed by SEC using a TSKgel G3000SWXL column (Tosoh Bioscience GmbH, Stuttgart, Germany) and an Agilent 1100 series HPLC system equipped with a UV/Vis detector operated at 210 nm (Agilent Technologies, Santa Clara, CA, USA). The mobile phase consisted of 150 mM potassium phosphate buffer pH 6.5 at a flow rate of 0.5 mL/min at room temperature.

3.13.   Adsorption of silicone particles to protein aggregates

To detect spontaneous association of free silicone particles with protein aggregates, a 2 mg/mL silicone microparticle suspension in histidine buffer was sonicated for 10 minutes. The suspension was mixed 1:1 with a stirred 2 mg/mL mAb solution diluted 1:50. This mixture was analyzed by flow imaging. For CLSM, stirred protein samples were mixed 1:1 with Bodipy stained silicone microparticles or silicone particles generated by buffer pumping through Bodipy stained Versilic tubing for 7 h. Mixed samples were incubated for 1.5 h before analysis.

3.14.   Statistics

Results are reported as mean values with standard deviation (SD) of three independent experiments. Data was analyzed using GraphPad Prism (Version 5.02 for Microsoft Windows, Graph Pad Software, San Diego, USA).

4. Results

4.1. Surface characterization of tubing material

The inner silicone tubing surface was characterized using 3D-LSM (Figure 1), as the surface roughness is an indicator for the degree of particle shedding during pumping.[27] Surface roughness is described by the arithmetical mean height of the surface (S_A) and the maximum height (S_Z). While fresh Accusil tubing features a smooth surface (S_A=0.25 ± 0.03 µm; S_Z=2.93 ± 0.42 µm), Versilic exhibits a markedly higher surface roughness (S_A=3.00 ± 0.19 µm; S_Z =23.08 ± 2.57 µm) with a wavelike surface structure.

(a)   (b)
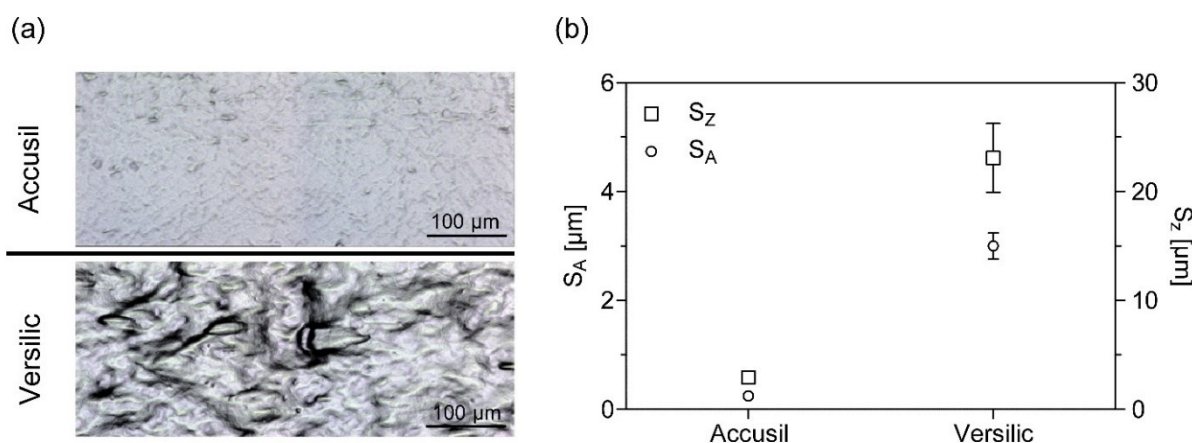
Figure 1 3D-LSM images (a) and surface roughness (b) of the inner wall of Accusil and Versilic tubing.

4.2. Particle formation upon pumping

Subsequently, protein solutions and buffer as control were pumped and analyzed for particle formation with three different techniques. Turbidity served as a qualitative indicator for particle formation, qLD to count in the nanometer to micrometer range and flow imaging to count and study the morphology of micrometer size particles (Figure 2). All pumped solutions were characterized by a substantial increase in particle numbers compared to the controls. Turbidity and particle numbers after pumping buffer were comparable for both silicone tubings with around 0.6 FNU and 4,000 particles ≥1 µm/mL. The signal intensity in qLD was below the cut-off level of noise for pumped buffer. The degree of particle formation was affected by the tubing material. Pumped mAb samples contained significantly higher particle numbers than the pumped buffer. Accusil tubing material resulted in lower particle levels than Versilic tubing material, with 1.8 ± 0.2 vs. 5.6 ± 0.1 FNU and 81,562 ± 5,441 vs. 450,709 ± 8,301 particles ≥ 1 µm/mL and $8.5 \cdot 10^6 \pm 0.6 \cdot 10^6$ vs. $5.1 \cdot 10^7 \pm 0.2 \cdot 10^7$ particles ≥ 0.3 µm/mL.
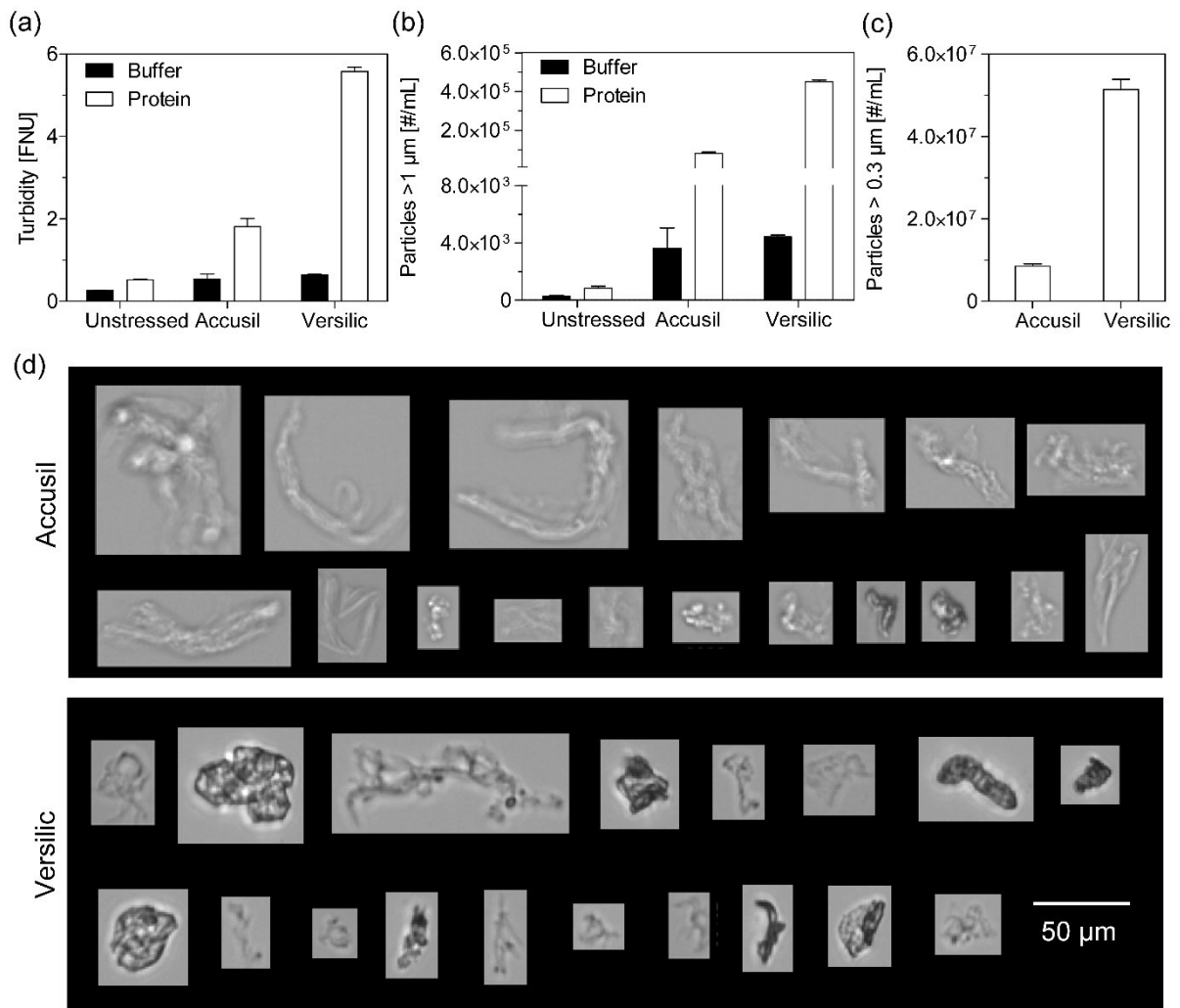
Figure 2 Particle analysis by turbidity (a), flow imaging (b) and qLD (c) of pumped buffer and mAb after 20 cycles through Accusil and Versilic tubing. Representative images from flow imaging of pumped mAb (d).

Morphological evaluation (Figure 2 d) was only possible for particles larger than 10 µm, as smaller particles appear blurry. The number concentration of the particles per mL larger than 10 µm increased drastically from less than 20 per mL to 200 per mL in buffer for both tubing materials, and 2,565 ± 233 and 18,816 ± 244 per mL in mAb solution for Accusil and Versilic, respectively. Particles exhibit a structure like ripped off protein film fragments folded up in the medium. Such type of particle was not present in the pumped buffer controls. In the following, samples pumped in Versilic tubing were used for a detailed microscopy-based analysis due to the higher particle concentration, whereas samples pumped in Accusil tubing were used for IFC to quantify mixed particles in optimum industry settings.

4.3. Component analysis using Raman microscopy

Figure 3 shows the chemical image of a representative protein particle with a size of approximately 12 × 12 µm^2. The surrounding of the particle within the region of interest (ROI) appears clear without any visible contaminants. 1600 spectra were acquired in a ROI of 20 x 20 µm^2.
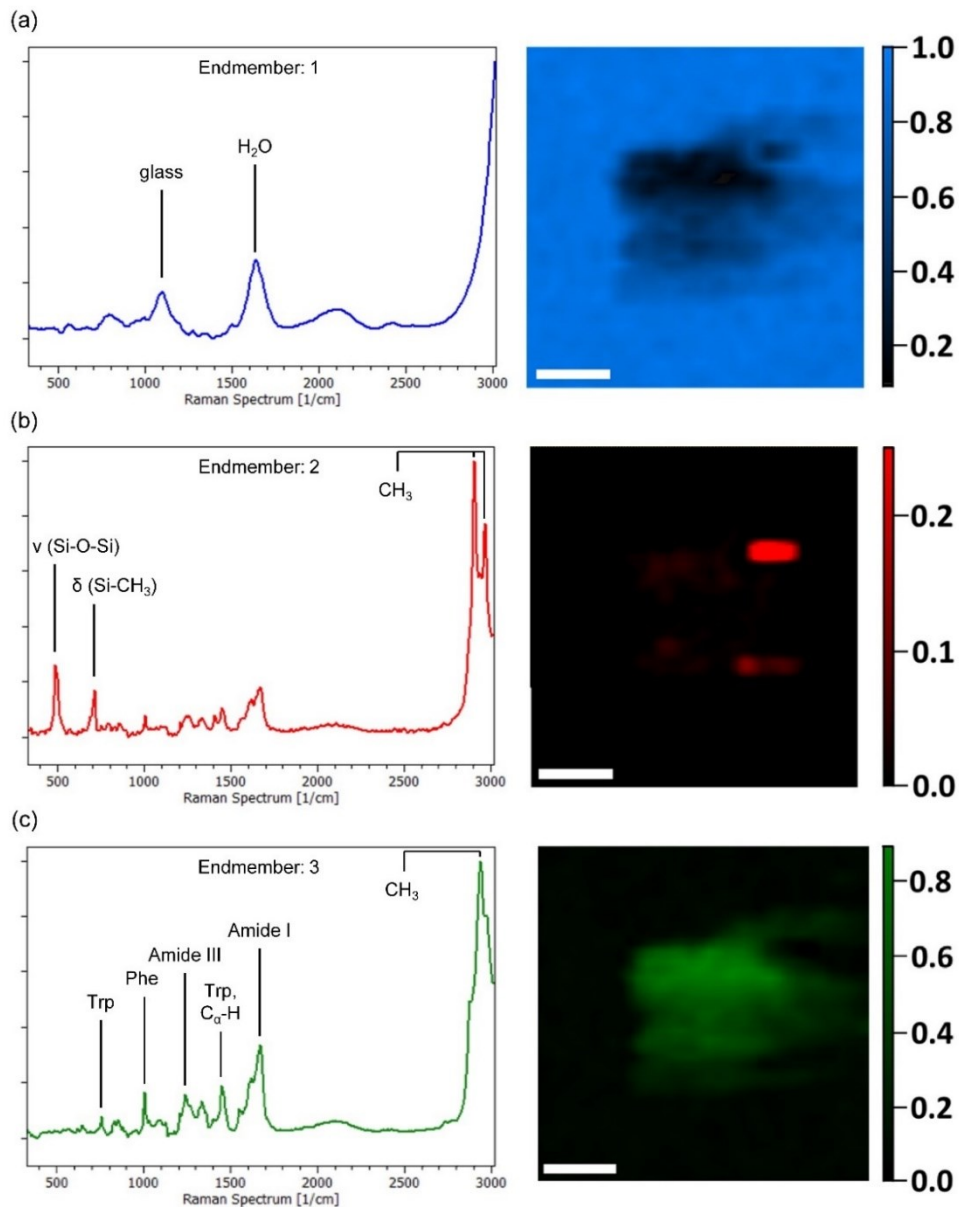
Figure 3 Calculated Raman spectra (left) and concentration maps (right) of the three detected endmembers: Raman spectral band intensities are allocated to the background (glass and water) (a), silicone nanoparticles (b) and protein (c). Scale bar represents 5 µm.

The different components glass, water, protein and silicone are called endmembers. The three endmembers were extracted from the Raman data via vertex component analysis (Table 1).

The concentration map of the first endmember represents the surrounding of the particle (background). The estimated Raman spectra of the first endmember shows a strong Raman band at 1100 cm^{-1} which is attributed to glass. The Raman bands at 1640 cm^{-1}, and 3400 cm^{-1} are assigned to bending and stretching vibrations of water. The Raman spectrum of the second endmember indicates an intense silicone signal besides of a weaker protein signal; hence, this component represents a mixture of silicone rubber and protein. The Raman fingerprint of silicone occurs at four distinct Raman wavenumbers which are all present in the extracted spectrum of the second component: the distinct band at 490 cm^{-1} evoked by ν(Si-O-Si) vibrations[50], the Raman band at 710 cm^{-1} attributed to (Si-CH$_3$) symmetric stretch vibrations, and the strong Raman bands at the wavenumbers at 2900 cm^{-1} and 2970 cm^{-1} representing C-H stretching vibrations.[49] The extracted Raman spectrum of the second endmember shows also protein specific Raman bands such as the phenylalanine band at 1000 cm^{-1} and the protein intrinsic amide I band at 1670 cm^{-1}.[44,48] The concentration map of the second endmember shows that silicone-characteristic Raman bands occur at four different spots of the scanned area. The concentration map of the third endmember represents the microscopically visualized particle. The extracted Raman spectrum of the third endmember shows exclusively protein specific Raman bands. The Raman band at 1000 cm^{-1} is assigned to phenylalanine.[44] The amide III band is apparent at 1240 cm^{-1}, whereas the tryptophan-characteristic bands are visible at 760 cm^{-1} and 1345 cm^{-1}.[51,46] The C-H deformation and stretching modes are represented at 1450 cm^{-1} and 2940 cm^{-1}, respectively.[47,49] The Raman band at 1670 cm^{-1} is assigned to the amide I vibration of the protein.[48]

Table 1 Raman band assignment of each component. ν stretching vibration; δ bending vibration

Component	Assignment	Wavenumber [cm^{-1}]	Ref.
Background	glass	1100	[40]
	δ(O-H) water	1640	[41]
	ν(O-H) water	3400	[42]
Protein	Tryptophan	760	[43]
	Phenylalanine	1000	[44]
	Amid II	1240	[45]
	C$_a$-H Tryptophan	1345	[46]
	δ(C-H)	1450	[47]
	Amid I	1670	[48]
	ν(C-H)	2940	[49]
Silicone rubber	ν(Si-O-Si)	490	[50]
	ν(Si-CH$_3$)	710	[50]
	C-H	2900	[49]
		2970	[49]

The unmixing of the hyperspectral data through VCA extracts endmember spectra. The according concentration maps visualize the spatial distribution of each component within the ROI, e. g. the distribution of silicone nanoparticles. In this example, the silicone particles appear to be located at the edge of the protein structure rather than within the protein particle.

More Raman images of protein structures were recorded to investigate the position of the silicone nanoparticles relative to the protein (Figure 4 a). The overlay of protein and silicone concentration maps reveals a random distribution of silicone particles (at the edge and in the middle of the protein structure). However, the 2-dimensional image does not reveal whether silicone particles are located on top, bottom or in the middle of the protein. Therefore, depth scans (z-stacks) were performed visualizing the spatial distribution of silicone nanoparticles in three dimensions (Figure 4 b).
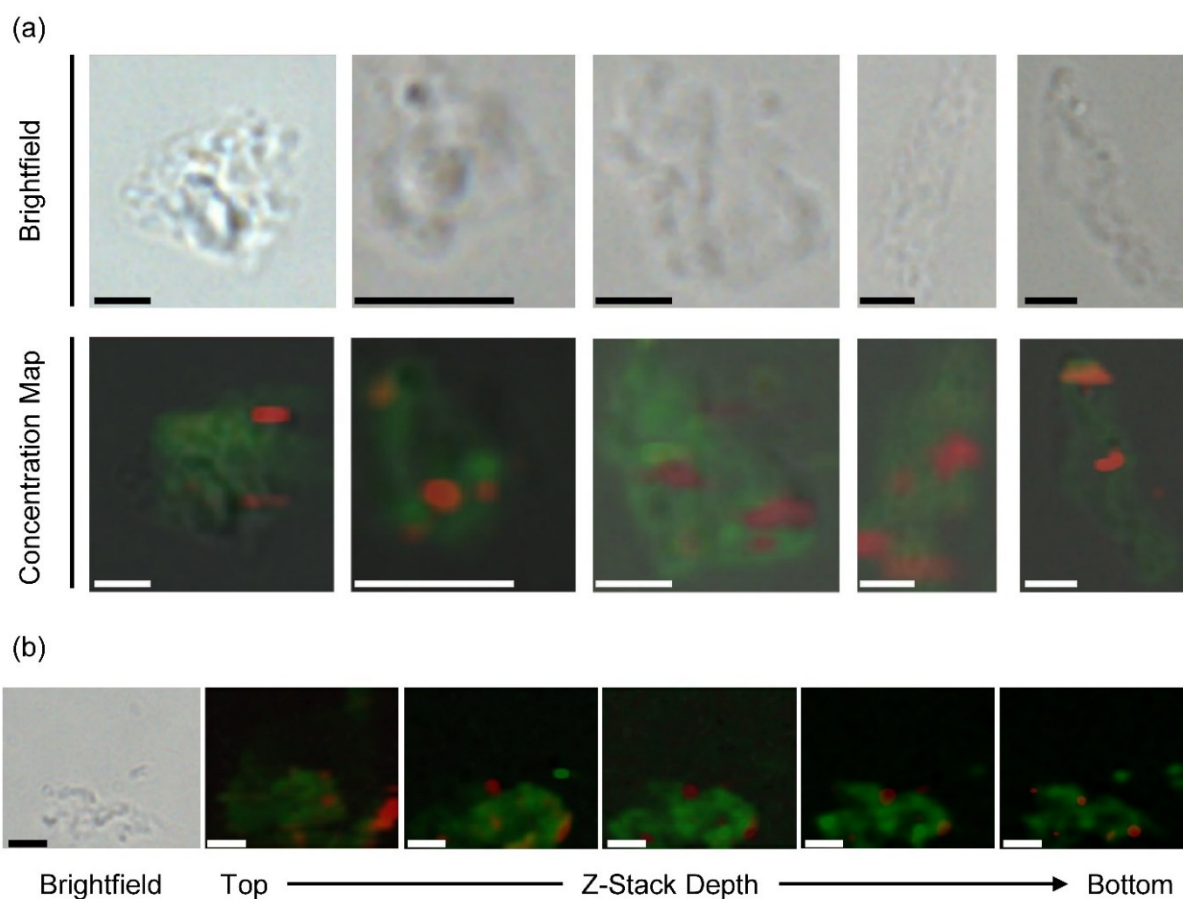
Figure 4 Microscopic images of particles in brightfield and calculated concentration maps (a) and z-scan (z-difference: 1 μm) through a single particle (b). Silicone majorities (red) were present around and inside the protein core (green). The scale bar corresponds to 5 μm.

Chemical depth profiles are achieved by recording Raman images at different heights/sample layers yielding a more comprehensive analysis of the silicone particle location. The depth

profiles of the protein particles indicate that silicone was not only located on the protein surface but also inside the particle.

4.4. Fluorescence-based particle identification using CLSM

Complementary to the observations by Raman microscopy, fluorescence-based methods were employed to identify and quantify the mixed particle species. The tubing material was stained before its use by incubation in an organic Bodipy solution. CLSM enables the analysis of the particle morphology and the distribution of the silicone nanoparticles inside the mixed particle. Only a single staining was possible in CLSM due to the quick photobleaching of ProteoStat (Figure 5).
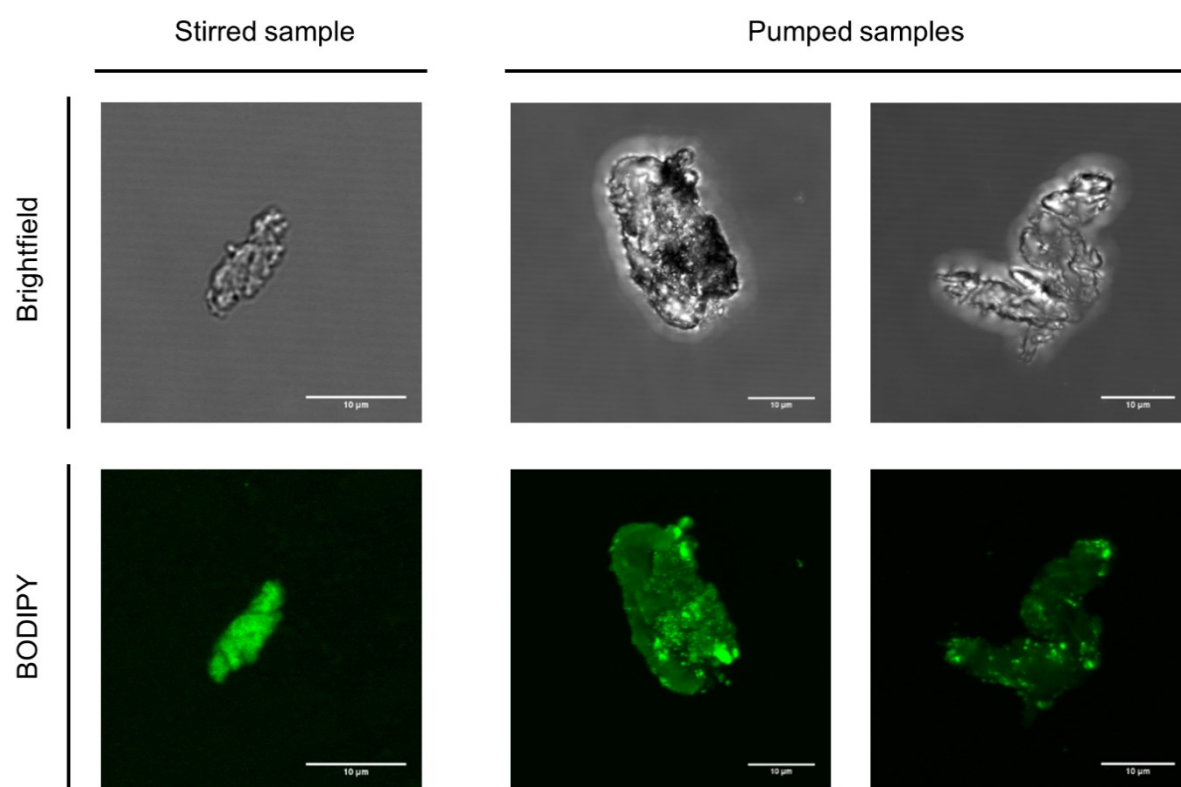
Figure 5 Representative brightfield and fluorescence micrographs of protein particles generated by stirring stained with 1 µmol Bodipy and generated during pumping through Bodipy stained Versilic tubing.

Protein particles independent of stress condition exhibited an irregular shape. Pure protein particles did not feature any intrinsic fluorescence, while staining these particles with 1 µmol Bodipy resulted in a diffuse fluorescence of the whole particle. In contrast, the pumped samples contain protein particles with several intense Bodipy positive signals attributed to silicone. Silicone particles varied in size, ranging from a few nanometers up to 2 µm.

4.5. Quantification of mixed species using IFC

While microscopic techniques are limited in the quantification of particles due to low sample throughput, we employed IFC to overcome these limitations. For sample generation, protein was pumped through Bodipy labeled tubing and aggregates were subsequently stained with ProteoStat to detect protein particles (Table 2). Data was presented in bivariate plots of BODIPY (Ch02) versus ProteoStat (Ch04) fluorescence intensity. Gates were drawn to classify the particles as either protein aggregates or silicone particles. Addition of ProteoStat to the buffer did not result in the formation of fluorescent particles e.g. by precipitation.

For the evaluation of the method, single particle type controls were run (Figure S 1) and demonstrated sufficient resolution of both signals. Labelled and unlabeled silicone beads showed a false positive signal in the protein aggregation gate. Such unspecific fluorescence is known for surfactant concentrations higher than 0.01%[52] due to interaction of ProteoStat with hydrophobic regions of the PS20 micelles.[53]

Table 2 Method development for IFC measurements.

	Bodipy Post-Staining Approach	Bodipy Pre-Staining Approach
Labelling of components:		
Silicone	Post-Staining with Bodipy	Pre-Staining Tubing with Bodipy
Protein Aggregates	Post-Staining with ProteoStat	Post-Staining with ProteoStat
Detection of mixed particles	Not possible	a) Silicone containing protein particles: Sample without ProteoStat staining b) Total amount of protein aggregates: Sample labelled with ProteoStat

Post-staining with Bodipy results in a Bodipy positive population for micrometer sized silicone beads and absence of Bodipy fluorescence in pure protein samples (Figure S 2). As free Bodipy could bind to protein aggregates pure protein particles could be detected false positive as mixed particles. Dye loading and thus fluorescence intensity of shed tubing particles could be adapted by the choice of the organic solvent which affects swelling and diffusion of dye into the tubing wall. Therefore, prestaining was considered as the more reliable preparation method for nanoparticle identification.

No fluorescent particles were detected in pumped buffer samples, while pumped protein samples showed signals in the protein aggregate population only after ProteoStat staining. Analyzing the protein samples unstained, a silicone particle population could be uncovered. ProteoStat seems to dominate the signals of silicone particles due to its high intensity

(Figure 6). For the detection of the mixed species, it is therefore necessary to evaluate the sample before and after staining with ProteoStat.
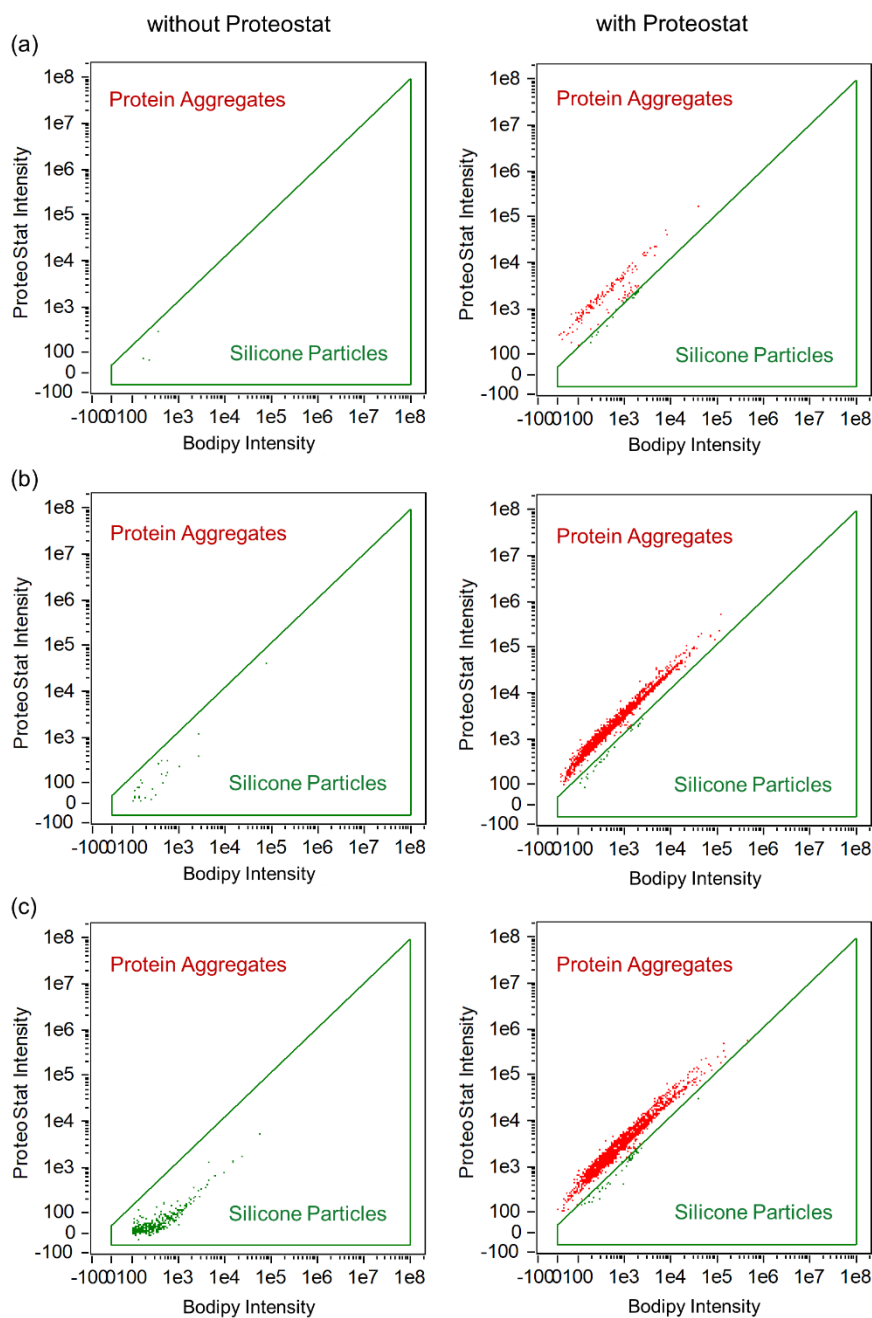
Figure 6 Bivariate Plots for buffer (a), 1 mg/mL mAb pumped through untreated (b) and Bodipy pre-stained Accusil tubing (c) before (left) and after staining with ProteoStat (right).

Samples were analyzed without additional silicone post staining for silicone nanoparticle containing protein particles and with additional ProteoStat post- staining to analyze the total number of protein particles (Figure 7). In mAb solutions pumped through naive and Bodipy labelled tubing, 407,968 ± 21,068 and 290,016 ± 20,610 protein particles per mL were detected, respectively. Due to instrument noise and spectral spillover the measurements of

buffer and mAb solution pumped through unlabeled tubing the instrument falsely indicated the presence of a few Bodipy stained particles. The mAb solution showed approximately 131,974 ± 7,279 Bodipy positive particles per mL after pumping through Bodipy labelled tubing indicating that 45% of the protein particles contained silicone particles.
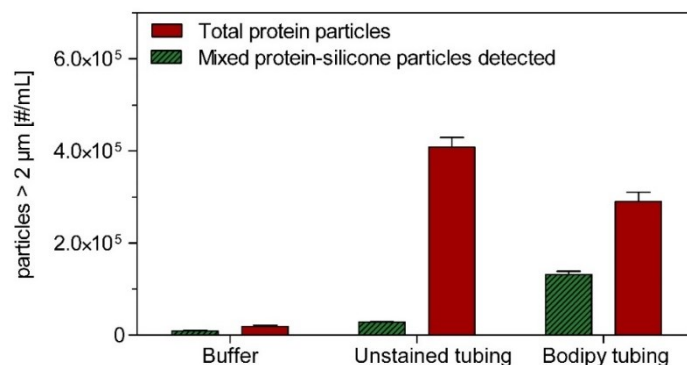
Figure 7 Number of detected mixed particles in buffer and 1 mg/mL mAb pumped through unstained and Bodipy stained Accusil tubing.

4.6. Protein adsorption to silicone particles

Shed silicone particles could not be produced in a sufficient large scale to allow reliable statistical analysis. Therefore, spherical silicone model microparticles with a specific surface area of 0.388 ± 0.002 m^2/g were utilized for adsorption studies (Figure 8 a). MAb molecules adsorbed quickly to the silicone particles (Figure 8 b + c) reaching an equilibrium of approximately 1.5 mg/m^2 after 24 h. Increasing mAb concentration only lead to a minor increase to 1.8 mg/m^2. Induction of protein oligomers could not be found in the bulk solution.

In CLSM, no mixed particles were detected after incubation of preformed protein aggregates with Bodipy labeled silicone model microparticles (Figure S 3 a). Furthermore, no decrease in total particle number concentration, which would indicate assembly of both components, could be found for incubated mixtures (Figure S 3 b).
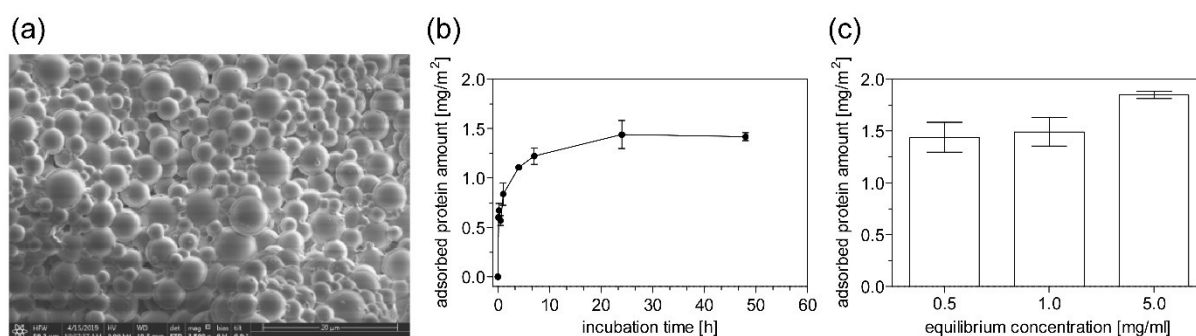
Figure 8 SEM images of model silicone particles (a). MAb adsorption to silicone particles over time (c = 0.5 mg/mL) (b) and as function of protein concentration after 24 h (c).

5. Discussion

Peristaltic pumps are routinely used in different stages of manufacturing and handling of biopharmaceuticals. Most manufacturing stages contain filtration steps for particle removal although there are some cases where filtration caused protein aggregation due to interfacial adsorption to the filter membrane.[54,55] Fill & finish operations lack final purification steps except filtration. Especially during filling, pumps could be the source of particle burden. Previous studies highlighted that upon peristaltic pumping, tubing material sheds[27] and protein aggregates can be formed.[21] Hence, potential formation of particles and aggregates is critical, as different size species may enter the final product in an unobstructed way.

We wanted to learn whether particles composed of both aggregated protein and shed silicone can form. Such mixed structures are suspected to induce immune responses.[28–30] At first, methods are needed to detect mixed protein species which are suitable for process development and root cause analysis. We therefore pumped a mAb solution using silicone tubing. Two silicone tubings with different surface roughness were tested to have a look on the effect of higher silicone particle spallation on protein aggregate formation. Independent of tubing material, pump roller-induced generation of particles above 1 μm were observed at a particle density less than 200 particles/mL per pump cycle. According to Saller et al., the shed silicone particles are typically around 180 nm in size. They found that the amount of shed particles is linked to the surface roughness of the inner tubing wall, which accords to our findings.[27] The tubing with higher roughness rendered increased levels of protein particles larger than 1 μm per pump cycle with approximately 23,000 compared to 4,000 particles per mL. This observation could be linked either to the difference in silicone shedding, or to the increasing surface area with increasing roughness prone to interfacial effects. With higher surface roughness on the nano- and micrometer scale, protein adsorption is enhanced beyond the corresponding increase in specific surface area,[56–58] which again may lead to increased protein aggregation and particle formation. It is assumed that protein particle formation is based on the detachment of the protein film from the tubing surface by roller movements[21] similar to effects known from piston pumps.[18] We speculate that, based on their morphology, the protein particles resemble fragmented protein film.

Multicomponent species can be discerned if components differ in specific properties such as morphology or density. The standard application is microflow imaging to tell between silicone oil droplets and protein particles, addressing a combination of different optical properties. Micrometer particles with nanometer-size contaminations cannot be further analyzed by this technique. Here, high resolution techniques with the ability for chemical identification are needed. In this study, Raman microscopy and fluorescence microscopic imaging were

employed to close this gap. The mechanism of mixed silicone and protein particle formation is still unclear. Mixed particles could form independently and attach to each other, or silicone particles could be nuclei for the formation of protein aggregates. Questions on the formation mechanism of the mixed protein particles cannot be answered with these methods but they can provide fundamental information on the composition of each detected particle and insight into contaminant distribution in protein particles.

Raman spectroscopy offers a variety of applications for pharmaceutical industry in early drug development, characterization of drug delivery systems, in-process measurements, product performance and quality control for the final product.[59] In brightfield microscopy, all particles resemble homogenous protein aggregates, without a hint of embedded or connected foreign species. By scanning the protein particles with Raman microscopy, the chemical distribution of the whole particle dimension was visualized. In a high number of particles, an additional chemical component besides protein could be identified. Heterogeneous particles showed spots of high Raman scattering at 490 cm^{-1}, 710 cm^{-1}, 2900 cm^{-1} and 2970 cm^{-1}, which is linked to silicone rubber shed from the tubing material during pumping.[60]

Heterogeneous particles were detected by Raman microscopy without sample staining. The unmixing of the hyperspectral data set via VCA provided a fast and reliable evaluation tool, which visualized the spatial distribution of silicone nanoparticles on the surface of a protein particle. The presented Raman method is applicable for a vast majority of particles with minor limitations for highly fluorescent or weakly Raman active species. Particles detected in brightfield mode exhibited a sufficiently strong Raman signal at moderate laser power without particle destruction, degradation or photobleaching. However, recording the Raman maps is a time-consuming task (roughly 2 hours / particle), hence, the current method suffers from poor sample throughput.

Complementary to Raman microscopy, mixed particles can be analyzed by fluorescence-based methods. This study aimed to differentiate protein and silicone using two non-covalently binding extrinsic fluorescence dyes that have selective affinity for each species with well-separated signals and require no purification step. Based on a previous study the combination of Bodipy and ProteoStat fits these requirements.[36] Silicone itself has no autofluorescence and needs labelling for detection. Bodipy is a highly fluorescent hydrophobic dye in non-polar and polar media with sharp and narrow emission peak at 503 nm. The tubing was stained by incubation with Bodipy and the dye migration enhanced by swelling of the tubing through organic solvents.[61] The Bodipy loading of the silicone matrix can also be tuned by the swelling properties of the organic solvent. This approach is limited to hydrophobic components, and it must be assured that the pump properties of the tubing are not changed by residual solvent.

Extrinsic labelling of the protein is necessary as the intrinsic fluorescence of proteins is not strong enough for detection. Covalent labeling of the protein a priori may change polarity, charge and ultimately surface binding, protein-protein interactions and protein aggregation.[62,63] Furthermore, covalent dye binding is not relevant when it comes to screening of a drug product. The protein staining dye ProteoStat was added to the samples prior to analysis. ProteoStat as a proprietary fluorescent rotor dye exhibits increased fluorescence when interacting with protein aggregate structures over a wide range of excipients including low to medium surfactant concentrations.[53]

We could not find a reference to the use of CLSM for the characterization of protein aggregates in biopharmaceuticals. Unfortunately, ProteoStat dye was quickly bleached whereas Bodipy showed good photochemical stability. Protein particles from stirred samples containing no silicone particles exhibited diffuse staining of the whole protein particle in presence of free Bodipy due to interactions with the hydrophobic cavities of protein aggregates.[64,65] In contrast, particles generated by pumping showed finely distributed silicone rubber remains attached to the protein particle. The sharp images taken in a few seconds with high resolution allowed morphological analysis and identification of silicone.

CSLM and Raman microscopy do not allow a fast quantification of protein particle concentration. Therefore, we set up an IFC method which could quantify both, protein-only and mixed protein silicone particles. IFC allows simultaneous acquisition of multiple spectral images in high quality and sensitivity for fast-moving objects by a charge-coupled device detector with a time-delay integration technology. Although post-staining of silicone with Bodipy was possible with micrometer-sized silicone beads, no mixed particles could be detected in the pumped samples using the post-staining approach. Additionally, post-staining with Bodipy comes with the risk of unspecific protein staining and interactions with the protein formulation. For micrometer-sized contaminants like silicone oil, post-staining with Bodipy may be less critical, as the fluorescence intensity would exceed any interferences from protein signal.[36] Consequently, silicone tubing was pre-labelled via incubation with organic solvents containing a higher BODIPY concentration of 2 mg/mL. Even with pre-labelling, the low fluorescence signal of the silicone nanoparticles was overwhelmed by the ProteoStat dye staining the protein. To distinguish mixed species, the pumped samples were analysed with and without ProteoStat staining, such that mixed particles were identified as BODIPY positive in the ProteoStat-unlabeled samples, and protein-only particles were identified as ProteoStat-positive events subtracted by the mixed particles. Free 180 nm[27] silicone rubber particles were not detectable as their size is below the SSC detection limit of around 200 nm, however silicone could be detected when attached to protein aggregates, presumably as multiple silicone particles were attached to individual protein aggregates.[36] Protein particles larger than 2 µm

were shown to contain at least 45% mixed particles for the pumped protein sample. To resolve smaller protein particles containing small amounts of silicone rubber particles, higher laser power and magnification could be beneficial. This method can be used for a wide range of formulations, but care should be taken when using surfactant concentrations > 0.01%. Interactions between the ProteoStat dye and the surfactant micelles can lead to increased background intensity resulting in a higher risk for false positive protein aggregates signal.

With the herein developed methods, it is now possible to distinguish and quantify protein particles containing foreign micro- and nanometer-sized particles. Raman microscopy, CLSM, and IFC together can provide important insights, as we demonstrate here for protein particles formed upon peristaltic pumping in silicone tubes. Due to the limitations in microscopic resolution and the low fluorescence intensity of the nanometer-sized particles, these approaches are limited to micrometer-sized protein particles.

Most foreign micro - and nanoparticle contaminations are coated by a protein monolayer and do not necessarily lead to protein particle formation.[12] But there are also materials like stainless steel particles, which induce conformational changes upon protein adsorption and lead to aggregation.[13,14] Spiking silicone particles did not induce an increase in protein aggregates in the course of a stability study[66], but the presence of surfactants in the tested formulations could have suppressed interfacial interactions. The chosen silicone rubber microparticles are formed from crosslinked linear dimethylpolysiloxane and resemble high purity silicone rubber. Density and surface charge should be very similar to the pt-cured tubing material, but the materials are not completely identical in material properties. We showed that approximately 1.8 mg/m^2 mAb adsorb to silicone particles, which is consistent with a monolayer formation.[12] There were no signs for formation or preferred adsorption of higher molecular weight species in SEC. Furthermore, the experiments were conducted in the absence of interfacial shear. These findings support the hypothesis that elevated protein particle formation in tubing with higher surface roughness is linked to an increase in adsorption area rather than to increased silicone rubber particle shedding. The adsorption is driven through an interplay of hydrophobic and electrostatic interactions between the positively charge mAb and the negatively charged silicone rubber[27] leading to an irreversibly bound monolayer.[67] Interactions between preformed aggregates and foreign species may be protein dependent, e. g lysozyme aggregates strongly attached on silicone oil droplets, mAb aggregates showed less interaction with silicone oil.[36] In case of our mAb, we did not find any evidence for subsequent adsorption of the silicone particles to protein aggregates. Silicone rubber particles could therefore become part of the aggregates if there is simultaneous disruption of protein film and detachment of underlying silicone rubber during roller movement.

6. Conclusion

Peristaltic pumping generates mAb particles containing nanometer sized silicone rubber fragments, which can be identified by Raman microscopy, CLSM and IFC. The silicone rubber particles do not serve as source of aggregation but are covered by protein and distributed in the total large protein aggregates. Raman microscopy as label-free method and CLSM using Bodipy stained tubing material could proof the presence of silicone fragments in protein particles. IFC could reveal that nearly half of the protein particles contained silicone rubber. The study indicated that mixed silicone rubber and protein particle are co-generated during pumping instead of subsequent absorption of both species. The developed methods possess great potential for chemical identification of protein aggregates contaminated with non-proteinaceous material to support process development and forensic root cause analysis.

7. Acknowledgements

8. References

1.   Walsh G. Biopharmaceutical benchmarks 2018. Nat Biotechnol. 2018;36(12):1136-1145. doi:10.1038/nbt.4305

2.   Rosenberg AS. Effects of Protein Aggregates: An Immunologic Perspective. AAPS J. 2006;8(3):E501-E507. doi:10.1208/aapsj080359

3.   Moussa EM, Panchal JP, Moorthy BS, et al. Immunogenicity of Therapeutic Protein Aggregates. J Pharm Sci. 2016;105(2):417-430. doi:10.1016/j.xphs.2015.11.002

4.   Mahler HC, Müller R, Friess W, Delille A, Matheus S. Induction and analysis of aggregates in a liquid IgG1-antibody formulation. European Journal of Pharmaceutics and Biopharmaceutics. 2005;59:407-417. doi:10.1016/j.ejpb.2004.12.004

5.   EP <2.9.19>. Particulate Contamination: Sub-Visible Particles. In: European Pharmacopoeia. 6th ed. European Directorate For The Quality Of Medicine; 2008.

6.   USP <788> Particulate matter in injections. In: United States Pharmacopeia. United States Pharmacopeial Convention; 2014.

7.   Singh SK, Afonina N, Awwad M, et al. An Industry Perspective on the Monitoring of Subvisible Particles as a Quality Attribute for Protein Therapeutics. J Pharm Sci. 2010;99(8):3302-3321. doi:10.1002/jps.22097

8.   Weinbuch D, Ruigrok M, Jiskoot W, Hawe A. Nanoparticulate Impurities Isolated from Pharmaceutical-Grade Sucrose Are a Potential Threat to Protein Stability. Pharm Res. 2017;34:2910-2921. doi:10.1007/s11095-017-2274-4

9.   Bee JS, Randolph TW, Carpenter JF, Bishop SM, Dimitrova MN. Effects of Surfaces and Leachables on the Stability of Biopharmaceuticals. J Pharm Sci. 2011;100(10):4158-4170. doi:10.1002/jps

10.   Gerhardt A, Mcgraw NR, Schwartz DK, Bee JS, Carpenter JF, Randolph TW. Protein Aggregation and Particle Formation in Prefilled Glass Syringes. J Pharm Sci. 2014;103(6):1601-1612. doi:10.1002/jps.23973

11.   Krayukhina E, Tsumoto K, Uchiyama S, Fukui K. Effects of syringe material and silicone oil lubrication on the stability of pharmaceutical proteins. J Pharm Sci. 2015;104(2):527-535. doi:10.1002/jps.24184

12.   Bee JS, Chiu D, Sawicki S, et al. Monoclonal Antibody Interactions With Micro- and Nanoparticles: Adsorption, Aggregation, and Accelerated Stress Studies. J Pharm Sci. 2009;98(9):3218-3238. doi:10.1002/jps

13.   Tyagi AK, Randolph TW, Dong A, Maloney KM, Hitscherich CJ, Carpenter JF. IgG Particle Formation during Filling Pump Operation: A Case Study of Heterogeneous Nucleation on Stainless Steel Nanoparticles. J Pharm Sci. 2009;98(1):94-104. doi:10.1002/jps.21419

14.   Bee JS, Davis M, Freund E, Carpenter JF, Randolph TW. Aggregation of a Monoclonal Antibody Induced by Adsorption to Stainless Steel. Biotechnol Bioeng. 2010;105(1):121-129. doi:10.1002/bit.22525

15.   Meireles M, Aimar P, Sanchez V. Albumin denaturation during ultrafiltration: Effects of operating conditions and consequences on membrane fouling. Biotechnol Bioeng. 1991;38(5):528-534. doi:10.1002/bit.260380511

16.   Cromwell MEM, Hilario E, Jacobson F. Protein aggregation and bioprocessing. AAPS J. 2006;8(3):E572-E579. doi:10.1208/aapsj080366

17.   Nayak A, Colandene J, Bradford V, Perkins M. Characterization of Subvisible Particle Formation During the Filling Pump Operation of a Monoclonal Antibody Solution. Journal of P. 2011;100(10):4198-4204. doi:10.1002/jps

18.   Kalonia CK, Heinrich F, Curtis JE, Raman S, Miller MA, Hudson SD. Protein Adsorption and Layer Formation at the Stainless Steel− Solution Interface Mediates Shear-Induced Particle Formation for an IgG1 Monoclonal Antibody. Mol Pharmaceutics. 2018;15(3):1319-1331. doi:10.1021/acs.molpharmaceut.7b01127

19.   Bausch UJ. Impact of Filling Processes on Protein Solutions. University Basel; 2008.

20.   Chandavarkar AS. Dynamics of Fouling of Microporous Membranes by Proteins. Massachusetts Institute of Technology; 1990.

21.   Her C, Carpenter JF. Effects of Tubing Type, Formulation, and Postpumping Agitation on Nanoparticle and Microparticle Formation in Intravenous Immunoglobulin Solutions Processed With a Peristaltic Filling Pump. J Pharm Sci. 2020;109(1):739-749. doi:10.1016/j.xphs.2019.05.013

22.   Denkinger SN. Modelle Zur Simulation Des Abfüllprozesses Biologisch-Pharmazeutischer Arzneimittel. Rheinische Friedrich-Wilhelms-Universität Bonn; 2010.

23.   Thomas CR, Geer D. Effects of shear on proteins in solution. Biotechnol Lett. 2011;33(3):443-456. doi:10.1007/s10529-010-0469-4

24.   Leong ASY, Disney AP, Gove DW. Spallation and Migration of silicone from blood-pump tubing in patients of hemodialysis. N Engl J Med. 1982;306(3):135-140. doi:10.1056/NEJM198201213060303

25.   Bommer J, Gemsa D, Waldherr R, Kessler J, Ritz E. Plastic Filing from Dialysis Tubing Induces Prostanoid Release from Macrophages. Vol 26.; 1984. doi:10.1038/ki.1984.177

26.   Laohapand T, Osman EM, Morley AR, Ward MK, Kerr DNS. Accumulation of silicone elastomer in regular dialysis. Proc EDTA. 1982;19:143-152.

27.   Saller V, Matilainen J, Grauschopf U, Bechtold-Peters K, Mahler HC, Friess W. Particle Shedding from Peristaltic Pump Tubing in Biopharmaceutical Drug Product Manufacturing. J Pharm Sci. 2015;104(4):1440-1450. doi:10.1002/jps.24357

28.   Van Beers MM c:, Gilli F, Schellekens H, Randolph TW, Jiskoot W. Immunogenicity of Recombinant Human Interferon Beta Interacting with Particles of Glass, Metal, and Polystyrene. Journal of Pharmaceutical Sciencesharmaceutical sciences. 2012;101(1):187-199. doi:10.1002/jps

29.   Chisholm CF, Baker AE, Soucie KR, Torres RM, Carpenter JF, Randolph TW. Silicone Oil Microdroplets Can Induce Antibody Responses Against Recombinant Murine Growth Hormone in Mice. J Pharm Sci. 2016;105(5):1623-1632. doi:10.1016/j.xphs.2016.02.019

30.   Chisholm CF, Soucie KR, Song JS, et al. Immunogenicity of Structurally Perturbed Hen Egg Lysozyme Adsorbed to Silicone Oil Microdroplets in Wild-Type and Transgenic Mouse Models. J Pharm Sci. 2017;106(6):1519-1527. doi:10.1016/j.xphs.2017.02.008

31.   Anderson JM, Ziats NP, Azeez A, Brunstedt MR, Stack S, Bonfield TL. Protein adsorption and macrophage activation on polydimethylsiloxane and silicone rubber. Journal of Biomaterials Science. 1996;7(2):159-169. doi:10.1163/156856295X00670

32.   Gambe-Gilbuena A, Shibano Y, Krayukhina E, Torisu T, Uchiyama S. Automatic Identification of the Stress Sources of Protein Aggregates Using Flow Imaging Microscopy Images. J Pharm Sci. 2020;109:614-623. doi:10.1016/j.xphs.2019.10.034

33.   Weinbuch D, Zölls S, Wiggenhorn M, et al. Micro-Flow Imaging and Resonant Mass Measurement (Archimedes)-Complementary Methods to Quantitatively Differentiate Protein Particles and Silicone Oil Droplets. J Pharm Sci. 2013;102:2152-2165. doi:10.1002/jps.23552

34.   Strehl R, Rombach-Riegraf V, Diez M, et al. Discrimination Between Silicone Oil Droplets and Protein Aggregates in Biopharmaceuticals: A Novel Multiparametric Image Filter for Sub-visible Particles in Microflow Imaging Analysis. Pharm Res. 2012;29:594-602. doi:10.1007/s11095-011-0590-7

35.   Ludwig DB, Trotter JT, Gabrielson JP, Carpenter JF, Randolph TW. Flow cytometry: A promising technique for the study of silicone oil-induced particulate formation in protein formulations. Anal Biochem. 2011;410(2):191-199. doi:10.1016/j.ab.2010.12.008

36.	Probst C. Characterization of Protein Aggregates, Silicone Oil Droplets, and Protein-Silicone Interactions Using Imaging Flow Cytometry. J Pharm Sci. 2020;109(1):364-374. doi:10.1016/j.xphs.2019.05.018

37.	Lankers M, Munhall J, Valet O. Differentiation between foreign particulate matter and silicone oil induced protein aggregation in drug solutions by automated Raman spectroscopy. Microscopy and Microanalysis. 2008;14(S 2):1612-1613. doi:10.1017/S1431927608086807

38.	Folzer E, Khan TA, Schmidt R, et al. Determination of the Density of Protein Particles Using a Suspended Microchannel Resonator. J Pharm Sci. 2015;104(12):4034-4040. doi:10.1002/jps.24635

39.	Nascimento JMP, Dias JMB. Vertex component analysis: A fast algorithm to unmix hyperspectral data. IEEE Transactions on Geoscience and Remote Sensing. 2005;43(4):898-910. doi:10.1109/TGRS.2005.844293

40.	White WB, Minser DG. Raman spectra and structure of natural glasses. J Non Cryst Solids. 1984;67(1-3):45-59. doi:10.1016/0022-3093(84)90140-6

41.	Tominaga Y, Fujiwara A, Amo Y. Dynamical structure of water by Raman spectroscopy. Fluid Phase Equilib. 1998;144(1-2):323-330. doi:10.1016/s0378-3812(97)00276-8

42.	Cárcamo JJ, Aliaga AE, Clavijo RE, Brañes MR, Campos-Vallette MM. Raman study of the shockwave effect on collagens. Spectrochim Acta A Mol Biomol Spectrosc. 2012;86:360-365. doi:10.1016/j.saa.2011.10.049

43.	Takeuchi H. Raman Structural Markers of Tryptophan and Histidine Side Chains in Proteins. Biopolymers (Biospectroscopy). 2003;72(5):305-317. doi:10.1002/bip.10440

44.	Lippert JL, Tyminski D, Desmeules PJ. Determination of the Secondary Structure of Proteins by Laser Raman Spectroscopy. J Am Chem Soc. 1976;98(22):7075-7080. doi:10.1021/ja00438a057

45.	Barron LD, Wen ZQ, Hecht L. Vibrational Raman Optical Activity of Proteins. J Am Chem Soc. 1992;114(2):784-786. doi:10.1021/ja00028a069

46.	Tobin MC. Raman spectra of crystalline lysozyme, pepsin, and alpha chymotrypsin. Science (1979). 1968;161(3836):68-69. doi:10.1126/science.161.3836.68

47.	Nakamura K, Era S, Ozaki Y, Sogami M, Hayashi T, Murakami M. Conformational changes in seventeen cystine disulfide bridges of bovine serum albumin proved by Raman spectroscopy. FEBS Lett. 1997;417(3):375-378. doi:10.1016/S0014-5793(97)01326-4

48.   Tfayli A, Piot O, Draux F, Pitre F, Manfait M. Molecular characterization of reconstructed skin model by Raman microspectroscopy: Comparison with excised human skin. Biopolymers. 2007;87(4):261-274. doi:10.1002/bip.20832

49.   Howell NK, Arteaga G, Nakai S, Li-Chan ECY. Raman Spectral Analysis in the C-H Stretching Region of Proteins and Amino Acids for Investigation of Hydrophobic Interactions. J Agric Food Chem. 1999;(47):924-933. doi:10.1021/jf981074l

50.   Österle W, Giovannozzi A, Gradt T, et al. Exploring the potential of Raman spectroscopy for the identification of silicone oil residue and wear scar characterization for the assessment of tribofilm functionality. Tribol Int. 2015;(90):481-490. doi:10.1016/j.triboint.2015.04.046

51.   Dupaix A, Bechet JJ, Yon J, Merlin JC, Delhayet M, Hill M. Resonance Raman spectroscopic studies of the interactions between trypsin and a competitive inhibitor. Proc Natl Acad Sci U S A. 1975;72(11):4223-4227. doi:10.1073/pnas.72.11.4223

52.   PROTEOSTAT ® Protein Aggregation Assay For microplates or flow cytometry Instruction Manual. Accessed March 23, 2020. www.enzolifesciences.com

53.   McClure SM, Ahl PL, Blue JT. High Throughput Differential Scanning Fluorimetry (DSF) Formulation Screening with Complementary Dyes to Assess Protein Unfolding and Aggregation in Presence of Surfactants. Pharm Res. 2018;35:81. doi:10.1007/s11095-018-2361-1

54.   Maa YF, Hsu CC. Investigation on fouling mechanisms for recombinant human growth hormone sterile filtration. J Pharm Sci. 1998;87(7):808-812. doi:10.1021/js980114x

55.   Bódalo A, Gómez JL, Gómez E, Máximo MF, Montiel MC. Study of L-aminoacylase deactivation in an ultrafiltration membrane reactor. Enzyme Microb Technol. 2004;35(2-3):261-266. doi:10.1016/j.enzmictec.2004.05.003

56.   Akkas T, Citak C, Sirkecioglu A, Güner FS. Which is more effective for protein adsorption: surface roughness, surface wettability or swelling? Case study of polyurethane films prepared from castor oil and poly(ethylene glycol). Polym Int. 2013;62(8):1202-1209. doi:10.1002/pi.4408

57.   Rechendorff K, Hovgaard MB, Foss M, Zhdanov VP, Besenbacher F. Enhancement of Protein Adsorption Induced by Surface Roughness. Langmuir. 2006;22(26):10885-10888. doi:10.1021/la0621923

58.   Deligianni DD, Katsala N, Ladas S, Sotiropoulou D, Amedee J, Missirlis YF. Effect of surface roughness of the titanium alloy Ti-6Al-4V on human bone marrow cell response and

on protein adsorption. Biomaterials. 2001;22(11):1241-1251. doi:10.1016/s0142-9612(00)00274-x

59.   Paudel A, Raijada D, Rantanen J. Raman spectroscopy in pharmaceutical product design. Adv Drug Deliv Rev. 2015;89:3-20. doi:10.1016/j.addr.2015.04.003

60.   Jayes L, Hard AP, Séné C, Parker SF, Jayasooriya UA. Vibrational Spectroscopic Analysis of Silicones: A Fourier Transform-Raman and Inelastic Neutron Scattering Investigation. Anal Chem. 2003;75(4):742-746. doi:10.1021/ac026012f

61.   Saller V, Matilainen J, Rothkopf C, et al. Preservative loss from silicone tubing during filling processes. European Journal of Pharmaceutics and Biopharmaceutics. 2017;112:109-118. doi:10.1016/j.ejpb.2016.11.021

62.   Cockrell GM, Wolfe MS, Wolfe JL, Schöneich C. Photoinduced aggregation of a model antibody-drug conjugate. Mol Pharm. 2015;12(6):1784-1797. doi:10.1021/mp5006799

63.   Teske CA, von Lieres E, Schröder M, Ladiwala A, Cramer SM, Hubbuch JJ. Competitive Adsorption of Labeled and Native Protein in Confocal Laser Scanning Microscopy. Biotechnol Bioeng. 2006;95(1):58-66. doi:10.1002/bit

64.   Marfin YS, Aleksakhina EL, Merkushev DA, Rumyantsev E V., Tomilova IK. Interaction of BODIPY Dyes with the Blood Plasma Proteins. J Fluoresc. 2016;26(1):255-261. doi:10.1007/s10895-015-1707-x

65.   Dorh N, Zhu S, Dhungana KB, et al. BODIPY-Based Fluorescent Probes for Sensing Protein Surface-Hydrophobicity. Sci Rep. 2015;5:18337. doi:10.1038/srep18337

66.   Saller V, Hediger C, Matilainen J, et al. Influence of particle shedding from silicone tubing on antibody stability. Journal of Pharmacy and Pharmacology. 2018;70(5):675-685. doi:10.1111/jphp.12603

67.   Marsh RJ, Jones RAL, Sferrazza M. Adsorption and displacement of a globular protein on hydrophilic and hydrophobic surfaces. Colloids Surf B Biointerfaces. 2002;23(1):31-42. doi:10.1016/S0927-7765(01)00204-1

9. Supplementary data
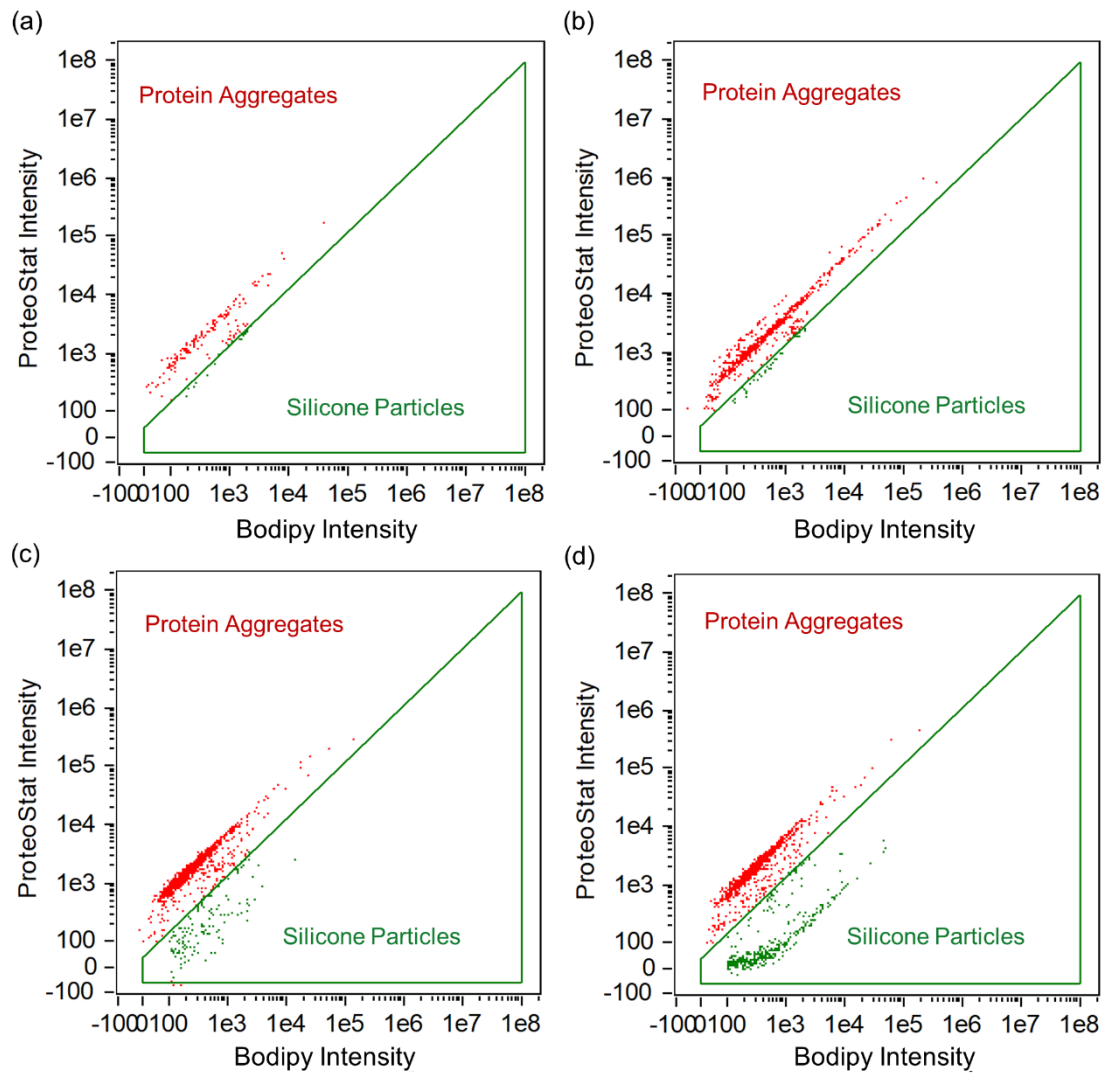
Figure S 1 IFC method validation by bivariate plots for buffer (a), shaken protein (b), unlabelded (c) and Bodipy labeled silicone beads (d) in presence of ProteoStat.
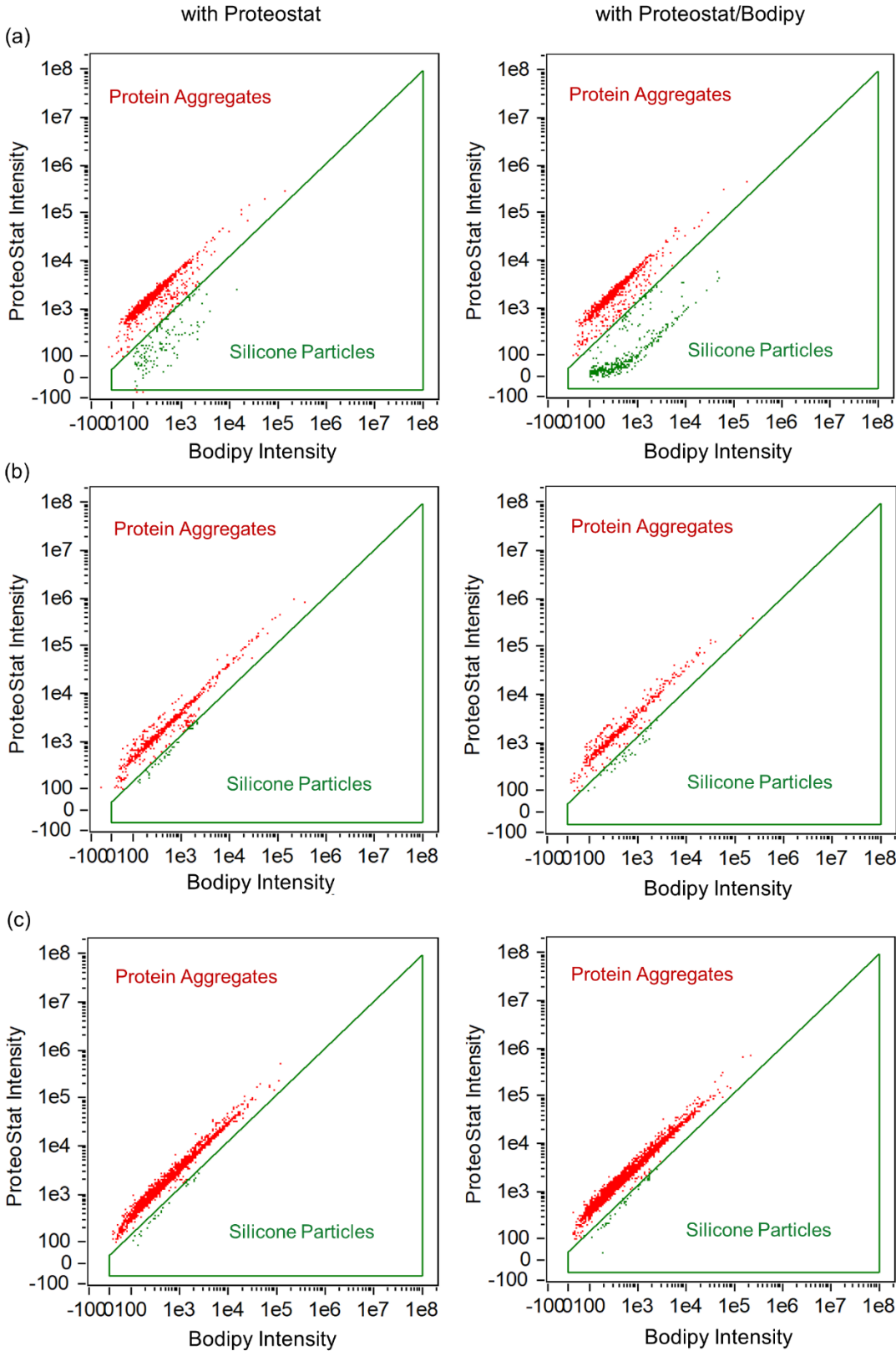
Figure S 2 Bivariate Plots for model silicone particles (a), 1 mg/mL mAb shear stressed (b) and 1 mg/mL mAb pumped through unlabeled Accusil tubing (c) stained with ProteoStat (left) and Bodipy (right).
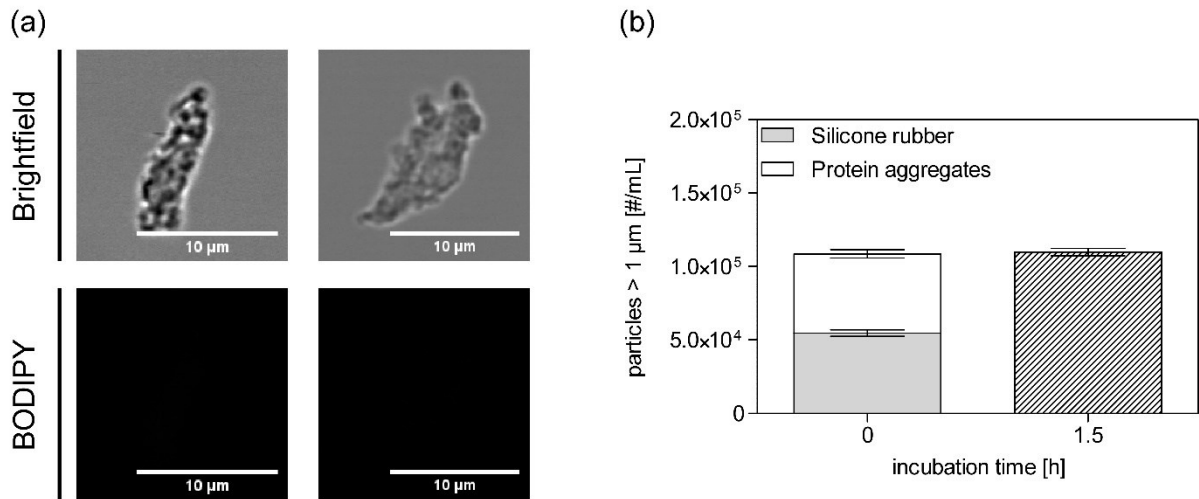
Figure S 3 Representative brightfield and fluorescence micrographs of protein particles incubated with shed silicone particles generated by 7 h pumped buffer through Bodipy stained Versilic tubing (a) and particle numbers for protein particles incubated with 1 mg/mL silicone microparticles for 1.5 h (b).

Chapter IV Proteins on the Rack: Mechanistic Studies on Protein Particle Formation During Peristaltic Pumping

[1]Department of Pharmacy, Pharmaceutical Technology and Biopharmaceutics, Ludwig-Maximilians-Universität München, Munich, Germany

Author contributions:

N.D. and W.F. conceived and designed the study. N.D. performed all experiments. N.D. analyzed data and wrote the original draft. W.F. revised and edited the manuscript. W.F. supervised the study.

Note from the authors:

The version included in this thesis is identical with the published article apart from minor changes.

1. Abstract

Peristaltic pumping can cause protein particle formation. The expected causes were unfolding by heat in the pump head, oxidative stress by cavitation generated during roller movement, interfacial adsorption to the tubing wall and mechanical stress by stretching of the tubing itself. The pump head reached 28 °C during experiments stayed well below the onset of the melting point of the proteins. Thus, heat may only be a relevant root cause for proteins containing domains with very low unfolding temperature. Analysis by terephthalic acid dosimetry and protein oxidation via RP-HPLC ruled out major induction of reactive hydroxyl radicals by pumping, indicating that cavitation does not play a significant role in particle generation. Addition of surfactants suppresses protein adsorption to the tubing wall and drastically reduced protein particle formation. This indicates that interfacial protein adsorption is a key element. Repeated stretching of tubing filled with protein solution led to the formation of protein particles, demonstrating that expansion and compression of the protein film on the tubing surface is the second key component for particle formation. Thus, protein particle generation during peristaltic pumping originates from the formation of a protein film on the tubing surface which gets stretched and compressed, leading to film fragments entering the bulk solution. This interplay of protein film formation and its rupture has been also observed at liquid/liquid or liquid/air interfaces.

Keywords: pumping, peristaltic pump, tubing, interface, protein(s), protein aggregation, particle formation, cavitation, stretching

Abbreviations: FNU - formazine nephelometric units; HGH - human growth hormone; HP-SEC - high-performance size-exclusion chromatography; HPW - highly purified water; H-TPA - 2-Hydroxyterephthalic acid; ID - inner diameter; IEP - isoelectric point; IL-11 - Interleukin-11; k_D - interaction parameter; mAb - model monoclonal antibody; MW - Molecular weight; PS20 - Polysorbate 20; qLD - quantitative laser diffraction; SDS - Sodium dodecyl sulfate; TFA - Trifluoroacetic acid; TFF - tangential flow filtration; T_m - melting point; TPA - Terephthalic acid

2. Introduction

Pumps are extensively used for transfer and filling in manufacturing of biopharmaceutics. Pumping of biopharmaceutics can lead to protein aggregation which impacts product quality.[1] Lobe pumping of albumin leads to aggregate formation due to the exposure to the pump environment and affects long term stability.[2] In a process like tangential flow filtration (TFF) where a protein formulation is circulated potentially for several hours, protein particle formation might be detrimental and pumping contributes substantially to the overall particle buildup during TFF.[3,4] Increased particle burden can lead to membrane fouling[5], increased viscosity[6], and reduced protein concentration and activity.[7,8] Reducing the particle burden during pumping is not only of interest from a technical point of view e.g. during TFF processes although particles formed may be removed by filtration. Particles generated upon pumping during final filling of drug product without an ultimate filtration reach the patient and may increase immunogenic risk.[9–11]

The aggregation mechanism depends on protein type and pump design. Exemplarily, stainless steel piston pumps lead to the formation of subvisible particles via disruption of protein film which adsorbs mainly by electrostatic interactions between protein and the stainless-steel surface.[12–14] Additionally, stainless-steel particles shed during pumping may serve as aggregation nuclei.[15–17] Furthermore, the higher number of particles formed by piston pumps may be triggered by the repeated exposure of protein to interfacial shear in the recirculation zone inside the cylinder.[13,18]

In contrast to piston pumps, studies on the aggregation mechanism in peristaltic pumps are limited. The particle formation propensity upon peristaltic pumping depends on formulation conditions and tubing type.[19,20] As peristaltic pumping is a complex combination of different mechanical stresses which potentially overlap with chemical stress the following factors are seen as potential drivers: temperature, exposure to interfaces, shear, and contaminants as nucleation sites.[21] Silicone tubing sheds particles into the product during pumping due to abrasion of the tubing piece in the pump head.[22] We could find mixed particles of protein containing nanometer sized silicone contaminants, but no evidence for the induction of protein aggregation by shed silicone particles.[23] Additionally, spiking silicone particles did not induce aggregation in two different mAb formulations up to 6 months storage at 2–8, 25, and 40°C.[24] In contrast, silicone oil droplets have been shown to trigger protein aggregation.[25,26]

This study aimed not only to close this knowledge gap and elucidate the mechanism underlying protein particle formation during peristaltic pumping but also to give advice for the reduction of pump related protein particles. Therefore, we used a combination of different analytical methods to isolate each potential contributor from the complex pumping mechanism. Protein

particle concentration, dependent on formulation and operation parameters, was analyzed using turbidity, flow imaging and quantitative laser diffraction (qLD) with different model proteins. To get deeper insight into the key elements that drive the protein aggregation, results from particle analysis were linked to the different physical and chemical parameters. Oxidative stress caused by cavitation was examined using Terephthalic Acid Dosimetry and analysis of protein oxidation. The temperature of the pump head was monitored by thermal imaging and compared to the onset of protein thermal unfolding. Finally, protein adsorption was quantified and interfacial shear was simulated by defined repeated stretching of filled tubing.

3. Materials and Methods

3.1. Materials

33.4 mg/ml monoclonal IgG1 antibody (148 kDa) in 20 mM histidine buffer pH 5.4 served as model monoclonal antibody (mAb). Interleukin-11 (IL-11, 15 mg/ml in 10 mM sodium phosphate + 300 mM glycine pH 7.0) and human growth hormone (HGH, 10 mg/ml in 10 mM sodium phosphate pH 7.0) served as model cytokines. Buffer ingredients were dissolved in highly purified water (HPW) from an Arium pro DI Ultrapure Water System (Sartorius Stedim Biotech GmbH, Goettingen, Germany) and pH was adjusted either with hydrochloric acid (VWR, Darmstadt, Germany) or sodium hydroxide (Bernd Kraft GmbH, Duisburg, Germany). Buffers were filtered through 0.2 µm cellulose acetate filters (47 mm ø, Sartorius Stedim Biotech GmbH). Protein and mAb formulations were filtered through 0.2 µm polyethersulfone membrane syringe filters (VWR) prior to experiments. Chemicals were obtained as follows: Histidine and Potassium dihydrogen phosphate from Applichem (Darmstadt, Germany); Glycine, Methionine, 2-Hydroxyterephthalic acid (H-TPA), Sodium dodecyl sulfate (SDS) and Terephthalic acid (TPA) from Sigma Aldrich (Steinheim Germany); Acetonitrile from Carl Roth (Karlsruhe, Germany); Sodium chloride from Bernd Kraft; Trifluoroacetic acid (TFA) from VWR; Hydrogen peroxide (H_2O_2), Polysorbate 20 (PS 20) and Sodium dihydrogen phosphate from Merck (Darmstadt, Germany); Ammonium iron(II) sulfate ($Fe(II)SO_4(NH_4)_2$) from Grüssing (Filsum, Germany).

3.2. Setup of Pumping Studies

Tubing sets made from Pt-cured silicone (Accusil Watson-Marlow, Falmouth, United Kingdom) with an inner diameter of 1.6 mm and a wall thickness of 1.6 mm were rinsed with 1 L HPW at 80 °C and steam sterilized (121 °C, 15 min, 2 bar). Tubing sets consisted of two 20 cm long pieces for the area in the pump head connected to 35 cm long tubing pieces via polypropylene Y-connectors (Kartell, VWR). The tubing set was fixed in a Flexicon PD12 peristaltic pump (Watson-Marlow Flexicon, Ringsted, Denmark) operated with a MC 12 control unit and flushed with 5 L HPW to remove external contaminants at 180 rpm. After priming to remove air in the tubing set, 6 mL of formulation buffer followed by 6 mL of 1 mg/ml protein solution was circulated for 20 passages through the pump head. Experiments were conducted under a laminar air flow cabinet with the exception of pumping at 8 °C where the pump assembly was moved into a climatic cabinet (Tritec, Hannover, Germany) for precooling overnight and experimental work. Samples were immediately analyzed after production.

3.3. Turbidity

Samples of 1.8 mL were examined for turbidity according to Ph. Eur. 2.2.1 using a Nephla turbidimeter (Dr. Lange, Duesseldorf, Germany). Data is presented in formazine nephelometric units (FNU).

3.4. Subvisible Particle Analysis

To estimate total particle amount, 5 mL sample was transferred in a batch cell and was analyzed by the Aggregates Sizer with the WingSALD bio software version 3.2.2 (Shimadzu Corporation, Kyoto, Japan). Calculations were based on a material specific refractive index of 1.46, an imaginary index of 0.1[27] and a protein particle density of 1.32 g/cm^3 [28]. The cut-off level of noise was set to 500.

Particles in the micrometer size range were analysed with a FlowCAM® 8100 (Fluid Imaging Technologies, Inc., Scarborough, ME, USA) equipped with a 10x magnification cell (81 µm × 700 µm). A total sample volume of 150 µl was analysed at a flow rate of 0.15 ml/min. Images were collected with an auto image frame rate of 28 frames/s and a sampling time of 60 s leading to an efficiency value higher than 70%. Particle identification was based on the following settings: 3 µm distance to the nearest neighbour, particle segmentation thresholds of 13 and 10 for the dark and light pixels, respectively. Particle size is displayed as the equivalent spherical diameter using VisualSpreadsheet® 4.7.6 software.

3.5. In silico comparison of IL-11 and HGH

For cytokine characterization respective PDB entries for IL11 (6O4O) and HGH (3HHR) were used, and missing residues were inserted with Modeller version 9.23. The PDB files were processed using the H++ webserver to adjust the protonation state of each titratable amino acid at pH 7.0 and calculate the IEP and the total charge of the protein. Molecular weight (MW) was determined from the FASTA sequence using the ExPASy proteomics Web server.

3.6. Fluorimetric Analysis of Thermal Protein Unfolding using nanoDSF

Standard nanoDSF capillaries were filled with 1 mg/ml protein solution and sealed using sealing paste as recommended by the manufacturer. The capillaries were placed in a Prometheus NT.48 (NanoTemper Technologies, Munich, Germany). The excitation power of the device was adjusted that the samples have fluorescence intensity at 330 and 350 nm between 1,000 and 10,000 counts after excitation at 280 nm (± 10 nm). A temperature ramp

of 1 °C/min was applied from 20 to 100 °C. The fluorescence intensity ratio (F350/F330) was plotted versus the temperature to derive the thermal unfolding transitions from the maximum of the first derivative of each measurement using the ThermControl software V2.1 (NanoTemper Technologies, Munich, Germany). Protein aggregation during heating was monitored using the backscattering detector of the device.

3.7. Dynamic Light Scattering

MAb samples with concentrations between 1 and 8 mg/ml were centrifuged for 10 min at 10,000 g. 25 µl of protein solution were filled in a 384 microwell plate (Corning, New York, United States) and centrifuged for 2 min at 2,000 rpm using a Heraeus Megafuge 40 centrifuge equipped with an M-20 well plate rotor (Thermo Fisher Scientific). Cytokine samples needed to be filtered through 0.02 µm Anotop 10 PVDF filters (Whatman, GE Healthcare, Buckinghamshire, United Kingdom) instead of centrifugation to allow reliable detection of the diffusion coefficient in 1536 well plates (Aurora Microplates, Scottsdale, Arizona, United States). Wells were sealed with silicone oil to avoid evaporation. After centrifugation the samples were measured at 25 °C with 20 acquisitions of 5 s using a DynaPro plate reader III (Wyatt Technology, Santa Babara,CA). The interaction parameter k_D was determined from the concentration dependence of the mutual diffusion coefficient D.

3.8. Thermal Imaging

To avoid a reflection induced impact on the infra-red signal the pump was covered in package tape. The pump was operated at 180 rpm for transferring HPW through 1.6 mm ID Accusil tubing for 6 h. To obtain the temperature profile thermal images were recorded with a Testo 880-1 thermal imaging camera (Titisee-Neustadt, Germany). Images were processed with an emissivity of 0.7 with the IRSoft Software (Testo). Temperature was additionally checked with an Infra Point Tastotherm MP 2000 (PEWA, Schwerte, Germany).

3.9. Terephthalic Acid Dosimetry

A 10 mM TPA solution in 12 mM phosphate buffer pH 7.4 was prepared as described in Ebrahiminia et al. [29]. 6 mL TPA solution was circulated 1,000 times at 30 rpm, 180 rpm and 600 rpm. The fluorescence of the pumped solutions at λ_{ex}= 315 nm, λ_{em}= 425 nm was immediately measured (Cary Eclipse 50, Agilent, Santa Clara, CA). To quantify free OH radicals originating from cavitation a calibration curve was recorded with H-TPA. Assay

integrity was tested using Fenton's reaction as positive control. Therefore a 10 mM TPA solution containing 0.6 mM $Fe(II)SO_4(NH_4)_2$ and 0.4% H_2O_2 was incubated for 60 min at room temperature.

3.10. Detection of Oxidized Protein Species

HGH and IL-11 oxidized species were obtained by incubating 10 mg/ml protein with 0% to 0.2% H_2O_2 for 24 h. The oxidation process was stopped by mixing the sample 1:1 (v/v) with 200 mM methionine in HPW. Pumped and oxidized HGH and IL-11 samples were analyzed using an ACQUITY UPLC I-Class system (Waters, Milford, MA, US) equipped with an Acquity UPLC Protein BEH C4 column (300Å, 1.7 μm, 2.1 mm x 50 mm, Waters) at 214 nm. The elution was carried out with a gradient solvent system with 0.4 mL/min flow rate at 40 °C. The mobile phase consisted of HPW + 0.1% TFA (A) and acetonitrile + 0.1% TFA (B). Starting from 80% A, the gradient went linearly from 80% to 20% A for 1 – 18 min. The gradient went to 100% B and subsequently back to starting conditions from 18 – 20 min.

3.11. Quantification of Protein Adsorption

For quantification of adsorbed protein, a 4 cm tubing piece was filled with 1 mL of 2 mg/mL protein formulation and incubated for 24 h at room temperature. After incubation, the tubing piece was washed three times with formulation buffer and filled with 1 mL desorption buffer (10 mM phosphate buffer pH 7.2 with 145 mM NaCl and 0.05 % SDS). After 24 h incubation, samples were analyzed with an Agilent 1100 device (Agilent Technologies, Boeblingen, Germany) equipped with a G1314A UV detector. Injection volume was increased to 400 μl by insertion of a 500 μl seat capillary and flow rate was set to 0.7 mL/min with the desorption medium as mobile phase. The desorbed protein amount was quantified via high-performance size-exclusion chromatography (HP-SEC) using a 7.8 x 300 mm TSK Gel G3000 SWXL column (Tosoh Bioscience, Stuttgart, Germany) at 210 nm. The total desorbed protein amount was calculated based on a protein specific 8-point calibration curve between 0.0001 and 0.01 mg/ml. All chromatograms were integrated manually using ChemStation software (Agilent Technologies).

3.12. Stretching Studies

To simulate the disruption of the protein film by stretching 130 mm silicone tubing pieces (ID 6.0 mm) sealed with silicone stoppers were filled with approximately 2.5 mL 1 mg/mL mAb 20 mM histidine pH 5.4 solution. The tubing piece was fixed with clamps leaving 120 mm tubing in the gap for stretching. Stretching by 10 mm was performed for 2,000 times at 4 mm/s by a TA.XTplus Texture Analyser (Stable Micro Systems, Surrey, UK). Protein solution was removed and analyzed for particles.

3.13. Statistical Significance

A t-test was carried out with * for $p \leq 0.05$, ** for $p \leq 0.01$ and *** for $p \leq 0.001$.

4. Results

4.1. Characterization of biophysical stability of model proteins

At first, we studied the particle formation propensity of one monoclonal antibody and two cytokines during peristaltic pumping. The mAb and IL-11 are positively charged (calculated total charge IL-11 at pH 7.0: +7) in their respective formulation, while HGH was negatively charged (calculated total charge at pH 7.0: -4).

The thermal stability of the proteins in their respective bulk solutions was analyzed to determine whether the heat exposure in the pump head could trigger unfolding and particle formation. Both cytokines followed a two-state thermal unfolding mechanism while the mAb showed three-state unfolding corresponding to its F_{ab} and F_c domains (Figure 1). Only IL-11 formed larger aggregates in the unfolded state as scattering started at its melting point (T_m).
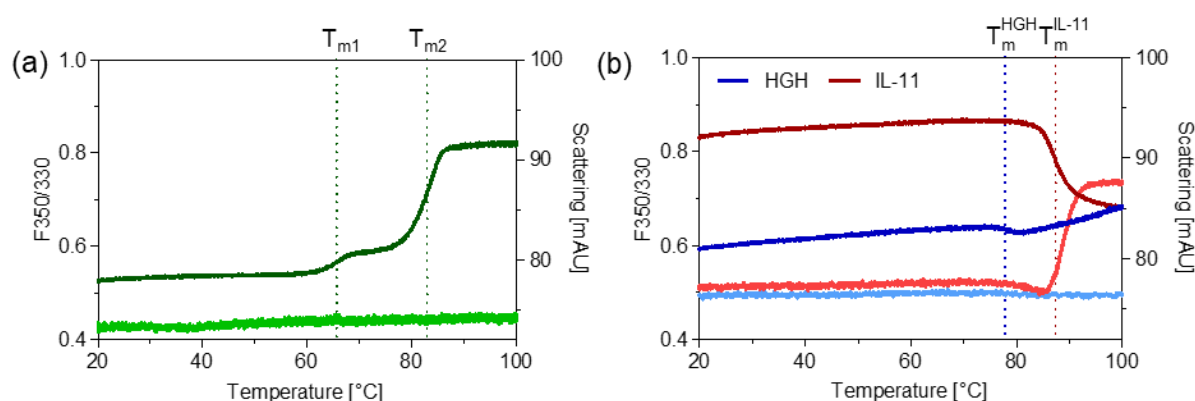
Figure 1 Thermal unfolding and scattering intensity curves of 1 mg/mL mAb (a) and HGH and IL-11 (b) in their respective bulk formulation. Corresponding light colors represent scattering intensity.

All three proteins were rather stable. The mAb showed the lowest onset temperature of unfolding at approximately 60 °C followed by HGH with 76 °C and IL-11 with 82 °C (Table 1).

Table 1 Characterization and thermal unfolding data from nanoDSF of model proteins in bulk formulation.

	Isoelectric point	MW [kDa]	Thermal unfolding [°C]		
			T_{onset}	T_m	$T_{onset-scattering}$
mAb	8.0 – 8.3	156	60.4 ± 0.2	T_{m1}: 65.6 ± 0.1	-
				T_{m2}: 82.9 ± 0.1	
HGH	5.4	22	75.8 ± 0.3	77.8 ± 0.1	-
IL-11	11.5	18	82.4 ± 0.1	87.4 ± 0.1	86.0 ± 0.1

The k_D value was used as a simple estimator for colloidal stability. The addition of PS20 had no substantial effect on the k_D value. Only in presence of 140 mM NaCl did k_D become negative (Table 2; Figure S1). Both cytokines exhibited negative k_D values. HGH had a lower k_D value than IL-11.

Table 2 k_D of mAb, HGH and IL-11 in different formulations.

Protein	Formulation	k_D [mL/g]		
mAb	20 mM histidine pH 5.4	13.87	±	0.33
	20 mM histidine + 140 mM NaCl pH 5.4	- 6.28	±	0.48
	20 mM histidine + 0.001% PS 20 pH 5.4	16.07	±	0.58
	20 mM histidine + 0.01% PS 20 pH 5.4	15.85	±	0.72
	20 mM histidine + 0.1% PS 20 pH 5.4	14.81	±	0.97
HGH	10 mM Naphosphate pH 7.0	- 11.86	±	1.72
IL-11	10 mM Naphosphate + 300 mM glycine pH 7.0	- 3.77	±	1.22

4.2. Particle formation during pumping

1 mg/ml mAb in 20 mM histidine pH 5.4 circulated exactly 20 times through the pump head and particle formation was analyzed via turbidity, flow imaging and qLD. Freshly filtered samples and pumped buffer did not show signals above the noise level in qLD. In all cases pumping buffer, as well as protein, led to the formation of particles (Figure 2). Overall, the turbidity values were in line with the particle numbers. Particle levels in the buffer were comparable for the different process parameters, apart from pumping at the highest speed of 600 rpm, which led to higher particle numbers. Pumping protein solutions resulted in markedly higher particle concentrations as compared to pumping buffer. The particle levels decreased with increasing rotation speed from 30 rpm (flow rate: 18 ml/min) to 180 rpm (flow rate: 109 ml/min). Increasing the rotation speed further to 600 rpm (flow rate: 332 ml/min) did not impact protein particle concentration. There was no difference between operating the instrument at 25 °C or completely refrigerated at 8 °C. When switching from continuous to filling mode (60 fills à 2 ml), we observed the same increased particle levels in the micrometer size range, irrespective of interval duration.
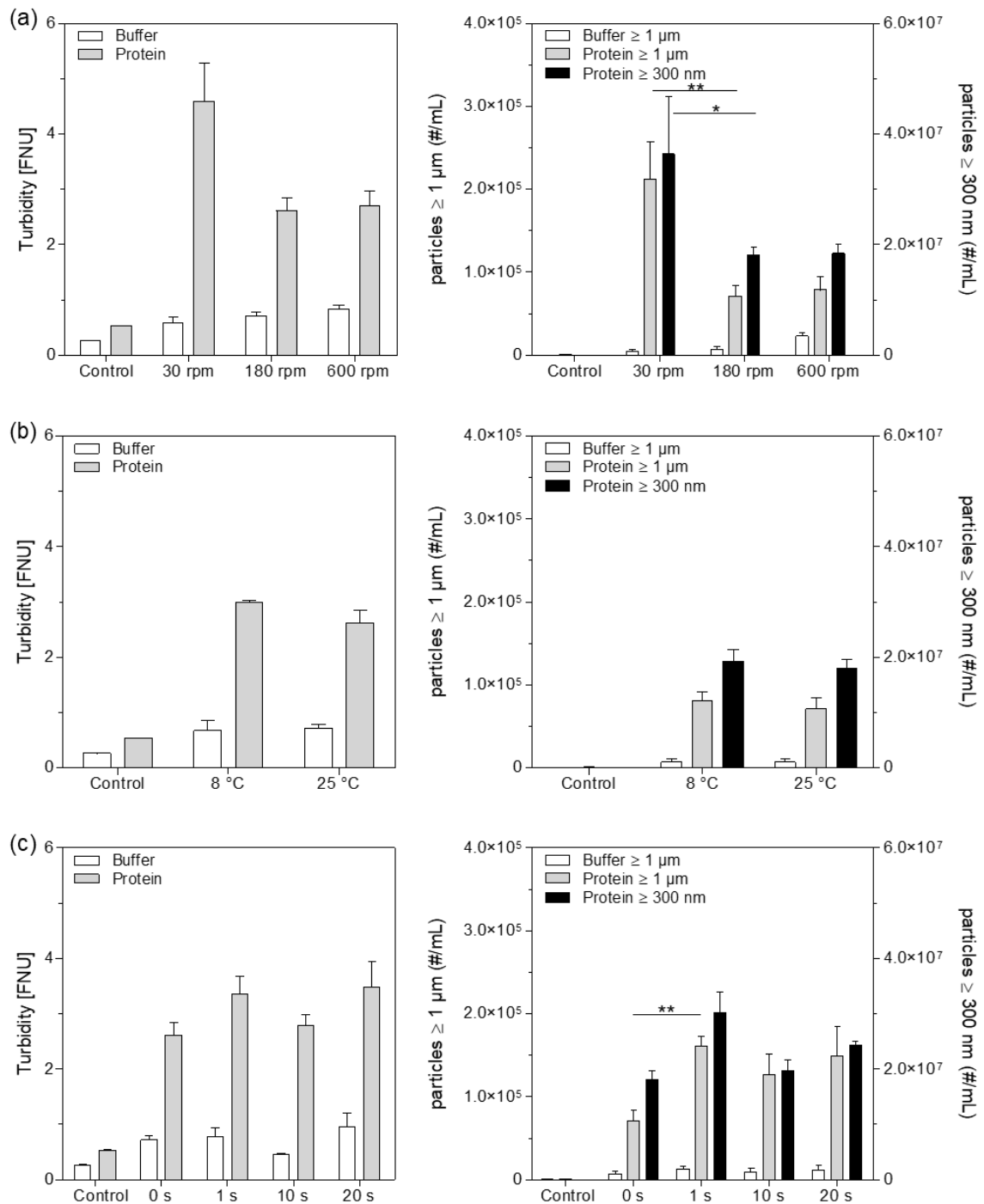
Figure 2 Turbidity (left) and particles in the micrometer and nanometer size range (right) after peristaltic pumping of 1 mg/mL mAb 20 mM histidine pH 5.4 at different rotation speeds (a), temperatures at 180 rpm (b) and filling intervals at 180 rpm (c). Control refers to unpumped buffer and protein formulation.

To identify interfacial triggers for protein particle formation, the formulation was varied (Figure 3). Addition of salt led to comparable total protein particle levels, but a higher number of micrometer sized particles. Size distribution data from FlowCam measurements revealed differences in the ≥ 25 µm particle concentration. Particles numbers for ≥ 25 µm increased

from 292 ± 42 particles per mL, without NaCl, to 832 ± 275. The addition of PS20, irrespective of the tested concentration, completely suppressed protein particle formation. Increased particle concentrations in buffer or mAb were detected compared to unpumped controls, despite the addition of PS20. A differentiation via particle image analysis is hardly possible (Figure S2); however, particles most likely originate from shed silicone from the inner tubing surface.

Both cytokine formulations showed a substantially higher particle number after pumping compared to the mAb formulation. While concentrations of nanometer sized protein particles were comparable in cytokine samples, protein particles ≥ 1 µm were significantly increased for IL-11. About 2,400 particles ≥ 25 µm per mL were detected both for HGH and IL-11. Already the particle concentration of the freshly filtered, unpumped HGH was slightly elevated, indicating higher sensitivity to interfacial stress.[30]
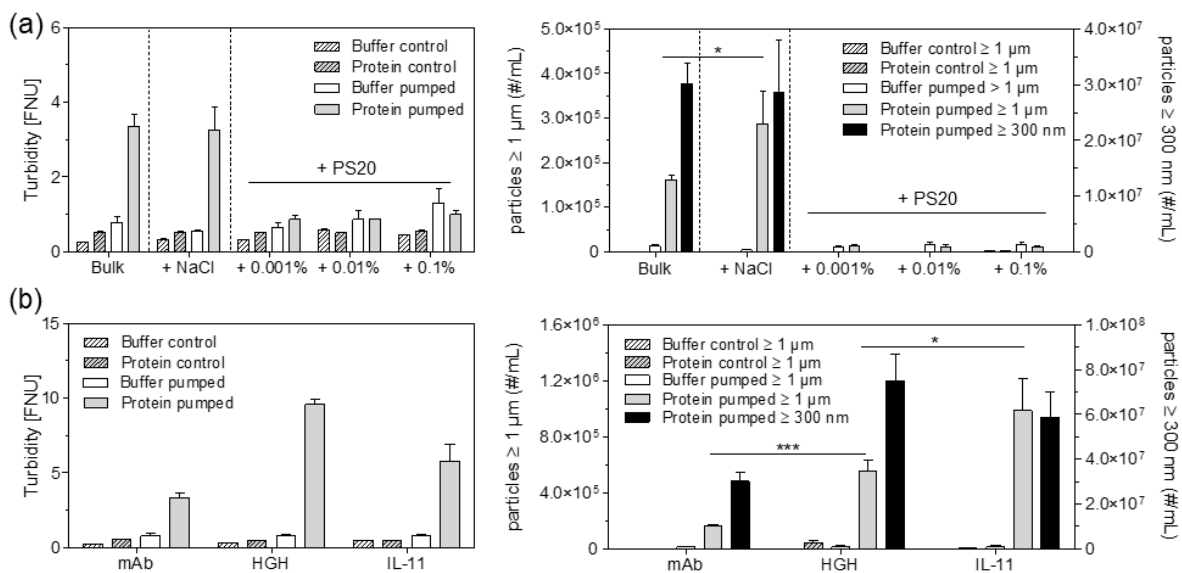
Figure 3 Turbidity (left) and particle formation in the micrometer and nanometer size range (right) after peristaltic pumping of 1 mg/mL mAb 20 mM histidine pH 5.4 with addition of 140 mM NaCl or 0.001, 0.01 or 0.1% PS20 (a). Comparison of mAb, HGH and IL-11 in their respective bulk formulation after peristaltic pumping (b). Pumping conditions are filling mode with 2 mL fill volume and 1 s filling interval at 180 rpm. Control refers to unpumped buffer and protein formulation.

4.3. Heat

To study the heat generation during the roller movement, HPW was pumped for 6 h at 180 rpm. Pump head and housing temperature increased over 3 h of pumping. A local hotspot was revealed at the driving unit which reached 36.8 ± 0.3°C while the temperature on top of the pump head increased only to 28.0 ± 0.4 °C (Figure 4; see complete temperature profile: Figure S3).
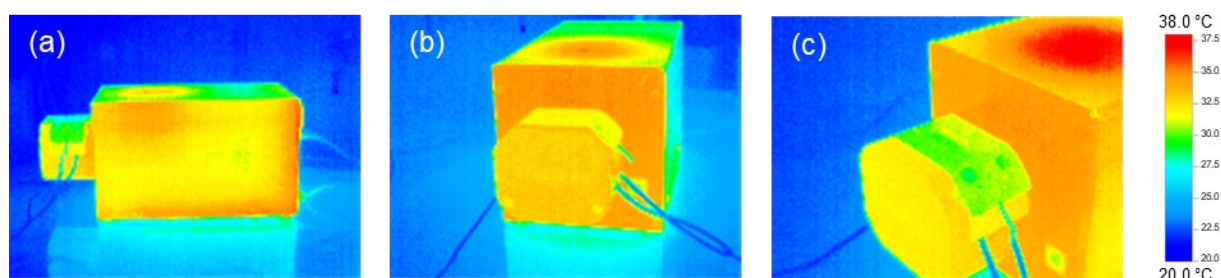
Figure 4 Temperature of the lateral (a) and front view of the pump (b) and the pump head (c) after 6 h pumping at 180 rpm.

4.4. Cavitation

By the conversion of TPA to fluorescent H-TPA it is possible to monitor hydroxyl radical formation by cavitation. Our linear calibration curve covered the range from 1.8 to 0.022 µM H-TPA. The assay reported no signals above the limit of detection for any of the pumped samples. Fenton´s reaction yielded in 7.0 ± 1.0 µM H-TPA, proving assay functionality.

Forced oxidation of HGH and IL-11 with H_2O_2 caused the formation of oxidized species in a H_2O_2 concentration dependent manner. While only one peak forms for HGH, IL-11 formed three subspecies as first Met^{58} is oxidized, followed with subsequent oxidation of Met^{122}.[31] Pumped HGH and IL-11 samples did not show any oxidized species after pumping (Figure 5). Thus, we did not find evidence for cavitation in our pump studies.
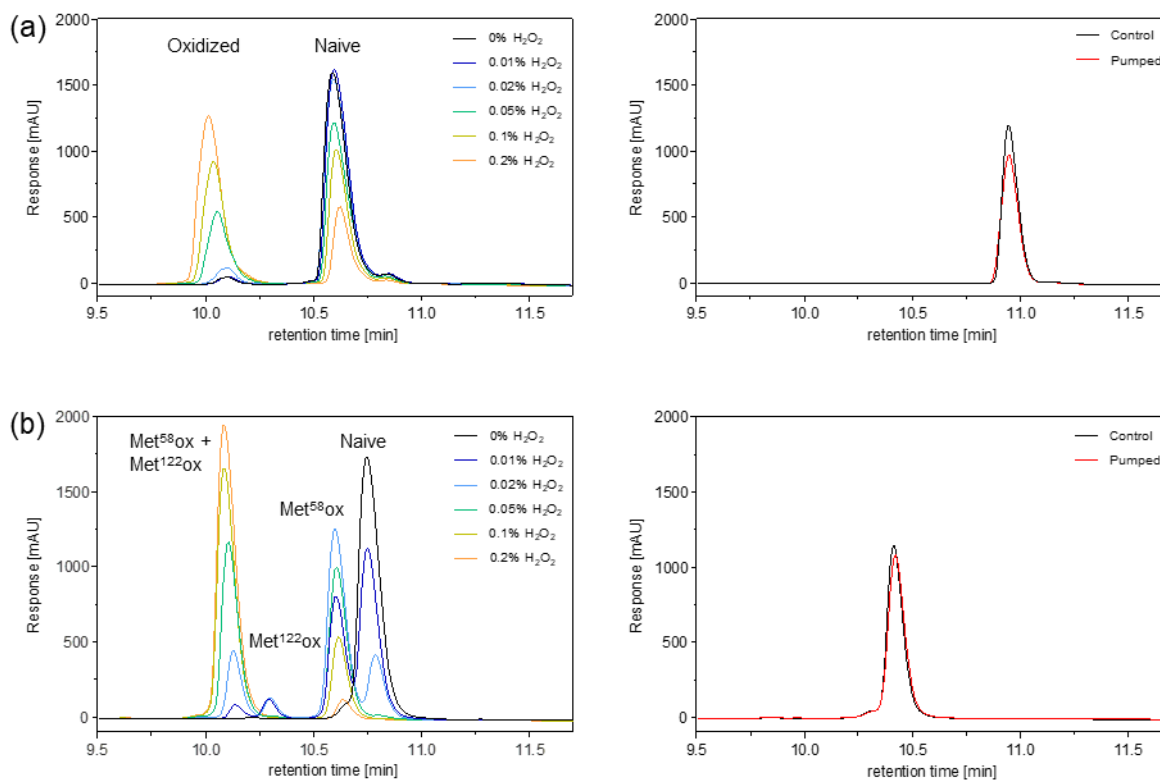
Figure 5 Chromatograms of HGH (a) and IL-11 (b) incubated with H_2O_2 (left) and pumped samples (right).

4.5. Interfacial protein adsorption

Due to their amphiphilic character, proteins adsorb to interfaces. We quantified the amount of protein irreversibly adsorbed to the the tubing surface (Figure 6) and found increasing ionic strength led to an increase of mAb adsorbed, from 4.0 ± 0.1 mg/m^2 at low and 5.3 ± 0.2 mg/m^2 at high ionic strength. Already, the lowest PS20 concentration of 0.001% [w/v] reduced protein adsorption substantially to 0.8 ± 0.4 mg/m^2. Protein adsorption was even more suppressed at 0.1% PS20 [w/v]. HGH adsorbed to a similar extent and IL-11 slightly less. Thus, all proteins form a film at the tubing surface.
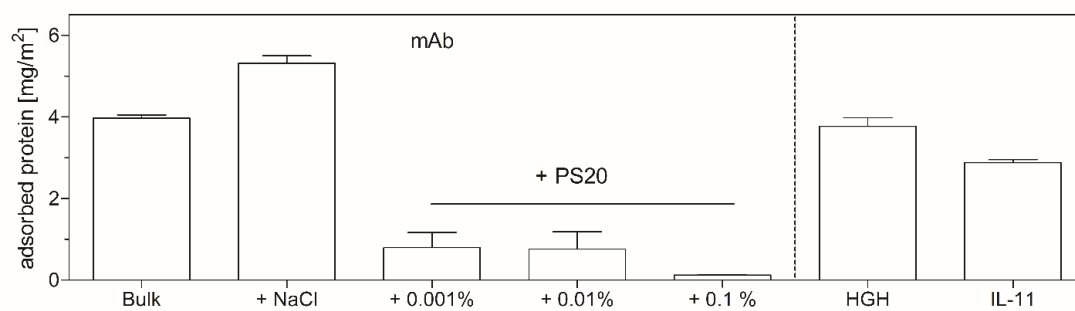
Figure 6 Amount of protein adsorbed to the tubing surface.

4.6. Repeated elongation and relaxation of tubing filled with protein solution

Additionally, we filled the tubing with mAb solution and exposed the tubing to 2,000 elongation and relaxations cycles (8.3% strain), stressing the adsorbed protein film (Figure 7). Unstretched tubing containing protein solution did not exhibit protein particle formation compared to the freshly filtrated protein formulation. Upon stretching the tubing, the particle level ≥ 1 µm per mL increased substantially to 24,000 ± 7,800. Particle concentration ≥ 10 µm and ≥ 25 µm per mL was increased to 285 ± 31 and 27 ± 12 compared to the unstretched tubing 54 ± 43 and 17 ± 12, respectively.
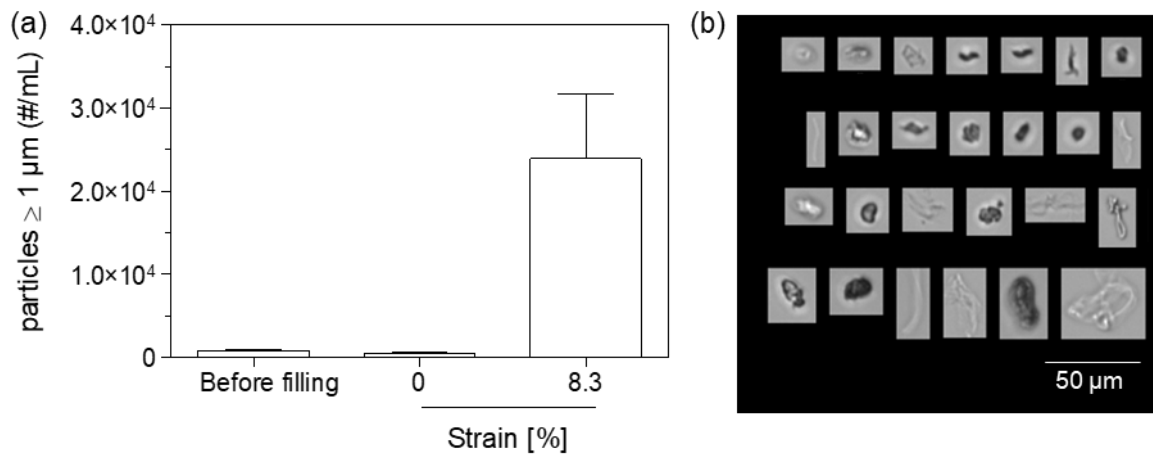
Figure 7 Subvisible particle formation in tubing filled with 1 mg/mL mAb 20 mM histidine pH 5.4 upon 2,000 elongation and relaxation cycles at 8.3% strain (a) and exemplary images of particles formed during stretching (b).

5. Discussion

Protein aggregation is a major challenge in processing and formulation of biopharmaceutics. During their production and purification, proteins are exposed to a variety of different mechanical and interfacial stresses. Pumps which are widely used for transferring and dosing the final product in manufacturing have turned out to contribute to the total particle burden. Aggregates formed during drug product filling into the final container without an ultimate filter downstream of the pump are critical for quality and safety. Until now, studies on the particle formation in peristaltic pumps have been limited and the root cause for protein particle formation has not been clearly identified.

In our current study we considered different peristaltic pumping parameters to identify relevant factors. We also investigated the effect of formulation, protein size and net charge on the particle formation propensity evaluating two cytokines, HGH and IL-11, and one mAb in different formulations. Independent of the process parameters, pumping resulted in an increase of the subvisible protein particle levels. Similar to previous studies, we did not find the formation of soluble aggregates in SEC for the mAb formulation, even after extensive pumping in preliminary tests.[12,13] Despite our findings, less stable proteins could potentially form soluble aggregates. In contrast to Her et al.[19], we found an increase in particle formation when prolonging the contact time between the protein and tubing surface at low rotation speed. This might be a hint towards an interface-mediated aggregation mechanism or increased exposure to the warm pump head. During rotation, the rollers generate friction resulting in heat, which, if the melting point is reached, could lead to protein unfolding followed by aggregation. To evaluate heat generated during roller movement as cause for protein aggregation, a heat temperature profile was recorded during pump operation. The pump head surface reached 28.0 ± 0.4 °C indicating a temperature of approximately 30 °C in the pump head. This is well below the melting temperature of the tested proteins, indicating that heat denaturation is unlikely in our models. For proteins which are more susceptible to temperature, the heat in the pump head could trigger aggregation. Additionally, considering that at 180 rpm (flow rate: 109 ml/min) the contact time of a protein to the pump head is less than a second and that cooling the device did not result in decreased protein aggregation, heat is not a key factor for protein aggregation in peristaltic pumping.

Interestingly, increasing the pump speed to 600 rpm, which might trigger shear associated aggregation or cavitation, only resulted in an increase in shed tubing particles in buffer due to material wear and fatigue. Protein particle levels, however, were comparable to material pumped at 180 rpm. Cavitation occurs in pumps if the static pressure of the liquid gets below the liquid's vapor pressure. This leads to the formation of small vapor bubbles, which explode

and release hydroxyl radicals, which could oxidize proteins. Duerkop et al.[32] found that high shear environment during cavitation experiments did not induce protein particle formation nor structural perturbation. The exposure to interfacial stress at the liquid/vapor bubble interface was seen as a driving force for aggregation and monomer loss. While Duerkop et al. did not identify hydroxyl radicals as the cause of aggregation, Randolph et al. showed that cavitation originating from vial dropping leads to HGH oxidation by hydroxyl radicals.[33] The met oxidized HGH form is less stable and more prone for aggregation.[34] IL-11 served as a second candidate for the detection of oxidation caused by pumping, as it gets quickly oxidized in presence of hydroxyl radicals.[31,35] The formation of hydroxyl radicals was additionally probed based on the conversion of non - fluorescent TPA to fluorescent H-TPA.[36] Though the potential for cavitation is positively correlated to pump speed, particle counts remained stable. Confirming theoretical calculations[18], oxidized species that are the result of cavitation could not be detected in any pumped samples. Therefore, despite the known propensity of oxidized species to form particles, the particles detected in this study were not produced by cavitation.

Thus, the particle formation propensity cannot be explained by chemical factors. The link between increased contact time and increased protein particle formation points towards solid-liquid interfacial interactions. Interfacial adsorption is a complex process triggered by a variety of factors including electrostatic and hydrophobic interactions, protein – protein interactions and conformational stability.[37,38] In surfactant-free formulations protein particle formation was observed irrespective of the protein type. A mAb formulation with reduced colloidal stability due to charge shielding through the addition of 140 mM NaCl[39–41], showed a similar total particle concentration with only a slightly higher number of particles ≥ 25 µm. Specifically, charge shielding may foster the build-up of larger aggregates due to attractive forces.[42] Although k_D values were comparable to the bulk formulation, adding PS20 to the formulation completely supressed protein particle formation. This latter result is in perfect agreement with the studies from Her et al.[19,20] In this study, we used k_D as a simplistic approach for colloidal stability estimation. Although k_D is used as a descriptor for interparticle interaction in protein solutions[43], this parameter does not provide a full picture of colloidal stability. Currently, computational and experimental approaches aim for a more accurate determination of colloidal stability.[44,45] Polysorbate suppresses protein adsorption by preferential location at the interface without forming complexes with the protein itself.[46,47] We could see similar effectiveness in protein adsorption reduction for PS80 and Poloxamer 188 (Figure S4); the two surfactants were already shown to be effective in protein particle reduction in pumping studies.[20] These findings verified that interfacial adsorption plays a key role in protein particle formation.

Protein films remain stable under flow conditions without protein particle formation.[12,48] We therefore elongated and relaxed tubing filled with protein solution outside the pump-head

repeatedly. This simple stress resulted in substantial protein particle formation which indicates that the rupture of the adsorbed protein film is a main factor in the particle formation upon peristaltic pumping. Based on the evidence in this study; protein aggregates originate from a protein film formed on the tubing surface and its subsequent rupture during roller movement; followed by film fragments entering the bulk solution. This mechanism is similar to the aggregation phenomena observed at the liquid-air[49,50], liquid-silicone oil interface[51] and in stainless steel piston pumps[12,14]. During pumping, the surface is continuously renewed due to the rolling mechanisms and repeated film formation will be induced. Extrapolating the adsorption speed of mAb to siliconized syringes[52], protein film formation takes place in less than a second at the chosen experimental conditions. The increased protein particle formation at low rotation speed might therefore originate from a 'self-healing' of the protein film during rotation due to the longer contact time similar to observations in piston pumps.[14] The protein adsorption rate can be influenced by electrostatic attraction and non – electrostatic interactions.[53] But despite repulsive electrostatic interactions between the negatively charged HGH and the negatively charged tubing[54], particle formation was comparable to the positively charged IL-11. Additionally, particle levels for the cytokines were way higher than those for the mAb, although adsorbed amounts of HGH and mAb were comparable. This might result from the higher diffusion speed of the smaller molecules.

6. Conclusion

Protein particle formation during peristaltic pumping was influenced by process parameters, formulation and protein type. At the lowest rotation speed, the protein particle levels were slightly higher. We therefore recommend the use of a rotation speed that balances between short contact time between tubing surface and protein, on the one hand, and maintaining tubing integrity on the other hand. Colloidal stability based on k_D thereby negligibly influenced protein particle concentration.

Heat generated during operation was way below the melting point of all tested proteins. There were also no signs for cavitation or protein oxidation. By screening for interfacial protein adsorption, we found that the reduced aggregation in surfactant-containing samples was linked to the suppression of protein adsorption to the tubing. In combination with defined stretching and relaxation of the tubing, protein adsorption led to particle formation. Protein particle formation during peristaltic pumping is therefore triggered by protein film formation on the tubing surface and its consecutive tearing during the roller movement, resulting in protein film fragments entering the bulk solution.

Thus, protein particle formation can be suppressed by the addition of surfactants, but techniques for surfactant-free samples are limited. To reduce particle burden upon pumping, formulation development should focus on the replacement of the protein at the interface. Still more work is needed to evaluate whether the tubing material itself, based on surface properties and material characteristics, can be optimized.

7. Acknowledgements

8. References

1.   USP <788> Particulate matter in injections. In: United States Pharmacopeia. United States Pharmacopeial Convention; 2014.

2.   Gomme PT, Hunt BM, Tatford OC, Johnston A, Bertolini J. Effect of lobe pumping on human albumin: investigating the underlying mechanisms of aggregate formation. Biotechnol Appl Biochem. 2006;43(2):103-111. doi:10.1042/ba20050147

3.   Callahan DJ, Stanley B, Li Y. Control of Protein Particle Formation During Ultrafiltration/Diafiltration Through Interfacial Protection. J Pharm Sci. 2014;103(3):862-869. doi:10.1002/jps.23861

4.   Meireles M, Aimar P, Sanchez V. Albumin Denaturation During Ultrafiltration: Effects of Operating Conditions and Consequences on Membrane Fouling. Biotechnol Bioeng. 1991;38(5):528-534. doi:10.1002/bit.260380511

5.   Chandavarkar AS. Dynamics of Fouling of Microporous Membranes by Proteins. Massachusetts Institute of Technology; 1990.

6.   Castellanos MM, Pathak JA, Colby RH. Both protein adsorption and aggregation contribute to shear yielding and viscosity increase in protein solutions. Soft Matter. 2014;10:122-131. doi:10.1039/c3sm51994e

7.   Virkar PD, Narendranathan TJ, Hoare M, Dunnill P. Studies of the effect of shear on globular proteins: Extension to high shear fields and to pumps. Biotechnol Bioeng. 1981;23(5):1169-1169. doi:10.1002/bit.260230525

8.   Yen JW. Denaturation and Aggregation of SS-Galactosidase during Tangential Flow Ultrafiltration. The Ohio State University; 1995.

9.   Rosenberg AS. Effects of Protein Aggregates: An Immunologic Perspective. AAPS J. 2006;8(3):E501-E507. doi:10.1208/aapsj080359

10.   Wang W, Singh SK, Li N, Toler MR, King KR, Nema S. Immunogenicity of protein aggregates - Concerns and realities. Int J Pharm. 2012;431(1-2):1-11. doi:10.1016/j.ijpharm.2012.04.040

11.   Moussa EM, Panchal JP, Moorthy BS, et al. Immunogenicity of Therapeutic Protein Aggregates. J Pharm Sci. 2016;105(2):417-430. doi:10.1016/j.xphs.2015.11.002

12.   Kalonia CK, Heinrich F, Curtis JE, Raman S, Miller MA, Hudson SD. Protein Adsorption and Layer Formation at the Stainless Steel− Solution Interface Mediates Shear-Induced

Particle Formation for an IgG1 Monoclonal Antibody. Mol Pharmaceutics. 2018;15(3):1319-1331. doi:10.1021/acs.molpharmaceut.7b01127

13. Nayak A, Colandene J, Bradford V, Perkins M. Characterization of subvisible particle formation during the filling pump operation of a monoclonal antibody solution. J Pharm Sci. 2011;100(10):4198-4204. doi:10.1002/jps.22676

14. Wu H, Randolph TW. Aggregation and Particle Formation During Pumping of an Antibody Formulation Are Controlled by Electrostatic Interactions Between Pump Surfaces and Protein Molecules. J Pharm Sci. 2020;109(4):1473-1482. doi:10.1016/j.xphs.2020.01.023

15. Bee JS, Davis M, Freund E, Carpenter JF, Randolph TW. Aggregation of a Monoclonal Antibody Induced by Adsorption to Stainless Steel. Biotechnol Bioeng. 2010;105(1):121-129. doi:10.1002/bit.22525

16. Bee JS, Chiu D, Sawicki S, et al. Monoclonal antibody interactions with micro- and nanoparticles: Adsorption, aggregation, and accelerated stress studies. J Pharm Sci. 2009;98(9):3218-3238. doi:10.1002/jps.21768

17. Tyagi AK, Randolph TW, Dong A, Maloney KM, Hitscherich C, Carpenter JF. IgG particle formation during filling pump operation: A case study of heterogeneous nucleation on stainless steel nanoparticles. J Pharm Sci. 2009;98(1):94-104. doi:10.1002/jps.21419

18. Dreckmann T, Boeuf J, Ludwig IS, Lümkemann J, Huwyler J. Low volume aseptic filling: Impact of pump systems on shear stress. European Journal of Pharmaceutics and Biopharmaceutics. 2020;147:10-18. doi:10.1016/j.ejpb.2019.12.006

19. Her C, Carpenter JF. Effects of Tubing Type, Formulation, and Postpumping Agitation on Nanoparticle and Microparticle Formation in Intravenous Immunoglobulin Solutions Processed With a Peristaltic Filling Pump. J Pharm Sci. 2020;109(1):739-749. doi:10.1016/j.xphs.2019.05.013

20. Her C, Tanenbaum LM, Bandi S, et al. Effects of Tubing Type, Operating Parameters, and Surfactants on Particle Formation During Peristaltic Filling Pump Processing of a mAb Formulation. J Pharm Sci. 2020;109(4):1439-1448. doi:10.1016/j.xphs.2020.01.009

21. Vázquez-Rey M, Lang DA. Aggregates in monoclonal antibody manufacturing processes. Biotechnol Bioeng. 2011;108(7):1494-1508. doi:10.1002/bit.23155

22. Saller V, Matilainen J, Grauschopf U, Bechtold-Peters K, Mahler HC, Friess W. Particle Shedding from Peristaltic Pump Tubing in Biopharmaceutical Drug Product Manufacturing. J Pharm Sci. 2015;104(4):1440-1450. doi:10.1002/jps.24357

23.   Deiringer N, Haase C, Wieland K, Zahler S, Haisch C, Friess W. Finding the Needle in the Haystack: High-Resolution Techniques for Characterization of Mixed Protein Particles Containing Shed Silicone Rubber Particles Generated During Pumping. J Pharm Sci. 2021;110(5):2093-2104. doi:10.1016/j.xphs.2020.12.002

24.   Saller V, Hediger C, Matilainen J, et al. Influence of particle shedding from silicone tubing on antibody stability. Journal of Pharmacy and Pharmacology. 2018;70(5):675-685. doi:10.1111/jphp.12603

25.   Jones LS, Kaufmann A, Middaugh CR. Silicone oil induced aggregation of proteins. J Pharm Sci. 2005;94(4):918-927. doi:10.1002/jps.20321

26.   Thirumangalathu R, Krishnan S, Ricci MS, Brems DN, Randolph TW, Carpenter JF. Silicone oil- and agitation-induced aggregation of a monoclonal antibody in aqueous solution. J Pharm Sci. 2009;98(9):3167-3181. doi:10.1002/jps.21719

27.   Totoki S, Yamamoto G, Tsumoto K, Uchiyama S, Fukui K. Quantitative laser diffraction method for the assessment of protein subvisible particles. J Pharm Sci. 2015;104(2):618-626. doi:10.1002/jps.24288

28.   Folzer E, Khan TA, Schmidt R, et al. Determination of the Density of Protein Particles Using a Suspended Microchannel Resonator. J Pharm Sci. 2015;104(12):4034-4040. doi:10.1002/jps.24635

29.   Ebrahiminia A, Mokhtari-Dizaji M, Toliyat T. Correlation between iodide dosimetry and terephthalic acid dosimetry to evaluate the reactive radical production due to the acoustic cavitation activity. Ultrason Sonochem. 2013;20(1):366-372. doi:10.1016/j.ultsonch.2012.05.016

30.   Maa YF, Hsu CC. Investigation on Fouling Mechanisms for Recombinant Human Growth Hormone Sterile Filtration. J Pharm Sci. 1998;87(7):808-812. doi:10.1021/js980114x

31.   Warne N, R. Koval, T. Crowley. Peracetic acid in the study of rhIL-11 methionine oxidation - European Pharmaceutical Review. European Pharmaceutical Review. Published 2008. Accessed May 14, 2019. https://www.europeanpharmaceuticalreview.com/article/1251/peracetic-acid-in-the-study-of-rhil-11-methionine-oxidation/

32.   Duerkop M, Berger E, Dürauer A, Jungbauer A. Impact of Cavitation, High Shear Stress and Air/Liquid Interfaces on Protein Aggregation. Biotechnol J. 2018;13(7):1800062. doi:10.1002/BIOT.201800062

33.   Randolph TW, Schiltz E, Sederstrom D, et al. Do not drop: Mechanical shock in vials causes cavitation, protein aggregation, and particle formation. J Pharm Sci. 2015;104(2):602-611. doi:10.1002/jps.24259

34.   Mulinacci F, Poirier E, Capelle MAH, Gurny R, Arvinte T. Influence of methionine oxidation on the aggregation of recombinant human growth hormone. European Journal of Pharmaceutics and Biopharmaceutics. 2013;85(1):42-52. doi:10.1016/j.ejpb.2013.03.015

35.   Yokota H, Saito H, Masuoka K, Kaniwa H, Shibanuma T. Reversed phase HPLC of Met 58 oxidized rhIL-11: oxidation enhanced by plastic tubes. J Pharm Biomed Anal. 2000;24(2):317-324. doi:10.1016/S0731-7085(00)00419-2

36.   Mason TJ, Lorimer JP, Bates DM, Zhao Y. Dosimetry in sonochemistry: the use of aqueous terephthalate ion as a fluorescence monitor. Ultrason Sonochem. 1994;1(2):S91-S95. doi:10.1016/1350-4177(94)90004-3

37.   Rabe M, Verdes D, Seeger S. Understanding protein adsorption phenomena at solid surfaces. Adv Colloid Interface Sci. 2011;162(1-2):87-106. doi:10.1016/j.cis.2010.12.007

38.   Bremer MGEG, Duval J, Norde W, Lyklema J. Electrostatic interactions between immunoglobulin (IgG) molecules and a charged sorbent. Colloids Surf A Physicochem Eng Asp. 2004;250(1-3):29-42. doi:10.1016/j.colsurfa.2004.05.026

39.   Roberts D, Keeling R, Tracka M, et al. Specific Ion and Buffer Effects on Protein−Protein Interactions of a Monoclonal Antibody. Mol Pharmaceutics. 2015;12(1):179-193. doi:10.1021/mp500533c

40.   Lehermayr C, Mahler HC, Mäder K, Fischer S. Assessment of net charge and protein-protein interactions of different monoclonal antibodies. J Pharm Sci. 2011;100(7):2551-2562. doi:10.1002/jps.22506

41.   He F, Woods CE, Becker GW, Narhi LO, Razinkov VI. High-throughput assessment of thermal and colloidal stability parameters for monoclonal antibody formulations. J Pharm Sci. 2011;100(12):5126-5141. doi:10.1002/jps.22712

42.   Koepf E, Schroeder R, Brezesinski G, Friess W. The missing piece in the puzzle: Prediction of aggregation via the protein-protein interaction parameter A∗2. European Journal of Pharmaceutics and Biopharmaceutics. 2018;128:200-209. doi:10.1016/j.ejpb.2018.04.024

43.   Zhang J, Liu XY. Effect of protein-protein interactions on protein aggregation kinetics. J Chem Phys. 2003;119(20):10972. doi:10.1063/1.1622380

44.   Calero-Rubio C, Saluja A, Roberts CJ. Coarse-Grained Antibody Models for "Weak" Protein−Protein Interactions from Low to High Concentrations. J Phys Chem B. 2016;120(27):6592-6605. doi:10.1021/acs.jpcb.6b04907

45.   Sorret LL, Dewinter MA, Schwartz DK, Randolph TW. Challenges in Predicting Protein-Protein Interactions from Measurements of Molecular Diffusivity. Biophys J. 2016;111:1831-1842. doi:10.1016/j.bpj.2016.09.018

46.   Kim HL, Mcauley A, Livesay B, Gray WD, Mcguire J. Modulation of Protein Adsorption by Poloxamer 188 in Relation to Polysorbates 80 and 20 at Solid Surfaces. J Pharm Sci. 2014;103(4):1043-1049. doi:10.1002/jps.23907

47.   Kanthe AD, Krause M, Zheng S, et al. Armoring the Interface with Surfactants to Prevent the Adsorption of Monoclonal Antibodies. ACS Appl Mater Interfaces. 2020;12(8):9977-9988. doi:10.1021/acsami.9b21979

48.   Thomas CR, Geer D. Effects of shear on proteins in solution. Biotechnol Lett. 2011;33(3):443-456. doi:10.1007/s10529-010-0469-4

49.   Koepf E, Eisele S, Schroeder R, Brezesinski G, Friess W. Notorious but not understood: How liquid-air interfacial stress triggers protein aggregation. Int J Pharm. 2018;537(1-2):202-212. doi:10.1016/j.ijpharm.2017.12.043

50.   Bee JS, Schwartz DK, Trabelsi S, et al. Production of particles of therapeutic proteins at the air-water interface during compression/dilation cycles. Soft Matter. 2012;8:10329-10335. doi:10.1039/c2sm26184g

51.   Mehta SB, Lewus R, Bee JS, Randolph TW, Carpenter JF. Gelation of a Monoclonal Antibody at the Silicone Oil-Water Interface and Subsequent Rupture of the Interfacial Gel Results in Aggregation and Particle Formation. J Pharm Sci. 2015;104(4):1282-1290. doi:10.1002/jps.24358

52.   Maruno T, Watanabe H, Yoneda S, et al. Sweeping of Adsorbed Therapeutic Protein on Prefillable Syringes Promotes Micron Aggregate Generation. J Pharm Sci. 2018;107(6):1521-1529. doi:10.1016/j.xphs.2018.01.021

53.   McUmber AC, Randolph TW, Schwartz DK. Electrostatic Interactions Influence Protein Adsorption (but Not Desorption) at the Silica−Aqueous Interface. J Phys Chem Lett. 2015;6:2583-2587. doi:10.1021/acs.jpclett.5b00933

54.   Roth J, Albrecht V, Nitschke M, et al. Surface functionalization of silicone rubber for permanent adhesion improvement. Langmuir. 2008;24(21):12603-12611. doi:10.1021/la801970s

9. Supplementary data
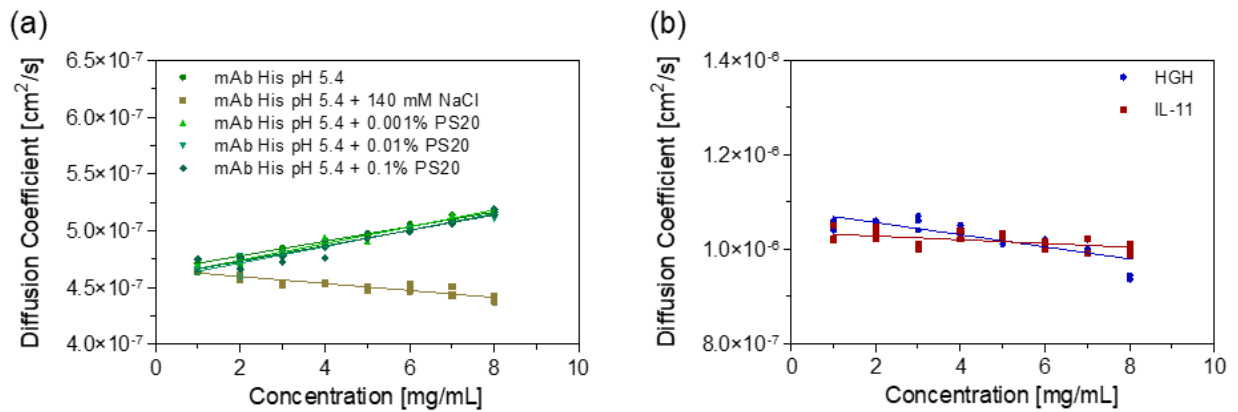
Figure S 1 Linear regression data for k_D determination of (a) the different mAb formulations and (b) the cytokines. Each data point represents one measurement out of the triplicates per concentration.

Figure S 2 Exemplary images of particles generated upon pumping pure buffer (a, c) or 1mg/mL mAb (b, d) with (c, d) or without (a, b) addition of 0.01% PS20 in filling mode at 180 rpm.
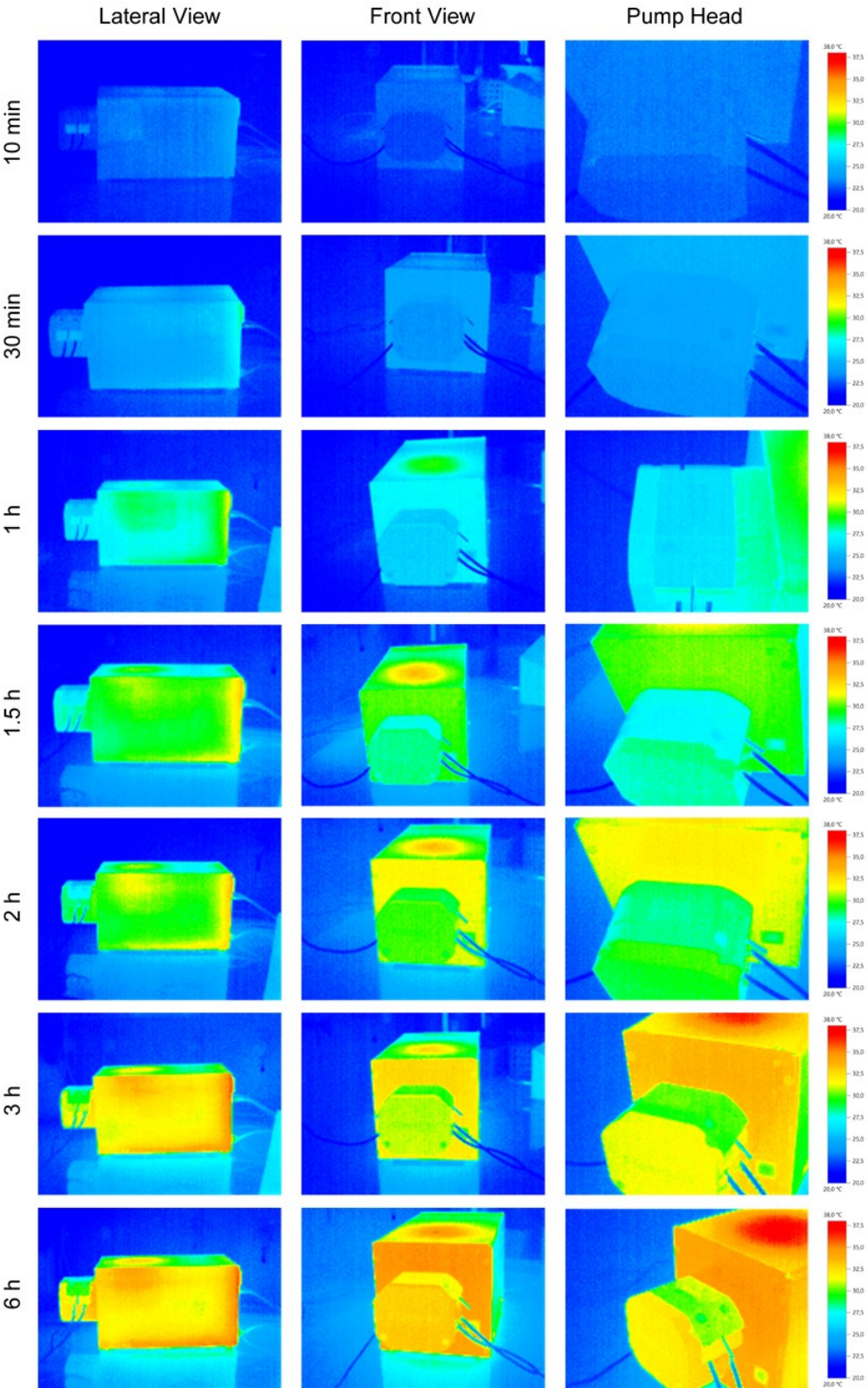
Figure S 3 Temperature profile of the peristaltic pump over 6 h of pumping at 180 rpm.
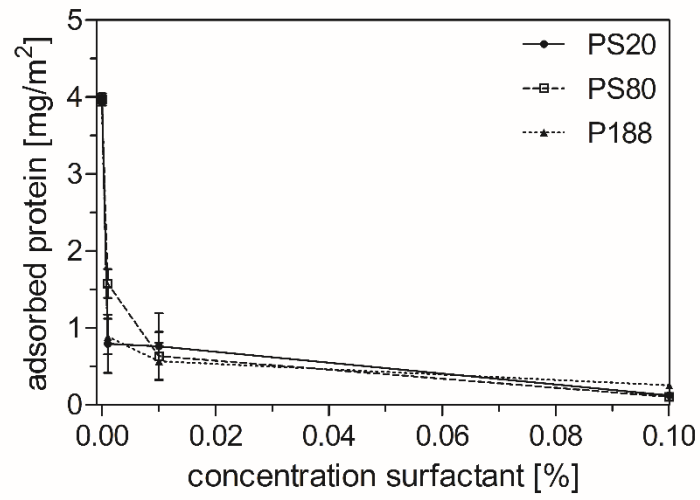
Figure S 4 Adsorbed equilibrium protein amount in presence of three surfactant types with concentrations ranging from 0 to 0.1% (w/v).

Chapter V Catching Speedy Gonzales: Driving forces for Protein Film Formation on Silicone Rubber Tubing During Pumping

Deiringer N[1], Rüdiger D[2], Luxbacher T[3], Zahler S[2], Friess W[1]. Catching Speedy Gonzales: Driving forces for Protein Film Formation on Silicone Rubber Tubing During Pumping. J Pharm Sci. **2022**;111(6):1577-1586. doi: 10.1016/j.xphs.2022.02.013.

[1]Department of Pharmacy, Pharmaceutical Technology and Biopharmaceutics, Ludwig-Maximilians-Universität München, Munich, Germany

[2] Department of Pharmacy, Pharmaceutical Biology, Ludwig-Maximilians-Universität München, Munich, Germany

[3]Anton Paar GmbH, Graz, Austria

Author contributions:

N.D. and W.F. conceived and designed the study. N.D. performed pumping and adsorption studies. T.L. performed zeta potential and electrophoretic measurements. N.D. and D.R. performed and evaluated AFM measurements. N.D. analyzed data and wrote the original draft. W.F., T.L., D.R. and S.Z. revised and edited the manuscript. W.F., S.Z. and T.L. supervised the study.

Note from the authors:

The version included in this thesis is identical with the published article apart from minor changes.

1. Abstract

Interfacial adsorption is a major concern in the processing of biopharmaceutics as it not only leads to a loss of protein, but also to particle formation. Protein particle formation during peristaltic pumping is linked to interfacial adsorption to the tubing and subsequent tearing of the formed protein film. In the current study, driving forces and rate of the adsorption of a monoclonal antibody to the silicone rubber surface during pumping, as well as particle formation, were studied in different formulations. Particle concentration and size distribution were influenced by the formulation parameters; specifically high ionic strength led to more particles and the build-up of particles larger than 25 µm. Formulation pH and ionic strength had an effect on the total amount of adsorbed protein. Adsorbed protein amounts increased when the Debye length of the protein was decreased, leading to a higher packing density. Atomic force microscopy and streaming potential determination revealed that the irreversible protein film formation on the hydrophobic tubing surface occurs in less than a second. Electrostatic interactions are the dominating factor for the initial adsorption speed. In intimate contact to the silicone rubber surface, hydrophobic interactions govern the protein adsorption. PS20 quickly coats the tubing surface which leads to an increase in hydrophilicity and shielding of electrostatic interactions, thereby efficiently inhibiting protein adsorption. Overall, atomic force microscopy and streaming potential determination possess great potential for the characterization of adsorbed protein films and the adsorption kinetic evaluation in high-speed mode. Protein adsorption to silicone tubing is driven by a combination of electrostatic and hydrophobic interactions which is effectively shielded by PS20.

Keywords: monoclonal antibody, pumping, biopharmaceutics, streaming potential, atomic force microscopy, silicone, protein adsorption, protein aggregation

Abbreviations: AFM - Atomic force microscopy; Gn·HCl - Guanidine hydrochloride; HP-SEC - high-performance size-exclusion chromatography; HPW – highly purified water; HS – AFM - high-speed AFM; ICD - Isothermal Chemical Denaturation; k_D – interaction parameter; mAb - monoclonal antibody; PDMS – Polydimethylsiloxane; PS20 - polysorbate 20

2. Introduction

Protein particle formation is a major concern in the processing of biopharmaceutics. During manufacturing and storage proteins are exposed to a variety of surfaces. As surface active molecules, proteins tend to adsorb to interfaces reversibly or irreversibly which can be triggered by structural perturbation. The adsorption process is governed by protein features like hydrophobicity, conformational and colloidal stability, as well as material characteristics.[1–3] On the one hand, interfacial adsorption results in protein loss. On the other hand, protein particles can form upon rupturing of the protein film at liquid-air and liquid-solid interfaces as agitation[4], stirring[5] or ejection from syringes leads to a substantial increase in subvisible and visible particles.[6] We previously observed pronounced particle formation during peristaltic pumping of protein solutions.[7] Various proteins adsorbed quickly to the silicone tubing used, and the formed protein film was ruptured during roller movement. We assume that during pumping a high protein adsorption rate plays a key role in the particle formation propensity. Protein adsorption to hydrophobic surfaces is difficult to monitor as the adsorption rate and the structural perturbation occur rather fast compared to hydrophilic surfaces.[1] Electrostatic and hydrophobic forces initiate protein adsorption via long-range and short-range interactions, respectively. Exemplary, protein particle formation in piston pumps was favoured by electrostatic interaction governing protein adsorption.[8] Identification of the driving forces during protein adsorption to tubing material could give hints on optimized formulations that reduce adsorption and particle formation during peristaltic pumping.

Atomic force microscopy (AFM) has been established for the characterization of protein film morphology and thickness on different materials.[9,10] Additionally, high-speed AFM (HS – AFM) can provide insights into the steps and the rate of protein film formation.[6] Unfortunately, HS-AFM is only an indicator for the protein film building process, but it does not enable a quantification of the adsorption. In contrast, a variety of methods allow the quantitative monitoring of protein adsorption kinetics to polymer surfaces like quartz crystal microbalance with dissipation monitoring,[11,12] neutron reflectometry[13] and surface plasmon resonance.[14] But these techniques typically require a model surface and tubings could not be investigated. To this end we evaluated streaming potential measurements on the tubing itself. Streaming potential measurements are based on the potential difference caused by the movement of counter charges from a charged surface. The flow of the counter charges is induced by the force exerted on the double layer due to a pressure gradient through a charged channel, capillary or membrane.[15] Streaming potential measurements do not only track protein adsorption label-free in high-speed mode, they also give evidence on the electrostatic charges present on the substrate before and after incubation.[16,17]

In our current study we evaluated the effect of formulation parameters on the protein particle formation propensity and identified the driving forces and kinetics of protein adsorption to silicone rubber tubings. Protein formulations were varied in ionic strength, pH and surfactant concentration to find the main driving forces during the adsorption process and their potential interplay. Protein stability and surface activity was measured by established biophysical methods and interfacial drop profile analysis. The protein film on the silicone rubber surface was visualized and characterized by AFM and streaming potential measurements. In order to track the protein adsorption kinetics in real time both techniques were setup in a high-speed mode. The findings from the adsorption kinetics and protein stability studies were linked to the protein particle formation propensity during pumping.

3. Materials and Methods

3.1. Materials

A 33.4 mg/mL monoclonal IgG1 antibody in 20 mM histidine buffer pH 5.4 was used as a model monoclonal antibody (mAb). Formulations at different pH and ionic strength (Table 1) were obtained from the 33.4 mg/mL stock by dilution in the respective buffer. Buffer ingredients were dissolved in highly purified water (HPW) from an Arium pro DI Ultrapure Water System (Sartorius Stedim Biotech GmbH, Goettingen, Germany) and pH was adjusted either with hydrochloric acid (VWR, Darmstadt, Germany) or sodium hydroxide (Bernd Kraft GmbH, Duisburg, Germany). Buffers were filtered through 0.2 µm cellulose acetate filters (47 mm ø, Sartorius Stedim Biotech GmbH). Protein and mAb formulations were filtered through 0.2 µm polyethersulfone membrane syringe filters (VWR) prior to experiments. Chemicals for experiments were purchased as follows: Guanidine hydrochloride (Gn·HCl), polysorbate 20 (PS20) and sodium dihydrogen phosphate from Merck (Darmstadt, Germany); Potassium chloride (KCl) from VWR; Sodium chloride (NaCl) from Bernd Kraft; Sodium dodecyl sulfate (SDS) from Sigma Aldrich (Steinheim Germany). The Sylgard 182 Silicone Elastomer Kit (The Dow Chemical Company, Midland, MI, USA) was kindly gifted by Biesterfeld Spezialchemie GmbH (Hamburg, Germany).

Table 1 Ionic strength (IS) calculation is based on the amount of Histidine · HCl and NaCl.

Formulation	IS [mM]
20 mM histidine pH 5.4	16.27
20 mM histidine pH 5.4 + 140 mM NaCl	156.27
20 mM histidine pH 7.4	0.84
20 mM histidine pH 7.4 + 140 mM NaCl	140.84

3.2. Preparation of silicone tubing sets

Accusil tubing sets (ID 1.6 mm, Watson-Marlow, Falmouth, United Kingdom) were assembled and cleaned as described elsewhere.[7] Cleaned tubing sets were flushed with 5 l HPW at 180 rpm prior to experiments using a Flexicon PD12 peristaltic pump (Watson-Marlow Flexicon, Ringsted, Denmark) operated with a MC 12 control unit. A total volume of 6 mL of a corresponding placebo buffer followed by the 1 mg/mL mAb formulation was circulated 20 times in filling mode (60 x 2 mL fills, 1 s interval, acceleration of 60) at 180 rpm. All pumping experiments were conducted under a laminar air flow cabinet. Experiments were performed as three independent pumping studies using a new tubing set each.

3.3. Particle analysis

Turbidity of samples from pumping studies were analyzed according to Ph. Eur. 2.2.1 using a Nephla turbidimeter (Dr. Lange, Duesseldorf, Germany). Subvisible particles were measured by the Aggregates Sizer with the WingSALD bio software version 3.2.2 (Shimadzu Corporation, Kyoto, Japan) and the FlowCAM® 8100 (Fluid Imaging Technologies, Inc., Scarborough, ME, USA). The Aggregates Sizer calculated protein particle concentration in a 5 mL batch cell based on a material specific refractive index of 1.46, an imaginary index of 0.1[18] and a protein particle density of 1.32 g/cm^3.[19] The cut-off level of noise was set to 500. Scattering from unpumped samples and pumped buffer samples were below the cut level of noise. A total sample volume of 150 µl was analysed using the FlowCam equipped with a 10x magnification cell (81 µm × 700 µm) at a flow rate of 0.15 mL/min. Images were collected with an auto image frame rate of 28 frames/s and a sampling time of 60 s (efficiency > 70%). Particle identification was based on the following settings: 3 µm distance to the nearest neighbour, particle segmentation thresholds of 13 and 10 for the dark and light pixels, respectively. Particle size as the equivalent spherical diameter is displayed using VisualSpreadsheet® 4.7.6 software.

3.4. Determination of the interaction parameter(k_D)

Varying mAb concentrations between 1 and 8 mg/mL were centrifuged for 10 min at 10,000 g. 25 µl of protein sample were filled in a 384 microwell plate (Corning, Corning, NY, USA) and centrifuged for 2 min at 2,000 rpm using a Heraeus Megafuge 40 centrifuge equipped with an M-20 well plate rotor (Thermo Fisher Scientific, Wilmington, USA). Wells sealed with silicone oil were measured at 25 °C with 20 acquisitions of 5 s using a DynaPro plate reader III (Wyatt Technology, Santa Babara, CA, USA). The interaction parameter k_D was derived from the concentration dependence of the mutual diffusion coefficient D:

$$D = D_0(1 + k_D c)$$

With D_0 = diffusion coefficient at infinite dilution and c = protein concentration.

For an estimation of a net attractive or a net repulsive interaction the osmotic second virial coefficient A_2^* was calculated from the TIM equation[20]:

$$A_2^* = \frac{k_D + 6.29}{1.19M}$$

With M representing the molar mass of the protein.

3.5. Determination of molecular weight

For the determination of the molecular mass by static light scattering samples with a mAb concentration of 4, 6, 8 and 10 mg/mL in histidine buffer pH 9 were analysed in a low volume quartz cuvette by the Litesizer 500 (Anton Paar, Graz, Austria). Each measurement was performed in duplicate at each mAb concentration.

3.6. Isothermal Chemical Denaturation (ICD)

Different denaturant concentrations were prepared by pipetting formulation buffer and denaturant stock (formulation buffer containing 6 M Gn·HCl) into a non-binding surface 384 well plate (Greiner, Frickenhausen, Germany) using Viaflo Assist equipped with a 16-channel 125 µL Viaflo pipette (Integra Biosciences, Konstanz, Germany). We used Gdn HCl as denaturant to avoid drawbacks from the weaker denaturant urea like partial unfolding, accepting that we affect the ionic strength. The protein stock was added to a final concentration of 1 mg/mL using a 16-channel 12.5 µL Viaflo pipette (Integra Biosciences). To avoid sample evaporation during incubation the well plate was sealed with EASYseal™ sealing film (Sigma Aldrich) after manual mixing. After 24 hours incubation at room temperature, the samples were analyzed with a FLUOstar Omega microplate reader (BMG Labtech, Ortenberg, Germany) by measuring intrinsic fluorescence intensity (λ_{ex}=280 nm; λ_{em1}= 330 nm and λ_{em2}= 350 nm). The measurements for both wavelengths were performed in multichromatic mode using 50 flashes per well with the same gain settings for each wavelength. The mean data of the triplicates was fitted to a three-state model using the biphasic model from Prism 5 (GraphPad Software, San Diego, CA, USA). The melting points (C_{m1} and C_{m2}) were derived from the fit representing the concentration leading to half-maximum unfolding of each unfolding transition.

3.7. Zeta potential and electrokinetic measurements

Streaming potential and streaming current measurements were performed with SurPASS 3 (Anton Paar GmbH, Graz, Austria) equipped with the measuring cell for flexible tubing (Figure S 1). A 70 mm tube sample was fixed on both ends using caps with an appropriate size that tighten the inlet and outlet of the tube sample by squeezing silicone gaskets. The cross-section of the tube sample was adjusted to comply with the requirements of a reliable streaming potential (streaming current) measurement on a capillary flow channel during 2.5 mM KCl rinsing. The central part of the tube sample was compressed gently by pushing the tube on a pedestal using a micrometre screw. After recording the pH dependence of the zeta potential for the inner surface of the pristine silicone tubing, the tubing was rinsed with HPW. For mAb

adsorption kinetic studies, the zeta potential of the pristine silicone tubing in 2.5 mM KCl at a chosen pH was recorded at a constant pressure (200 mbar) and a constant volume flow rate (73 ± 16 mL/min) serving as a baseline. As a second step the KCl solution was replaced by a 0.025 mg/mL mAb solution at pre-adjusted pH. As a last step the mAb solution was replaced with fresh 2.5 mM KCl pre-adjusted to the corresponding pH. For monitoring the effect of the non-ionic surfactant PS20 an additional adsorption step with KCl buffer containing 0.004% [w/v] PS20 was added before protein adsorption. After kinetic studies the pH dependence of the zeta potential for the inner surface of the silicone tubing after adsorption and desorption of mAb was recorded. Experiment durations were adapted until equilibrium conditions were reached. Data from adsorption kinetics measurements was fitted via nonlinear regression to the ´plateau followed by one phase association´ model from Prism 5 to obtain the adsorption rate.

3.8. Quantification of protein adsorption

To quantify the adsorbed protein, a 4 cm tubing piece (ID 6.0 mm) was filled with 1 mL of 2 mg/mL protein formulation. After 24 h incubation at room temperature, the tubing piece was washed three times with formulation buffer and refilled with 1 mL desorption buffer (10 mM phosphate buffer pH 7.2 with 145 mM NaCl and 0.05 % [w/v] SDS). After 24 h incubation, samples were analysed with an Agilent 1100 HPLC system (Agilent Technologies, Boeblingen, Germany) at 210 nm with a G1314A UV detector. To quantify the small protein amounts the injection volume was increased to 400 µl by insertion of a 500 µl seat capillary. The desorbed protein amount was quantified via high-performance size-exclusion chromatography (HP-SEC) using a 7.8 x 300 mm TSK Gel G3000 SWXL column (Tosoh Bioscience, Stuttgart, Germany) at a flow rate of 0.7 mL/min with the desorption medium as mobile phase. Based on an 8-point calibration curve (0.0001 to 0.01 mg/mL) the total desorbed protein amount could be determined. All chromatograms were analyzed using ChemStation software (Agilent Technologies).

3.9. Interfacial drop profile analysis

To study protein behaviour at the silicone oil interface, a 50 µl drop mAb solution (c = 1 mg/mL) was formed in a silicone oil (viscosity: 100 cSt; Optimal Products, Bad Oeynhausen, Germany) filled in an optical glass cuvette (Hellma, Müllheim, Germany). The interfacial tension was monitored over 30 minutes via a profile analysis tensiometer (PAT-1, Sinterface Technologies, Ltd., Germany). The pendant drop on a stainless-steel capillary (Ø 2.1 mm) was formed by the

automated syringe. Drop images were captured by a CCD camera at 1 frame/s and processed (PAT-1 software, Sinterface Technologies) to obtain drop volume, surface area, and interfacial tension based on the Young–Laplace equation. Interfacial tension was calculated based on solution densities of 1 g/cm^3 and 0.972 g/cm^3 for the mAb and silicone oil phase, respectively. Results are converted to surface pressure Π by subtraction of the pure buffer signal. The initial surface pressure Π_0 was estimated by the 'two phase association' kinetic model from Prism 5.

3.10.   Atomic force microscopy

AFM images were performed using NanoWizard® 4 (JPK, Berlin, Germany) with integrated Axiovert 200 inverted microscope (Zeiss, Jena, Germany) and SPM software (JPK, Berlin, Germany). The cantilever qp-BioAC-CB1 (NanoWorld, Neuenburg, Switzerland; resonance frequency 90 kHz, spring constant 0.3 N/m) was used in the QI™ Mode (Advanced Imaging) and calibrated with the contact free method at room temperature.

For imaging of the tubing surface, pieces of Accusil tubing (ID 6.0 mm) were glued on glass slides. By gluing a ring serving as reservoir wall, the tubing surface could be covered with buffer. A defined spot of the tubing was measured in buffer before and after incubation with 1 mg/mL mAb for 30 min. The following values have been set: setpoint 0.5 nN; z-length 4 µm; speed 300 µm/s; 20x20 µm^2 area with 350x350 pixels.

For protein film thickness and high-speed AFM measurements, ultra-flat PDMS coated surfaces were obtained by coating muscovite Mica V1-quality (Electron Microscopy Sciences, Hatfield, PA, USA) with the silicone elastomer kit. Ten parts of elastomer base and one part of curing agent [w/w] were mixed and after degassing 10 drops were applied on a mica sheet mounted on a KLM spincoater 1.4 (Schaefer Technologie, Langen, Germany) equipped with a KNF Laboport vacuum pump (Freiburg, Germany) operated at 200 rps for 30 s followed by ramping to 15 rps in 30 s. The PDMS coating was cured at 150 °C for one hour at 11 mbar. Successful coating was verified by water contact angle determination using drop shape analysis (Figure S 2). Coated Mica sheets were accepted for measurements only if the water contact angle was above 105°. Coated mica sheets were glued into petri dishes.

The PDMS surface was measured in air before incubation with the following values: setpoint 0.4 – 0.6 nN; z-length 0.4 µm; speed 300 µm/s; 10x10 µm^2 area with 256x256 pixels. The PDMS surface was incubated with 2 mL 1 mg/mL mAb solution at pH values 5.4 or 7.4 for 10 min and subsequently washed three times with respective formulation buffer. First, the protein surface was imaged. Afterwards an area of 1x1 µm^2 was scratched off by using the AFM contact mode in one scan (512x512 pixel) with maximum force (≈18 nN). Protein layer

thickness was estimated from the measured height profile of the resulting hole. The following values were set for imaging the protein surface and the scratched areas: setpoint 0.3 – 0.6 nN; z-length 0.4 µm; speed 181.82 µm/s; 5x5 µm^2 area with 256x256 pixels.

For the high-speed imaging the USC-F0.3-k0.3 cantilever (NanoWorld; resonance frequency 300 kHz, spring constant 0.3 N/m) was used in the Fast Imaging Mode and calibrated with the contact free method at room temperature. Petri dishes with coated mica sheets were filled with buffer. During the measurement, the protein solution was injected into the buffer via a microfluidic insert to observe the deposition of the protein in real time leading to a final protein concentration of 0.1 mg/mL. An area of 500x500 nm^2 was scanned at 200x100 pixels with a line rate of 100 Hz. The setpoint oscillation amplitude was between 3.44 nm and 5.51 nm.

All images were processed and optimized with Data Processing software version 6.0.50 (JPK, Berlin, Germany). First, a polynomial fit was subtracted from each scan line independently. A histogram is calculated for each scan line, and only the data between the lower (0%) and upper (70%) limits is used for fitting the polynomial. The second step was to replace outlier pixel values with the median value of neighbouring pixels. The last step was to use low-pass filter (2-dimensional Savitzky–Golay smoothing; smoothing width: 5, order: 2).

3.11.   Gold staining of mAb adsorbed to coated mica sheets

To verify protein adsorption during HS-AFM measurements coated mica sheets glued in petri dishes were incubated with 0.1 mg/mL mAb in 20 mM His/HCl pH 5.4 buffer for 13 s and 300 s. To remove residual salts on the surface that might interfere with the gold staining, incubated mica dishes were washed three times with corresponding placebo buffer followed by three times HPW. After washing, the petri dishes were filled with 2 mL gold staining solution (Colloidal gold total protein stain, BioRad Laboratories, Munich, Germany) and incubated at room temperature for 3 days. Stained samples were washed with deionized water and dried by compressed air.

4. Results

4.1. Protein particle formation upon pumping

At first, we studied the impact of pH and ionic strength on protein particle formation upon pumping of a mAb solution (Table 2). For buffer formulations, turbidity and particle number went up only marginally. In contrast, mAb formulations exhibited a marked increase in turbidity from approximately 0.5 to 3-3.5 FNU, and correspondingly, the number of particles ≥ 300 nm, increased from below the detection limit to approximately 26 x 10^6 per mL after pumping. The number of particles ≥ 1 μm per mL was substantially higher with approx. 150,000 for formulations without NaCl and 250,000 with NaCl as compared to approx. 400 before pumping. The formation of particles ≥ 10 μm and ≥ 25 μm was similar for all formulations, except for those with a buffer of low ionic strength and pH 5.4.

Table 2 Particle size distribution after pumping 1 mg/mL mAb in buffer pH 5.4 and 7.4 with and without addition of NaCl. Data at pH 5.4 from Deiringer et al.[7]

Formulation	Turbidity [FNU]	Particle concentration [#/mL]			
		≥ 300 nm	≥ 1 μm	≥ 10 μm	≥ 25 μm
pH 5.4	3.3 ± 0.3	30.2 x 10^6 ± 3.7 x 10^6	161,284 ± 10,920	2,513 ± 480	292 ± 42
+ 140 mM NaCl	3.3 ± 0.6	28.7 x 10^6 ± 9.6 x 10^6	287,475 ± 71,884	4,510 ± 1,448	832 ± 275
pH 7.4	3.6 ± 0.1	26.3 x 10^6 ± 2.5 x 10^6	148,036 ± 9,290	4,707 ± 1,038	743 ± 239
+ 140 mM NaCl	2.8 ± 0.2	20.3 x 10^6 ± 1.6 x 10^6	235,156 ± 43,433	2,999 ± 398	546 ± 104

4.2. Effect of formulation on protein interfacial behavior, conformational and colloidal stability

As protein particle formation upon pumping occurred in all formulations, but to a slightly different extent, the interfacial behaviour, the conformational as well as the colloidal stability of the mAb were tested as a function of the formulation. Conformational stability was monitored via chemical denaturation, as thermal denaturation would be substantially impacted by the pH shift of the histidine buffer upon heating.[21] The ICD data fitted well to a complex unfolding behaviour following a three-state model[21] (Figure 1). According to literature, the first transition can be assigned to the unfolding of the CH2 domain, while the second transition is linked to the unfolding of the Fab or the CH3 domain.[22]
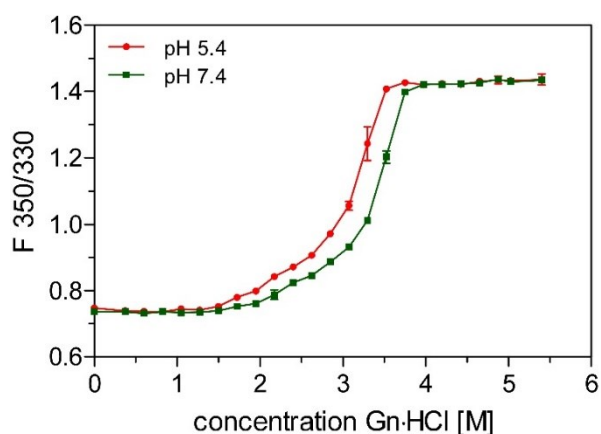
Figure 1 Isothermal chemical denaturation of 1 mg/mL mAb in different formulations.

C_m values only showed slight differences in unfolding propensity (Table 3). The formulation at pH 7.4 showed a higher resistance to unfolding induced by Gn·HCl compared to formulations at pH 5.4. These findings are in line with previously published literature.[23,24]

Table 3 Melting points (C_{m1} and C_{m2}) calculated from the biphasic fit model ($R^2 > 0.998$) of ICD, k_D and A_2^* of mAb formulations. The 95 % lower and 95 % upper confidence intervals for C_m values are reported in brackets.

Formulation	C_{m1} [M]	C_{m2} [M]	k_D [mL/g]	A_2^* [mL·mol/g^2]· 10^{-4}
pH 5.4	2.4 (2.2 - 2.5)	3.2 (3.2 - 3.3)	13.9 ± 0.3[7]	1.1 ± < 0.05
pH 5.4 + 140 mM NaCl	-	-	- 6.3 ± 0.5[7]	0.0 ± < 0.05
pH 7.4	2.7 (2.6 - 2.8)	3.5 (3.5 - 3.5)	28.0 ± 1.6	1.9 ± < 0.05
pH 7.4 + 140 mM NaCl	-	-	- 7.1 ± 0.4	0.0 ± < 0.05

The colloidal stability was characterized via k_D which can be transferred into an A_2^* value with the obtained molecular mass of $M_W = 156 \pm 6$ kDa of the mAb (Table 3). Without NaCl, increasing repulsive forces were observed with increasing pH. The addition of NaCl shielded the charge effect, leading to net balanced repulsion and attraction irrespective of pH.

Additionally, we studied the mAb adsorption behaviour at the interface between formulation and silicone oil, simulating the silicone rubber surface. We did not observe a lag phase, but a slow consistent increase in surface pressure (Figure 2). In the two buffers without NaCl, the increase was more substantial at pH 7.4. At high ionic strength in presence of NaCl, initial adsorption was very fast reaching higher surface pressure levels as compared to the salt-free low ionic strength buffers (Table 4).
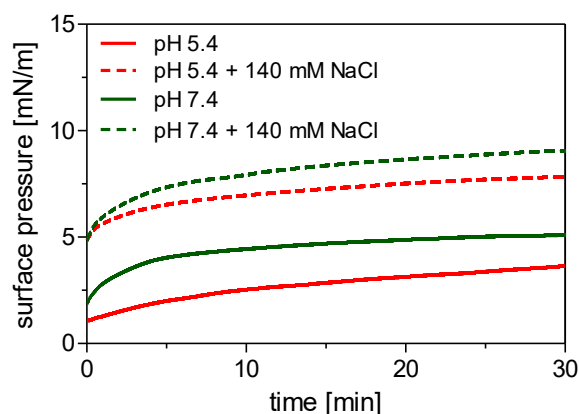
Figure 2 Surface activity measurements of 1 mg/mL mAb in different formulations (mean of n = 3).

Table 4. Initial surface pressure Π_0 obtained from extrapolation of the exponential model fit and surface pressure after 30 min (Π_{30}).

Formulation	Π_0[mN/m]	Π_{30}[mN/m]
pH 5.4	1.0 ± 0.2	3.7 ± 0.4
pH 5.4 + 140 mM NaCl	4.4 ± 0.1	7.9 ± 0.3
pH 7.4	1.5 ± 0.3	5.1 ± 0.2
pH 7.4 + 140 mM NaCl	4.4 ± 0.1	9.1 ± 0.5

4.3. Characterization of the mAb film on silicone rubber

The amount of adsorbed mAb was only slightly impacted by pH and ionic strength. At pH 5.4, 4.0 ± 0.1[7] and 5.3 ± 0.2[7] mg/m^2 respectively adsorbed compared to 4.6 ± 0.1 and 5.2 ± 0.2 mg/m^2 respectively at pH 7.4 in absence and presence of NaCl. At pH 9.0, an additional pH studied in the streaming potential measurements, adsorption was more pronounced with 6.8 ± 0.4 mg/m^2.

AFM showed that the tubing surface was irregular with deep holes resulting in height differences up to 1.6 µm (Figure 3). The protein filled the cavities and led to a smooth surface with height differences of less than 50 nm.
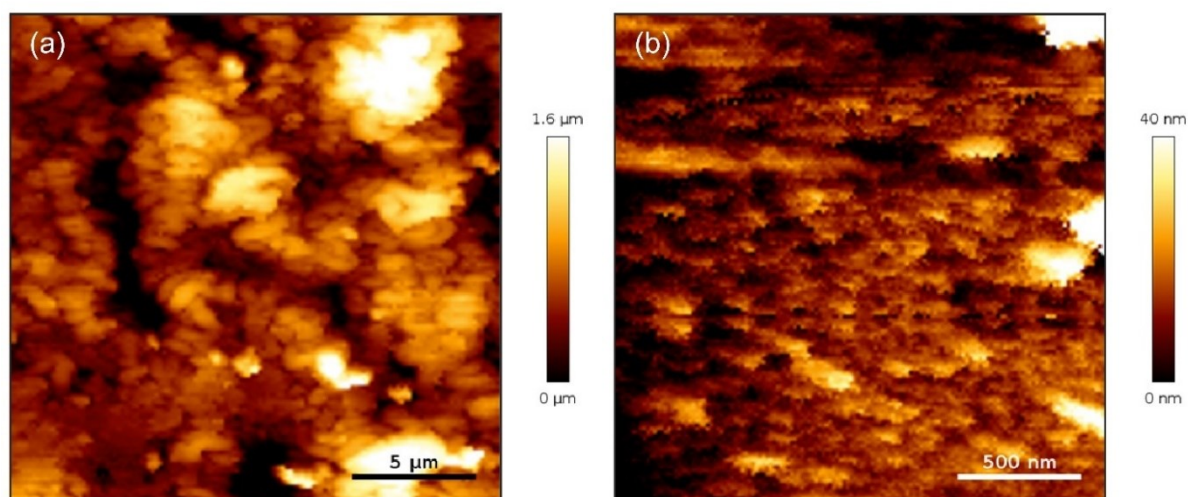
Figure 3 AFM images of tubing surface (a) before and (b) after incubation with 1 mg/mL mAb in 20 mM histidine buffer pH 5.4. Note that the height bars are of different scale and the image after incubation is zoomed in for proper morphology evaluation.

The protein film thickness could not be analysed directly on the silicone rubber tubing via AFM. Instead, PDMS coated mica sheets were used as model substrates with a strongly hydrophobic surface (similar water contact angle as silicone rubber[25], Figure S 2) and a smooth surface with less than 15 nm differences in height (Figure S 3). While the mAb formed clusters on top of the initial protein film at pH 5.4 with approximately 8 nm in height, a smooth and flat film of 3 to 4 nm was observed at pH 7.4 (Figure 4).
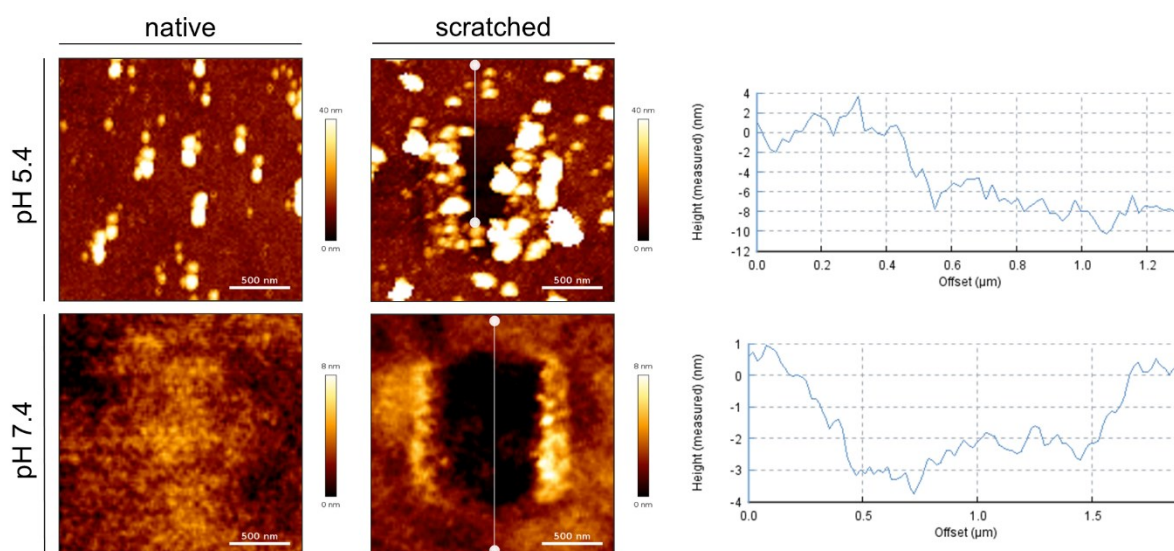
Figure 4 AFM images of mAb film on PDMS coated mica sheets in 20 mM histidine at pH 5.4 and pH 7.4. The white line represents the section for determination of the height profile. Additional measurements are presented in Figure S 3.

4.4. Electrochemical characterization of the mAb film on silicone rubber

The contribution of electrokinetic forces of either the tubing, the mAb or PS20 to adsorption was characterized by monitoring the zeta potential on the tubing itself in the presence of mAb and PS20. The high buffer capacity of the histidine buffer and different electric conductivities at different pH levels (pH 5.4: 400-500 mS/m; pH 7.4: 40-50 mS/m) impeded automated pH scans of the zeta potential after adsorption and desorption of mAb. Reference measurements supported the use of 2.5 mM KCl (conductivity: 35 mS/m) as background electrolyte for this study (Figure S 5a).
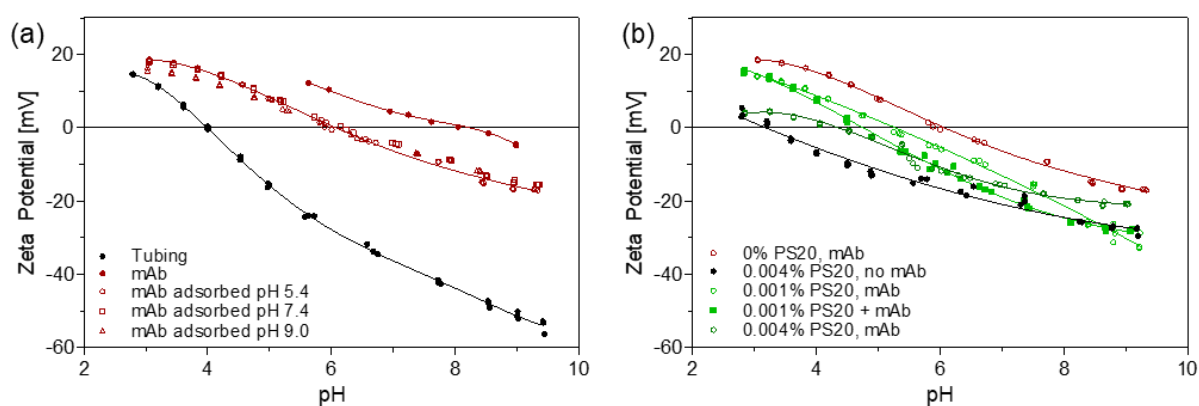
Figure 5 pH dependence of zeta potential after adsorption of mAb on silicone tubing using different experimental conditions. (a) Effect of mAb adsorption at different pH values. (b) Effect of surfactant concentration and PS20 pre-adsorption to the tubing at pH 5.4. PS20, mAb represents the mAb adsorption after priming the tubing with PS20 while PS20 + mAb means the adsorption of a mixture of mAb and PS20.

Zeta potential titrations revealed an IEP of 4.1 for the silicone tubing and 8.1 for the mAb (Figure 5a). After adsorption of mAb on the inner surface of the silicone tubing, the zeta potential and IEP changed significantly from the single components indicating protein attachment. Independent of the buffer pH employed, the adsorbed mAb layer on the tubing showed the same charging behaviour.

Furthermore, we examined the effect of the concentration and time dependent addition of PS20 on mAb adsorption (Figure 5b). Incubating the pristine silicone tubing with 0.004% [w/v] PS20 led to attachment of PS20, indicated by a substantial increase in zeta potential, and caused a shift of the IEP to pH 3.2 compared to the pristine tubing (IEP of pH 4.1). Priming the tubing with 0.001% [w/v] PS20 reduced the affinity of the protein towards the surface of the tubing. At the adsorption equilibrium of 0.004% [w/v], PS20 (Figure S 5b) adsorption of the mAb is further decreased. Compared to PS20 priming, when pumping a mixture of mAb and PS20, the surfactant decreased mAb adsorption even more effectively.

4.5. Adsorption kinetics on silicone tubing

We characterized the adsorption kinetics by employing HS-AFM and streaming potential measurements. Real-time monitoring by HS-AFM (Figure 6) revealed that protein film formation occurred in less than 13 s. Morphology of the formed film did not significantly differ from the pristine PDMS sheet. To verify the presence of a protein film on the PDMS surface, coated mica sheets were incubated with the mAb at the same conditions as during HS-AFM measurements. We successfully proved the presence of a protein film during our measurements via protein sensitive gold staining[26] (Figure 6). With increasing protein incubation time, stain intensity increased. Unfortunately, the first HS-AFM images could only be captured 13 s after mAb addition due to the adjustment of the cantilever.
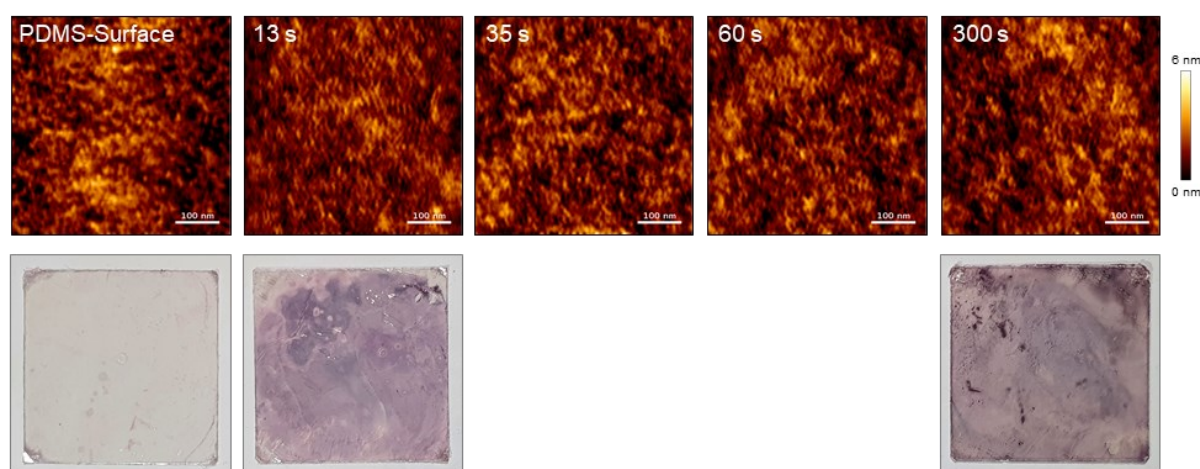
Figure 6 HS-AFM images (top) and corresponding gold staining (bottom) of PDMS coated mica sheets upon incubation with 0.1 mg/mL mAb in 20 mM histidine buffer pH 5.4 over 300 s.

To overcome the resolution gap of the HS-AFM and to detect electrostatic effects on mAb adsorption kinetics, streaming potential measurements were conducted at pH 5.4, 7.4 and 9.0 (Figure 7). The temporal changes in the streaming potential were measured during the adsorption of 0.025 mg/mL mAb and the subsequent rinse cycle with the aqueous 2.5 mM KCl solution adjusted to the respective pH.
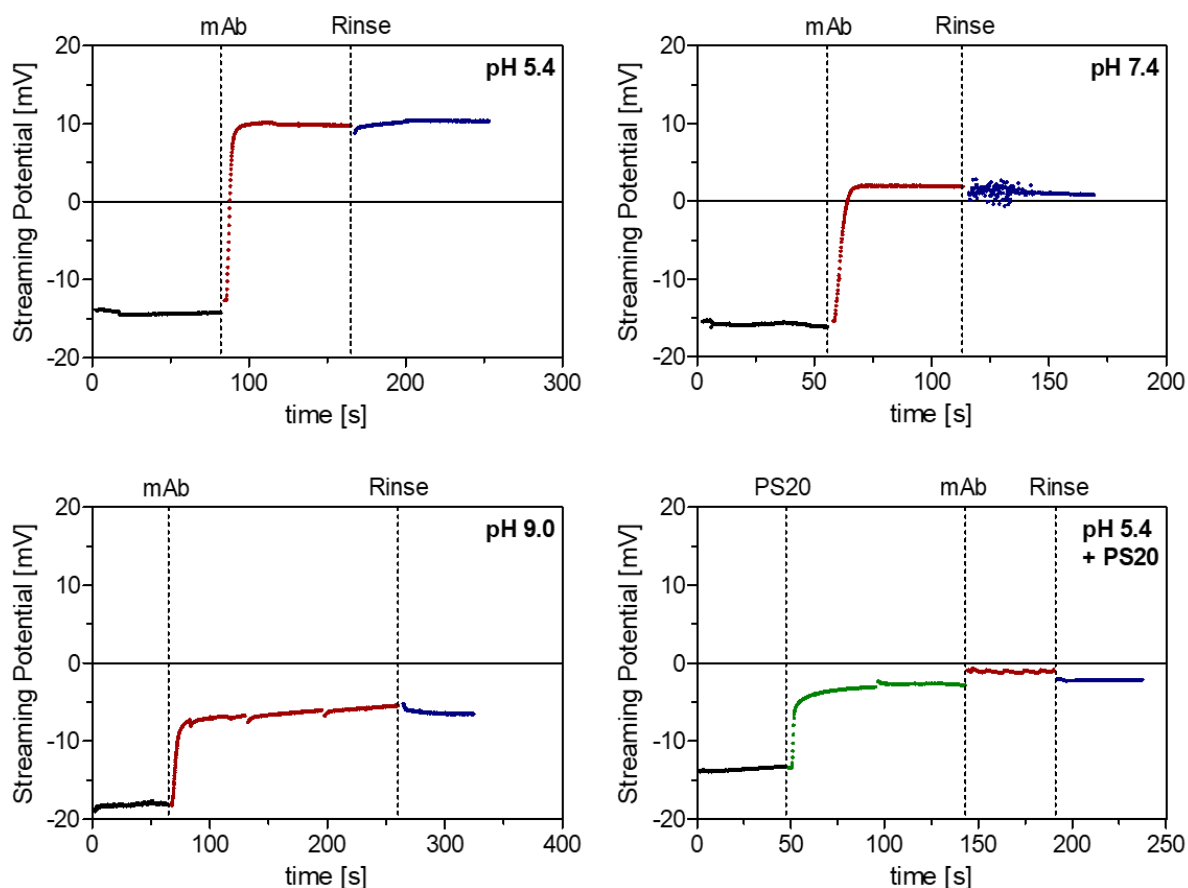
Figure 7 Streaming potential of inner tubing surface in 2.5 mM KCl after addition of mAb, 0.004% PS20 followed by a rinse with 2.5 mM KCl at the respective pH.

All conditions led to mAb adsorption in less than 10 seconds until equilibrium was reached. A charge reversal upon adsorption of the net positively charged mAb at pH 5.4 and 7.4 was observed. In comparison, at pH 9.0 adsorption of the net negatively charged mAb reaching the plateau took noticeably longer. Initial adsorption rates (Figure S 6, R^2 > 0.994) decreased from 0.53 s^{-1} to 0.41 s^{-1} and 0.29 s^{-1} with increasing pH and the initial adsorption phase took about 3, 5 and 6 s with increasing pH. The subsequent rinse cycle with 2.5 mM KCl and the respective pH had no effect on the streaming potential, indicating an irreversible mAb adsorption.

Priming the tubing surface with PS20 strongly reduced mAb adsorption as the streaming potential remained negative after incubation with mAb. The initial PS20 adsorption rate reached 1.4 s^{-1} and took only 1 s. Flushing the primed tubing with mAb resulted in only a minimal streaming potential increase, which was reversible with the subsequent rinse cycle.

5. Discussion

Adsorption of proteins to material surfaces during manufacturing has been widely investigated.[27–29] Protein adsorption is a serious issue in peristaltic pumping if the protein film is ruptured during the tubing strain, which results in film fragments entering the bulk solution.[7] We designed a study to analyse the effect of formulation on mAb particle formation propensity during peristaltic pumping and to link the results to the outcome of mechanistic protein adsorption studies. The addition of salt should reduce the electrostatic potential and inhibit electrostatic interfacial interactions, and variation of pH should impact conformational stability and protein charge. Her and Carpenter found an influence of the formulation on the protein particle formation propensity during peristaltic pumping; specifically, an increase in particle numbers in PBS due to a lower colloidal stability of the antibody tested.[30] In contrast, the formulation only slightly influenced the total particle concentration in our study. An increase in ionic strength (irrespective of pH) led to a substantial shielding of the electrostatic interactions between the mAb molecules, as supported by A_2^* values, and allowed the formation of more micrometre-sized aggregates.[31,32] Therefore, shielding protein-protein interactions counteracted the potentially reduced aggregation resulting from the shielding of electrostatic interactions with the surface. At low ionic strength the repulsive protein-protein interactions become predominant.[32–36] Furthermore, at low ionic strength the pH value did not impact protein particle formation propensity, although formation of large particles might be facilitated at pH 7.4 compared to pH 5.4 due to a lower net repulsive charge close to the isoelectric point.[32]

Adsorption of the mAb can be linked to the aggregation propensity upon pumping. Irrespective of the formulation, the adsorbed protein amounts indicate the formation of multiple protein layers.[37] AFM revealed a rough surface of the tubing with height differences of approximately 1.2 μm, which is in good agreement with 3D laser scanning microscopy results from a previous study.[38] After incubation with the mAb, a rather flat film with superficial protein clusters of around 40 nm in height was obtained. The dimensions of the clusters, around 100 nm, indicate that these clusters are formed by multiple antibody entities.[39] These large, irregularly shaped agglomerate structures of the protein film have already been observed on various materials like glass,[9,40] graphite[41] and mica[42]. It is argued that these protein clusters originate either from sedimentation and adherence of larger protein particles from the bulk[40], or from nucleation promoting the adsorption of further molecules.[41,42] Interestingly, the clusters were only present at pH 5.4, whereas we obtained a smooth film at pH 7.4.

Interestingly, film thickness at pH 5.4 increased as compared to pH 7.4, despite contradictory findings with regards to the amount of adsorbed protein. A rapid increase in surface pressure

at pH 7.4, which is near the isoelectric point of the mAb, indicates more pronounced protein-protein and protein-surface interactions compared to pH 5.4.[43–45] Debye length is a parameter for the packing density of the proteins, which is linked to the damping distance of the electric potential of a fixed charge in an electrolyte.[46] Generally speaking, a strong interfacial protein network has its maximum amount of protein at the isoelectric point and high ionic strength due to attractive forces between the proteins or shielding of the inner protein charges, which result from a decrease of the effective Debye length.[47] At pH 7.4 which is close to the IEP, electrostatic protein-protein repulsions are low due to a minimum of the Debye length[48] and allow higher packing densities, leading to a maximized mass load.[49–51] Different heights of the films might indicate a more compact layer due to a denser packing of the mAb and less solvation at pH 7.4. The factors influencing layer solvation are a result of the size, shape and structure of the protein, as well as their packing arrangement upon adsorption. Similarly, α-chymotrypsin tends to form more continuous layers resulting in a flat surface at the isoelectric point.[50] Additionally, increased conformational stability at pH 7.4 might slightly impact the film properties. For instance, the soft α-synuclein layer is diffuse and soft with a high percentage of solvation, whereas the rigid lysozyme forms a layer which was densely packed, rigid and has low water content although both proteins have a similar molecular weight.[52] The presented data does not allow any conclusions on the denaturation of the mAb at the interface. While denaturation was not observed at the liquid-air interface,[53] studies on hydrophobic substrates confirmed conformational changes of lysozyme upon adsorption.[54]

The addition of NaCl increased adsorbed mAb amounts at both pH levels due to the decrease in Debye length by efficiently reducing the electric potential of the protein molecules for lateral interactions, leading to a smaller effective size.[55] Additionally, the electrostatic screening also decreases the interactions between protein and water which leads to more excluded volume.[56] This in turn may contribute to an increase in packing density.[57–59] Additionally, adsorption rate might also be impacted by hampering attractive interactions.[60]

During pumping the surface is quickly recreated. Protein adsorption is a fast process and difficult to monitor. HS-AFM demonstrated that a PDMS surface was covered with protein in less than 13 s at a protein concentration 10-fold lower than the one utilized in the pumping experiments. Interestingly, the protein film was flat without the clusters seen after static incubation for 10 min. Also, Maruno et al.[10] found the formation of wobbling protein clusters long after the initial superficial film adsorption on glass syringes by HS-AFM.[61] Thus, the protein clusters form at a later stage.

Adsorption is typically driven by a combination of electrostatic interactions and hydrophobic interactions with different contribution. For example, aggregation in stainless steel piston

pumps is electrostatically controlled.[8] In contrast, electrostatic interactions contribute only to a minor extent to the adsorption of lysozyme and other various proteins on indium tin oxide.[62] Time-resolved streaming potential measurements were conducted to gain further insights. Interestingly, we observed fast adsorption irrespective of charge-based net repulsive or attractive electrostatic interactions between mAb and tubing. Thus, the net electric potential seems to play a minor role in adsorption. Adsorbed protein could be removed by a buffer rinse, which is commonly observed on hydrophobic surfaces.[1] At different pH levels, initial adsorption speed increased with increasing electrostatic attraction. This leads to the conclusion that the adsorption speed seems to be governed by overcoming an electrostatic barrier which is favoured at strong attractive forces between oppositely charged species. Adsorption speed is hampered by both net negatively charged species, but local positively charged patches at the protein surface might allow electrostatically driven adsorption. Increasing ionic strength might shield the repulsive electrostatic interactions, increasing adsorption speed.[63] The isoelectric point can be used as an indicator for the overall charge to estimate the potential for electrostatic interactions. Factors that also influence the adsorption to the charged surface are charge regulation within the protein and the presence of charged patches.[64,65] The electrostatic interactions are important for initial adsorption speed, but adsorption at intimate contact to the surface is driven by short term hydrophobic or van der Waals interactions.[63] Overall, our findings can be transferred to other proteins with alike characteristics in hydrophobicity, excess surface charge or local charge patches. These factors, in turn impact the adsorption rate, amount of adsorbed protein and aggregate formation.

To further elucidate the relevance of hydrophobic interactions for the protein adsorption to the tubing, the non-ionic surfactant PS20 was used to shield hydrophobic interactions. Priming the tubing with PS20 led to a reduction of the absolute value of the tubing's zeta potential. This indicates shielding of the superficial charges together with an increase in surface hydrophilicity.[66] Only small amounts of protein loosely attached to the surfactant-primed tubing. Priming the tubing with PS20 close to its critical micelle concentration of 0.006% [w/v][67] could decrease mAb attachment even more effectively. The adsorption rate of the surfactant was even higher than that of the mAb, indicating the smaller PS20 molecules race to the tubing surface and coat it before mAb can adsorb.[68] These results are in line with our previous study where mAb adsorption was effectively reduced and particle formation during pumping substantially decreased in the presence of PS20.[7] The experiments with PS20 substantiate the hypothesis that mAb adsorption on silicone tubing is an interplay of an electrostatically dominated fast initial adsorption phase and hydrophobic interactions driving the final adsorption phase. Extrapolating our results from AFM and streaming potential measurements to the pumping conditions, full surface coverage occurs in less than a second irrespective of

pH and might explain similar total particle concentrations. The results suggest that the difference in size distribution originates from a subsequent build-up of aggregates depending on its colloidal stability after protein film detachment.

6. Conclusion

Our work gives insights into the mechanism of protein adsorption to hydrophobic surfaces and its impact on particle formation during pumping. The adsorption of a monoclonal antibody and its film characterization were performed by AFM and streaming potential measurements. Both methods proved themselves as powerful techniques to monitor the adsorption and morphologic features of the protein film in a high-speed manner. Streaming potential measurements showed that the initial fast adsorption phase is governed by electrostatic interactions between protein molecules and the tubing surface. Protein adsorption also takes place if both components exhibit the same charge, which emphasizes the importance of remaining positively charged patches on the protein surface. In intimate contact with the tubing surface, the short-range hydrophobic interactions control the final attachment. The packing density and the adsorbed amount are influenced by the Debye length, which affects lateral protein-protein interaction, as well as the solvation and conformational stability of the protein. These hydrophobic and electrostatic interactions can successfully be shielded by the use of surfactants, which coat the surface and increase its hydrophilicity. In summary, the adsorption to silicone tubing is a complex interplay between protein-protein and protein-surface interactions of electrostatic and hydrophobic nature. The formulation composition could influence the protein particle concentration especially in the micrometre size range. High ionic strength and a pH close to the isoelectric point foster the formation of aggregates ≥ 25 μm. Overall, the results from the current study emphasize the importance of a mature formulation development to reduce the particle formation upon pumping and all other applications where proteins come into contact with a variety of surfaces in a high shear environment.

7. Acknowledgements

8. References

1.   Marsh RJ, Jones RAL, Sferrazza M. Adsorption and displacement of a globular protein on hydrophilic and hydrophobic surfaces. Colloids Surf B Biointerfaces. 2002;23(1):31-42. doi:10.1016/S0927-7765(01)00204-1

2.   Bergfreund J, Bertsch P, Fischer P. Adsorption of proteins to fluid interfaces: Role of the hydrophobic subphase. J Colloid Interface Sci. 2021;584:411-417. doi:10.1016/j.jcis.2020.09.118

3.   Bergfreund J, Bertsch P, Kuster S, Fischer P. Effect of Oil Hydrophobicity on the Adsorption and Rheology of β-Lactoglobulin at Oil−Water Interfaces. Langmuir. 2018;34(16):4929-4936. doi:10.1021/acs.langmuir.8b00458

4.   Koepf E, Eisele S, Schroeder R, Brezesinski G, Friess W. Notorious but not understood: How liquid-air interfacial stress triggers protein aggregation. Int J Pharm. 2018;537(1-2):202-212. doi:10.1016/j.ijpharm.2017.12.043

5.   Sediq AS, van Duijvenvoorde RB, Jiskoot W, Nejadnik MR. No Touching! Abrasion of Adsorbed Protein Is the Root Cause of Subvisible Particle Formation During Stirring. J Pharm Sci. 2016;105(2):519-529. doi:10.1016/j.xphs.2015.10.003

6.   Maruno T, Watanabe H, Yoneda S, et al. Sweeping of Adsorbed Therapeutic Protein on Prefillable Syringes Promotes Micron Aggregate Generation. J Pharm Sci. 2018;107(6):1521-1529. doi:10.1016/j.xphs.2018.01.021

7.   Deiringer N, Friess W. Proteins on the Rack: Mechanistic Studies on Protein Particle Formation During Peristaltic Pumping. J Pharm Sci. 2022;111(5):1370-1378. doi:10.1016/j.xphs.2022.01.035

8.   Wu H, Randolph TW. Aggregation and Particle Formation During Pumping of an Antibody Formulation Are Controlled by Electrostatic Interactions Between Pump Surfaces and Protein Molecules. J Pharm Sci. 2020;109(4):1473-1482. doi:10.1016/j.xphs.2020.01.023

9.   Mathes JM. Protein Adsorption to Vial Surfaces – Quantification, Structural and Mechanistic Studies. Ludwig-Maximilians-University Munich; 2010.

10.   Denis FA, Hanarp P, Sutherland DS, et al. Protein Adsorption on Model Surfaces with Controlled Nanotopography and Chemistry. Langmuir. 2002;18(3):819-828. doi:10.1021/la011011o

11.   Cordeiro AL, Rückel M, Bartels F, Maitz MF, Renner LD, Werner C. Protein adsorption dynamics to polymer surfaces revisited-A multisystems approach. Biointerphases. 2019;14(5):051005. doi:10.1116/1.5121249

12.   Saller V. Interactions of Formulation as Disposables in Biopharmaceutical Drug Product Manufacturing. Ludwig-Maximilians-University Munich; 2015.

13.   Zhang Z, Orski S, Woys AM, et al. Adsorption of polysorbate 20 and proteins on hydrophobic polystyrene surfaces studied by neutron reflectometry. Colloids Surf B Biointerfaces. 2018;168:94-102. doi:10.1016/j.colsurfb.2018.04.036

14.   Green RJ, Davies J, Davies MC, Roberts CJ, Tendler SJB. Surface plasmon resonance for real time in situ analysis of Protein adsorption to polymer surfaces. Biomoterials. 1997;18(5):405-413. doi:10.1016/S0142-9612(96)00141-X

15.   Peeters JMM, Mulder MH v, Strathmann H. Streaming potential measurements as a characterization method for nanofiltration membranes. Colloids Surf A Physicochem Eng Asp. 1999;150(1-3):247-259. doi:10.1016/S0927-7757(98)00828-0

16.   Norde W, Rouwendal E. Streaming potential measurements as a tool to study protein adsorption kinetics. J Colloid Interface Sci. 1990;139(1):169-176. doi:10.1016/0021-9797(90)90454-V

17.   Payerl C, Bračič M, Zankel A, et al. Nonspecific protein adsorption on cationically modified Lyocell fibers monitored by zeta potential measurements. Carbohydr Polym. 2017;164:49-56. doi:10.1016/j.carbpol.2017.01.088

18.   Totoki S, Yamamoto G, Tsumoto K, Uchiyama S, Fukui K. Quantitative laser diffraction method for the assessment of protein subvisible particles. J Pharm Sci. 2015;104(2):618-626. doi:10.1002/jps.24288

19.   Folzer E, Khan TA, Schmidt R, et al. Determination of the Density of Protein Particles Using a Suspended Microchannel Resonator. J Pharm Sci. 2015;104(12):4034-4040. doi:10.1002/jps.24635

20.   Menzen T, Friess W. Temperature-ramped studies on the aggregation, unfolding, and interaction of a therapeutic monoclonal antibody. J Pharm Sci. 2014;103(2):445-455. doi:10.1002/jps.23827

21.   Svilenov H, Markoja U, Winter G. Isothermal chemical denaturation as a complementary tool to overcome limitations of thermal differential scanning fluorimetry in predicting physical stability of protein formulations. European Journal of Pharmaceutics and Biopharmaceutics. 2018;125:106-113. doi:10.1016/j.ejpb.2018.01.004

22.   Liu H, Chumsae C, Gaza-Bulseco G, Goedken ER. Domain-level stability of an antibody monitored by reduction, differential alkylation, and mass spectrometry analysis. Anal Biochem. 2010;400(2):244-250. doi:10.1016/j.ab.2010.02.004

23.   Sahin E, Grillo AO, Perkins MD, Roberts CJ. Comparative Effects of pH and Ionic Strength on Protein-Protein Interactions, Unfolding, and Aggregation for IgG1 Antibodies. J Pharm Sci. 2010;99(12):4830-4848. doi:10.1002/jps.22198

24.   Xu J, Namanja A, Chan SL, et al. Insights into the Conformation and Self-Association of a Concentrated Monoclonal Antibody using Isothermal Chemical Denaturation and Nuclear Magnetic Resonance. J Pharm Sci. 2021;110(12):3819-3828. doi:10.1016/j.xphs.2021.09.005

25.   Zhou X, Zhang Y, Shi X, Fan D. Preparation, Characterization, and Preliminary Biocompatibility Evaluation of Carbon Ion-Implanted Silicone Rubber. In: Elastomers. InTech; 2017. doi:10.5772/intechopen.69251

26.   Eu B, Cairns A, Ding G, Cao X, Wen ZQ. Direct visualization of protein adsorption to primary containers by gold nanoparticles. J Pharm Sci. 2011;100(5):1663-1670. doi:10.1002/jps.22410

27.   Hollowell P, Li Z, Hu X, et al. Recent Advances in Studying Interfacial Adsorption of Bioengineered Monoclonal Antibodies. Molecules. 2020;25(9):2047. doi:10.3390/molecules25092047

28.   Vázquez-Rey M, Lang DA. Aggregates in monoclonal antibody manufacturing processes. Biotechnol Bioeng. 2011;108(7):1494-1508. doi:10.1002/bit.23155

29.   Cromwell MEM, Hilario E, Jacobson F. Protein aggregation and bioprocessing. AAPS J. 2006;8(3):E572-E579. doi:10.1208/aapsj080366

30.   Her C, Carpenter JF. Effects of Tubing Type, Formulation, and Postpumping Agitation on Nanoparticle and Microparticle Formation in Intravenous Immunoglobulin Solutions Processed With a Peristaltic Filling Pump. J Pharm Sci. 2020;109(1):739-749. doi:10.1016/j.xphs.2019.05.013

31.   Koepf E, Schroeder R, Brezesinski G, Friess W. The missing piece in the puzzle: Prediction of aggregation via the protein-protein interaction parameter A∗2. European Journal of Pharmaceutics and Biopharmaceutics. 2018;128:200-209. doi:10.1016/j.ejpb.2018.04.024

32.   Majhi PR, Ganta RR, Vanam RP, Seyrek E, Giger K, Dubin PL. Electrostatically Driven Protein Aggregation: β -Lactoglobulin at Low Ionic Strength. Langmuir. 2006;22(22):9150-9159. doi:10.1021/la053528w

33.   Roberts D, Keeling R, Tracka M, et al. Specific Ion and Buffer Effects on Protein−Protein Interactions of a Monoclonal Antibody. Mol Pharmaceutics. 2015;12(1):179-193. doi:10.1021/mp500533c

34.   Pindrus MA, Shire SJ, Yadav S, Kalonia DS. The Effect of Low Ionic Strength on Diffusion and Viscosity of Monoclonal Antibodies. Mol Pharm. 2018;15(8):3133-3142. doi:10.1021/acs.molpharmaceut.8b00210

35.   Lehermayr C, Mahler HC, Mäder K, Fischer S. Assessment of net charge and protein-protein interactions of different monoclonal antibodies. J Pharm Sci. 2011;100(7):2551-2562. doi:10.1002/jps.22506

36.   Sorret LL, Dewinter MA, Schwartz DK, Randolph TW. Challenges in Predicting Protein-Protein Interactions from Measurements of Molecular Diffusivity. Biophys J. 2016;111(9):1831-1842. doi:10.1016/j.bpj.2016.09.018

37.   Bee JS, Chiu D, Sawicki S, et al. Monoclonal antibody interactions with micro- and nanoparticles: Adsorption, aggregation, and accelerated stress studies. J Pharm Sci. 2009;98(9):3218-3238. doi:10.1002/jps.21768

38.   Deiringer N, Haase C, Wieland K, Zahler S, Haisch C, Friess W. Finding the Needle in the Haystack: High-Resolution Techniques for Characterization of Mixed Protein Particles Containing Shed Silicone Rubber Particles Generated During Pumping. J Pharm Sci. 2021;110(5):2093-2104. doi:10.1016/j.xphs.2020.12.002

39.   Harris LJ, Skaletsky E, Mcpherson A. Crystallographic Structure of an Intact IgG1 Monoclonal Antibody. J Mol Biol. 1998;275(5):861-872. doi:10.1006/jmbi.1997.1508

40.   Zidar M, Posnjak G, Muševič I, Ravnik M, Kuzman D. Surfaces Affect Screening Reliability in Formulation Development of Biologics. Pharm Res. 2020;37(2):1-11. doi:10.1007/s11095-019-2733-1

41.   Cullen DC, Lowe CR. AFM Studies of Protein Adsorption: 1. Time-Resolved Protein Adsorption to Highly Oriented Pyrolytic Graphite. J Colloid Interface Sci. 1994;166(1):102-108. doi:10.1006/jcis.1994.1276

42.   Kim DT, Blanch HW, Radke CJ. Direct Imaging of Lysozyme Adsorption onto Mica by Atomic Force Microscopy. Langmuir. 2002;18(15):5841-5850. doi:10.1021/la0256331

43.   Kim SH, Kinsella JE. Surface Activity of Food Proteins: Relationships Between Surface Pressure Development, Viscoelasticity of Interfacial Films and Foam Stability of Bovine Serum Albumin. J Food Sci. 1985;50(6):1526-1530.

44.   Shieh IC, Patel AR. Predicting the Agitation-Induced Aggregation of Monoclonal Antibodies Using Surface Tensiometry. Mol Pharm. 2015;12(9):3184-3193. doi:10.1021/acs.molpharmaceut.5b00089

45.   Rao CS, Damodaran S. Is Surface Pressure a Measure of Interfacial Water Activity? Evidence from Protein Adsorption Behavior at Interfaces. Langmuir. 2000;16(24):9468-9477. doi:10.1021/la0007168

46.   Israelachvili J. Intermolecular and Surface Forces. 2nd ed. Academic Press; 1992.

47.   Rühs PA, Scheuble N, Windhab EJ, Mezzenga R, Fischer P. Simultaneous Control of pH and Ionic Strength during Interfacial Rheology of β-Lactoglobulin Fibrils Adsorbed at Liquid/Liquid Interfaces. Langmuir. 2012;28(34):12536-12543. doi:10.1021/la3026705

48.   Dong Y, Laaksonen A, Cao W, Ji X, Lu X. AFM Study of pH-Dependent Adhesion of Single Protein to TiO2 Surface. Adv Mater Interfaces. 2019;6(14):1900411. doi:10.1002/admi.201900411

49.   Bremer MGEG, Duval J, Norde W, Lyklema J. Electrostatic interactions between immunoglobulin (IgG) molecules and a charged sorbent. Colloids Surf A Physicochem Eng Asp. 2004;250(1-3):29-42. doi:10.1016/j.colsurfa.2004.05.026

50.   Demanèche S, Chapel JP, Monrozier LJ, Quiquampoix H. Dissimilar pH-dependent adsorption features of bovine serum albumin and a-chymotrypsin on mica probed by AFM. Colloids Surf B Biointerfaces. 2009;70(2):226-231. doi:10.1016/j.colsurfb.2008.12.036

51.   Höök F, Rodahl M, Kasemo B, Brzezinski P. Structural changes in hemoglobin during adsorption to solid surfaces: Effects of pH, ionic strength, and ligand binding. Proc Natl Acad Sci U S A. 1998;95(21):12271-12276. doi:10.1073/pnas.95.21.12271

52.   Ouberai MM, Xu K, Welland ME. Effect of the interplay between protein and surface on the properties of adsorbed protein layers. Biomaterials. 2014;35(24):6157-6163. doi:10.1016/j.biomaterials.2014.04.012

53.   Koepf E, Schroeder R, Brezesinski G, Friess W. The film tells the story: Physical-chemical characteristics of IgG at the liquid-air interface. European Journal of Pharmaceutics and Biopharmaceutics. 2017;119:396-407. doi:10.1016/j.ejpb.2017.07.006

54.   Sethuraman A, Vedantham G, Imoto T, Przybycien T, Belfort G. Protein unfolding at interfaces: Slow dynamics of α-helix to β-sheet transition. Proteins: Structure, Function and Genetics. 2004;56(4):669-678. doi:10.1002/prot.20183

55.   Jia Y, Liu XY. Self-assembly of protein at aqueous solution surface in correlation to protein crystallization. Appl Phys Lett. 2005;86(2):023903. doi:10.1063/1.1846153

56.   Li Y, Shrestha M, Luo M, et al. Salting Up of Proteins at the Air/Water Interface. Langmuir. 2019;35(43):13815-13820. doi:10.1021/acs.langmuir.9b01901

57.   Rabe M, Verdes D, Zimmermann J, Seeger S. Surface Organization and Cooperativity during Nonspecific Protein Adsorption Events. J Phys Chem B. 2008;112(44):13971-13980. doi:10.1021/jp804532v

58.   Fang F, Szleifer I. Competitive adsorption in model charged protein mixtures: Equilibrium isotherms and kinetics behavior. J Chem Phys. 2003;119(2):1053-1065. doi:10.1063/1.1578992

59.   Maldonado-Valderrama J, Miller R, Fainerman VB, Wilde PJ, Morris VJ. Effect of Gastric Conditions on β-Lactoglobulin Interfacial Networks: Influence of the Oil Phase on Protein Structure. Langmuir. 2010;26(20):15901-15908. doi:10.1021/la102294u

60.   Jones KL, O'Melia CR. Protein and humic acid adsorption onto hydrophilic membrane surfaces: effects of pH and ionic strength. J Memb Sci. 2000;165(1):31-46. doi:10.1016/S0376-7388(99)00218-5

61.   Maruno T, Watanabe H, Yoneda S, et al. Sweeping of Adsorbed Therapeutic Protein on Prefillable Syringes Promotes Micron Aggregate Generation. J Pharm Sci. 2018;107(6):1521-1529. doi:10.1016/j.xphs.2018.01.021

62.   Bos MA, Shervani Z, Anusiem ACI, Giesbers M, Norde W, Kleijn JM. Influence of the electric potential of the interface on the adsorption of proteins. Colloids Surf B Biointerfaces. 1994;3(1-2):91-100. doi:10.1016/0927-7765(93)01109-5

63.   McUmber AC, Randolph TW, Schwartz DK. Electrostatic Interactions Influence Protein Adsorption (but Not Desorption) at the Silica−Aqueous Interface. J Phys Chem Lett. 2015;6(13):2583-2587. doi:10.1021/acs.jpclett.5b00933

64.   Boubeta FM, Soler-Illia GJAA, Tagliazucchi M. Electrostatically Driven Protein Adsorption: Charge Patches versus Charge Regulation. Langmuir. 2018;34(51):15727-15738. doi:10.1021/acs.langmuir.8b03411

65.   Cloutier TK, Sudrik C, Mody N, Hasige SA, Trout BL. Molecular computations of preferential interactions of proline, arginine.HCl, and NaCl with IgG1 antibodies and their impact on aggregation and viscosity. MAbs. 2020;12(1):1816312. doi:10.1080/19420862.2020.1816312

66.   Zimmermann R, Freudenberg U, Schweiß R, Küttner D, Werner C. Hydroxide and hydronium ion adsorption — A survey. Current Opinion in Colliod & Interface Science. 2010;15(3):196-202. doi:10.1016/j.cocis.2010.01.002

67.   Wan LSC, Lee PFS. CMC of Polysorbates. J Pharm Sci. 1974;63(1):136-137. doi:10.1002/jps.2600630136

68.   Kanthe AD, Krause M, Zheng S, et al. Armoring the Interface with Surfactants to Prevent the Adsorption of Monoclonal Antibodies. ACS Appl Mater Interfaces. 2020;12(8):9977-9988. doi:10.1021/acsami.9b21979

9. Supplementary data
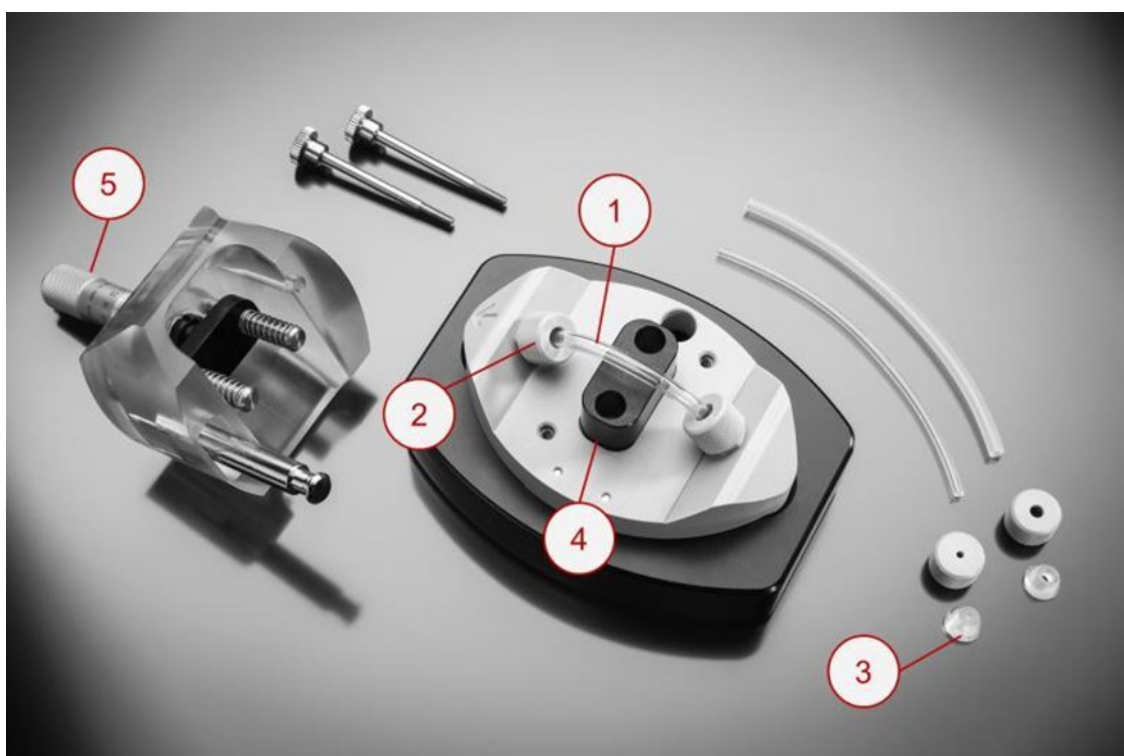
Figure S 1 Measuring Cell for Flexible Tubing for SurPASS 3. The tube sample (1) is fixed on both ends using caps (2) that tighten the inlet and outlet of the tube sample by squeezing silicone gaskets (3). The cross-section of the tube sample is adjusted to comply with the requirements of a reliable streaming potential measurement on a capillary flow channel. The central part of the tube sample is compressed gently by pushing the tube on a pedestal (4) using a micrometer screw (5).
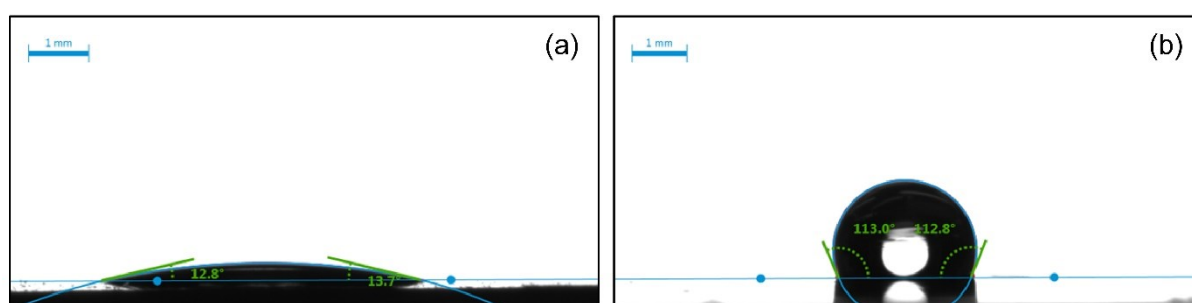
Figure S 2 Contact angle of water on (a) pristine and (b) PDMS coated mica sheets.
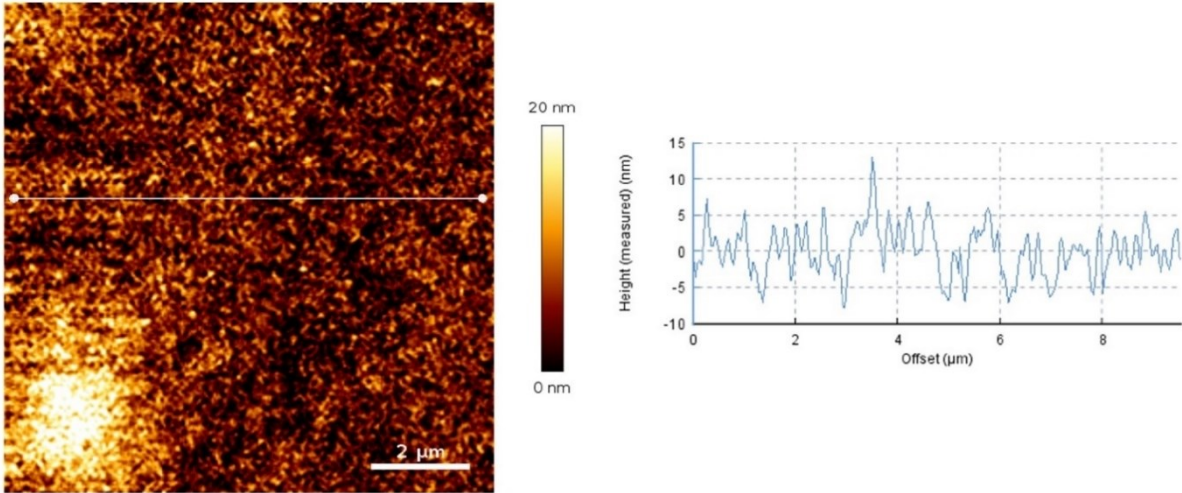
Figure S 3 AFM image of pristine PDMS coated mica sheet. The white line represents the section of the determination of the corresponding height profile.
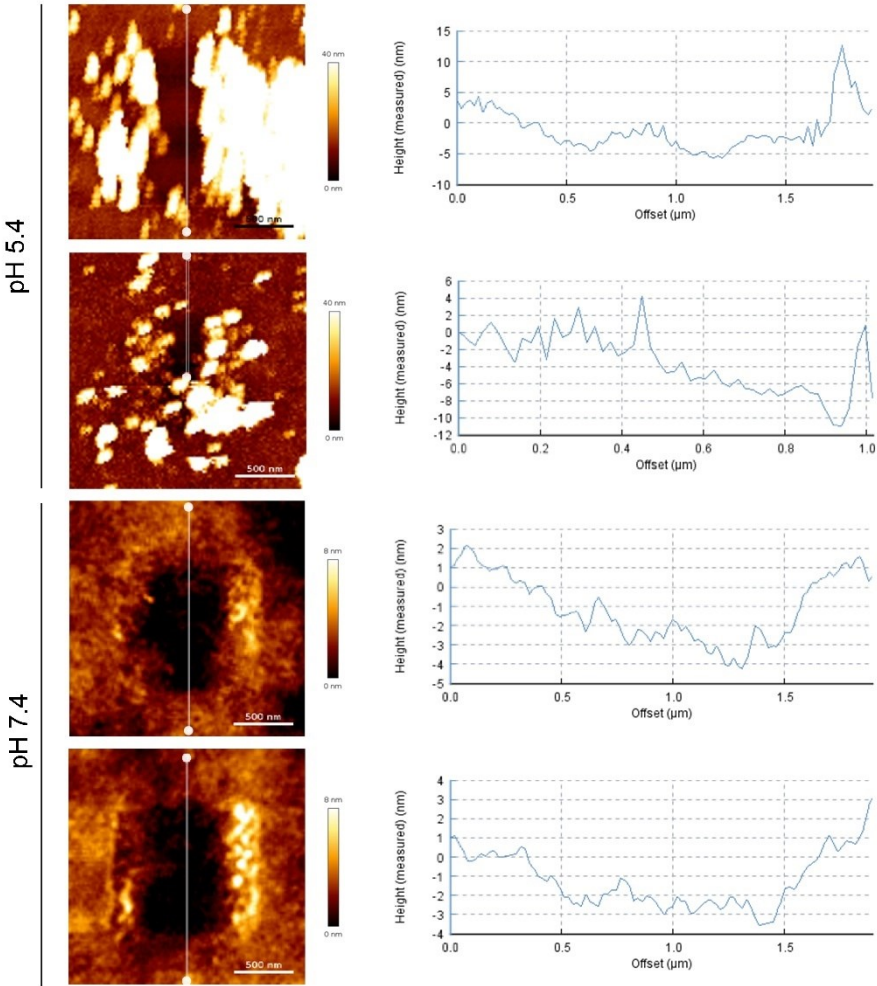
Figure S 4 AFM images of mAb film on PDMS coated mica sheets in 20 mM histidine at pH 5.4 and pH 7.4. The white line represents the section for determination of the height profile.
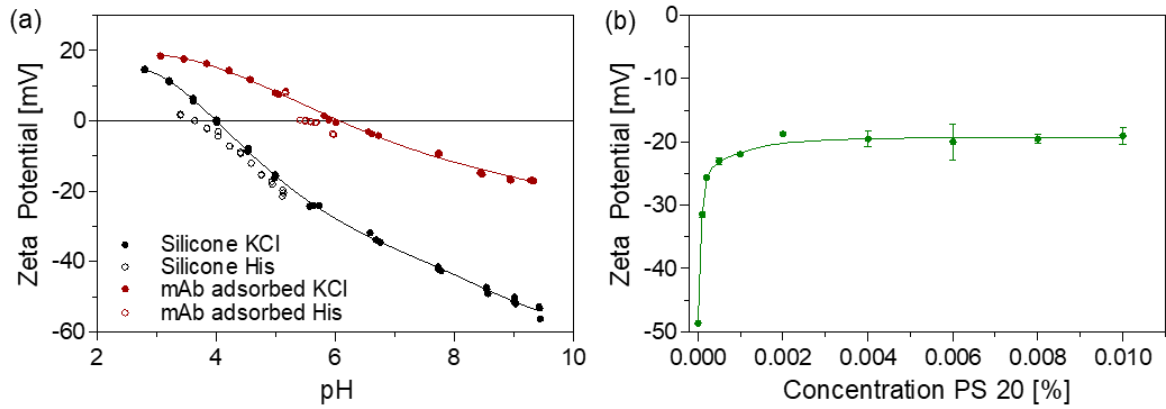
Figure S 5 Zeta potential of (a) silicone tubing with and without preadsorption of mAb in 20 mM histidine and 2.5 mM KCl pH 5.4. (b) Zeta potential of silicone tubing in presence of different PS20 concentrations in 4 mM PBS pH 7.4.
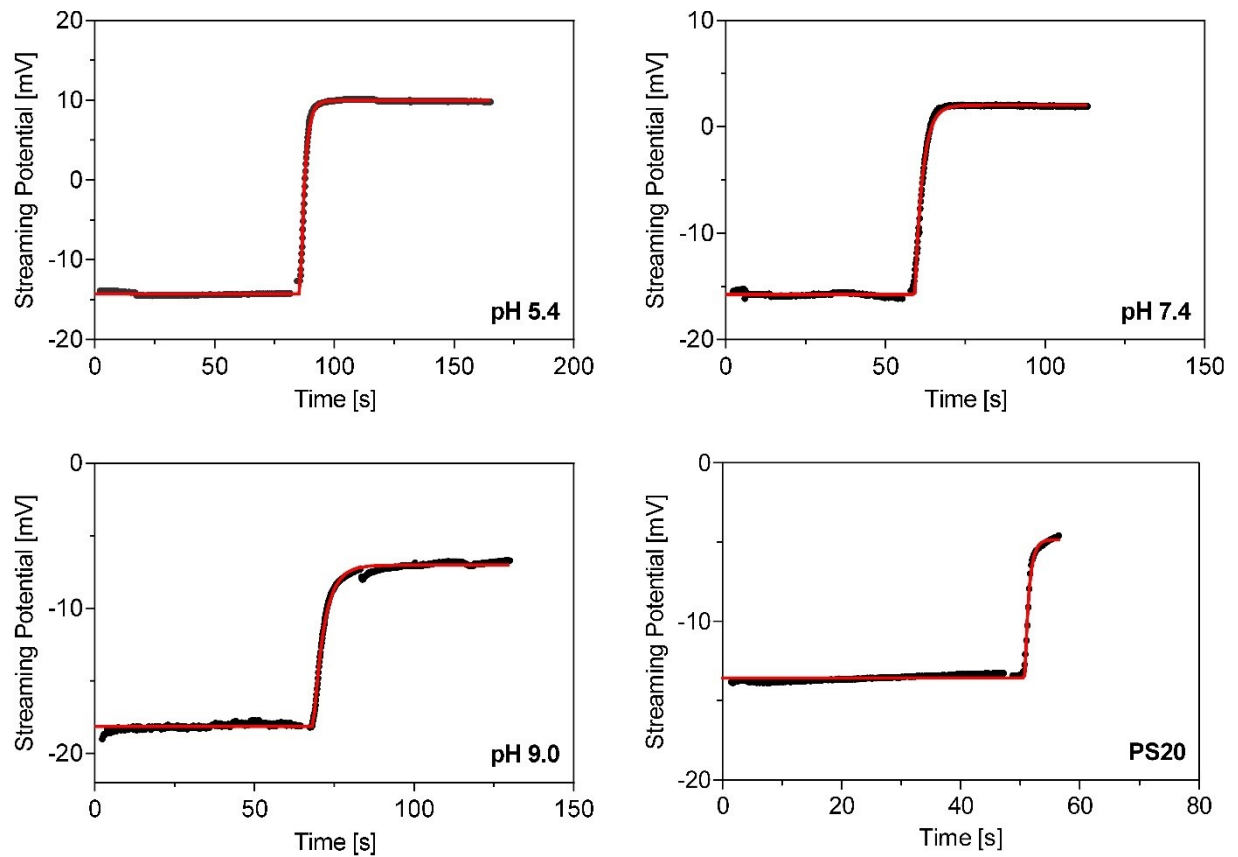
Figure S 6 Fitted experimental data from streaming potential measurements. For pH 9.0 and PS20 only the initial adsorption cycle was fitted.

Chapter VI Reaching the breaking point: Effect of tubing characteristics on protein particle formation during peristaltic pumping

Deiringer N[1] and Friess W[1]. Reaching the breaking point: Effect of tubing characteristics on protein particle formation during peristaltic pumping. Int J Pharm. **2022**; 627: 122216. doi: 10.1016/j.ijpharm.2022.122216.

[1]Department of Pharmacy, Pharmaceutical Technology and Biopharmaceutics, Ludwig-Maximilians-Universität München, Munich, Germany

Author contributions:

N.D. and W.F. conceived and designed the study. N.D. performed all experiments. N.D. analyzed data and wrote the original draft. W.F. revised and edited the manuscript. W.F. supervised the study.

Note from the authors:

The version included in this thesis is identical with the published article apart from minor changes.
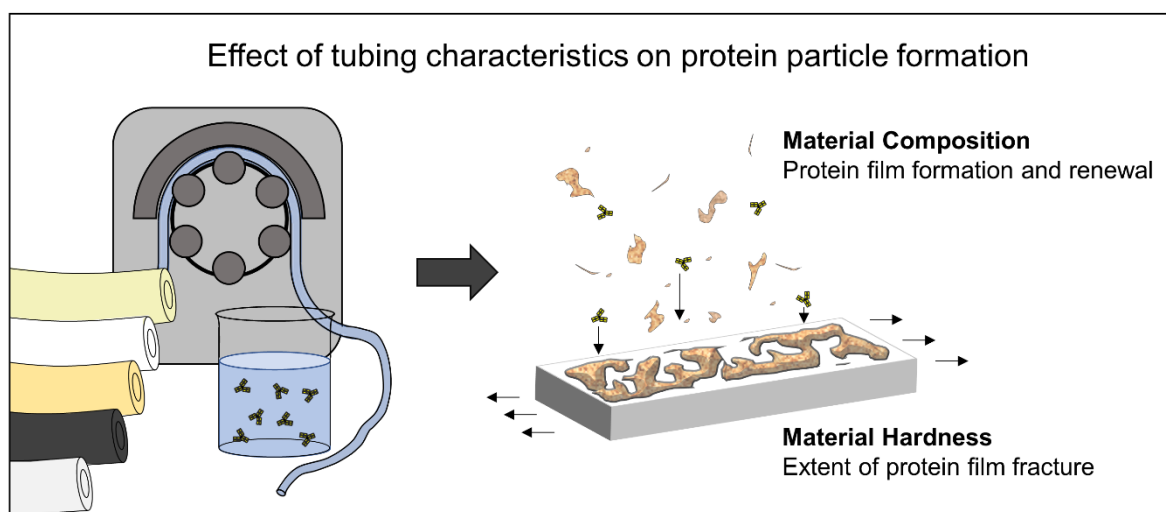
1. Abstract

Peristaltic pumping has been identified as a cause for protein particle formation during manufacturing of biopharmaceuticals. To give advice on tubing selection, we evaluated the physicochemical parameters and the propensity for tubing and protein particle formation using a monoclonal antibody (mAb) for five different tubings. After pumping, particle levels originating from tubing and protein differed substantially between the tubing types. An overall low shedding of tubing particles by wear was linked to low surface roughness and high abrasion resistance. The formation of mAb particles upon pumping was dependent on the tubing hardness and surface chemistry. Defined stretching of tubing filled with mAb solution revealed that aggregation increased with higher strain beyond the breaking point of the protein film adsorbed to the tubing wall. This is in line with the decrease in protein particle concentration with increasing tubing hardness. Furthermore, material composition influenced particle formation propensity. Faster adsorption to materials with higher hydrophobicity is suspected to lead to a higher protein film renewal rate resulting in higher protein particle counts. Overall, silicone tubing with high hardness led to least protein particles during peristaltic pumping. Results from this study emphasize the need of proper tubing selection to minimize protein particle generation upon pumping.

Keywords: protein aggregation, pumping, tubing, protein particles, hydrophobicity, protein adsorption, interface

Abbreviations: 3D-LSM - 3D laser scanning microscopy; DLS - Dynamic light scattering; FNU - formazine nephelometric units; HPW – highly purified water; ID – inner diameter; IFP - interfacial pressure; IFT - interfacial tension; mAb - monoclonal antibody; OD – outer diameter; qLD - quantitative laser diffraction; S_A - mean arithmetic height; SDS - sodium dodecyl sulfate; S_Z - maximum height

2. Introduction

Protein aggregates, in particular larger particles, are a quality and safety concern of biopharmaceuticals.[1–4] Protein aggregation is a complex process involving different pathways including but not limited to unfolding, self-association, interfacial effects and chemical degradation.[5–7] Consequently, risks have to be assessed and measures have to be taken in order to reduce the particle formation during manufacturing. Pumping is an essential unit operation for transfer and filling. In various studies pumping has been identified as a source for protein particle formation.[8–14] For rotary piston and peristaltic pumps it is proposed that aggregation is based on protein adsorption to the pump or tubing surface followed by protein film disruption when in operation.[8,9,12,15] Additionally, stainless steel or rubber particles shed from the equipment are suspected to be nuclei for protein aggregation.[16,17] Silicone particles shed from the tubing can be associated with protein in larger aggregates formed upon peristaltic pumping[18], but did not lead to enhanced protein aggregation during storage at up to 40 °C for up to 6 months.[19]

Nayak et al.[20] found the least protein particle formation by peristaltic pumping comparing different pump setups. The main advantage of peristaltic pumps is the single use of the inserted tubing to avoid extensive cleaning and cross contamination. A limited selection of polymers is available for tubings for peristaltic pumping due to the need for high abrasion resistance and elasticity. Additionally, chemical and migration resistance are required for product safety. Exemplarily, leachables from polyvinyl chloride disposables possess the potential for causing protein aggregation[21] and for adverse effects in patients.[21–24] Another problem associated with tubings is particle shedding from the inner tubing wall due to friction in the pump head. Shed plastic particles may be transferred into the product and impact its quality.[25] Her et al.[13,14] highlighted that the tubing type can affect protein particle formation upon pumping, but the underlying mechanism could not be fully resolved. Knowledge about tubing material properties related to protein aggregation upon pumping would be highly valuable for selection and optimization of tubing for pumping in general and specifically of biologics.

In the current study we want to link tubing properties to the extent of material shedding and protein particle formation upon peristaltic pumping. We studied five chemically and mechanically different types of tubing. The tubings were characterized with respect to surface free energy, surface roughness, indentation force, and tensile strength. In a next step particle formation upon pumping pure buffer and a monoclonal antibody (mAb) solution was analysed via turbidity, flow imaging, and quantitative laser diffraction. These results were flanked by studies of the protein film formed on the inner tubing wall considering both amount and rate of protein adsorption. Finally, the effect of defined stretching of the tubing on protein particle

concentration was evaluated. The combination of the results from the current study should give new insights into the mode of protein particle formation during peristaltic pumping. Thus, we enable advice for the selection of tubing material for handling and manufacturing of protein drugs minimizing the risk of protein particle formation.

3. Materials and Methods

3.1. Materials

For pumping studies, a mAb in 20 mM histidine buffer pH 5.4 was used. Buffer ingredients were dissolved in highly purified (HPW) from an arium® pro DI Ultrapure Water System (Sartorius Stedim Biotech GmbH, Goettingen, Germany) and pH was adjusted either with hydrochloric acid (VWR, Darmstadt, Germany) or sodium hydroxide (Bernd Kraft GmbH, Duisburg, Germany). Finally, the buffer was filtered using pressurized nitrogen and 0.2 µm cellulose acetate filters (47 mm ø, Sartorius Stedim Biotech GmbH). Protein concentration was verified by UV absorption at 280 nm using a Nanodrop Micro-Volume UV-Vis spectrometer (Nano Drop 2000, Thermo Scientific, Wilmington, USA) at the protein specific extinction coefficient of 1.51 m^2/mg. Prior to experiments, the protein sample was filtered with 0.2 µm polyethersulfone membrane syringe filters (VWR International GmbH, Ismaning, Germany).

Tubing materials used are stated in Table 1. Each tubing material was available with an inner diameter (ID)/outer diameter (OD) ratio of 1.6 mm/ 4.8 mm and approximately 6.0 mm/ 10.0 mm. Chemicals were obtained as follows: histidine from Applichem (Darmstadt, Germany); ethylene glycol, hexadecane and sodium dihydrogen phosphate from Merck (Darmstadt, Germany); hexane (puriss, ≥99) and sodium dodecyl sulfate (SDS) from Sigma Aldrich (Steinheim Germany); perfluorohexane from Thermofisher (Kandel, Germany); silicone oil 100 cst from Optimal Products (Bad Oeynhausen, Germany).

Table 1 Specifications of tubings used in pumping studies.

Abbreviation	Material	Shore A hardness
SiR	Silicone rubber, pt-cured, post-cured	55 - 65
FKM	Fluoroelastomer (Viton®)	~ 60
TPV	vulcanized alloy consisting of ethylene propylene diene monomer rubber in a thermoplastic matrix of polypropylene (Santoprene®)	65 ± 5
ePTFE-SiR	composite of expanded PTFE and pt-cured silicone	85 ± 10
ePTFE-FKM	composite of expanded PTFE and pt-cured perfluoro-elastomer	85 ± 10

3.2. Sample preparation

Pumping experiments were conducted under a laminar air flow cabinet to avoid external particle contamination. Occlusion pressure of the Flexicon PD12 peristaltic pump (Watson-Marlow Flexicon, Ringsted, Denmark) was adjusted with the 6.0 mm ID/ 10.2 mm OD silicone tubing to approximately 1.3 bar upon operation in air (accuracy class 2.5 manometer from WIKA Alexander Wiegand SE & Co. KG, Klingenberg, Germany). The setting led to a gap

width of 3 mm. Tubing sets were cleaned and assembled as previously described.[9] For experiments the 1.6 mm ID/ 4.8 mm OD tubing set was inserted in the pump head. First 6 ml of buffer followed by 6 ml of 1 mg/mL mAb solution were circulated 20 times in continuous mode at 180 rpm with an acceleration of 60. Experiments were performed in triplicates with new tubing sets.

3.3. Detection of particles

Samples of 1.8 mL were examined for turbidity using a Nephla turbidimeter (Dr. Lange, Duesseldorf, Germany). Data is presented in formazine nephelometric units (FNU).

For estimation of particle size distribution and total particle amount, the samples were analysed with quantitative laser diffraction (qLD). Protein particles were analyzed in a batch cell with a total sample volume of 5 mL using the Aggregates Sizer with WingSALD bio software version 3.2.2 (Shimadzu Corporation, Kyoto, Japan). Particles were calculated based on a material specific refractive index of 1.46, an imaginary index of 0.1[26] and a protein particle density of 1.32 g/cm^3 [27] with a cut-off level of noise of 500. Pumped buffer and freshly filtrated samples did not show any detectable signal.

Samples were additionally analyzed with a FlowCAM® 8100 (Fluid Imaging Technologies, Inc., Scarborough, ME, USA) equipped with a 10x magnification cell (81 µm × 700 µm) with the following settings: sample volume of 150 µl; flow rate of 0.15 ml/min; auto image frame rate of 28 frames/s and a sampling time of 60 s. Settings resulted in an efficiency value higher than 70%. Particle identification was based on a 3 µm distance to the nearest neighbour, particle segmentation thresholds of 13 and 10 for the dark and light pixels respectively. Particle sizes are presented as the equivalent spherical diameter from VisualSpreadsheet® 4.7.6 software.

3.4. Dynamic light scattering

Dynamic light scattering (DLS) measurements were performed in 384-well plates (Corning, New York, US) using a DynaPro plate reader (Wyatt Technologies, Santa Barbara, US). Each well was measured with 5 acquisitions of 5 seconds at 25 °C. Resulting data was analysed with the DYNAMICS software using a viscosity of 0.891 mPa·s and a refractive index of 1.333.

3.5. Contact angle measurements

To evaluate surface free energy of the tubing material (~ 6.0 mm ID), 5 µl of each test liquid was placed on the inner surface of a tubing. The contact angle was measured using a Kruess Drop Shape Analyzer DSA25 (Kruess GmbH, Hamburg, Germany) via sessile drop method. The curved baseline was manually adjusted and the drop was fitted by the circle method. Each drop was measured 20 s after the drop formation with 1 s delay between measurements over 3 s. To obtain the surface free energy, the Owens-Wendt-Rabel-Kaelble analysis was performed by the ADVANCE software v1.1.0.2 based on the test liquids surface tension parameters of water, ethylene glycol and hexadecane.

3.6. 3D laser scanning microscopy

Surface roughness of the inner tubing walls (1.6 mm ID/ 4.8 mm OD) was determined using a Keyence VK-X200 (3D-LSM) equipped with a CF Plan ELWD 50x objective (Keyence GmbH, Neu-Isenburg, Germany). Two micrographs of small tubing pieces which were captured with the VK Viewer software in 'Expert Mode' at the standard settings were stitched. Three representative regions of 100 x 100 µm^2 were used for surface roughness calculations by the MultiFileAnalyzer version 1.3.1.120. Before evaluation tubing curvature was corrected via the correct tilt – sec curved surface function and artefacts were eliminated by a medium height cut level. Data for 6.0 mm ID tubings can be found in the supplementary information.

3.7. Texture analysis experiments

The indentation force of the tubing material (1.6 mm ID/ 4.8 mm OD) was determined with a Texture Analyser (TA.XT plus, Stable Micro Systems, Godalming, UK) equipped with a cylindrical test probe with a diameter of 12.7 mm. The indentation force was measured at an indentation depth of 1 mm at a pre-test speed of 1.0 mm/s and test speed of 2.0 mm/s. Tubing pieces which were within and outside of the pump head were evaluated after pumping studies.

The tensile strength of tubing material was analyzed similar to DIN:EN ISO 527-3 guideline. A 70 mm long tubing piece (1.6 mm ID/ 4.8 mm OD) was fixed to the Texture Analyser leading to 50 mm tubing length in the gap for stretching. The tubing was stretched with a speed of 1.2 mm/min. Stress is calculated based on the cross-sectional area of the tubing. A prestress of 0.05 N/mm^2 was used to guarantee sufficient stretching and reproducibility between measurements.

Disruption of the protein film by shear was simulated with a 130 mm tubing piece (~ 6.0 mm ID) filled with 1 mg/mL mAb in 20 mM histidine pH 5.4, sealed with silicone stoppers and fixed with clamps on the Texture Analyser (120 mm tubing in the gap for stretching). Tubing was stretched for 2,000 times at different speed and distance parameters. Protein solution was recovered and analysed for particles.

3.8. Interfacial drop profile analysis

To study protein adsorption behaviour at hydrophobic liquid interfaces, the interfacial tension (IFT) of a hanging drop on a stainless-steel capillary (Ø 2.1 mm) was monitored over 30 minutes with a profile analysis tensiometer (PAT-1, Sinterface Technologies, Ltd., Germany). For experiments involving silicone oil (density: 0.972 g/cm^3) and hexane (density: 0.659 g/cm^3) the optical glass cuvette (Hellma, Müllheim, Germany) was filled with the oil phase. A 50 µl or 20 µl drop mAb solution (c = 1 mg/ml; density: 1.000 g/cm^3) in silicone oil or hexane was formed by the automated syringe. Due to the density difference for the perfluorohexane (density: 1.699 g/cm^3) the setup needed to be inverted. The IFT of a 20 µl drop of perfluorohexane was detected against the 1 mg/mL mAb solution as surrounding medium. Drop images were captured by CCD camera at 1 frame/s. Drop volume, surface area, and IFT were calculated based on the Young–Laplace equation. Results were converted to interfacial pressure (IFP) Π by subtraction of the surface tension against HPW. The initial IFP Π_0 was estimated by the 'two phase association' kinetic model from GraphPad Prism (Version 5.02 for Microsoft Windows, Graph Pad Software, San Diego, USA).

3.9. Adsorbed amount

For the quantification of the protein amount adsorbed to tubing at equilibrium, tubing pieces (~ 6.0 mm ID) were incubated with 1 mL of 2 mg/mL mAb solution for 24 h at room temperature.[9] After removing the incubation solution, inner was rinsed three times with 1 mL of formulation buffer to remove unbound mAb. Subsequently, the adsorbed protein was detached by incubation in desorption buffer (10 mM phosphate buffer pH 7.2 with 145 mM NaCl and 0.05% SDS) for 24 h. The detached protein was subsequently quantified using SEC-HPLC at 210 nm with the desorption buffer as running buffer.

3.10.   Statistical analysis

Data is presented as mean with standard deviation of three independent experiments. Data was evaluated using GraphPad Prism.

4. Results

4.1. Characterization of material properties

We evaluated five different tubing types: a thermoplastic vulcanizate (TPV), silicone rubber (SiR) and fluorine rubber (FKM) without and with an expanded PTFE layer (ePTFE-SiR and ePTFE-FKM). The inner surface structure and roughness which has been shown to be related to tubing particle formation[25] was determined via 3D-LSM (Figure 1a, b). Apart from TPV, all tubings had a smooth surface without any indentations substantiated by low mean arithmetic height (S_A) and the maximum height (S_Z) values. While the inner surface of SiR and FKM showed a rather wave like appearance, ePTFE-SiR and ePTFE-FKM had a honeycomb structure. In contrary, TPV had an irregular and rough surface with deep indentations represented by high S_A and S_Z values. All tubings had nearly no polar contribution (< 0.5 mN/m) to their surface free energy (Figure 1c) emphasizing their hydrophobic character. The surface free energy was lower for FKM based tubing with approximately 15 mN/m compared to approximately 20 mN/m for the other tubing materials.
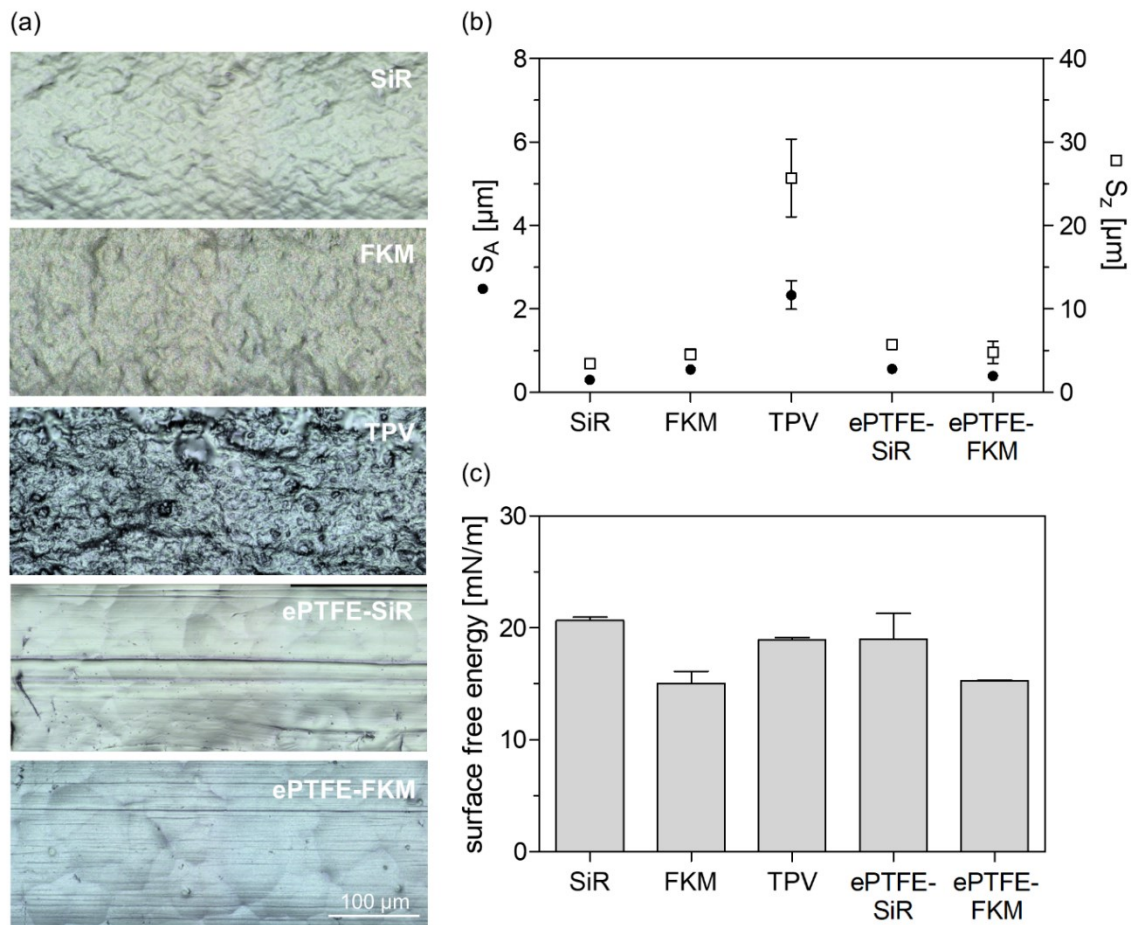
Figure 1 Images from 3D-LSM (a), surface roughness (b) and the dispersive contribution of the surface free energy (polar contributions < 0.5 mN/m) (c) of the different tubing materials.

To test for material fatigue after pumping the indentation force was evaluated for pieces inside and outside of the pump head (Figure 2a). Sections outside the pump head are expected to have the same behaviour as the untreated tubing. Apart from the FKM tubing, all tubings exhibited a decreased indentation force after pumping. The fatigue was most pronounced for TPV with a decrease of indentation force by roughly one third compared to approximately 10% for the remaining tubing types. Additionally, we characterized the mechanical properties of the tubings via the tensile strength (Figure 2b). All tubings ranged in a comparable stress range until approximately 15% strain. Upon further increase in strain, the ePTFE composite materials drastically increased in stress while the remaining materials reached a plateau.
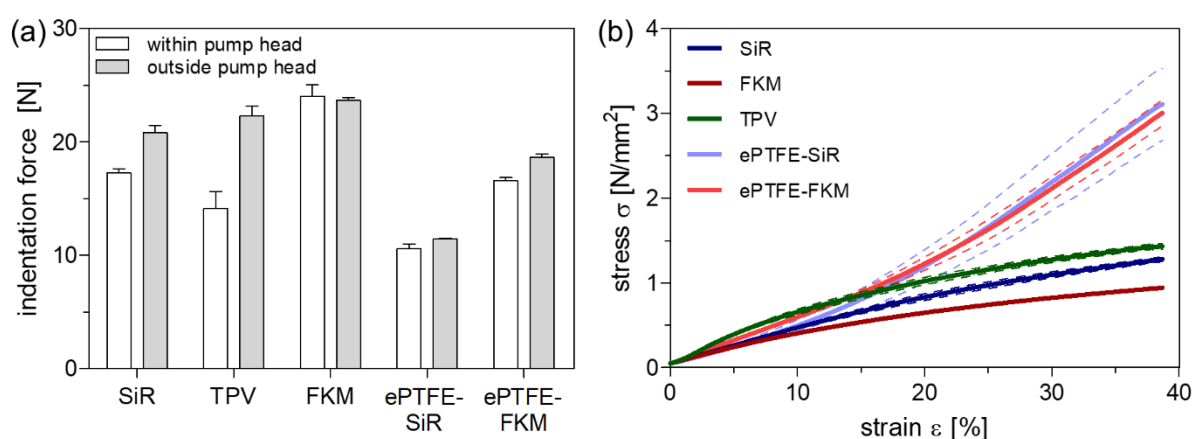
Figure 2 Analysis of tubing resistance during mechanical stress by indentation force (a) and tensile strength (b). Corresponding dashed lines represent standard deviation.

4.2. Particle formation upon pumping

At first, we compared the particle shedding propensity of the tubings pumping buffer (Figure 3; Table S1). Particle levels were low with less than 10,000 particles ≥ 1 µm per mL after 20 passages through the pump head; only with TPV approx. 40,000 were reached. Interestingly, FKM based tubings exhibited a lower particle spallation compared to the silicone-based ones.
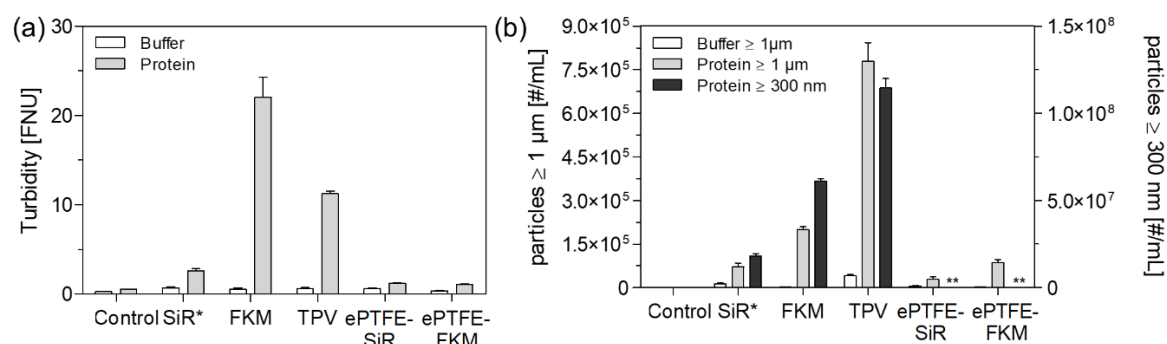
Figure 3 Turbidity (a) and subvisible particle concentration (b) after pumping buffer and 1 mg/mL mAb solution. Control represents freshly filtrated solutions before pumping. *Data from Deiringer and Friess.[9] ** not detectable.

Pumping mAb solution resulted in higher particle concentrations compared to buffer samples. Turbidity measurements, apart from FKM samples, were in line with observations from flow imaging microscopy (FIM) and qLD measurements. The high turbidity value from FKM tubing indicated formation of high amounts of small particles below the detection range of qLD. For particles $\geq$ 1 µm per mL, we observed a trend following ePTFE-SiR < SiR < ePTFE-FKM < FKM < TPV. Composite materials yielded in a lower total protein particle concentration compared to their equivalents. QLD measurements followed the trend depicted by flow imaging microscopy in the non-composite tubings. Particle levels for the composite tubings were below the detection limit of qLD. The presence of small protein aggregates in the samples pumped through the composite materials could be observed with DLS. Protein particle size distribution from FIM after pumping mAb (Table 2) revealed that composite materials trend to formation of fewer but bigger aggregates.

Table 2 Particle size distribution from FIM mAb solution pumped through different tubings. *Data from Deiringer and Friess.[9]

	Particle concentration [#/mL]											
	1 – 5 µm			5 – 10 µm			10 – 25 µm			> 25 µm		
SiR*	67,328	±	11,809	3,223	±	1,429	505	±	229	34	±	50
FKM	185,852	±	7,553	11,684	±	1,855	2,269	±	535	236	±	104
TPV	707,566	±	52,082	58,870	±	10,507	11,531	±	2,851	876	±	294
ePTFE-SiR	21,458	±	6,035	3,606	±	1,287	2,072	±	814	869	±	313
ePTFE-FKM	71,596	±	6,659	9,011	±	1,870	4,834	±	1,522	1,136	±	432

4.3. Characterization of protein film formation

Additionally, the amount of protein adsorbed to the different tubing material was analysed (Figure 4). Significantly more mAb adsorbed to TPV with 5.3 ± 0.3 mg/m^2 compared to approximately 4.0 mg/m^2 for the remaining materials.
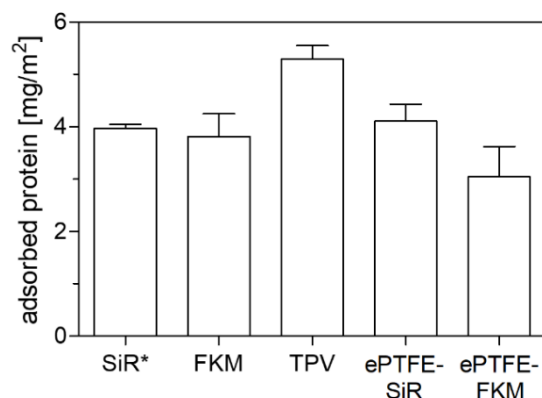
Figure 4 mAb amount adsorbed to different tubing materials. *SiR data from Deiringer and Friess.[9]

We simulated the formation of the mAb film on the different tubing surfaces utilizing silicone oil, hexane, and perfluorohexane as artificial models (Figure 5). The IFT against water increased from 33.0 mN/m for silicone oil, to 54.1 mN/m for hexane and 59.5 mN/m for perfluorohexane corresponding to an increase in hydrophobicity. The difference in subphase polarity makes a direct comparison difficult as the extent of decrease in IFP would be disproportional between polar and apolar oils.[28] The IFP normalized by the initial IFP of the water/oil interface revealed a steep increase from Π_0 by 0.17 ± 0.01 and 0.11 ± 0.02 for hexane and its fluorinated analogue, respectively. In presence of mAb the IFP increased without lag phase. Normalized IFP values at 30 min (Π_{30}) for hexane even increased to 0.43 ± 0.01 compared to 0.33 ± 0.02 for perfluorohexane. The mAb/silicone oil interface had the lowest normalized IFP Π_0 of 0.03 ± 0.01 which increased to Π_{30} of 0.11 ± 0.01.
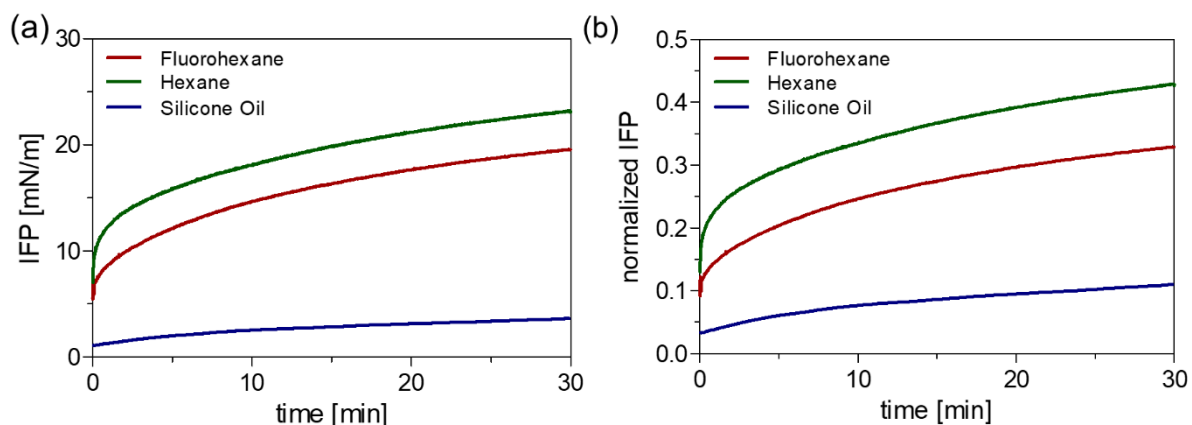
Figure 5 Interfacial pressure profiles (a) and its normalized presentation (b) for 1 mg/mL mAb in 20 mM histidine pH 5.4 in presence of different subphases. Data was normalized against the water baseline for each oil. Silicone oil data from Deiringer et al.[29] Mean from n = 3.

4.4. Protein particle formation during stretching and compression

Repeated stretching of tubings filled with mAb solution outside the pump head led to the formation of protein particles depending on speed, strain, and tubing material (Figure 6). Surface roughness were comparable to the 1.6 mm tubings used during pumping studies (Figure S1). Increasing the speed from 1 (experiment duration t: 70 min) to 4 cm/s (t: 24 min) led to less particle formation (190,378 ± 24,902 vs. 113,165 ± 4,085 ≥ 1 µm per mL). At a strain of 4% (t: 16 min) particle levels did not differ from the unstretched control sample whereas with further increase of the strain to 8% and 13% (t: 32 min) particle levels increased markedly. Particle formation was tubing material dependent. Particle levels were increased to 113,164 ± 4,084 particles ≥ 1 µm per mL for TPV compared to 23,930 ± 7,778 and 41,215 ± 14,112 particles ≥ 1 µm per mL for SiR and FKM, respectively. Composite materials exhibited higher particle levels compared to their equivalents.
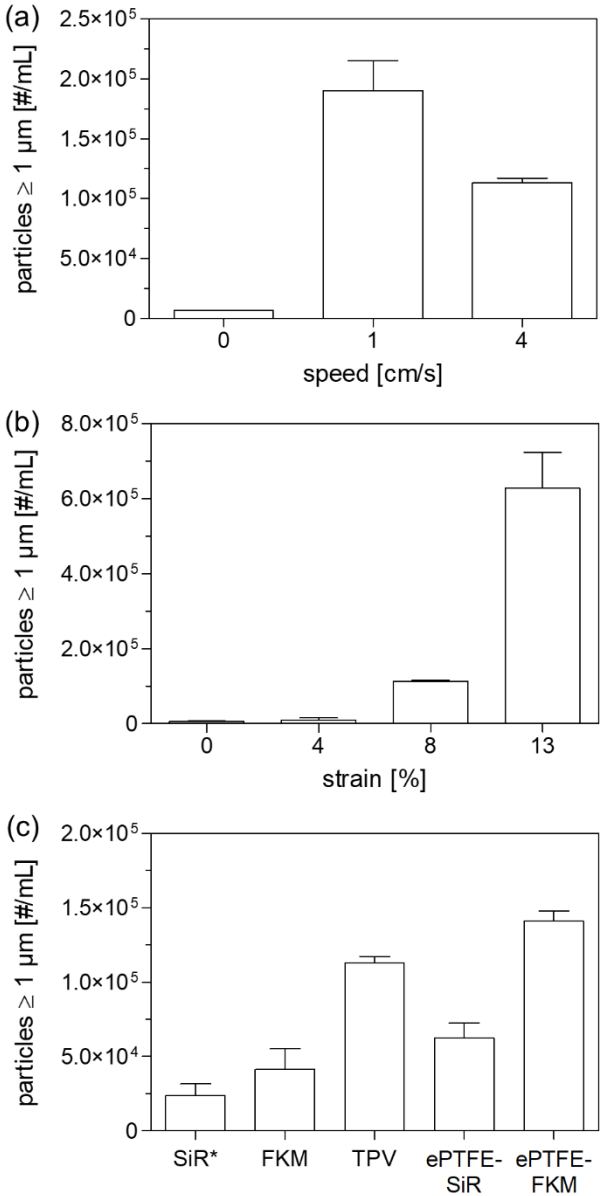
Figure 6 Particle concentration after stretching tubing filled with 1 mg/mL mAb for 2,000 times depending on speed at 8% strain in TPV (a), strain at 4 cm/s in TPV (b) and tubing material at 8% strain and 4 cm/s (c). *SiR data from Deiringer and Friess.[9]

5. Discussion

Peristaltic pumps have been associated with a low risk of protein particle formation.[11,15,20] Our results show that this view must be put into perspective as the type of tubing strongly impacts the formation of protein particles.

We evaluated five different tubings based on three different materials, SiR, FKM, and TPV and ePTFE-SiR and ePTFE-FKM as composite materials with PTFE. All tubings shed plastic particles due to the stress in the pump head. Saller et al.[25] found that the number of shed particles in silicone tubing is related to the surface roughness of the tubing. Although these particles do not necessarily impact mAb stability[18,19] the particle burden is of general concern in for biologics products. Apart from TPV, plastic particle shedding was extremely low with less than 10,000 particles ≥ 1 µm/mL upon 20 pump cycles. The increased particle levels from TPV might be related to its high surface roughness. The very low particle levels of FKM based tubings correspond to its high abrasion resistance.[30,31] Overall, the particle burden from tubing abrasion is negligible compared to the increase in particle levels upon pumping protein.

We previously showed that protein particle formation upon pumping can be linked to protein enrichment at the tubing surface and subsequent rupture of the protein film upon roller movement. Shed film fragments enter the bulk solution.[9] The adsorption process is influenced by the protein characteristics on one hand and the surface properties on the other hand. In a previous study, we found that the adsorption process to silicone tubing was governed by both electrostatic and hydrophobic interactions.[29] Surface properties of the tubing that impact the adsorption are surface hydrophobicity, surface energy, charge and morphology.[32] Tubings have a low surface free energy, with hardly any polar contribution and mainly hydrophobic interactions are expected. The fluorinated carbon structures show a lower surface free energy and higher hydrophobicity compared to hydrocarbon structures due to the greater molecular cross-sectional area of fluorine compared to hydrogen increasing energy penalty for hydration.[33–35] Surface free energy values obtained in this study are in a comparable range to literature values.[36,37] Smaller differences to surface free energy values in literature can originate from differences in surface roughness, chemical heterogeneity, number and type of standard liquids as well as calculation method.[38–42] Despite comparable surface free energy, protein adsorption to TPV was higher compared to SiR based tubing. This effect is most likely linked to the higher surface roughness and thus accessible surface area for TPV.[43,44] However, the amount of adsorbed protein did not correlate with protein particle formation upon pumping. Despite high amounts of protein particles formed, it has been shown that monomer and high molecular species content are typically not significantly affected by pumping.[9,12,14,15,20]

As hydrodynamic shear does not substantially contribute to protein particle formation,[45] mechanical disruption of the protein film plays a key role in protein particle formation.[9] Computational fluid dynamics analyses indicate that the tubing in front and after the moving roller is extensively stretched with the highest shear within the gap of the roller and the pump head.[11,46] Mechanical shear which resembles the stretching and compression of the tubing within the pump head is a complex overlay of three main actions (Figure 7). Firstly, insertion in the pump head leads to a stretching of the outer tubing wall and a compression of the inner wall. Upon motion of the rollers, the tubing is squeezed and thereby transversally and longitudinally stretched. The stretch of the tubing upon insertion and transversal squeezing is fixed by the dimensions of the pump head and the gap width. In contrast, the longitudinal stretching is dependent on the material properties. Manopoulos et al.[47] estimated a maximum deformation of 30% for a silicone tubing in their setup.
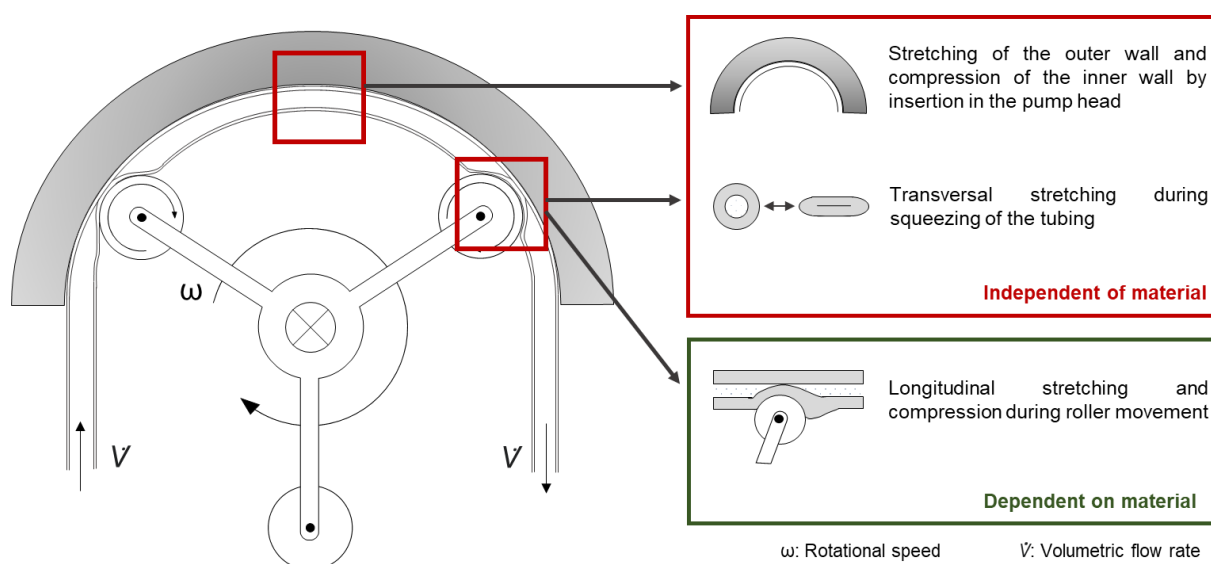
Figure 7 Simplified presentation of the contributors of shear stress on the tubing walls. Figure is inspired by Berg and Dallas.[48]

The isolated longitudinal stretching of the tubing served as simplistic approach for further analysis of the particle formation by film rupture. Increasing the strain beyond 4% resulted in substantial particle formation beyond a level that would be expected from varying the stretching speed. The observations made with tubing are in line with compression studies at the liquid/air interface. Particle formation at the liquid/air interface increased from a certain compression factor on reaching a plateau at higher compression factors.[49,50] The viscoelastic film withstands a certain strain depending on rigidity until reaching the yielding point, breaking up and releasing particles into the bulk. Mechanical properties of the protein film depend on one hand on the protein and one the other hand on the subphase. To the protein end packing density, self-

interaction and intrinsic stability of the individual molecules in the interfacial network play a role.[51–54] To the material end, hardness translates into the strain on the protein film impacting the degree of protein film fragmentation. Thus, tubings with higher tensile strength caused substantially less but bigger particles compared to more flexible tubings. Hardness information provided by the manufacturers fitted well to the observed trend in our tensile strength measurements. Thus, hardness can give an orientation for tubing selection as it may also reflect the tubing wear and potential plastic particle formation upon operation.

Nonetheless, tubing hardness does not explain the higher particle levels for TPV compared to SiR. In literature, the effect of the composition of the surface on particle formation has been striking. Shaking unlubricated prefilled glass and polymer-based syringes yielded in comparable protein particle levels.[55] In contrast, in hydrodynamic flow or friction experiments surface material influenced residual monomer and subvisible particle levels.[12,56,57] Adsorption to the polymer surface is mainly governed by hydrophobicity and surface charge.[58] In the case of silicone tubing, we showed the importance of electrostatic interaction for the initial adsorption speed and of hydrophobic interactions for final attachment and film morphology.[29] We now show by stretching different tubing material at the same strain level that the base polymer affects protein particle concentration. Differences between protein particle formation upon pumping with different tubing materials might be linked to initial protein adsorption speed, network complexity, and adhesion tendency to the surface. These factors increase with subphase hydrophobicity and interfacial energy. Bergfreund et. al.[28] evaluated the influence of different subphase chemistry and hydrophobicity of oils on protein adsorption kinetics and protein film rheology. More apolar oils lead to higher normalized surface pressure values and faster adsorption through structural rearrangement and an increase of network complexity.[28] Protein adsorption speed and normalized surface pressure values for hexane and perfluorohexane were substantially higher compared to the more polar silicone oil. Surprisingly, perflourohexane led to a lower normalized interfacial pressure in presence of protein than hexane despite highest hydrophobicity. This might be attributed to lower interfacial energy of perfluorohexane. These simplistic model oils indicate a dependency of the protein film formation on the chemical composition of the subphase. But one has to be careful transferring the findings for oils 1:1 to tubings due to the substantial differences in polymer chain length, surface heterogeneity, and complexity. Apart from FKM, protein particle formation in stretching experiments followed the trend in adsorption speed depicted by PAT results in both the composite and the non-composite group. Surprisingly, upon defined stretching FKM tubing led to particle levels comparable to SiR tubing despite its higher hydrophobicity. This could result from its fluorine content of 65-67%. The amount of flourine is a poor indicator for hydrophobicity as energy levels depend non-linearly on fluorine content.[59] While fully

fluorinated surfaces exhibit high hydrophobicity, surfaces containing hydrogen and fluorine can increase the surface polarity even beyond the fully hydrogenated surface due to a longer range near-surface electric field.[59] The presence of the ePTFE matrix in the composite group seems to foster protein particle formation even further upon defined stretching. The results from stretching experiments demonstrate that also material composition affects the protein adsorption kinetics in terms of initial adsorption speed as well as the renewal of the protein film after rupture. Interestingly, tubing stretching results suggest that hydrophobic interactions are key for protein particle formation. The results and conclusions from this study can in principle be transferred to linear peristaltic pumps which also cause protein particle formation.[11] Protein particle formation dependent on contact material was as well observed for rotary piston pumps.[8,15,20] Irrespective of pump design which leads to differences in shear stress, flow behaviour and deformation of the contact material, the properties of the contact material itself influence protein particle formation.

Overall, the results indicate that the ePFTE-SiR tubing performed best due to high material stiffness and low interfacial adsorption speed. Nevertheless, a general recommendation on tubing base material is difficult as material features depend on melt composition including base components, polymer additives like stabilizers or processing agents as well as the manufacturing process all defined by manufacturers. Furthermore, at the biotech manufacturing site the tubing choice is also dependent on factors including process requirements, availability, and cost.

6. Conclusion

The choice of tubing for peristaltic pumps is important for controlling protein particle formation during pumping of biopharmaceutics. Overall, the present study identified factors which need to be considered. Plastic particle shedding from the tubing surface depends on surface roughness and abrasion resistance of the material and the levels are negligible compared to protein particles. Protein particle formation is substantially influence by the tubing type and is a combination of material composition and hardness. Tubing hardness impacts the longitudinal stretch during roller movement. Rupture of the protein film adsorbed to the tubing depends on the fracture point of the protein network and the hardness of the tubing. Once the fracture point is reached upon stretching the tubing, total protein particle concentration is negatively correlated to tubing hardness. At the same time high tubing hardness shifts protein particle formation towards bigger particle sizes. Higher hydrophobicity of the tubing material increases protein adsorption speed leading to faster film formation and renewal which correlate with more pronounced protein particle formation. In summary, we recommend choosing the tubing piece within the pump head based on its base material and hardness. In the range of the tested tubings, a composite of expanded PTFE and Pt-cured silicone rubber served as the optimal candidate for pumping biopharmaceuticals. However, tubing choice is a case-to-case decision which has to take many other factors into consideration including costs, process requirements, and leachables.

7. Acknowledgements

8. References

1.   Moussa EM, Panchal JP, Moorthy BS, et al. Immunogenicity of Therapeutic Protein Aggregates. J Pharm Sci. 2016;105(2):417-430. doi:10.1016/j.xphs.2015.11.002

2.   Rosenberg AS. Effects of Protein Aggregates: An Immunologic Perspective. AAPS J. 2006;8(3):E501-E507. doi:10.1208/aapsj080359

3.   USP <788> Particulate matter in injections. In: United States Pharmacopeia. United States Pharmacopeial Convention; 2014.

4.   EP <2.9.19>. Particulate Contamination: Sub-Visible Particles. In: European Pharmacopoeia. 6th ed. European Directorate For The Quality Of Medicine; 2008.

5.   Wang W, Roberts CJ. Protein aggregation – Mechanisms, detection, and control. Int J Pharm. 2018;550(1-2):251-268. doi:10.1016/j.ijpharm.2018.08.043

6.   Wang W, Nema S, Teagarden D. Protein aggregation-Pathways and influencing factors. Int J Pharm. 2010;390(2):89-99. doi:10.1016/j.ijpharm.2010.02.025

7.   Mahler HC, Friess W, Grauschopf U, Kiese S. Protein Aggregation: Pathways, Induction Factors and Analysis. J Pharm Sci. 2009;98(9):2909-2934. doi:10.1002/jps.21566

8.   Wu H, Randolph TW. Aggregation and Particle Formation During Pumping of an Antibody Formulation Are Controlled by Electrostatic Interactions Between Pump Surfaces and Protein Molecules. J Pharm Sci. 2020;109(4):1473-1482. doi:10.1016/j.xphs.2020.01.023

9.   Deiringer N, Friess W. Proteins on the Rack: Mechanistic Studies on Protein Particle Formation During Peristaltic Pumping. J Pharm Sci. 2022;111(5):1370-1378. doi:10.1016/j.xphs.2022.01.035

10.   Gomme PT, Hunt BM, Tatford OC, Johnston A, Bertolini J. Effect of lobe pumping on human albumin: investigating the underlying mechanisms of aggregate formation. Biotechnol Appl Biochem. 2006;43(2):103-111. doi:10.1042/ba20050147

11.   Dreckmann T, Boeuf J, Ludwig IS, Lümkemann J, Huwyler J. Low volume aseptic filling: Impact of pump systems on shear stress. European Journal of Pharmaceutics and Biopharmaceutics. 2020;147:10-18. doi:10.1016/j.ejpb.2019.12.006

12.   Kalonia CK, Heinrich F, Curtis JE, Raman S, Miller MA, Hudson SD. Protein Adsorption and Layer Formation at the Stainless Steel− Solution Interface Mediates Shear-Induced Particle Formation for an IgG1 Monoclonal Antibody. Mol Pharmaceutics. 2018;15(3):1319-1331. doi:10.1021/acs.molpharmaceut.7b01127

13.   Her C, Carpenter JF. Effects of Tubing Type, Formulation, and Postpumping Agitation on Nanoparticle and Microparticle Formation in Intravenous Immunoglobulin Solutions Processed With a Peristaltic Filling Pump. J Pharm Sci. 2020;109(1):739-749. doi:10.1016/j.xphs.2019.05.013

14.   Her C, Tanenbaum LM, Bandi S, et al. Effects of Tubing Type, Operating Parameters, and Surfactants on Particle Formation During Peristaltic Filling Pump Processing of a mAb Formulation. J Pharm Sci. 2020;109(4):1439-1448. doi:10.1016/j.xphs.2020.01.009

15.   Roffi K, Li L, Pantazis J. Adsorbed protein film on pump surfaces leads to particle formation during fill-finish manufacturing. Biotechnol Bioeng. 2021;118(8):2947-2957. doi:10.1002/bit.27801

16.   Tyagi AK, Randolph TW, Dong A, Maloney KM, Hitscherich C, Carpenter JF. IgG particle formation during filling pump operation: A case study of heterogeneous nucleation on stainless steel nanoparticles. J Pharm Sci. 2009;98(1):94-104. doi:10.1002/jps.21419

17.   Bee JS, Davis M, Freund E, Carpenter JF, Randolph TW. Aggregation of a Monoclonal Antibody Induced by Adsorption to Stainless Steel. Biotechnol Bioeng. 2010;105(1):121-129. doi:10.1002/bit.22525

18.   Deiringer N, Haase C, Wieland K, Zahler S, Haisch C, Friess W. Finding the Needle in the Haystack: High-Resolution Techniques for Characterization of Mixed Protein Particles Containing Shed Silicone Rubber Particles Generated During Pumping. J Pharm Sci. 2021;110(5):2093-2104. doi:10.1016/j.xphs.2020.12.002

19.   Saller V, Hediger C, Matilainen J, et al. Influence of particle shedding from silicone tubing on antibody stability. Journal of Pharmacy and Pharmacology. 2018;70(5):675-685. doi:10.1111/jphp.12603

20.   Nayak A, Colandene J, Bradford V, Perkins M. Characterization of subvisible particle formation during the filling pump operation of a monoclonal antibody solution. J Pharm Sci. 2011;100(10):4198-4204. doi:10.1002/jps.22676

21.   Snell JR, Monticello CR, Her C, et al. DEHP Nanodroplets Leached From Polyvinyl Chloride IV Bags Promote Aggregation of IVIG and Activate Complement in Human Serum. J Pharm Sci. 2020;109(1):429-442. doi:10.1016/j.xphs.2019.06.015

22.   Schröter A, Mahler HC, Sayed N ben, Koulov A v., Huwyler J, Jahn M. 4-Hydroxynonenal – A toxic Leachable from clinically used Administration Materials. J Pharm Sci. 2021;110(9):3268-3275. doi:10.1016/j.xphs.2021.05.014

23.   Latini G, Ferri M, Chiellini F. Materials Degradation in PVC Medical Devices, DEHP Leaching and Neonatal Outcomes. Curr Med Chem. 2010;17:2979-2989.

24.   Tickner JA, Schettler T, Guidotti T, Mccally M, Rossi M. Health Risks Posed by Use of Di-2-Ethylhexyl Phthalate (DEHP) in PVC Medical Devices: A Critical Review. Am J Ind Med. 2001;39:100-111.

25.   Saller V, Matilainen J, Grauschopf U, Bechtold-Peters K, Mahler HC, Friess W. Particle Shedding from Peristaltic Pump Tubing in Biopharmaceutical Drug Product Manufacturing. J Pharm Sci. 2015;104(4):1440-1450. doi:10.1002/jps.24357

26.   Totoki S, Yamamoto G, Tsumoto K, Uchiyama S, Fukui K. Quantitative laser diffraction method for the assessment of protein subvisible particles. J Pharm Sci. 2015;104(2):618-626. doi:10.1002/jps.24288

27.   Folzer E, Khan TA, Schmidt R, et al. Determination of the Density of Protein Particles Using a Suspended Microchannel Resonator. J Pharm Sci. 2015;104(12):4034-4040. doi:10.1002/jps.24635

28.   Bergfreund J, Bertsch P, Fischer P. Adsorption of proteins to fluid interfaces: Role of the hydrophobic subphase. J Colloid Interface Sci. 2021;584:411-417. doi:10.1016/j.jcis.2020.09.118

29.   Deiringer N, Rüdiger D, Luxbacher T, Zahler S, Friess W. Catching Speedy Gonzales: Driving forces for Protein Film Formation on Silicone Rubber Tubing During Pumping. J Pharm Sci. 2022;111(6):1577-1586. doi:10.1016/j.xphs.2022.02.013

30.   Colas A, Malczewiski R, Ulmann K. Silicone Tubing for Pharmaceutical Processing. Dow Corning, Life Sciences. Published online 2004:1-9.

31.   Bahal SM, Romansky JM. Spalling and Sorption of Tubing for Peristaltic Pumps. Pharm Dev Technol. 2002;7(3):317-323. doi:10.1081/PDT-120005728

32.   Rabe M, Verdes D, Seeger S. Understanding protein adsorption phenomena at solid surfaces. Adv Colloid Interface Sci. 2011;162(1-2):87-106. doi:10.1016/j.cis.2010.12.007

33.   Dalvi VH, Rossky PJ. Molecular origins of fluorocarbon hydrophobicity. PNAS. 2010;107(31):13603-13607. doi:10.1073/pnas.0915169107

34.   Hayes LJ. Surface Energy of flourinated Surfaces. J Fluor Chem. 1976;8:69-88.

35.   Lee S, Park JS, Lee TR. The Wettability of Fluoropolymer Surfaces: Influence of Surface Dipoles. Langmuir. 2008;24:4817-4826. doi:10.1021/la700902h

36.   Owens DK, Wendt RC. Estimation of the surface free energy of polymers. J Appl Polym Sci. 1969;13(8):1741-1747. doi:10.1002/app.1969.070130815

37.   Al-Assi M, Kassem E. Evaluation of adhesion and hysteresis friction of rubber-pavement system. Applied Sciences . 2017;7(10):1029. doi:10.3390/app7101029

38.   Correia NT, Ramos JJM, Saramago BJ v, Calado JCG. Estimation of the Surface Tension of a Solid: Application to a Liquid Crystalline Polymer. J Colloid Interface Sci. 1997;189:361-369.

39.   Michalski MC, Hardy J, Saramago BJ v. On the Surface Free Energy of PVC/EVA Polymer Blends: Comparison of Different Calculation Methods. J Colloid Interface Sci. 1998;208:319-328.

40.   Wolansky G, Marmur A. Apparent contact angles on rough surfaces: the Wenzel equation revisited. Colloids Surf A Physicochem Eng Asp. 1999;156:381-388.

41.   Kwok DY, Ng H, Neumann AW. Experimental Study on Contact Angle Patterns: Liquid Surface Tensions Less Than Solid Surface Tensions. J Colloid Interface Sci. 2000;225:323-328. doi:10.1006/jcis.2000.6749

42.   Rudawska A, Jacniacka E. Analysis for determining surface free energy uncertainty by the Owen-Wendt method. Int J Adhes Adhes. 2009;29(4):451-457. doi:10.1016/j.ijadhadh.2008.09.008

43.   Rechendorff K, Hovgaard MB, Foss M, Zhdanov VP, Besenbacher F. Enhancement of Protein Adsorption Induced by Surface Roughness. Langmuir. 2006;22(26):10885-10888. doi:10.1021/la0621923

44.   Akkas T, Citak C, Sirkecioglu A, Güner FS. Which is more effective for protein adsorption: surface roughness, surface wettability or swelling? Case study of polyurethane films prepared from castor oil and poly(ethylene glycol). Polym Int. 2013;62(8):1202-1209. doi:10.1002/pi.4408

45.   Thomas CR, Geer D. Effects of shear on proteins in solution. Biotechnol Lett. 2011;33(3):443-456. doi:10.1007/s10529-010-0469-4

46.   Mavrodontis N. Performance assessment of a Peristaltic Pump. Simuleon FEA Blog. Published 2020. Accessed August 12, 2021. https://info.simuleon.com/blog/performance-assessment-of-a-peristaltic-pump

47.   Manopoulos C, Savva G, Tsoukalis A, et al. Optimal design in roller pump system applications for linear infusion. Computation. 2020;8(2):35. doi:10.3390/COMPUTATION8020035

48.	Berg JM, Dallas T. Peristaltic Pumps. In: Li D, ed. Encyclopedia of Microfluidics and Nanofluidics. 2nd ed. Springer Science+Business Media; 2015:2693-2701.

49.	Koepf E, Eisele S, Schroeder R, Brezesinski G, Friess W. Notorious but not understood: How liquid-air interfacial stress triggers protein aggregation. Int J Pharm. 2018;537(1-2):202-212. doi:10.1016/j.ijpharm.2017.12.043

50.	Bee JS, Schwartz DK, Trabelsi S, et al. Production of particles of therapeutic proteins at the air-water interface during compression/dilation cycles. Soft Matter. 2012;8:10329-10335. doi:10.1039/c2sm26184g

51.	Martin AH, Stuart MAC, Bos MA, van Vliet T. Correlation between Mechanical Behavior of Protein Films at the Air/Water Interface and Intrinsic Stability of Protein Molecules. Langmuir. 2005;21:4083-4089. doi:10.1021/la047417t

52.	Lin GL, Pathak JA, Hyun Kim D, et al. Interfacial dilatational deformation accelerates particle formation in monoclonal antibody solutions. Soft Matter. 2016;12(14):3285-3470. doi:10.1039/c5sm02830b

53.	Martin A, Bos M, Cohen Stuart M, van Vliet T. Stress-Strain Curves of Adsorbed Protein Layers at the Air/Water Interface Measured with Surface Shear Rheology. Langmuir. 2002;18:1238-1243. doi:10.1021/la011176x

54.	Bos MA, Grolle K, Kloek W, van Vliet T. Determination of Fracture Stresses of Adsorbed Protein Layers at Air-Water Interfaces. Langmuir. 2003;19:2181-2187. doi:10.1021/la020675a

55.	Krayukhina E, Tsumoto K, Uchiyama S, Fukui K. Effects of syringe material and silicone oil lubrication on the stability of pharmaceutical proteins. J Pharm Sci. 2015;104(2):527-535. doi:10.1002/jps.24184

56.	Grigolato F, Arosio P. Synergistic effects of flow and interfaces on antibody aggregation. Biotechnol Bioeng. 2020;117(2):417-428. doi:10.1002/bit.27212

57.	Brückl L, Hahn R, Sergi M, Scheler S. A systematic evaluation of mechanisms, material effects, and protein-dependent differences on friction-related protein particle formation in formulation and filling steps. Int J Pharm. 2016;511(2):931-945. doi:10.1016/j.ijpharm.2016.08.006

58.	Cordeiro AL, Rückel M, Bartels F, Maitz MF, Renner LD, Werner C. Protein adsorption dynamics to polymer surfaces revisited-A multisystems approach. Biointerphases. 2019;14(5):051005. doi:10.1116/1.5121249

59.   Mayrhofer L, Moras G, Mulakaluri N, Rajagopalan S, Stevens PA, Moseler M. Fluorine-Terminated Diamond Surfaces as Dense Dipole Lattices: The Electrostatic Origin of Polar Hydrophobicity. J Am Chem Soc. 2016;138(12):4018-4028. doi:10.1021/jacs.5b04073

9. Supplementary data

Table S 1 Particle size distribution of pumped buffer depending on tubing type. *Data originates from Deiringer and Friess.[9]

	Particle concentration [#/mL]										
	1 – 5 µm			5 – 10 µm			10 – 25 µm			> 25 µm		
SiR*	6,403	±	2,552	556	±	508	135	±	163	3	±	6
FKM	1,648	±	1,009	181	±	41	97	±	48	37	±	41
TPV	39,642	±	3,122	1,867	±	481	246	±	62	82	±	37
ePTFE-SiR	4,743	±	1,433	571	±	340	177	±	101	54	±	86
ePTFE-FKM	2,063	±	1,209	217	±	46	105	±	62	58	±	12
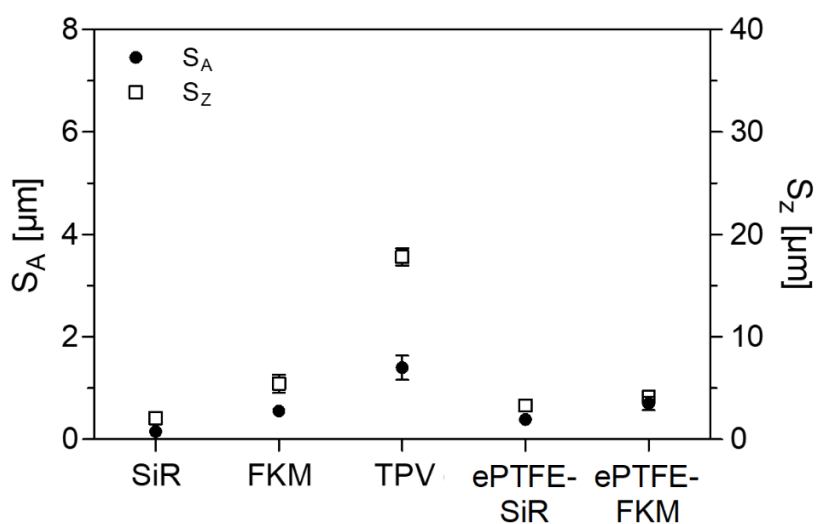
Figure S 1 Determination of surface roughness of the inner wall of 6.0 mm ID tubings.

Chapter VII Afraid of the wall of death? Considerations on monoclonal antibody characteristics that trigger aggregation during peristaltic pumping

Deiringer N[1], and Friess W[1]. Afraid of the wall of death? Considerations on monoclonal antibody characteristics that trigger aggregation during peristaltic pumping. Int J Pharm. **2023**; 633: 122635. doi: 10.1016/j.ijpharm.2023.122635.

[1]Department of Pharmacy, Pharmaceutical Technology and Biopharmaceutics, Ludwig-Maximilians-Universität München, Munich, Germany

Author contributions:

N.D. and W.F. conceived and designed the study. N.D. performed all experiments. N.D. analyzed data and wrote the original draft. W.F. revised and edited the manuscript. W.F. supervised the study.

Note from the authors:

The version included in this thesis is identical with the published article apart from minor changes.
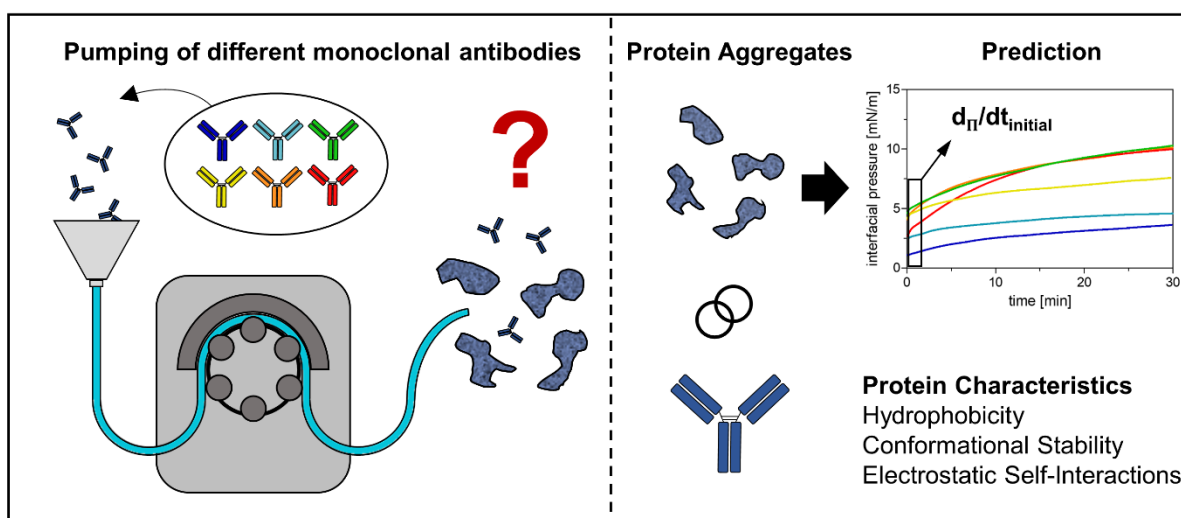
1. Abstract

Protein aggregation is of major concern in manufacturing of biopharmaceutics. Protein aggregation upon peristaltic pumping for filtration, transfer or filling is triggered by protein adsorption to the tubing surface and subsequent film rupture during roller movement. While the impact of tubing type and formulation has been studied in more detail, the contribution of the protein characteristics is not fully resolved. We studied the aggregation propensity of six monoclonal antibodies during peristaltic pumping and characterized their colloidal and conformational stability, hydrophobicity, and surface activity. A high affinity to the surface resulting in faster adsorption and film renewal was key for the formation of protein particles ≥ 1 µm. Film formation and renewal were influenced by the antibody hydrophobicity, potential for electrostatic self-interaction and conformational stability. The initial interfacial pressure increase within the first minute can serve as a good predictor for antibody adsorption and particle formation propensity. Our results highlight the complexity of protein adsorption and emphasize the importance of formulation development to reduce protein particle formation by avoidance of adsorption to interfaces.

Keywords: protein aggregation, pumping, protein adsorption, IgG antibody(s), tubing, subvisible particles, protein formulation, bioprocess development

Abbreviations: FNU – formazine nephelometric unit; HIC – hydrophobic interaction chromatography; HPW – highly purified water; ICD – isothermal chemical denaturation; IEF – isoelectric focusing; qLD – quantitative laser diffraction

2. Introduction

Protein particle formation during manufacturing and storage is critical for quality, safety and efficacy as well as functionality of manufacturing processes.[1,2] Protein aggregates can be associated with an increased potential for immune response and antidrug antibody formation interfering with therapy success.[3] Aggregation mechanisms are manifold and can be triggered by factors like interfacial interactions, temperature or external particles shed from equipment.[4] Specifically, particles that are generated in the very last final filling of drug product may reach the patient and can additionally be seeds for further aggregation.[5,6] A mechanistic understanding of factors triggering aggregation during filling can help to improve the process and ultimately the drug product.

Nayak et al.[7] ranked different pump types based on their protein particle formation propensity. In this context, the piston pump was linked to tremendous protein particle formation while the other pump types were less critical. Peristaltic pumping has also been reported as an origin of protein particle formation of biopharmaceutics in recent publications.[8–10] According to our previous study, peristaltic pumps lead to protein particle formation by rupture of the protein film formed on the tubing surface.[10] We found that protein adsorption to the tubing is driven by electrostatic and hydrophobic interactions resulting in a film formation rate of less than a second.[11] The extent of protein particle formation depends on the tubing material.[8,9,12] We identified material hardness and chemical composition as key factors.[12] These pump studies focused on the aggregation mechanism and the tubing material. The effect of the protein was not investigated in detail, although interfacially triggered aggregation is known to be affected by the protein characteristics as well, specifically shown for the liquid/air interface.[13–16] Exemplary, Shieh and Patel[14] concluded that protein rearrangement and conformational change at the liquid/air interface substantially impact the extent of aggregation. Koepf et al.[13] linked enhanced protein aggregation at the liquid/air interface with more attractive protein-protein interactions. Kumar et al.[17] observed higher levels of insoluble aggregates upon agitation for protein molecules that show stronger hydrophobic interactions. Thus, the identification of protein characteristics that influence protein particle formation upon peristaltic pumping could give additional insights into the aggregation mechanism which supports formulation development and ultimately product quality.

In the current study six monoclonal antibodies (mAbs) were analyzed for their protein particle formation propensity upon peristaltic pumping through silicone tubing. Protein particles in the micrometer and nanometer size range were characterized by turbidity, quantitative laser diffraction (qLD) and flow imaging. We characterized the colloidal and conformational stability, hydrophobicity, interfacial activity by the interaction parameter A_2^*, thermal and isothermal

chemical denaturation using guanidine hydrochloride, hydrophobic interaction chromatography and interfacial drop profile analysis. In addition, the amount of mAb adsorbed on the tubing surface was quantified via an adsorption-desorption assay. We then tried to link the mAb properties with the adsorbed amount and the particle formation propensity.

3. Materials and Methods

3.1. Materials

All reagents and buffer excipients were obtained in analytical grade. Acetic acid was purchased from VWR (Darmstadt, Germany). Ammonium sulphate ((NH4)2SO4) was obtained from Bernd Kraft. Guanidine hydrochloride (Gn·HCl) and sodium chloride (NaCl) were supplied by Merck (Darmstadt, Germany). Methanol and trichloroacetic acid originated from Fluka (Buchs, Switzerland) and Applichem (Darmstadt, Germany), respectively. Sodium dodecyl sulphate (SDS) was obtained from Sigma Aldrich (Darmstadt, Germany).

Protein concentrations were verified via UV absorption at 280 nm using a Nanodrop Micro-Volume UV-Vis spectrometer (Nano Drop 2000, Thermo Scientific, Wilmington, USA) with the protein specific extinction coefficient ranging from 1.49 – 1.70 mL·g-1·cm-1. Formulation buffer was prepared by dissolving histidine (Applichem) in highly purified water (HPW) from an arium® pro DI Ultrapure Water System (Sartorius Stedim Biotech, Goettingen, Germany). After pH adjustment by hydrochloric acid (HCl, VWR), formulation buffer was filtered using pressurized nitrogen and 0.2 μm cellulose acetate filters (47 mm ø, Sartorius Stedim Biotech). Protein formulations were filtered with 0.2 μm polyethersulfone membrane syringe filters (VWR International, Ismaning, Germany).

3.2. Sample preparation

Pt-cured silicone Accusil tubing sets (ID: 1.6 mm, wall thickness: 1.6 mm, Watson-Marlow, Falmouth, United Kingdom) were assembled by connecting two 20 cm long pieces placed in the pump head to 35 cm long pieces via polypropylene Y-connectors (Kartell, VWR International, Darmstadt). Sets were rinsed with 500 ml HPW at 80 °C and steam sterilized (121 °C, 15 min, 2 bar).

All pumping experiments were conducted using a Flexicon PD12 peristaltic pump (Watson-Marlow Flexicon, Ringsted, Denmark) under laminar air flow to avoid external particle contamination. Tubing sets were prerinsed by pumping 5 L HPW in continuous mode at 180 rpm. For sample preparation, 6 mL formulation buffer followed by 6 ml of 1 mg/mL protein solution were circulated for 20 times at 180 rpm at an acceleration of 60 in filling mode (60 x 2 mL; 1 s interval). Pumping experiments were performed three times per mAb with a new tubing set each.

3.3. Turbidity

Sample turbidity was analyzed according to Ph. Eur. 2.2.1 using a Nephla turbidimeter (Dr. Lange, Duesseldorf, Germany) and 1.8 mL sample. Data is presented in formazine nephelometric units (FNU).

3.4. Detection of subvisible particles

Particle size distribution and total particle amount were analyzed using the Aggregates Sizer with WingSALD bio software version 3.2.2 (Shimadzu Corporation, Kyoto, Japan) in a batch cell with 5 mL sample volume. Calculations were based on a a protein particle refractive index of 1.46, an imaginary index of 0.1[18] and density of 1.32 g/cm^3 [19] with a cut-off level of noise of 500. Freshly filtrated samples and pumped buffer exhibited signals below the cut-off level.

Additionally, samples were analysed with a FlowCAM® 8100 (Fluid Imaging Technologies, Inc., Scarborough, ME, USA) with a 10x magnification cell (81 µm × 700 µm) using 150 µl. The settings for image collection (flow rate: 0.15 mL/min, auto image frame rate: 28 frames/s, sampling time: 60 s) resulted in an efficiency value higher than 70%. Particle identification was based on 3 µm distance to the nearest neighbour, particle segmentation thresholds of 13 and 10 for the dark and light pixels respectively. Particle size was reported as the equivalent spherical diameter using VisualSpreadsheet® 4.7.6 software for data collection and analysis.

3.5. Quantification of mAb adsorption

Adsorption of mAb to silicone tubing was determined based on a desorption assay as described previously.[10] Briefly summarized, silicone tubing was filled with 2 mg/mL mAb in 20 mM histidine pH 5.4. After 24 h incubation and washing with formulation buffer, adsorbed mAb was desorbed with desorption buffer (10 mM phosphate buffer pH 7.2 with 145 mM NaCl and 0.05% SDS) for 24 h. Recovered desorbed protein was quantified via high-performance size-exclusion chromatography (HP-SEC) using a 7.8 x 300 mm TSK Gel G3000 SWXL column (Tosoh Bioscience, Stuttgart, Germany) at 210 nm (Agilent 1100 device (Agilent Technologies, Boeblingen, Germany) equipped with a G1314A UV detector at 400 µl injection volume eluting with desorption buffer at 0.7 mL/min. The mAb concentration was calculated based on a mAb specific 8-point calibration curve between 0.0001 and 0.01 mg/mL.

3.6. Hydrophobic interaction chromatography

Hydrophobic interaction chromatography (HIC) analysis was performed on an Agilent 1200 device (Agilent Technologies) with a G1314B UV detector at 280 nm eluting with a gradient elution (buffer A: 20 mM histidine/HCl pH 6 containing 1.5 M $(NH_4)_2SO_4$; buffer B: 20 mM histidine/HCl, pH 6) using a 35 x 4.6 mm TSKgel Butyl-NR column (Tosoh Bioscience) at 25 °C at 1 mL/min. The column was equilibrated for 2 min in 100% buffer A, followed by a linear gradient from 0-100% buffer B until 68 min and 100% buffer A until 74 min. Prior to analysis mAb samples (c = 1 mg/mL) were diluted with buffer A to 0.33 mg/mL, and 20 µg mAb were injected.

3.7. Fluorimetric Analysis of Thermal Protein Unfolding

Standard capillaries filled with 1 mg/mL mAb solution were sealed with sealing paste. The capillaries were analyzed with a Prometheus NT.48 (NanoTemper Technologies, Munich, Germany). Fluorescence intensity at 330 and 350 nm with excitation at 280 nm (± 10 nm) was monitored from 20 to 100 °C at 1 °C/min. Unfolding transitions were derived from the temperature dependent fluorescence intensity ratio (F350/F330) by the maximum of the first derivative using the ThermControl software V2.1 (NanoTemper Technologies, Munich, Germany).

3.8. Isothermal Chemical Denaturation (ICD)

Formulation buffer and denaturant stock (formulation buffer containing 6 M Gn·HCl) were pipetted into a non-binding surface 384 well plate (Greiner) using Viaflo Assist equipped with a 16-channel 125 µL Viaflo pipette (Integra Biosciences, Konstanz, Germany) to prepare the desired denaturant concentrations. Protein sample was added to a final concentration of 1 mg/mL. After manual mixing the well plate was sealed with EASYseal™ sealing film (Steinheim, Germany), incubated for 24 h at room temperature and analyzed with a FLUOstar Omega microplate reader (BMG Labtech, Ortenberg, Germany) (λ_{ex}=280 nm; λ_{em1}= 330 nm and λ_{em2}= 350 nm) in multichromatic mode using 50 flashes per well. The mean of triplicates was autofitted to the biphasic model from Prism (Figure S 1) to derive melting points (C_m).

3.9. Isoelectric Focusing

The isoelectric point (IEP) of the mAbs was determined by isoelectric focusing (IEF) on a Multiphor II™ electrophoresis system with an EPS 3501 XL power supply and a Multitemp III

thermostatic circulator (GE Healthcare, Freiburg, Germany). Protein samples were diluted to 1 mg/mL in 20 mM histidine buffer pH 5.4. A volume of 5 µL of protein samples and protein standard Serva Liquid Mix IEF Marker 3-10 were loaded on the Precast Servalyt® Blank Precotes® electrophoresis gels (125x125x0.3 mm) with a pH gradient from 3 to 10 (Serva Electrophoresis, Heidelberg, Germany). After electrophoresis, the gel was fixed with 20% (w/v) trichloroacetic acid and stained with Serva Violett 17 according to the manufacturer's protocol. Background was destained 4 x 15 min in acetic acid:methanol:HPW (10:40:50 (v/v/v)) and 3 x 5 min in HPW. The gel was scanned in wet state using a ChemiDoc Imaging System (Bio-Rad Laboratories, Feldkirchen, Germany). The IEP values of the mAbs were evaluated based on the position of the marker bands (n = 1).

3.10.   Theoretical charge states of mAbs

Homology models of the different mAbs were generated with BioLuminate (Schrödinger Release 2022-4, Schrödinger LLC, NY) using the antibody prediction module. The protein preparation wizard was used to fill gaps and set the protonation states according to pH 5.4. In addition, a restrained minimization using the OPLS3e force field was performed. Overall charges were calculated with the Protein Surface Analysis module. Debye length λ_D at 298 K was estimated by

$$\lambda_D = \sqrt{\frac{\varepsilon_0 \varepsilon_r k_B T}{2 * 10^3 N_A e^2 I_c}}$$

With ε_0 representing the permittivity of free space, ε_r the dielectric constant of water, k_B the Boltzmann constant, T the absolute temperature, N_A the Avogadro constant, e the elementary charge and I_c the ionic strength of the histidine buffer.

3.11.   Interfacial drop profile analysis

To study the rate of protein adsorption to a silicone oil interface, the volume of an initially 50 µL drop of mAb solution (c = 1 mg/mL) was monitored over 30 minutes via a profile analysis tensiometer (PAT-1, Sinterface Technologies, Ltd., Germany). The drop was formed by the automated syringe with a stainless-steel capillary (Ø 2.1 mm) immersed in silicone oil 100 cst (Optimal Products, Bad Oeynhausen, Germany) filled in a glass cuvette (Hellma, Müllheim, Germany). Drop images were captured by a CCD camera at 1 frame/s and processed (PAT-1 software, Sinterface Technologies) to obtain drop volume, surface area, and interfacial tension

based on the Young–Laplace equation. The density of the mAb solutions was 1.000 g/cm^3 measured by a portable density meter (Anton Paar, Graz, Austria). The density for silicone oil was set to 0.972 g/cm^3. Results were converted to interfacial pressure Π by subtraction of the pure buffer signal. As slight fluctuations impacted the fitting quality and the results were impacted by drop volume adjustment in the first 10 s, the initial rate of interfacial pressure increase was determined from a second order polynomial fit of the LOWESS curve of the mean using 10 points in smoothing window for the timeframe from 11 to 90 s.

3.12.   Dynamic Light Scattering

The interaction parameter k_D was derived by dynamic light scattering. To remove aggregates, mAb solutions in the concentration range between 1 and 8 mg/mL were centrifuged for 10 min at 10,000 G, 25 µl per sample was filled in a 384 microwell plate (Corning) and the plate centrifuged for 2 min at 3,400 G using a Heraeus Megafuge 40 centrifuge equipped with an M-20 well plate rotor (Thermo Fisher Scientific). After centrifugation, silicone oil was used for sealing of the wells to avoid evaporation. After a second centrifugation step, samples were measured using a DynaPro plate reader III (Wyatt Technology, Santa Babara, CA) with 20 acquisitions of 5 s at 25 °C. The interaction parameter k_D was derived from the concentration dependence of the mutual diffusion coefficient D. In a next step, k_D was converted to osmotic second virial coefficient A_2^* using the TIM equation.[20]

3.13.   Statistical analysis

Results are reported as mean values with standard deviation of three samples from three different experiments if not indicated otherwise. Data from interfacial drop profile analysis (n = 2) is presented as mean ± range. Correlation of data sets was evaluated by Pearson's correlation coefficient r_p or Spearman's rank correlation coefficient r_s and respective p-values from a two-tailed test with ns for not significant (p > 0.05), * for p ≤0.05, ** for p ≤ 0.01 and *** for p ≤ 0.001. Data was analyzed using GraphPad Prism (Version 5.02 for Microsoft Windows, Graph Pad Software, San Diego, USA).

4. Results

4.1. Biophysical characterization of the mAbs

Six IgG1 mAbs produced by CHO cells with a molecular weight ranging from 148 to 156 kDa served as models. To get a comprehensive picture of the biophysical characteristics of the mAbs hydrophobicity, IEP, theoretical charge and colloidal stability were determined (Table 1). Hydrophobicity increased from mAb_1 to mAb_6, ranking mAb_1 and mAb_2 as the most hydrophilic ones, mAb_3 as moderate hydrophilic, mAb_4 and mAb_5 as moderate hydrophobic and mAb_6 as hydrophobic. The peaks were asymmetric, had shoulders, mAb_4 peak was rather broad and mAb_6 revealed 4 distinct peaks of different hydrophobicity (Figure S 2). The IEF gel (Figure S 3) showed several bands corresponding to isoforms for each mAb. The IEP values for mAb_{1-5} were above 7.4 with mAb_2 being more basic while mAb_6 had an IEP around 6.5. All mAbs were positively charged at pH 5.4 with theoretical charges ranging from +31 to +15. The Debye length is approximately 2.4 nm in the given buffer conditions.

Table 1 Biophysical parameters of mAb_{1-6}.

	HIC retention time [min]	IEP [pH]	Theoretical charge	A_2^* [mL·mol/g^2]· 10^{-4}
mAb_1	14.6 ± 0.1	8.0 - 8.3	+31	1.1 ± < 0.1**
mAb_2	15.7 ± 0.1	8.3 - 9.5	+28	1.5 ± 0.1
mAb_3	19.5 ± 0.1	7.4 - 8.0	+27	- 1.3 ± < 0.1
mAb_4	29.7 ± 0.1	7.8 - 8.0	+22	0.9 ± 0.1
mAb_5	29.5 ± 0.0	7.4 - 7.8	+25	0.3 ± < 0.1
mAb_6	36.2 ± 0.0*	6.0 - 6.9	+15	- 1.7 ± < 0.1

* Hydrophobic variants at 31.7, 35.2, 38.7 and 42.2 min were averaged based on peak area.
** Data from Deiringer and Friess.[10]

A_2^* derived from the interaction parameter k_D via the TIM equation reflects protein self-interaction which is an important factor of the colloidal stability of the mAbs (Figure 1a). Net repulsive intermolecular interactions were detected for mAb_1, mAb_2 and mAb_4. In contrast, mAb_3 and mAb_6 exhibited significant net attractive interactions. Only marginally net repulsive intermolecular interactions were detected for mAb_5. To rank conformational stability of the mAbs their unfolding behavior in presence of a denaturant and upon temperature increase were monitored. Chemical unfolding with Gn·HCl showed a three-state unfolding behavior for all mAbs (Figure 1b). Specifically, mAb_4 showed a pronounced plateau between both melting points. Resistance to Gn·HCl induced unfolding based on C_{m2} increased in the order $mAb_6 < mAb_5 < mAb_3 < mAb_2 < mAb_1 < mAb_4$ (Table 2). Thermal unfolding curves (Figure 1c) for each mAb were described by the onset temperature of signal increase (T_{onset}) and two melting points T_{m1} and T_{m2} (Table 2). Apart from mAb_5, the mAbs exhibited three-state unfolding

behavior. Unfolding of mAb_5 led to a signal overshooting before reaching a plateau. Interestingly, mAb_3 started to unfold already around 55 °C compared to a T_{onset} of approximately 60 °C for the other mAbs. T_{m1} ranged from approximately 64 to 69 °C and T_{m2} from 79 to 83 °C. No scattering was observed during heating for all mAbs indicating minimal formation of large aggregates.
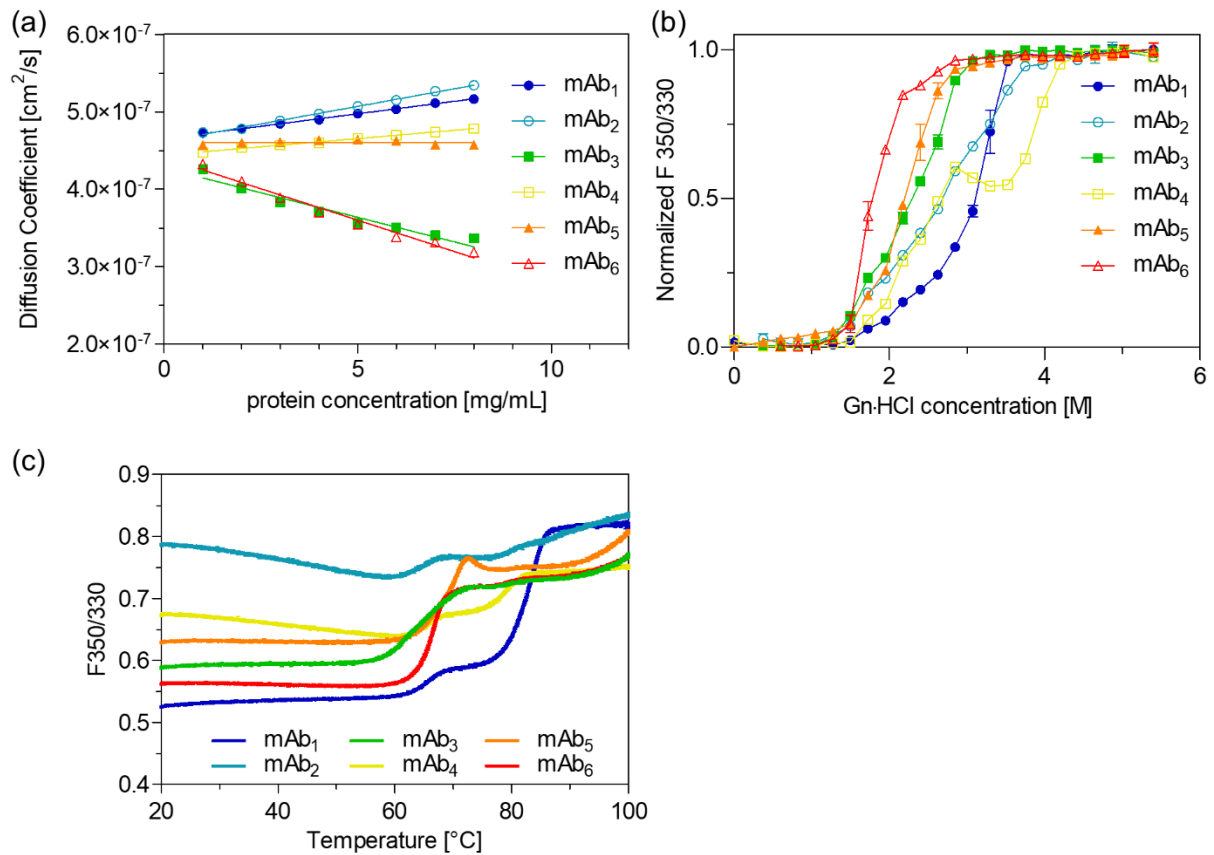
Figure 1 Concentration dependence of the diffusion coefficient for k_D determination (a) and isothermal (b) and thermal (c) unfolding curves of mAb_{1-6}.

Table 2 Thermal and isothermal unfolding of mAb_{1-6}. The 95% lower and 95% upper confidence intervals for C_m values are reported in brackets.

	Temperature [°C]			Concentration Gn·HCl [M]	
	T_{onset}	T_{m1}	T_{m2}	C_{m1}	C_{m2}
mAb_1	60.4 ± 0.2*	65.6 ± 0.1*	82.9 ± 0.1*	2.4 (2.2 - 2.5) **	3.2 (3.2 - 3.3) **
mAb_2	58.7 ± 0.1	64.6 ± 0.0	80.3 ± 0.1	1.8 (1.6 - 2.2)	3.1 (2.9 - 3.2)
mAb_3	55.4 ± 0.1	63.5 ± 0.2	80.1 ± 0.0	2.0 (1.9 - 2.0)	2.7 (2.7 - 2.7)
mAb_4	60.7 ± 0.3	65.7 ± 0.0	79.0 ± 0.0	2.2 (2.2 - 2.2)	3.9 (3.9 - 3.9)
mAb_5	59.8 ± 0.1	69.0 ± 0.0	80.8 ± 0.2	1.9 (1.4 - 2.1)	2.3 (2.2 - 2.3)
mAb_6	59.1 ± 0.1	66.3 ± 0.0	79.3 ± 0.1	1.7 (undefined)	1.9 (1.9 - 2.0)

* Data from Deiringer and Friess.[10]
** Data from Deiringer et al.[11]

4.2. Interfacial adsorption behavior of the mAbs

Silicone oil was used to mimic the silicone tubing surface in kinetic studies of mAb adsorption due to the chemical and structural similarity. For all mAbs the interfacial pressure increased rapidly without a lag phase followed by a flattening of the curve after approximately 5 to 10 min (Figure 2). Mab$_1$ and mAb$_2$ showed a low adsorption tendency with a comparably low initial interfacial pressure increase $d\Pi/dt_{initial}$ of less than 0.4 mN/m/min reaching approximately 4 mN/m after 30 min (Π_{30}) (Table 3). In contrast, mAb$_4$ showed a high interfacial pressure jump within a few seconds followed by a similar $d\Pi/dt_{initial}$ reaching a Π_{30} of approximately 7 mN/m. Although starting from approximately 2 mN/m, interfacial pressure increased rapidly for mAb$_6$ reaching a Π_{30} of approximately 10 mN/m. In comparison, interfacial pressure of mAb$_3$ and mAb$_5$ started from approximately 4 mN/m and reached the same Π_{30} as mAb$_6$.
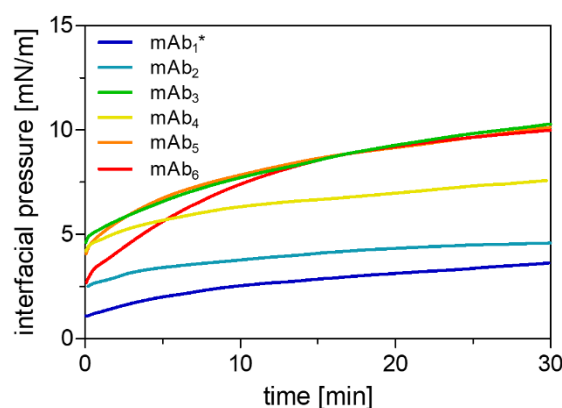
Figure 2 Mean interfacial pressure profiles of the protein solution – silicone oil interface for mAb$_{1-6}$. *Data from Deiringer et al.[11]

Adsorption was additionally characterized by the amount of protein adsorbed per tubing surface area. In equilibrium between approx. 3.5 and 8.0 mg/m^2 were reached. mAb$_6$ showed by far the highest affinity to silicone tubing.

Table 3 Interfacial adsorption behavior of mAb$_{1-6}$.

	Surface activity		mAb adsorbed [mg/m^2]
	$d\Pi/dt_{initial}$ [mN/m/min]	Π_{30} [mN/m]	
mAb$_1$	0.25	3.7 ± 0.4*	4.0 ± 0.1**
mAb$_2$	0.40	4.6 ± 0.3	3.5 ± 0.1
mAb$_3$	0.55	10.3 ± 0.3	5.2 ± 0.0
mAb$_4$	0.50	7.4 ± 0.4	4.6 ± 0.3
mAb$_5$	1.10	10.1 ± 0.1	5.7 ± 0.3
mAb$_6$	1.25	10.0 ± 0.2	7.9 ± 0.7

* Data from Deiringer et al.[11]
** Data from Deiringer and Friess[10]

4.3. Protein particle formation upon pumping

Protein particle formation was monitored by turbidity, flow imaging and qLD. Upon pumping buffer, particle concentrations and turbidity increased from approximately 300 particles to 7,000 ≥ 1 µm per mL and 0.3 to 0.8 FNU (Figure 3). The mAb starting solution showed approximately 0.7 FNU, less than 700 particles ≥ 1 µm per mL and were below the LOD in qLD. For all protein formulations we found substantial particle formation by pumping but to a different extent. After pumping the turbidity values ranged between 3.0 and 7.2 FNU, particles ≥ 1 µm per mL between 130,000 and 560,000 and particles ≥ 300 nm per mL between 23,300,000 and 53,000,000 per mL.
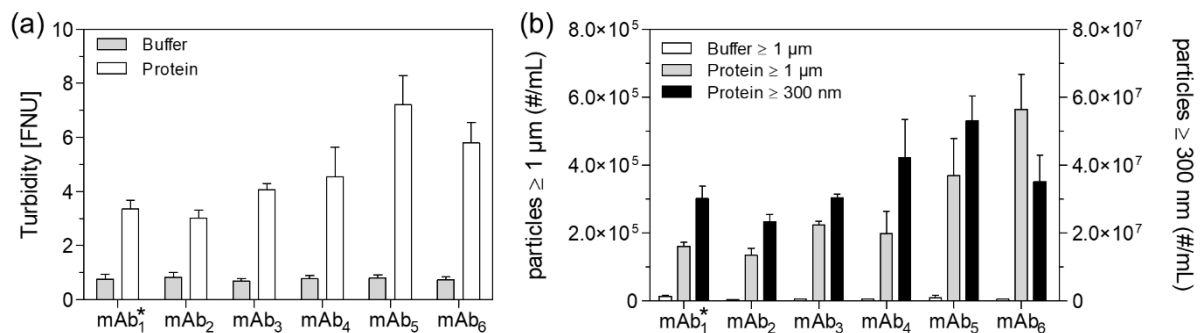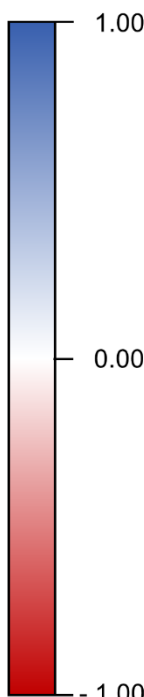
Figure 3 Turbidity (a) and particles ≥ 1 µm per mL and ≥ 300 nm per mL (b) after peristaltic pumping of 1 mg/mL mAb$_{1-6}$. *Data from Deiringer and Friess[10]

4.4. Relationship between protein characteristics, adsorbed amount, and protein particle formation

Based on Pearson's correlation coefficient r_p and p-value we tried to identify mAb characteristics which are key factors for mAb adsorption and particle formation (Figure 4). Adsorption and protein particle formation propensity were ranked against single protein properties (proximity to IEP, hydrophobicity, A_2^* and melting points) and complex descriptors for the adsorption process (dΠ/dt$_{initial}$ and Π_{30}). The adsorbed amount correlated with the proximity of the formulation pH to the IEP. A weaker correlation was detected for theoretical charge, hydrophobicity and A_2^*. While turbidity and particles ≥ 300 nm correlated significantly (r_p = 0.88, p ≤ 0.05), no significant correlation between particles ≥ 1 µm and the other particle descriptors was detected. Only with T$_{m1}$ a weak significant correlation with particles ≥ 300 nm or turbidity was observable in our study. In contrast, the concentration of particles ≥ 1 µm strongly correlated to adsorbed amount and proximity to IEP. Also, hydrophobicity, theoretical charge and conformational stability described by C$_{m2}$ correlated to the concentration of particles ≥ 1 µm but to a lesser degree. While we did not find a significant correlation for Π_{30}

to particle formation, $d\Pi/dt_{initial}$ appeared to be a good predictor for adsorbed amount, turbidity, as well as concentration of particles ≥ 1 µm. To uncover possible nonlinear relationships a rank correlation method was performed. Spearman´s rank correlation coefficient r_s (Figure S 4) confirmed a strong significant monotonic relationship for adsorbed amount and concentration of particles ≥ 1 µm to proximity to IEP ($r_s = -1.00$, $p \leq 0.01$). As well, $d\Pi/dt_{initial}$ could be significantly linked to adsorbed amount and concentration of particles ≥ 1 µm. Interestingly, also a weak monotonic correlation between turbidity and adsorbed amount ($r_s = 0.89$, $p \leq 0.05$) as well as proximity to IEP ($r_s = -0.89$, $p \leq 0.05$) was identified. Furthermore, a weak monotonic correlation between A_2^* and adsorbed amount or concentration of particles ≥ 1 µm was found ($r_s = -0.94$, $p \leq 0.05$).

		Adsorbed amount	Turbidity	Particles ≥ 300 nm	Particles ≥ 1 µm
Adsorbed amount			0.71 ns	0.37 ns	0.98 ***
Proximity to IEP*		-0.97 **	-0.72 ns	-0.47 ns	-0.92 **
Theoretical charge		-0.86 *	-0.56 ns	-0.32 ns	-0.84 *
Hydrophobicity		0.84 *	0.80 ns	0.65 ns	0.84 *
A_2^*		-0.84 *	-0.41 ns	-0.06 ns	-0.73 ns
Chemical unfolding	C_{m1}	-0.55 ns	-0.40 ns	0.00 ns	-0.60 ns
	C_{m2}	-0.78 ns	-0.60 ns	-0.17 ns	-0.82 *
Thermal unfolding	T_{onset}	-0.10 ns	0.18 ns	0.40 ns	0.03 ns
	T_{m1}	0.36 ns	0.84 *	0.85 *	0.50 ns
	T_{m2}	-0.44 ns	-0.27 ns	-0.17 ns	-0.38 ns
Surface activity	$d\Pi/dt_{initial}$	0.92 **	0.88 *	0.57 ns	0.96 ***
	Π_{30}	0.77 ns	0.75 ns	0.54 ns	0.69 ns

Color scale: 1.00 / 0.00 / -1.00

Figure 4 Pearson correlation of mAb properties with adsorbed amount, turbidity, and particle concentration. Color scale reflects trends in Pearson coefficient. *Proximity of formulation pH to IEP was calculated based on the dominant band of IEF gel.

5. Discussion

Aggregation and particle formation during manufacturing and storage of protein pharmaceuticals is a major concern for product quality, safety, and efficacy. Peristaltic pumping has been shown to lead to protein particle formation. Protein molecules adsorb to the tubing surface, forming a film within less than a second[11], which gets ruptured upon roller motion resulting in protein film fragments entering the bulk.[10] A continuous renewal of the film takes place during operation which is impacted by characteristics of the tubing[12], the protein as well as the formulation.[10]

We pumped six mAbs to get a better mechanistic understanding of protein characteristics that influence the film and particle formation. MAb differ in their conformational stability and their potential for self- and interfacial interactions and the behaviour depends on the surrounding environment. This study used mAb concentrations of 1 mg/mL leading to viscosity and flow characteristics close to pure buffer. Higher protein concentrations resulting in increased viscosity and less distance between protein molecules may impact the protein aggregation propensity. The protein particle formation upon peristaltic pumping might on one hand depend on the adsorption process and on the other hand on the fate of the fragments formed upon rupture affected by the bulk formulation properties. Silicone tubing is based on crosslinked polysiloxane associated with surface free energy around 20 mN/m with nearly no polar contribution.[12] Above the IEP around 4.1[11] the tubing surface carries negative charge due to preferential adsorption of hydroxide ions.[21] The adsorption process to silicone tubing is governed by electrostatic and hydrophobic interactions.[11] The total amount adsorbed, and the film formation rate are influenced by different factors like protein-protein interactions, conformational stability, and hydrophobicity.[22–25] The relationship between two variables described by Pearson´s or Spearman´s correlation coefficients confirmed a marked number of strong correlations. We observed a strong correlation between adsorbed amount and proximity of formulation pH to IEP which reflects the Debye length. The Debye length of a protein is important for the protein-protein interactions.[26,27] Near the IEP the Debye length and thus the protein´s effective diameter is minimal. This allows denser packing of the individual protein molecules leading to an increase in the adsorbed protein amount.[27] Specifically for mAb_6 with an IEP close to the formulation pH, reflected by the lowest theoretical charge, showed high adsorption. The calculated theoretical charge correlated less with the adsorbed amount compared to the more general parameter proximity of formulation pH to IEP. In line with observations that protein hydrophobicity is linked to a higher susceptibility of hydrophobic interaction with the surface, hydrophobicity correlated with the adsorbed mAbs amount, but

only slightly.[23] Additionally, attractive protein-protein interactions depicted by a negative A_2^* seem to favour a more compact protein layer.

Upon pumping, the formed film is ruptured and subsequently renewed. During operation, a high potential for interfacial interactions is expected to speed up the renewal and is consequently linked to the particle formation propensity. We studied and quantified different particle size ranges via turbidity, qLD and flow imaging. A high correspondence between turbidity and qLD data is not surprising as both methods quantify signals based on light scattering of the sample. Turbidity and qLD estimate particle concentration by direct measurement of incident scattered light or converting light scattering pattern based on an algorithm to particle concentrations, respectively. The result is impacted by particle size distribution, morphology and in case of qLD the quality of estimators for calculation. In contrast, flow imaging counts the particles and is therefore more precise with respect to the analysis of aggregation propensity. This may explain why we could only find a weak correlation with T_{m1} while the number of particles ≥ 1 µm correlated with several estimators. The flow imaging data strongly correlated with the adsorbed amount emphasizing that the affinity of the mAb to the tubing is a key element for protein particle formation. We described the adsorption rate by $d\Pi/dt_{initial}$, the slope during initial adsorption and Π_{30}, the interfacial pressure after 30 min. The interfacial pressure is a complex descriptor which depends on several protein characteristics like self-interaction, hydrophobicity, and structural stability, and which is not necessarily linked to the adsorbed amount.[14] This explains why the magnitude of Π_{30} did not correlate with particle formation or adsorbed amount. Shieh and Patel[14] identified the $d\Pi/dt_{initial}$ as a semiquantitative predictor for the aggregation propensity of an antibody at the air-liquid interface. This also holds true for the the amount of mAb adsorbed to the tubing as well as turbidity and particle ≥ 1 µm concentration of the mAb solutions after upon pumping. Thus, a higher affinity of the protein to the surface results in the formation of more particles. High levels of adsorption and attractive protein-protein interactions have been linked to more pronounced aggregate formation in presence of silicone oil.[28] In line, Spearman's rank correlation indicated that A_2^* could serve as an estimator for protein particle formation, but not necessarily in a linear manner.

Thus, protein particle formation propensity ≥ 1 µm is linked to the Debye length, the protein hydrophobicity and conformational stability. Low electrostatic hinderance and high hydrophobicity increase the affinity to the tubing. Structurally stable proteins are less prone for surface-induced conformational changes and adsorption to the surface is weaker[29], whereas less structurally stable proteins rearrange more quickly at the interface leading to increased affinity to the surface and interactions with neighboring protein molecules.[22] Low structural stability might explain the high Π_{30} of the rather hydrophilic mAb$_3$ compared to mAb$_1$ and mAb$_2$.

Overall, it is difficult, maybe even impossible, to predict the aggregation tendency of proteins based on only one feature described by a simple estimator. The IEP for example is only a measure of the electrical charge neutrality of the whole structure while ignoring any aggregation prone patches or the distribution of charges on the protein surface. Computational models may help to better understand protein aggregation propensity in the bulk and at interfaces, but these models can still not cover the full complexity of the phenomena.[30–33] Although our sample set was limited to six mAbs, we could get a better understanding of the mechanisms driving protein adsorption and aggregation during peristaltic pumping. Increasing the number of mAbs in various formulation conditions may allow to establish a complex model that combines different estimators to predict protein aggregation at the solid/liquid interface. In addition, we provide some guidance on how to reduce protein particle formation. Key element is avoidance of protein adsorption which can be achieved by addition of surfactants to cover the tubing surface.[11] Additionally, a formulation pH remarkably lower than the IEP increases the Debye length, reduces adsorption and ultimately particle formation; but the pH benefit needs to be balanced with the conformational and the chemical protein stability.

6. Conclusion

This study aimed to link mAb characteristics with protein particle formation propensity in protein solutions upon peristaltic pumping. More attractive protein-protein interactions and higher protein hydrophobicity were found to lead to a higher amount of adsorbed mAb which in return correlated with the number of particles ≥ 1 µm formed. During the pumping process, the renewal rate of the protein film, driven by electrostatic and hydrophobic interactions, plays a dominant role. Additionally, a smaller Debye length reflecting reduced electrostatic protein-protein repulsions could increase the adsorption rate. Furthermore, stronger hydrophobic interactions either of the native protein form or as a result of partial unfolding related to a low conformational stability increases the affinity of the protein to the hydrophobic surface. The initial interfacial pressure increase can serve as a good predictor for surface activity and particle formation propensity. Thus, this study with six different mAbs gives substantial insights into driving forces contributing to protein particle formation upon pumping, and it provides some guidance to avoid this phenomenon and with that improve the quality, safety and efficacy of protein drug products.

7. Acknowledgements

8. References

1.   Vázquez-Rey M, Lang DA. Aggregates in monoclonal antibody manufacturing processes. Biotechnol Bioeng. 2011;108(7):1494-1508. doi:10.1002/bit.23155

2.   Wang W, Singh SK, Li N, Toler MR, King KR, Nema S. Immunogenicity of protein aggregates - Concerns and realities. Int J Pharm. 2012;431(1-2):1-11. doi:10.1016/j.ijpharm.2012.04.040

3.   Moussa EM, Panchal JP, Moorthy BS, et al. Immunogenicity of Therapeutic Protein Aggregates. J Pharm Sci. 2016;105(2):417-430. doi:10.1016/j.xphs.2015.11.002

4.   Philo JS, Arakawa T. Mechanisms of Protein Aggregation. Curr Pharm Biotechnol. 2009;10(4):348-351. doi:10.2174/138920109788488932

5.   Sahin Z, Demir YK, Kayser V. Global kinetic analysis of seeded BSA aggregation. European Journal of Pharmaceutical Sciences. 2016;86:115-124. doi:10.1016/j.ejps.2016.03.007

6.   Gomes D, Kalman RK, Pagels RK, Rodrigues MA, Roberts CJ. Parallel chromatography and in situ scattering to interrogate competing protein aggregation pathways. Protein Science. 2018;27(7):1325-1333. doi:10.1002/pro.3435

7.   Nayak A, Colandene J, Bradford V, Perkins M. Characterization of subvisible particle formation during the filling pump operation of a monoclonal antibody solution. J Pharm Sci. 2011;100(10):4198-4204. doi:10.1002/jps.22676

8.   Her C, Carpenter JF. Effects of Tubing Type, Formulation, and Postpumping Agitation on Nanoparticle and Microparticle Formation in Intravenous Immunoglobulin Solutions Processed With a Peristaltic Filling Pump. J Pharm Sci. 2020;109(1):739-749. doi:10.1016/j.xphs.2019.05.013

9.   Her C, Tanenbaum LM, Bandi S, et al. Effects of Tubing Type, Operating Parameters, and Surfactants on Particle Formation During Peristaltic Filling Pump Processing of a mAb Formulation. J Pharm Sci. 2020;109(4):1439-1448. doi:10.1016/j.xphs.2020.01.009

10.   Deiringer N, Friess W. Proteins on the Rack: Mechanistic Studies on Protein Particle Formation During Peristaltic Pumping. J Pharm Sci. 2022;111(5):1370-1378. doi:10.1016/j.xphs.2022.01.035

11.   Deiringer N, Rüdiger D, Luxbacher T, Zahler S, Friess W. Catching Speedy Gonzales: Driving forces for Protein Film Formation on Silicone Rubber Tubing During Pumping. J Pharm Sci. 2022;111(6):1577-1586. doi:10.1016/j.xphs.2022.02.013

12.   Deiringer N, Friess W. Reaching the breaking point: Effect of tubing characteristics on protein particle formation during peristaltic pumping. Int J Pharm. 2022;627:122216. doi:10.1016/j.ijpharm.2022.122216

13.   Koepf E, Schroeder R, Brezesinski G, Friess W. The missing piece in the puzzle : Prediction of aggregation via the protein-protein interaction parameter A * 2. European Journal of Pharmaceutics and Biopharmaceutics. 2018;128:200-209. doi:10.1016/j.ejpb.2018.04.024

14.   Shieh IC, Patel AR. Predicting the Agitation-Induced Aggregation of Monoclonal Antibodies Using Surface Tensiometry. Mol Pharm. 2015;12(9):3184-3193. doi:10.1021/acs.molpharmaceut.5b00089

15.   Duerkop M, Berger E, Dürauer A, Jungbauer A. Impact of Cavitation, High Shear Stress and Air/Liquid Interfaces on Protein Aggregation. Biotechnol J. 2018;13(7):1800062. doi:10.1002/BIOT.201800062

16.   Maruno T, Watanabe H, Yoneda S, et al. Sweeping of Adsorbed Therapeutic Protein on Prefillable Syringes Promotes Micron Aggregate Generation. J Pharm Sci. 2018;107(6):1521-1529. doi:10.1016/j.xphs.2018.01.021

17.   Kumar V, Dixit N, Zhou L, Fraunhofer W. Impact of short range hydrophobic interactions and long range electrostatic forces on the aggregation kinetics of a monoclonal antibody and a dual-variable domain immunoglobulin at low and high concentrations. Int J Pharm. 2011;421(1):82-93. doi:10.1016/j.ijpharm.2011.09.017

18.   Totoki S, Yamamoto G, Tsumoto K, Uchiyama S, Fukui K. Quantitative laser diffraction method for the assessment of protein subvisible particles. J Pharm Sci. 2015;104(2):618-626. doi:10.1002/jps.24288

19.   Folzer E, Khan TA, Schmidt R, et al. Determination of the Density of Protein Particles Using a Suspended Microchannel Resonator. J Pharm Sci. 2015;104(12):4034-4040. doi:10.1002/jps.24635

20.   Menzen T, Friess W. Temperature-ramped studies on the aggregation, unfolding, and interaction of a therapeutic monoclonal antibody. J Pharm Sci. 2014;103(2):445-455. doi:10.1002/jps.23827

21.   Zimmermann R, Dukhin S, Werner C. Electrokinetic measurements reveal interfacial charge at polymer films caused by simple electrolyte ions. Journal of Physical Chemistry B. 2001;105(36):8544-8549. doi:10.1021/jp004051u

22.   Bergfreund J, Bertsch P, Fischer P. Adsorption of proteins to fluid interfaces: Role of the hydrophobic subphase. J Colloid Interface Sci. 2021;584:411-417. doi:10.1016/j.jcis.2020.09.118

23.   Cordeiro AL, Rückel M, Bartels F, Maitz MF, Renner LD, Werner C. Protein adsorption dynamics to polymer surfaces revisited-A multisystems approach. Biointerphases. 2019;14(5):051005. doi:10.1116/1.5121249

24.   Rabe M, Verdes D, Seeger S. Understanding protein adsorption phenomena at solid surfaces. Adv Colloid Interface Sci. 2011;162(1-2):87-106. doi:10.1016/j.cis.2010.12.007

25.   Norde W. My voyage of discovery to proteins in flatland ...and beyond. Colloids Surf B Biointerfaces. 2008;61(1):1-9. doi:10.1016/j.colsurfb.2007.09.029

26.   Israelachvili J. Intermolecular and Surface Forces. 2nd ed. Academic Press; 1992.

27.   Dong Y, Laaksonen A, Cao W, Ji X, Lu X. AFM Study of pH-Dependent Adhesion of Single Protein to TiO2 Surface. Adv Mater Interfaces. 2019;6(14):1900411. doi:10.1002/admi.201900411

28.   Kannan A, Shieh IC, Negulescu PG, Suja VC, Fuller GG. Adsorption and Aggregation of Monoclonal Antibodies at Silicone Oil−Water Interfaces. Mol Pharmaceutics. 2021;18:1656-1665. doi:10.1021/acs.molpharmaceut.0c01113

29.   Ouberai MM, Xu K, Welland ME. Effect of the interplay between protein and surface on the properties of adsorbed protein layers. Biomaterials. 2014;35(24):6157-6163. doi:10.1016/j.biomaterials.2014.04.012

30.   March D, Bianco V, Franzese G. Protein unfolding and aggregation near a hydrophobic interface. Polymers (Basel). 2021;13(1):1-14. doi:10.3390/polym13010156

31.   Arsiccio A, Mccarty J, Pisano R, Shea JE. Effect of Surfactants on Surface-Induced Denaturation of Proteins: Evidence of an Orientation-Dependent Mechanism. J Phys Chem B. 2018;122(49):11390-11399. doi:10.1021/acs.jpcb.8b07368

32.   Prabakaran R, Rawat P, Thangakani AM, Kumar S, Gromiha MM. Protein aggregation: in silico algorithms and applications. Biophysicl Reviews. 2021;13:71-89. doi:10.1007/s12551-021-00778-w

33.   van der Kant R, Karow-Zwick AR, van Durme J, et al. Prediction and Reduction of the Aggregation of Monoclonal Antibodies. J Mol Biol. 2017;429(8):1244-1261. doi:10.1016/j.jmb.2017.03.014

9. Supplementary data
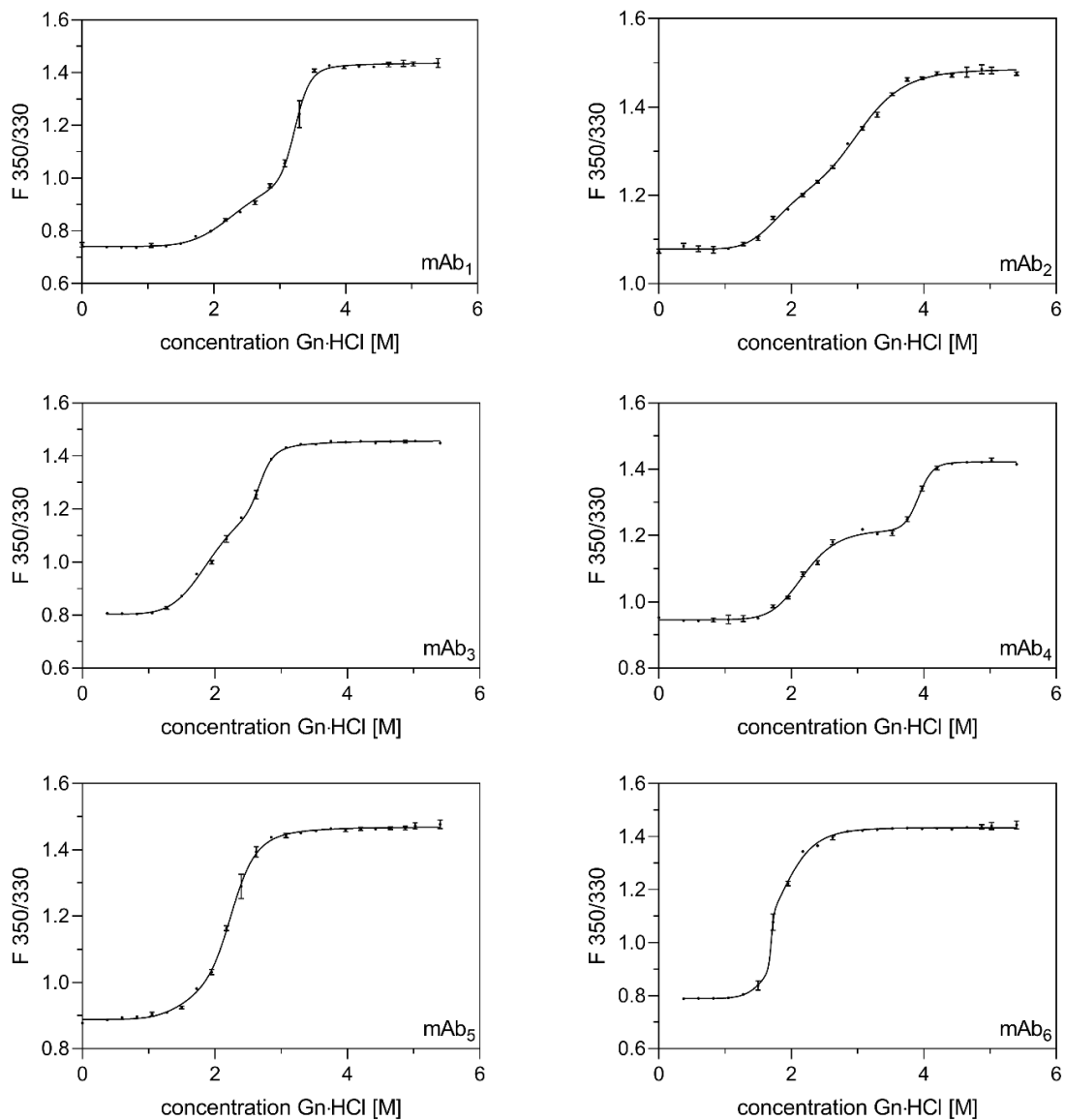
Figure S 1 Fitted raw data from ICD measurements for all mAbs ($R_2 > 0.998$). Note: For mAb_4 the value for 2.85 M was excluded to allow proper fitting of the plateau.
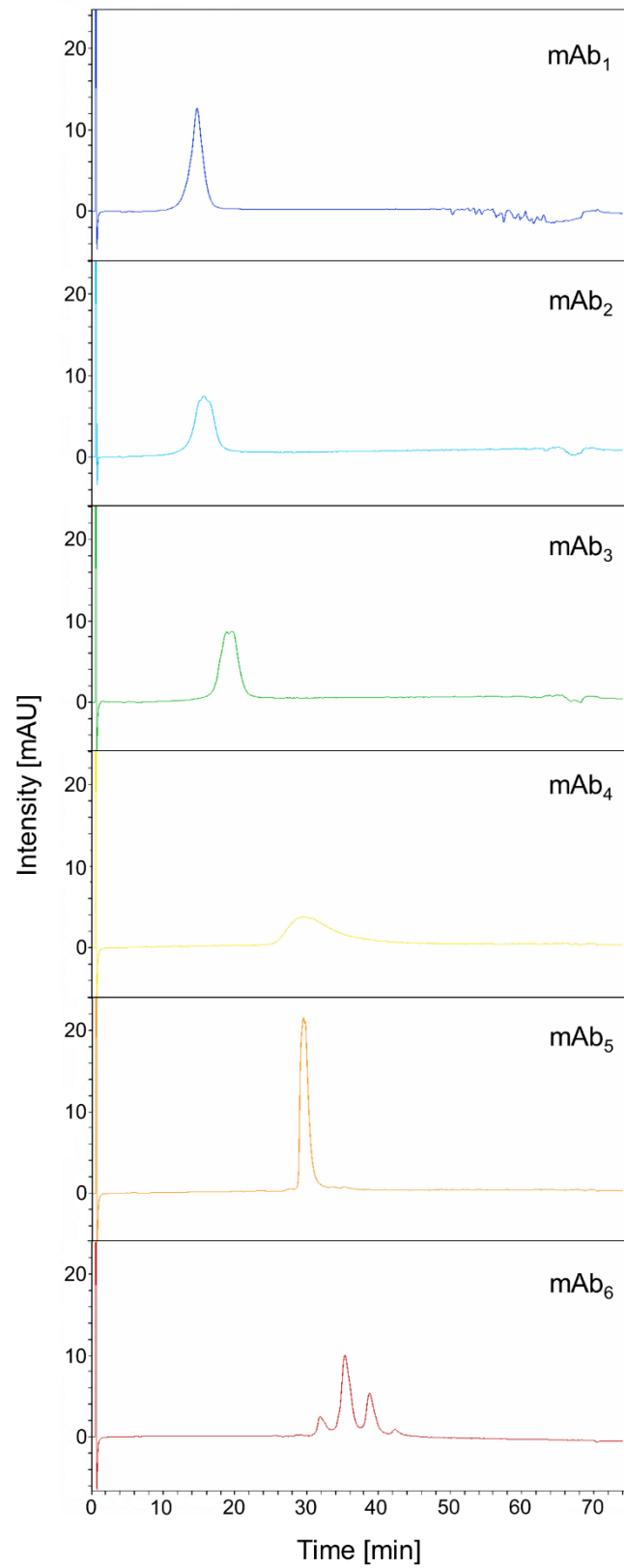
Figure S 2 HIC chromatograms for hydrophobicity ranking of mAbs. Signals are shown between − 6 mAU and 24 mAU.
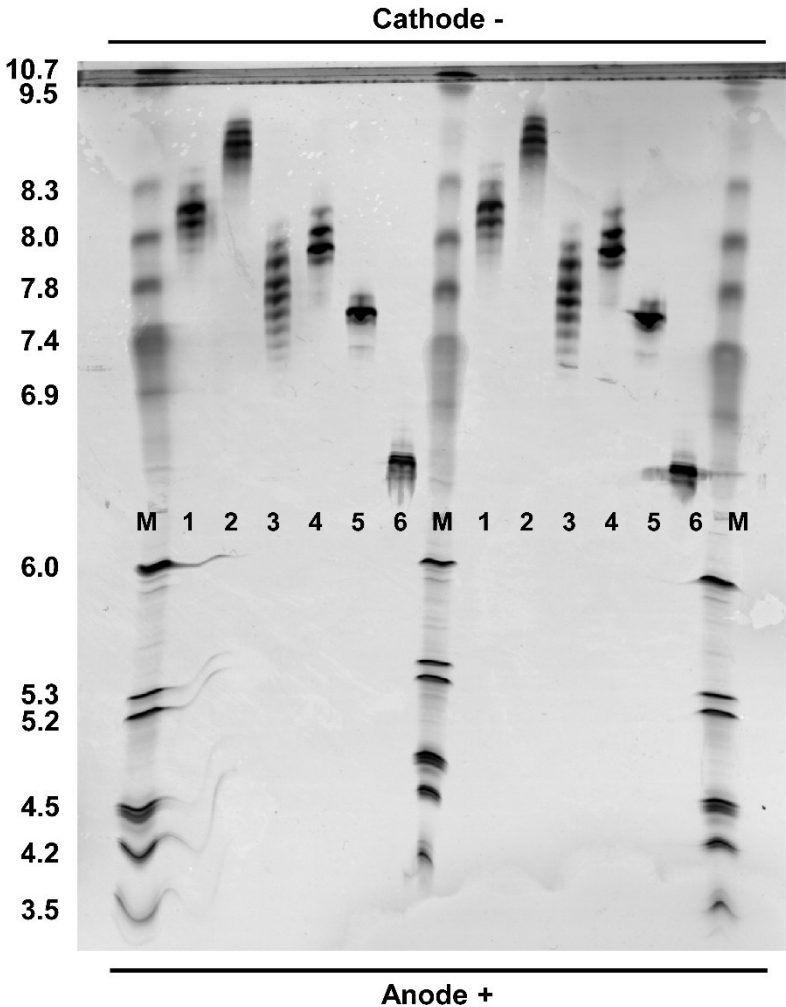
Figure S 3 IEF gel for IEP determination of the model mAb_1-mAb_6 based on marker (M) bands.

		Adsorbed amount	Turbidity	Particles ≥ 300 nm	Particles ≥ 1 µm
Adsorbed amount			0.89 *	0.71 ns	1.00 **
Proximity to IEP*		-1.00 **	-0.89 *	-0.71 ns	-1.00 **
Theoretical charge		-0.77 ns	-0.77 ns	-0.71 ns	-0.77 ns
Hydrophobicity		0.77 ns	0.77 ns	0.71 ns	0.77 ns
A_2^*		-0.94 *	-0.71 ns	-0.54 ns	-0.94 *
Chemical unfolding	C_{m1}	-0.43 ns	-0.26 ns	-0.03 ns	-0.43 ns
	C_{m2}	-0.77 ns	-0.54 ns	-0.26 ns	-0.77 ns
Thermal unfolding	T_{onset}	-0.09 ns	0.26 ns	0.43 ns	-0.09 ns
	T_{m1}	0.60 ns	0.83 ns	0.77 ns	0.60 ns
	T_{m2}	-0.31 ns	-0.26 ns	-0.31 ns	-0.31 ns
Surface activity	$d\Pi/dt_{initial}$	0.94 *	0.83 ns	0.66 ns	0.94 *
	Π_{30}	0.71 ns	0.60 ns	0.54 ns	0.71 ns

Figure S 4 Spearman rank correlation of mAb properties with adsorbed amount, turbidity, and particle concentration. Color scale reflects trends in Spearman's rank coefficient. *Proximity of formulation pH to IEP was calculated based on the dominant band of IEF gel.

Chapter VIII Modification of Tubings for Peristaltic Pumping of Biopharmaceutics

[1]Department of Pharmacy, Pharmaceutical Technology and Biopharmaceutics, Ludwig-Maximilians-Universität München, Munich, Germany

[2]Department of Pharmacy, Center for Drug Research, Ludwig-Maximilians-University Munich, Munich, Germany

Author contributions:

N.D. and W.F. conceived and designed the study. N.D. characterized PDMS-PEG polymers and conducted pumping studies with DBE 712 modified TPV tubing and poloxamer modified silicone tubing. S.A. conducted WCA measurements on PDMS and method development of DBE modified tubing including extended pumping and HGH studies. N.D. evaluated the data of pumping studies. C.M. performed and evaluated GC-MS measurements. N.D. wrote the original draft. W.F. and C.M. revised and edited the manuscript. W.F. supervised the study.

Note from the authors:

The version included in this thesis is identical with the published article apart from minor changes.
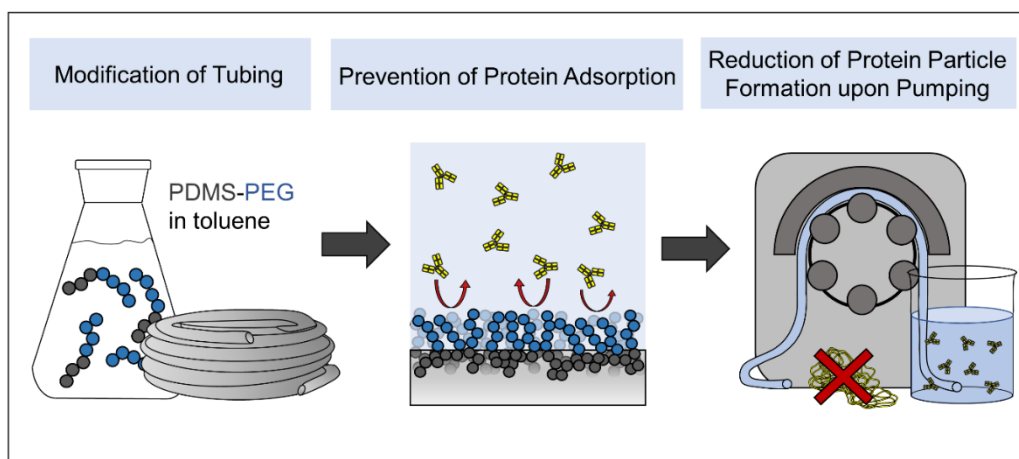
1. Abstract

Protein particle formation during peristaltic pumping of biopharmaceuticals is due to protein film formation on the inner tubing surface followed by rupture of the film by the roller movement. Protein adsorption can be prevented by addition of surfactants as well as by increasing the hydrophilicity of the inner surface. Attempts based on covalent surface coating were mechanically not stable against the stress of roller movement. We successfully incorporated surface segregating smart polymers based on a polydimethylsiloxane (PDMS) backbone and polyethylene glycol (PEG) side blocks in the tubing wall matrix. For this we applied an easy, reproducible, and cost-effective process based on soaking of tubing in toluene containing the PDMS-PEG copolymer. With this tubing modification we could drastically reduce protein particle formation during peristaltic pumping of a monoclonal antibody and human growth hormone (HGH) formulation in silicone and thermoplastic elastomer-based tubing. The modification did not impact the tubing integrity during pumping while hydrophilicity was increased, and protein adsorption was prevented. Free PDMS-PEG copolymer might have an additional stabilizing effect, but less than 50 ppm of the PDMS-PEG copolymer leached from the modified tubing during 1 h of pumping in the experimental setup. In summary, we present a new method for the modification of tubings which reduces protein adsorption and particle formation during any operation involving peristaltic pumping, *e.g.* transfer, filling, or tangential flow filtration.

2. Introduction

Protein particle formation during manufacturing and storage is a serious concern. The product may fail to meet the pharmacopoeial requirement of being essentially free of visible particles as well as the subvisible particle limits.[1,2] Additionally, these large protein aggregates are suspected to cause an enhanced response in patients or a loss in therapeutic efficacy.[3] This implies that the formation of protein particles during the whole manufacturing process is understood and minimized in order to assure product safety and efficacy.

An important unit operation during manufacturing of biopharmaceuticals is peristaltic pumping. This procedure is applied for ultra- or diafiltration, transfer or filling. But peristaltic pumping leads to a substantial increase in protein particles dependent on tubing material, protein, and formulation.[4–7] Proteins adsorb to the tubing wall, driven by electrostatic and hydrophobic interactions, and the formed protein film is compressed, decompressed and ultimately torn off by the roller movement.[6,7] The need for resistance to high mechanical shear in combination with sufficient flexibility and the strict limitations on leachables restricts the polymers used as base material for tubings in pharmaceutical manufacturing to a small group including silicone, some thermoplastic elastomers and fluorinated polymers. Exemplarily polyvinyl chloride (PVC) may leach the plasticizer di(2-ethylhexyl) phthalate which can lead to protein aggregation and might trigger complement activation and the potentially genotoxic 4-hydroxynonenal.[8,9] The polymers used render tubings with a hydrophobic surface. This enhances protein adsorption and thus particle formation as compared to a hydrophilic surface. Addition of surfactants can effectively prevent the formation of protein particle.[4–6] But this approach is not applicable in case of operations in which surfactants are hindering like in tangential flow filtration (TFF) or in early down scale.

Silicone tubing made of polydimethylsiloxane (PDMS) is one of the commonly used tubings in the context of peristaltic pumping of protein pharmaceuticals. But proteins have a strong tendency to adsorb to the hydrophobic PDMS surface.[10,11] In contrast, protein adsorption to very hydrophilic surfaces is reduced due to higher energetic cost of surface dehydration.[12,13] Hydrophilization of polymeric surfaces in order to avoid protein adsorption is established e.g. in microfluidic applications or cell culture.[14,15] A wide range of techniques like plasma treatment, physisorption, grafting to or grafting from approaches[16] or coating with surfactants[17] showed extensive reduction in protein adsorption by increasing the hydrophilicity of PDMS. These techniques mostly modify the PDMS surface. In preliminary tests we modified the inner tubing surface by an established silanization approach[18,19] which results in a few nm thin surface layer of polyethylene glycol (PEG).[20] Surface hydrophilicity was strongly increased until full wetting (Figure S1). But the PEG coating became abraded mechanically by the rollers in the pump

head already within 4 h pumping at 180 rpm (Figure 1). Thus, this surface coating which may additionally suffer from low scalability, limited shelf life or a labour-intensive multistep modification process[16] is not a viable approach to achieve the goal of a reduction of protein particle formation.
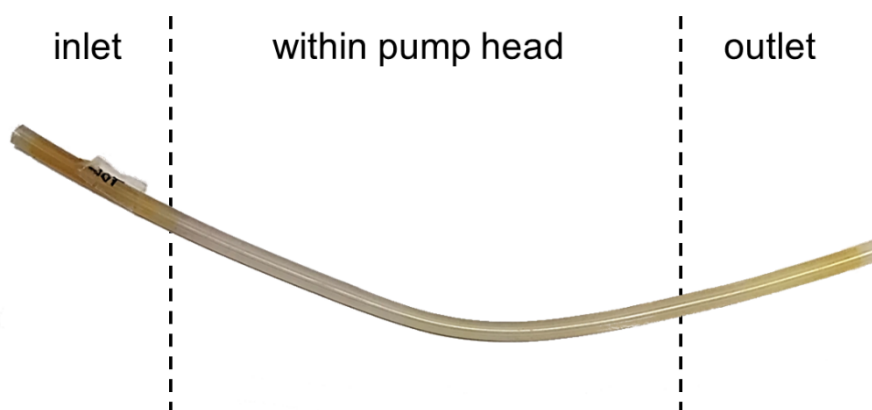
Figure 1 PEG staining of PDMS tubing silanized with 55 mg/mL PEG-silane in toluene after 4 h of pumping 6 mL 20 mM histidine pH 5.4 buffer. Yellow staining indicates the presence of bound PEG.

To overcome these limitations and to reach a stable hydrophilic surface Gökaltun et al.[21] included a surface segregating smart copolymers built from PDMS as basic structure with pegylated sections. By mixing the polymer with a PDMS base followed by polymerization *via* heat curing, they obtained PDMS sheets with increased hydrophilicity and strongly reduced protein adsorption. In theory, the copolymers segregate to the surface when exposed to water which leads to rearrangement of the PEG chains towards the interface rendering surface hydrophilicity.[22] Beyond increasing hydrophilicity, PEG protruding from the surface might further reduce protein adsorption by the large excluded volume and the unique conformational adaptability of PEG chains.[23] Benefits of this approach are high scalability, long storage life, easiness of manufacturing and low costs.[21,24] These benefits make the use of surface segregating smart (PDMS-PEG) copolymers a highly interesting approach for modifying PDMS tubing.

In our study, we aimed to overcome protein particle formation during peristaltic pumping by developing a new modification of tubing material. The modification method was to be easy, quick and cost effective while preserving product quality and safety. Furthermore, the beneficial effect must be sustainable during long time pumping. We modified silicone tubings by embedding different PDMS-PEG copolymers. We first characterized the surface-active behaviour of the segregating polymers. Embedding into the tubing bulk was achieved *via* incubation and swelling of the tubing in a toluene solution containing the PDMS-PEG copolymer followed by drying and deswelling. The effectiveness of the tubing modification was

evaluated in pump studies using a model monoclonal antibody formulation with a focus on protein particle concentration evaluation *via* flow imaging and turbidity and confirmed with human growth hormone (HGH) as smaller protein of different secondary and tertiary structure. To broaden the scope of application we embedded the PDMS-PEG copolymers also in a tubing made from thermoplastic vulcanizate. To evaluate persistence of PDMS-PEG incorporation during pumping, turbidity and protein particle concentration were monitored over 24 h.

3. Materials and Methods

3.1. Materials

1 mg/mL monoclonal antibody (mAb) in 20 mM histidine buffer pH 5.4 and 1 mg/mL HGH in 10 mM sodium phosphate buffer pH 7.0 were used. Concentrations of mAb (ε= 1.51; 156 kDa) and HGH (ε= 0.72; 22 kDa) were verified *via* A280 with a Nanodrop 2000 (Thermo Fisher Scientific, Wilmington, NC, USA) prior to experiments. All buffer and protein samples were filtered through a 0.2 µm polyethersulfone (PES) sterile syringe filter (VWR, Radnor, PA, USA).

Reagents were obtained as follows: 3-[Methoxy-(polyethyleneoxy)-propyl]-trimethoxysilane (PEG-silane) 90%, 6-9 polyethylene oxide units from Abcr (Karlsruhe, Germany); Barium chloride dihydrate from Grüssing (Filsum, Germany); Dimethylsiloxane-ethylene oxide block/graft copolymers (DBE 224, DBE 311, DBE 712, DBE 814) from Gelest (Morrisville, NC, USA); Disodium hydrogen phosphate dihydrate, ethanol and toluene from VWR; Dimethylsulfoxide (DMSO) and hydrochloric acid from Bernd Kraft (Duisburg, Germany); Iodine sublime, potassium iodide, polysorbate 20 (PS 20), and sodium chloride from Merck (Darmstadt, Germany); L-histidine from AppliChem (Darmstadt, Germany); Pluronics from BASF (Ludwigshafen, Germany); Sodium dihydrogen phosphate from Glatt (Binzen, Germany); Sodium dodecyl sulfate (SDS) and toluene D8 from Sigma Aldrich (St. Louis, MO, USA). Highly purified water (HPW) produced with an Arium water purification system (Sartorius, Aubagne, France) was used for buffer preparation. The heat-cure Sylgard 182 Silicone Elastomer Kit (Dow, Midland, MI, USA) was kindly gifted by Biesterfeld Spezialchemie (Hamburg, Germany).

Silicone tubing with 1.6 mm and 6.0 mm bore (Accusil, Watson Marlow, Falmouth, UK) and a thermoplastic vulcanizate (TPV) tubing with 1.6 mm bore (AET Lezaud, St. Wendel, Germany) were used.

3.2. Covalent coating with PEG-silane

Silicone tubing pieces of 200 mm were treated in a Zepto plasma oven (Diener electronic, Ebhausen, Germany) to activate the tubing surface by oxidation which allows anchoring of PEG-silane. Vacuum was built up for 10 min, then the chamber was filled with oxygen for 2 min and plasma cleaning was performed at 0.3 mbar for 3 min with a power of 40 W. Immediately after treatment, tubings were filled with 55 mg/mL PEG-silane solution in toluene and incubated for 1.5 h at room temperature. Subsequently, tubings were washed with 100 mL ethanol followed by 100 mL HPW to remove unbound PEG-silane. The tubing was vacuum dried in a

VO 200 oven (Memmert, Schwabach, Germany) at 120 °C and 11 mbar for 45 min to remove residual solvents.

3.3. Incorporation of PDMS-PEG copolymers

The 200 mm tubing piece was filled with 2%, 5% and 10% (*m/v*) PDMS-PEG copolymers or 5% (*m/v*) poloxamers in toluene. The ends were connected to 2 mL glass syringes filled with the polymer solution to avoid evaporation. After incubation up to 5 h, the tubing was flushed with 100 mL ethanol followed by 100 mL HPW to remove residual polymers. To remove toluene the tubing was vacuum dried in a VO 200 oven (Memmert, Schwabach, Germany) at 120 °C and 11 mbar for 45 min.

3.4. Pumping studies

Tubing sets were cleaned as described previously.[6] Only the 200 mm piece which is placed in the pump head was modified. Tubing sets were assembled by connecting 350 mm long tubing pieces to each end of a 200 mm long tubing piece. Tubings were flushed with 200 mL HPW to remove any external particles. At first, 6 mL formulation buffer and subsequently 6 mL of 1 mg/mL protein solution was circulated using a Flexicon PD 12 peristaltic pump (Watson-Marlow Flexicon, Ringsted, Denmark) operated with a MC 12 control unit. The pump was operated at 180 rpm ($\triangleq$ 109 mL/min) for 1 h at room temperature which results in 500 passages of the sample through the 1.6 mm bore tubing. For 24 h pumping studies tubings with 6.0 mm bore and 45 mL sample volume were used with the same setup.

3.5. Subvisible particle analysis

Subvisible particles were analysed with a FlowCAM® 8100 (Fluid Imaging Technologies, Inc., Scarborough, ME, USA) equipped with a 10x magnification cell (81 µm × 700 µm). The following parameters were set for particle detection: sample volume of 150 µL, flow rate of 0.15 mL/min, auto image frame rate of 28 frames/s and a sampling time of 60 s. These settings lead to an efficiency value higher than 70%. Particles were identified using VisualSpreadsheet® 4.7.6 software (settings: 3 µm distance to the nearest neighbour; particle segmentation thresholds of 13 and 10 for the dark and light pixels) and results were displayed as the equivalent spherical diameter. Additionally, samples of 1.8 mL were examined for turbidity using a Nephla turbidimeter (Dr. Lange, Düsseldorf, Germany).

3.6. Detection of pegylated species

The presence of pegylated species in the tubing was visualized by incubation of the tubing for 15 min in an iodine solution prepared from 2 g iodine sublime and 4 g potassium iodide in 100 mL HPW followed by rinsing with 100 mL HPW to remove residual staining solution.[25]

PDMS-PEG copolymers leaching into pumped samples was quantified by mixing 1.5 mL of pumped formulation buffer with 375 µL of iodine solution and 187 µL of 5% (*m/v*) aqueous barium chloride solution and turbidity detection using a Nephla turbidimeter (Dr. Lange, Düsseldorf, Germany).[26] Polymer concentration in solution could be determined based on a 7-point calibration curve of the PDMS-PEG copolymer (Figure S2).

3.7. Tensiometry

Surface tension measurements were performed using a K100 MK2 tensiometer (Krüss, Hamburg, Germany) equipped with a F12 thermostat (Julabo, Ostfildern, Germany) and a 765 Dosimat (Metrohm, Leinfelden-Echterdingen, Germany). To check for equipment cleanliness the surface tension of HPW was determined before every measurement (requirement: 72.0 ± 0.1 mN/m). A total of 35 concentrations per DBE polymer was measured using a platinum iridium plate in a custom-made glass vessel[27] by automated dilution of the copolymer stock (0.1% (*m/v*) for DBE 712 and 814; 0.03% (*m/v*) for DBE 311) in HPW using the Dosimat. Experiments (n=3) were performed at 25 °C. The critical micelle concentration (CMC) was determined from the sharp break in surface tension vs. logarithm of surfactant concentration plots using LabDesk 3.1 software (Krüss, Hamburg, Germany).

3.8. Solubility

Water solubility of the copolymers DBE 224 and 311 was evaluated by adding 100 mg of copolymer to 15 mL of water and incubating for 72 h at room temperature under shaking. The saturated solution was centrifuged at 17,000 *g* with a Heraeus Megafuge 16R (Thermofisher Scientific, Waltham, MA, USA) for 10 min, 5 mL of the supernatant were transferred into 10 R vials (Schott, Mainz, Germany), water was evaporated at 80 °C for 24 h with an oven (Binder, Tuttlingen, Germany) and the amount of dissolved copolymer was determined *via* differential weighing.

3.9. Protein adsorption

Protein adsorbed on the tubing before and after 24 h of pumping was quantified as previously described[6] based on the detachment of adsorbed protein by incubation with SDS followed by size-exclusion-chromatography.

3.10.   Stress strain curves

Elasticity and stress strain behaviour of the modified and non-modified tubing were evaluated using a Ta.XT plus Texture Analyzer (Stable Micro Systems, Godalming, UK). Tubing pieces of 70 mm length were clamped into the apparatus resulting in 50 mm of tubing within the gap for stretching. Samples were pulled at 5 mm/min for 70 mm. Strain rate was set 0% at a prestress of 0.05 N/mm^2 to guarantee sufficient stretching. The elastic modulus was calculated from the slope of the stress-strain curve in the linear region between 0 and 10% strain.

3.11.   Contact angle measurements

Water contact angle measurements on tubing or coated glass slides were performed using a Drop Shape Analyzer DSA25E (Krüss, Hamburg, Germany). A water drop of 3.0 µL was placed on the surface and the contact angle was evaluated based on a circle fit. Coated glass slides were prepared by mixing PDMS-PEG copolymer with the silicone elastomer kit followed by heat curing of the mixture on microscope slides at 120 °C for 45 min at 11 mbar.

3.12.   Detection of copolymer incorporated in tubing

Silicone or TPV tubing was filled with 5% (*m/v*) DBE 712 in toluene and incubated for 5 h. After flushing with 100 mL ethanol and 100 mL HPW, toluene was slowly removed under vacuum for 12 h at 40 °C and 24 h at 60°C using a VO 200 oven (Memmert, Schwabach, Germany). The amount of incorporated copolymer was determined *via* differential weighing. Weight differences for TPV after drying were corrected for a dried TPV incubated with toluene only.

3.13.   Determination of residual toluene content

Residual toluene content was analysed by static headspace-gas chromatography-mass spectrometry (HS-GC-MS). An Agilent Technologies 7890B gas chromatograph (Waldbronn, Germany), equipped with an Agilent J&W DB-624 UI ultra-inert capillary column (6% cyanopropyl phenyl and 94% polydimethylsiloxane) 30 m × 0.25 mm × 1.4 µm and an Agilent

Technologies 7010B triple quadrupole detector with high efficiency source was used for analysis. A tubing sample of 40 mm was placed into a 20 mL headspace vial, 20 µL of toluene d8 (1 mg/mL in DMSO) as internal standard was added, and the vial was closed tightly. After sealing, the sample was analysed by HS-GC-MS. Conditions of static HS-GC-MS are included in the supplementary information (Table S1). The MS was operated in scan mode (*m/z* 45-120; EI 70 eV). The retention times and the molecule peaks of toluene (9.33 min, *m/z* 92) and toluene d8 (9.29 min, *m/z* 100) were used as qualifier ions and the base peaks *m/z* 91 and 98 as quantifier ions.

3.14.   Statistical significance

If not indicated otherwise, experiments were repeated three times with a new tubing set each. Data is then represented as mean ± standard deviation. Statistical significance was evaluated based on an unpaired two-tailed t-test.

4. Results

4.1. Characterization of PDMS-PEG polymers

We evaluated different surface segregating smart copolymers with different PEG content and molecular weight (Table 1). While the copolymers DBE 224 and 311 were poorly soluble in water, DBE 712 and 814 were freely soluble. For all copolymers except for DBE 224 the CMC was below 0.02% (m/v). Although a CMC could not be detected for DBE 224 due to immediate suspension formation in water, a saturated DBE 224 solution reached a surface tension ($\sigma_{saturation}$) of 26.7 ± 2.9 mN/m indicating high surface activity. The saturated aqueous solutions of the other polymers showed an even lower surface tension with the lowest value of 20.7 ± 0.1 mN/m for DBE 712.

Table 1 Characterization of chemical structure, solubility, and surface activity of PDMS-PEG copolymers (n=3).

Copolymer	PEG [%][28]	Molecular Weight [Da][28]	Solubility [g/100g]	CMC [% (m/v)]	$\sigma_{saturation}$ [mN/m]
DBE 224	25	10,000	< 0.1	not detectable	26.7 ± 2.9
DBE 311	30 - 35	800 - 1,200	< 0.1	0.0161 ± 0.0015	22.9 ± 0.1
DBE 712	60 - 70	600	Freely soluble	0.0082 ± 0.0002	20.7 ± 0.1
DBE 814	80	1,000	Freely soluble	0.0127 ± 0.0002	21.9 ± 0.2

Exemplarily for DBE 712 its surfactant effect on reduction of particle formulation during peristaltic pumping was evaluated by pumping a 1 mg/mL mAb solution containing 0.01% DBE 712 (Figure 2). Upon pumping of pure buffer with unmodified and modified tubing the particle level increased to the same extent. This most likely results from rubber particles shed from the inner tubing wall.[28] The protein particle levels as effectively reduced by the modification as by addition of 0.01% PS 20 to the formulation.
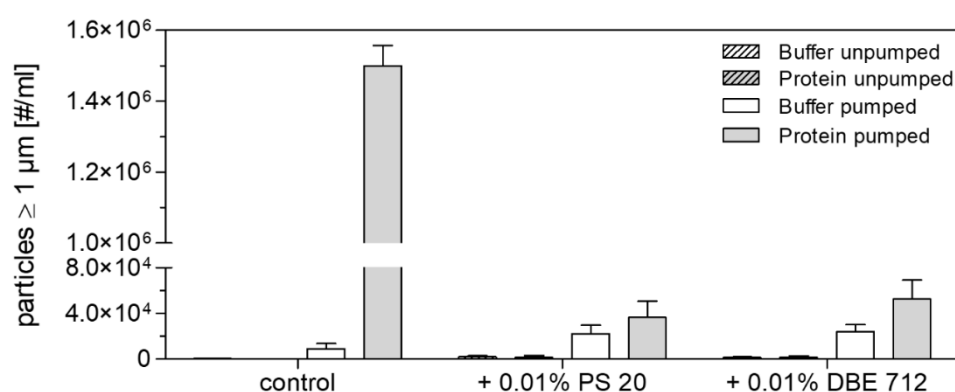
Figure 2 Particles ≥ 1 µm per mL after pumping formulation buffer and 1 mg/mL mAb in 20 mM histidine pH 5.4 with and without the addition of 0.01% PS 20 or DBE 712 through silicone tubing (n=3). Turbidity data is presented in Figure S3.

PDMS-PEG copolymers tend to self-assemble at the interface in contact with water to create a hydrophilic PEG-layer. Water contact angles decreased over time with increasing copolymer concentrations (Figure 3). Incorporation of 0.5% (*m/v*) DBE 712 decreased the water contact angle effectively below 10° within 10 min, whereas 0.1% and 0.25% DBE 712 was less effective. Both the more hydrophobic DBE 311 and the more hydrophilic DBE 814 showed a slower and less effective water contact angles reduction than DBE 712. At 2.5% DBE 311 or DBE 814 full wetting was achieved within 50 min. Lower concentrations led to a slower decrease in water contact angle reaching values above 20° after 50 min. In contrast to the other copolymers, PDMS sheets containing DBE 224 exhibited a 5 min lag phase followed by a rather slow less pronounced decrease of the water contact angle compared to the more hydrophilic PDMS-PEG copolymers.
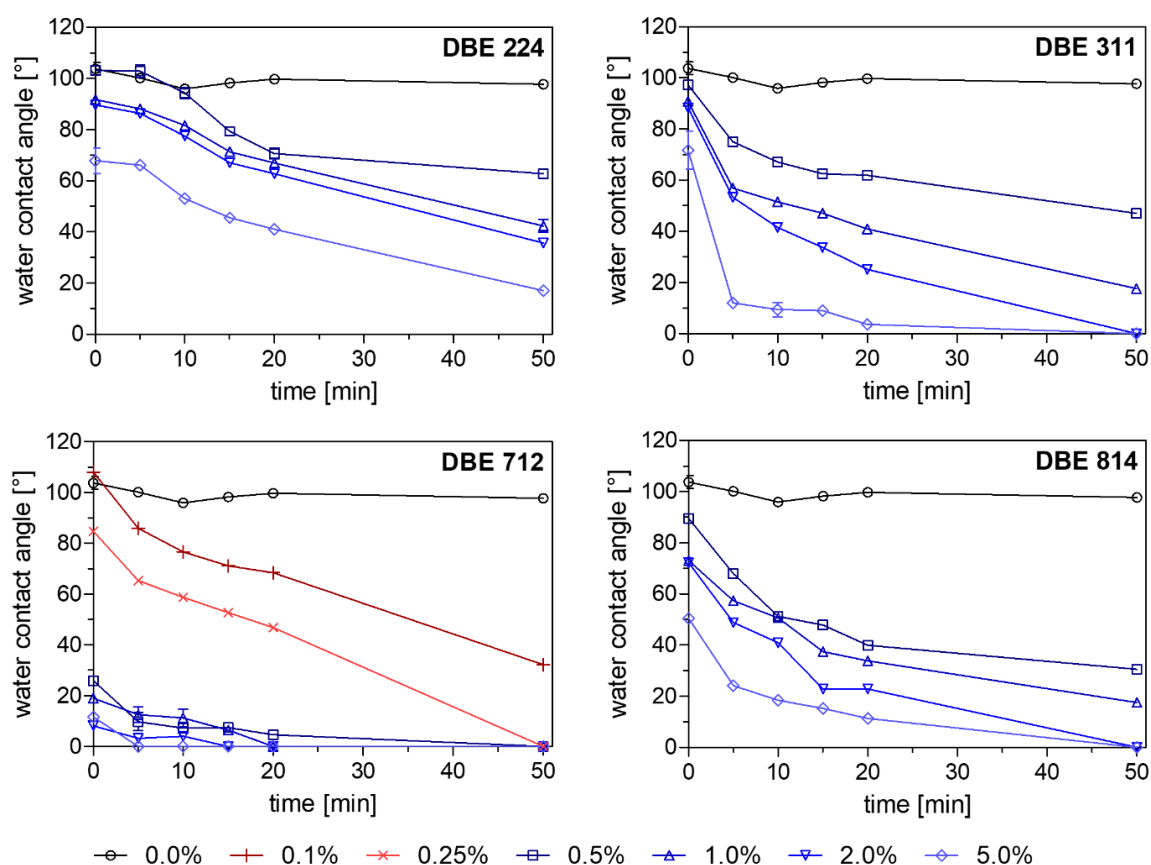
Figure 3 Water contact angle on PDMS-PEG copolymers PDMS sheets as a function of polymer type, concentration and waiting time (n=3). Standard deviations of measurements are small and sometimes superimposed by symbols.

4.2. Development of tubing modification

To incorporate the copolymer in the tubing we developed a swelling/ deswelling approach. The choice of solvent for the copolymer was essentially based on its PDMS tubing swelling ability to reach high levels of incorporated copolymer amounts. In preliminary experiments with

ethanol and toluene we observed the highest swelling efficacy with toluene. The swelling was gone after drying. Toluene could be removed at 120 °C under vacuum for 45 min leading to a residual concentration of 4.6 ± 0.6 µg/cm ($\triangleq 24.9 \pm 3.1$ ppm (m/m)) toluene in the PDMS tubing. Prolonging the drying time to 24 h did not further reduce the residual toluene amount (5.4 ± 0.5 µg/cm $\triangleq 29.6 \pm 2.5$ ppm (m/m)).

To find the optimum combination of copolymer concentration, incubation time and tubing polymer type parameters we varied the incubation parameters and pumped formulation buffer and mAb for 1 h (Figure 4). Modification of the tubing at all tested combinations did not impact elasticity (Table S2), shape, transparency or shedding of particles from the tubing itself.
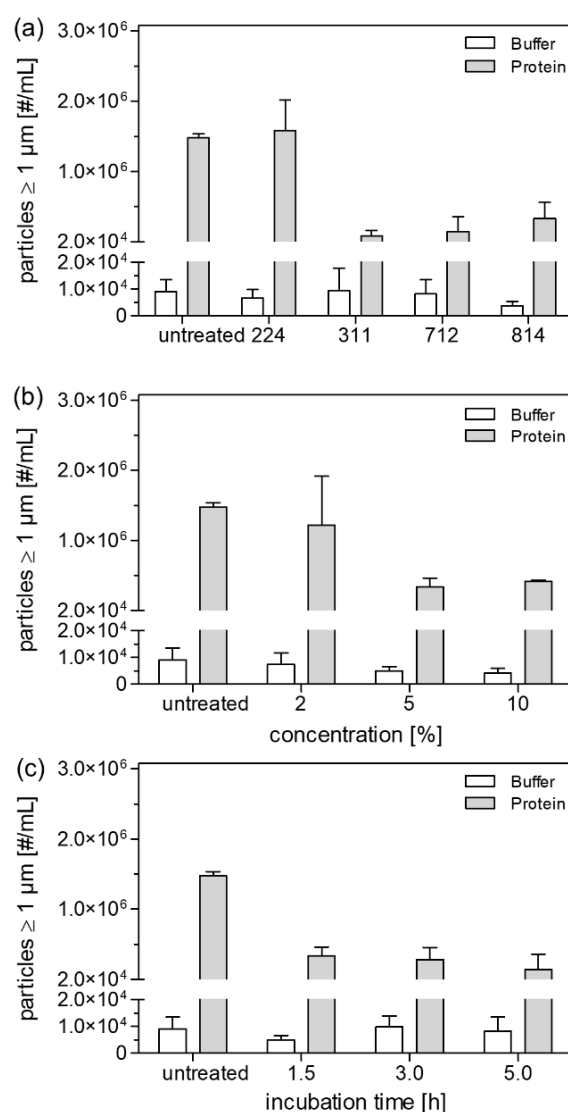
Figure 4 Particles ≥ 1 µm per mL after pumping 6 mL formulation buffer and 6 mL 1 mg/mL mAb in 20 mM histidine pH 5.4 through untreated or modified silicone tubing for 1 h. Tubing (n=3) was either incubated with different PDMS-PEG copolymers at 5% (m/v) for 5 h (a), different concentrations of DBE 712 for 1.5 h (b) or different duration with 5% (m/v) DBE 712 (c). Turbidity data is presented in Figure S4.

Upon pumping mAb through the PDMS-PEG modified tubings, turbidity and protein particle concentration increase were markedly less compared to untreated tubing. Incorporation of DBE 224 reduced turbidity from 35.3 ± 8.3 to 13.0 ± 1.4 FNU compared to the untreated tubing while protein particle concentration ≥ 1 μm per mL remained unaffected. The other PDMS-PEG polymers were even more effective and reduced both turbidity and particle concentration to approximately 3 FNU and 150,000 particles ≥ 1 μm per mL, respectively. To identify the optimal parameters for modification, PDMS-PEG concentration in the incubation solution and incubation time were varied using DBE 712. Incubation with 2% (*m/v*) DBE 712 for 1.5 h reduced turbidity only to 15.5 ± 5.0 FNU while particle formation ≥ 1 μm per mL were unaffected. Incubation with 5% (*m/v*) DBE 712 decreased the turbidity and protein particle levels to 5.1 ± 1.3 FNU and approx. 350,000 ± 125,000 particles ≥ 1 μm per mL, respectively. Increasing the DBE 712 concentration further to 10% (*m/v*) did not additionally decrease protein particle formation and turbidity. Prolonging the incubation time from 1.5 to 3 and 5 h significantly reduced turbidity ($p < 0.05$) to 2.5 ± 0.5 FNU but had no effect on protein particle concentration.

Overall, the amount of copolymer detected in formulation buffer was low with a maximum of approximately 50 ppm after pumping for 1 h (Table 2). Only 4 ppm were detected for the most hydrophobic copolymer DBE 224 higher levels resulted for the more hydrophilic DBE 712 and DBE 814. Additionally, the amount of copolymers detected in pumped formulation buffer after 1 h increased for tubings incubated in copolymer solution of higher concentration (2% vs. 10%; $p < 0.05$) or for longer time (1.5 h vs. 5 h; $p < 0.01$).

Table 2 PDMS-PEG copolymer detected in 20 mM histidine pH 5.4 buffer after pumping 6 mL for 1 h through modified silicone tubing (n=3). * Estimated based on the DBE 712 calibration considering the PEG fraction since calibration curves for DBE 224 and 311 could not be obtained due to suspension formation upon contact with water and iodine solution.

Copolymer	Concentration [%]	Incubation time [h]	Copolymer detected [ppm]
DBE 712	2	1.5	5.1 ± 0.7
	5	1.5	12.9 ± 2.6
	10	1.5	24.3 ± 7.9
	5	3	36.7 ± 22.2
	5	5	44.8 ± 8.2
DBE 224	5	5	4.0 ± 1.0*
DBE 311	5	5	12.4 ± 7.5*
DBE 814	5	5	34.1 ± 17.6

Staining the tubings with iodine solution confirmed the successful incorporation of the copolymers (Figure 5). All modified tubings revealed strong yellow to brownish colouring before and after pumping compared to the untreated tubing. The brownish colour originates from high concentrations of iodine - PEG complexes within the tubing and small traces of entrapped substrate. Additionally, all modified tubings exhibited a homogenous distribution of the copolymer throughout the entire tubing wall which was stable during pumping.
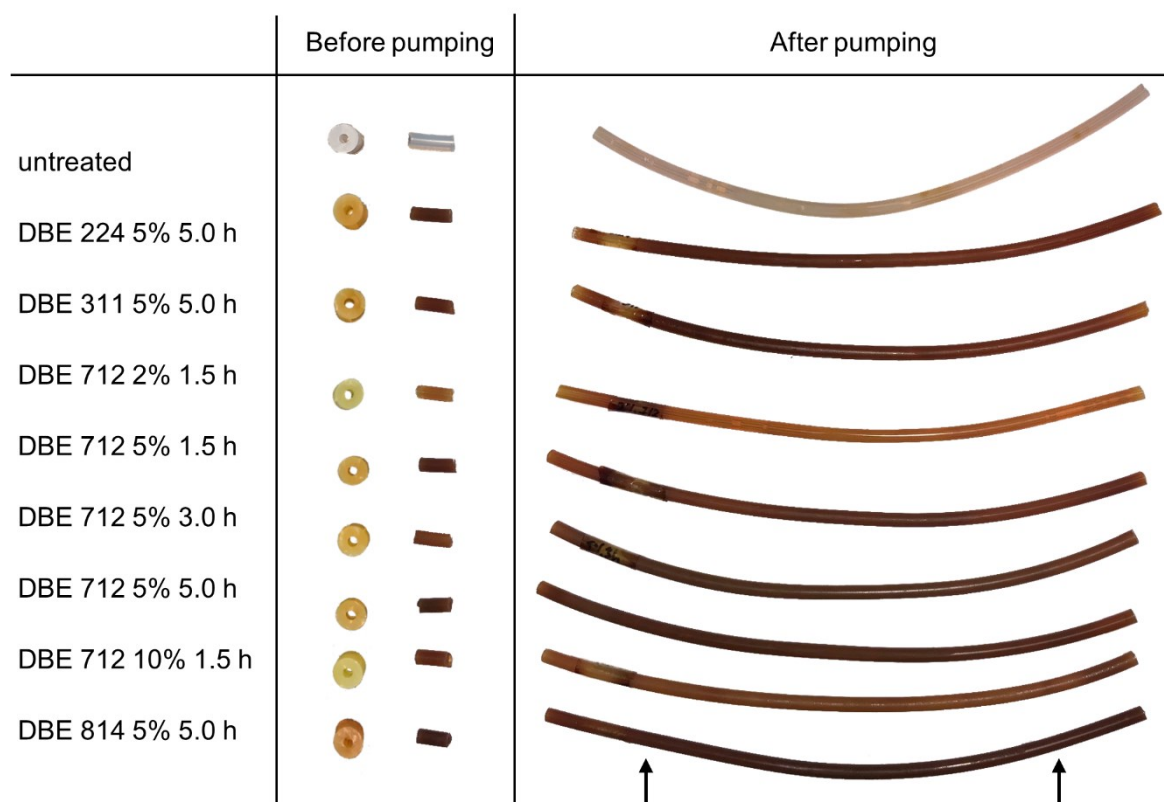
Figure 5 Copolymer visualization in modified tubings before and after pumping by iodine staining for tubings modified with different copolymer at different conditions. Segment between the arrows was mounted in the pump head.

Tubings were modified at 5% (*m/v*) for 5 h with DBE 712 which is already well characterized for biocompatibility.[21] This setup led to an embedded mass of DBE 712 of 0.88 ± 0.01% (*m/m*). The modification with PDMS-PEG copolymers completely suppressed mAb adsorption to the silicone tubing. Even after 24 h of pumping, mAb adsorption was not detectable on the PDMS-PEG modified silicone tubing compared to 5.2 ± 0.4 mg/m^2 mAb adsorbed to the untreated tubing. Additionally, water contact angles decreased to 76.5 ± 0.8° before and 73.9 ± 0.4° after 24 h pumping compared to 111.2 ± 0.6° of the untreated tubing (Figure 6).
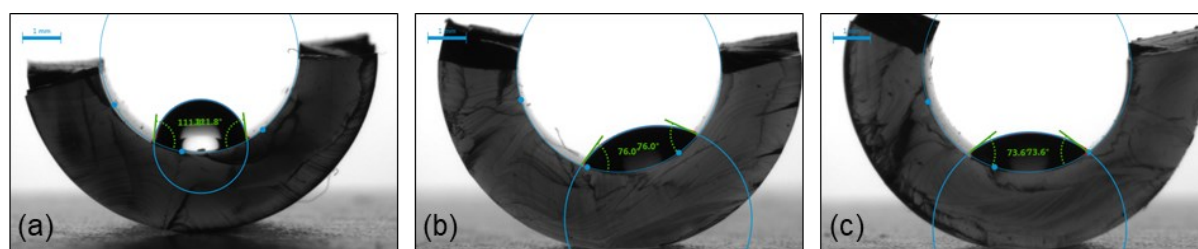
Figure 6 Water contact angle of the inner tubing surface of the untreated silicone tubing (a) and the DBE 712 modified silicone tubing before (b) and after 24 h of pumping formulation buffer (c).

To learn more about the impact of the segregating property of the copolymers, additionally tubings were modified with poloxamer (P) 182, 184 and 188. Iodine staining demonstrated a less marked penetration of the poloxamers. After pumping, poloxamer could not be detected in formulation buffer. Modification with P 182 and P 184 did not show a significant ($p > 0.05$) effect on turbidity and protein particle levels. In contrast, P 188 incorporation into the tubing did result in a significant reduction ($p < 0.01$) in particle concentration ≥ 1 µm by approximately 65% but turbidity was also not significantly different from untreated tubing ($p > 0.05$). In summary, the positive effect of P 188 is by far less compared to that when of tubing modification with PDMS-PEG copolymers (Figure 7).
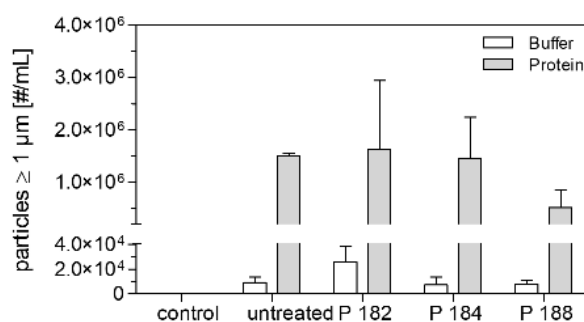
Figure 7 Particles ≥ 1 µm in 6 mL formulation buffer or 6 mL 1 mg/mL mAb samples pumped for 1 h in silicone tubing modified with different poloxamers. Modification conditions were 5% (*m/v*) poloxamer in toluene incubated for 5 h (n=3). Control represents an unpumped sample. Turbidity data is presented in Figure S5.

In the next step, the positive effect of tubing modification was to be studied with a different type of protein, HGH which is known to be sensitive to pumping stress.[6] We used tubing modified with 5% (*m/v*) DBE 712 for 5 h and detected 34.7 ± 4.4 ppm in formulation buffer after 1 h pumping. Pumping HGH for 1 h through unmodified silicone tubing resulted in a massive increase in turbidity from 1.4 ± 0.3 to 57.4 ± 15.8 FNU and formation of almost 3.5 ×10^6 particles ≥ 1 µm/mL (Figure 8). Modification of the tubing with DBE 712 drastically reduced HGH particle formation with a turbidity after pumping of only approx. 3 FNU and 0.2 ×10^6 particles ≥ 1 µm/mL.
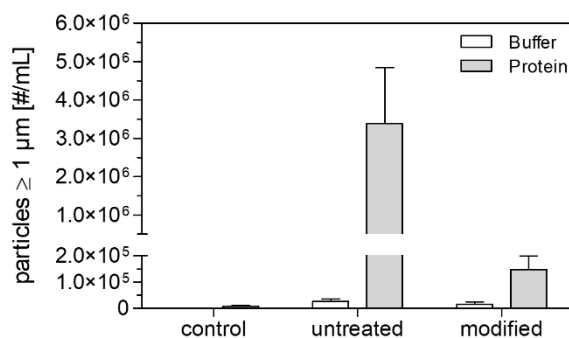
Figure 8 Particles ≥ 1 µm per mL after pumping formulation buffer and 1 mg/mL HGH in 10 mM sodium phosphate pH 7.0 through DBE 712 modified silicone tubing for 1 h (n=3). Control refers to unpumped sample. Turbidity data is presented in Figure S6.

4.3. Stability of tubing modification upon extended pumping

Especially in TFF operations pumping duration last several hours. Therefore, we stressed the sustainability of the tubing modified tubing by pumping for 24 h (n = 1). Particle ≥ 1 µm burden in formulation buffer was comparable for modified and untreated tubing over 7 h and slightly higher in the modified tubing after 24 h (Figure 9). Whereas pumping of mAb over 24 h with untreated tubing resulted in a drastic linear increase of turbidity up to approx. 2,000 FNU and particle ≥ 1 µm level to almost 200×10^6 per mL. Modifying the tubing drastically reduced protein particle formation in a sustained manner over 24 h (100 FNU and 7.5×10^6 particles ≥ 1 µm/mL after 24 h). The amount of copolymer detected in formulation buffer increased over time reaching 135.4 ppm after 24 h (Table 3).
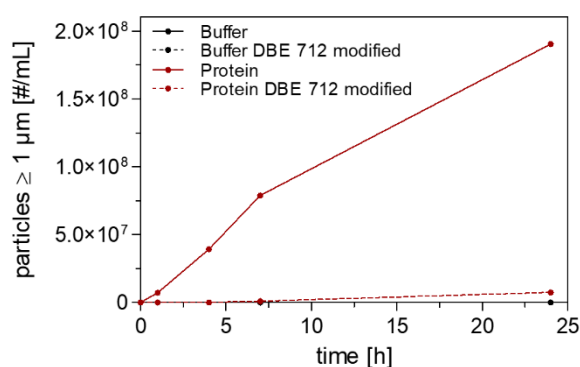
Figure 9 Particles ≥ 1 µm per mL after pumping formulation buffer and 1 mg/mL mAb in 20 mM histidine pH 5.4 through DBE 712 modified silicone tubing for 24 h (n=1). Particles ≥ 1 µm are presented as mean of three replicate measurements. Turbidity data is presented in Figure S7.

Table 3 Copolymer detected after pumping 45 mL 20 mM histidine buffer pH 5.4 through DBE 712 modified 6.0 mm silicone tubing over 24 h (n=1).

Time [h]	Total detected copolymer [ppm]
1	17.4
4	48.0
7	66.7
24	135.4

4.4. Application of tubing modification method for TPV tubing

The tubing method may also be applicable to tubings made of other base materials. We therefore modified TPV tubing by incubation in 5% DBE 712 in toluene for 5 h followed by washing and toluene removal. Modification of the tubing led to the incorporation of 0.93 ± 0.01% (*m/m*) DBE 712. After pumping of formulation buffer, turbidity was only slightly higher for the modified tubing compared to the untreated tubing (4.2 ± 1.1 FNU vs. 0.9 ± 0.4 FNU) whereas particle concentrations ≥ 1 μm per mL were not significantly different ($p > 0.05$). In pumped formulation buffer 10.2 ± 5.9 ppm of DBE 712 was detected after 1 h. After pumping mAb, turbidity and particle concentration could be reduced by approximately 90% by modifying the TPV tubing with DBE 712 (Figure 10). Overall, turbidity and protein particle concentration ≥ 1 μm per mL in untreated TPV tubing were significantly higher compared to untreated silicone tubing.

Figure 10 Particles ≥ 1 μm per mL after pumping 6 mL formulation buffer and 6 mL 1 mg/mL mAb in 20 mM histidine pH 5.4 through unmodified and DBE 712 modified TPV tubing for 1 h (n=3). Control refers to unpumped sample. Turbidity data is presented in Figure S8.

5. Discussion

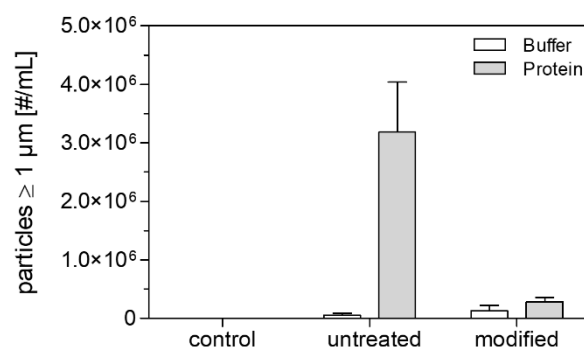Peristaltic pumping can lead to formation of protein particles which might impact product quality and safety of biologics. Protein particles originate from the rupture of the protein film formed on the tubing surface during roller movement.[6] A common method to reduce protein adsorption is by hydrophilic coating of the material surface. But in case of tubings, the high mechanical stress in the pump head leads to abrasion of the coating. We went a different route by incorporating PDMS-PEG copolymers into the tubing wall.

PDMS-PEG copolymers consist of a hydrophobic PDMS anchor and hydrophilic modifications with PEG. The four tested PDMS-PEG copolymers were of different molecular weight (600 - 10,000 Da) and hydrophilicity (PEG content 25 - 80%). One of the most important parameters for amphiphilic molecules is their CMC. The CMC depends on the molecules and the solvent properties. Solvent properties influencing CMC are *e.g.* addition of electrolytes, ionic strength and the presence of protein.[29–32] At the CMC full surface coverage by the surfactant at the interface is expected. A relatively low CMC is therefore favourable in order to reach high surfactant efficacy. All tested PDMS-PEG copolymers are surface active and lower the surface tension of water to less than 27 mN/m at surface saturation. Copolymer characteristics influencing CMC are the hydrophobic block content and molecular weight.[33–35] The detectable PDMS-PEG CMCs were below 0.02% (*m/v*) in water. As expected, CMC for DBE 712 was lower than that of DBE 814 due to a higher hydrophobicity. Surprisingly, the CMC for DBE 311 was higher than DBE 712 despite a higher hydrophobicity. In comparison, PS 20 leads to a surface tension in between 33 and 35 mN/m at saturation[36–38] with a CMC of 0.006% (*m/v*).[38,39] During pumping experiments the addition of DBE 712 to the protein solution reduced protein particle concentration as effective as PS 20. In summary, the tested PDMS-PEG copolymers have surface-active potential in solution.

To estimate the increase in hydrophilicity of surfaces, PDMS-PEG copolymers were incorporated in PDMS sheets. All copolymers led to a time dependent substantial decrease in the water contact angle, reflecting a surface hydrophilicity increase, which is in theory associated with the reorganization of the copolymers exposing the PEG chains to the hydrophilic phase.[22] Within the tested PDMS-PEG copolymers, DBE 712 (Molecular Weight (MW) 600 Da; PEG 60 - 70%) increased the surface hydrophilicity most drastically which can be explained by a rapid reorganization of the rather short chain polymer at the surface. In contrast, the bigger and more hydrophobic DBE 224 (MW 10,000 Da; PEG 25%) showed a lag time before increasing surface hydrophilicity and was less effective in increasing surface hydrophilicity. DBE 814 (MW 1,000 Da; PEG 80%) also induced a fast increase in surface hydrophilicity whereas the small but more hydrophobic DBE 311 (MW 800 – 1,200 Da; PEG

30 – 35%) was less efficient. Thus, smaller and more hydrophilic PDMS-PEG copolymers were more suitable for the purpose of increasing surface hydrophilicity.

The four different PDMS-PEG copolymers were incorporated into PDMS tubing *via* swelling the tubing in a toluene solution containing the copolymer followed by evaporation of the solvent. In preliminary studies toluene had turned out to be the most promising solvent as it penetrates into the tubing and allows copolymer ingress into the tubing. Its swelling capacity for PDMS is substantially higher compared to ethanol and other protic solvents.[40] Due to health risks of toluene upon frequent exposure, the permitted daily exposure of 8.9 mg toluene per day and the concentration limit of 890 ppm are stated by the Pharmacopeia.[41] After vacuum drying, the residual toluene within a 20 cm long tubing piece which could be used in the pump head could at maximum release 0.1 mg, an amount that can be considered as non-critical. Drawbacks of toluene are the extraction of unpolymerized components[40], incompatibility with a wide range of rubbers[42] and potential impact on mechanical properties. We did not observe any effect of toluene on tubing appearance, shedding propensity as demonstrated by pumping formulation buffer, and stretching behaviour. Thus, this setup is an easy method to modify tubings in lab scale. For commercial manufacturing of the modified tubing melt extrusion of a polymer mixture is expected to be the method of choice since that swelling and deswelling in toluene comes with the drawback of residual toluene potentially leaching into the product.

We varied polymer type, concentration of copolymer in the incubation solution as well as incubation time. At all test conditions we observed migration of copolymer throughout the whole tubing wall. Tubing modification with DBE 311, 712 and 814 resulted in significant reduction of protein particle formation upon pumping whereas the large and more hydrophobic DBE 224 was less effective. The effect of the process parameters was evaluated for DBE 712, the small hydrophilic copolymer, for which toxicity data is available. A higher concentration of PDMS-PEG copolymer in the incubation solution of 5 or 10% turned out to be superior to a lower concentration of 2% (*m/v*) DBE 712 in toluene. The incubation time was of less importance and 1.5 h of incubation was sufficient.

PDMS-PEG copolymer in the pumped solution may results from leaching or abrasion. We found up to 50 ppm of DBE 712 and 814 after recirculating pumping of 6 mL for 1 h and lower concentrations for the more hydrophobic copolymers. This leads to a maximum leaching of approximately 0.1 ppm per pump cycle. The PDMS-PEG copolymer concentration in formulation buffer after pumping was below the CMC in all cases. At larger scale, by direct mixing of the copolymer into the melt leaching of PDMS-PEG copolymer might be reduced.

For comparison we employed poloxamers as alternative PEG based copolymers. In contrast to the PDMS-PEG copolymers with their PEG side blocks attached to a PDMS backbone,

poloxamers are of a triblock nature. Wu *et al.*[43] embedded P 407 in PDMS and observed a reduction in protein adsorption at the modified surface. In our studies incorporation of P 182 and P 184 into PDMS tubing did not have a beneficial effect on protein particle formation upon pumping. P 188, the most hydrophilic of the poloxamers tested, reduced protein particle formation but turbidity of the pumped sample was improved over untreated tubing. Overall, modification with poloxamers was by far less effective than modification with PDMS-PEG copolymers. A possible cause might be a low solubility of poloxamers in silicone as assumed by Wu and Hjort [43]. Furthermore, poloxamers have a higher molecular weight ranging from 2,500 to 8,400 g/mol compared to the effective PDMS-PEG copolymers DBE 311, 712, and 814.

After successful modification of PDM tubing with DBE 712, water contact angles decreased to approximately 75° and protein adsorption was prevented. Gökulthan *et al.*[21] found that upon storage the hydrophilic character is stable for at least 20 months. We could show that even under the intense mechanical stress of 24 h pumping, the hydrophilicity and protein repelling properties were preserved. Particle concentration and turbidity increased linearly for both the untreated and modified tubing which indicated a constant particle formation per interval. Modification of the tubing drastically reduced the particle concentration by approximately 95% upon 24 h of operation. Thus, tubing modification is also applicable for processes lasting for several hours like TFF.

HGH is even more sensitive to stress induced by pumping compared to mAb.[6] Modifying the tubing with DBE 712 decreased turbidity and protein particle concentration ≥ 1 µm by approximately 95%. Her *et al.*[4,5] observed that protein particle formation is tubing material dependent. In fact, we detected a higher protein aggregation propensity in untreated TPV compared to silicone tubing. Modification of TPV tubing with DBE 712 successfully reduced protein aggregation to a level comparable to modified silicone tubing. Despite the chemical dissimilarity embedding of DBE 712 in TPV was successful most likely because of the hydrophobic interactions between the tubing and the hydrophobic anchor of the copolymer. While our lab scale approach is limited by the swelling capacity of the tubing, extrusion of a polymer mixture expands the applicability of the developed hydrophilization by smart segregating block copolymers to materials which swell only poorly in organic solvents.

6. Conclusion

Protein particle formation is a concern during the manufacturing of biopharmaceutics. In this context, peristaltic pumps had been identified as contributor to the overall protein particle burden. In the current manuscript we developed a promising method to modify tubings to reduce protein particle formation drastically. The approach is based on the incorporation of PDMS-PEG copolymers into the tubing material. On lab scale we successfully achieved this by swelling of the tubing material in a toluene solution of the copolymer and removal of residual toluene *via* vacuum drying after washing. The modification process did not alter tubing appearance, material shedding, and elasticity. Four PDMS-PEG copolymers DBE 224, 311, 712 and 814 with different molecular weight and hydrophilicity were incorporated through the complete tubing wall. Upon pumping mAb with the modified silicone tubing, the PDMS-PEG copolymers reduced protein particle formation by approximately 90%, only the hydrophobic DBE 224 was less effective. Less protein particles are formed due to a reduced protein adsorption caused by an increased tubing surface hydrophilicity through migration of the PDMS-PEG copolymers to the surface. This approach was also effective in case of the more sensitive HGH. The modification can withstand at least 24 h of pumping which makes long-term use during *e.g.* TFF possible. Incorporation of PDMS-PEG copolymer reduced protein particle formation also in case of TPV tubing. This supports the use of the presented tubing modification approach for different scenarios and tubing materials involved in processing of biologics. Our simple and cost-effective solvent-based method can be easily applied in a research lab environment. For a broader application, the copolymer can be admixed to melt which is extruded when manufacturing tubings.

7. Acknowledgements

8. References

1.   EP <2.9.19>. Particulate Contamination: Sub-Visible Particles. In: European Pharmacopoeia. 6th ed. European Directorate For The Quality Of Medicine; 2008.

2.   USP <788> Particulate matter in injections. In: United States Pharmacopeia. United States Pharmacopeial Convention; 2014.

3.   Moussa EM, Panchal JP, Moorthy BS, et al. Immunogenicity of Therapeutic Protein Aggregates. J Pharm Sci. 2016;105(2):417-430. doi:10.1016/j.xphs.2015.11.002

4.   Her C, Carpenter JF. Effects of Tubing Type, Formulation, and Postpumping Agitation on Nanoparticle and Microparticle Formation in Intravenous Immunoglobulin Solutions Processed With a Peristaltic Filling Pump. J Pharm Sci. 2020;109(1):739-749. doi:10.1016/j.xphs.2019.05.013

5.   Her C, Tanenbaum LM, Bandi S, et al. Effects of Tubing Type, Operating Parameters, and Surfactants on Particle Formation During Peristaltic Filling Pump Processing of a mAb Formulation. J Pharm Sci. 2020;109(4):1439-1448. doi:10.1016/j.xphs.2020.01.009

6.   Deiringer N, Friess W. Proteins on the Rack: Mechanistic Studies on Protein Particle Formation During Peristaltic Pumping. J Pharm Sci. 2022;111(5):1370-1378. doi:10.1016/j.xphs.2022.01.035

7.   Deiringer N, Rüdiger D, Luxbacher T, Zahler S, Friess W. Catching Speedy Gonzales: Driving forces for Protein Film Formation on Silicone Rubber Tubing During Pumping. J Pharm Sci. 2022;111(6):1577-1586. doi:10.1016/j.xphs.2022.02.013

8.   Schröter A, Mahler HC, Sayed N ben, Koulov A v., Huwyler J, Jahn M. 4-Hydroxynonenal – A toxic Leachable from clinically used Administration Materials. J Pharm Sci. 2021;110(9):3268-3275. doi:10.1016/j.xphs.2021.05.014

9.   Snell JR, Monticello CR, Her C, et al. DEHP Nanodroplets Leached From Polyvinyl Chloride IV Bags Promote Aggregation of IVIG and Activate Complement in Human Serum. J Pharm Sci. 2020;109(1):429-442. doi:10.1016/j.xphs.2019.06.015

10.   Chumbimuni-Torres KY, Coronado RE, Mfuh AM, et al. Adsorption of proteins to thin-films of PDMS and its effect on the adhesion of human endothelial cells. RSC Adv. 2011;1(4):706-714. doi:10.1039/c1ra00198a

11.   Anderson JM, Ziats NP, Azeez A, Brunstedt MR, Stack S, Bonfield TL. Protein adsorption and macrophage activation on polydimethylsiloxane and silicone rubber. J Biomater Sci Polym Ed. 1995;7(2):159-169. doi:10.1163/156856295X00670

12.   Vogler EA. Protein adsorption in three dimensions. Biomaterials. 2012;33(5):1201-1237. doi:10.1016/j.biomaterials.2011.10.059

13.   Rabe M, Verdes D, Seeger S. Understanding protein adsorption phenomena at solid surfaces. Adv Colloid Interface Sci. 2011;162(1-2):87-106. doi:10.1016/j.cis.2010.12.007

14.   Zhou J, Ellis AV, Voelcker NH. Recent developments in PDMS surface modification for microfluidic devices. Electrophoresis. 2010;31(1):2-16. doi:10.1002/elps.200900475

15.   Goddard JM, Hotchkiss JH. Polymer surface modification for the attachment of bioactive compounds. Progress in Polymer Science (Oxford). 2007;32(7):698-725. doi:10.1016/j.progpolymsci.2007.04.002

16.   Gokaltun A, Yarmush ML, Asatekin A, Usta OB. Recent advances in nonbiofouling PDMS surface modification strategies applicable to microfluidic technology. Technology (Singap World Sci). 2017;05(01):1-12. doi:10.1142/s2339547817300013

17.   Dou YH, Bao N, Xu JJ, Meng F, Chen HY. Separation of proteins on surface-modified poly(dimethylsiloxane) microfluidic devices. Electrophoresis. 2004;25(17):3024-3031. doi:10.1002/elps.200405986

18.   Schmolke H, Demming S, Edlich A, et al. Polyelectrolyte multilayer surface functionalization of poly(dimethylsiloxane) (PDMS) for reduction of yeast cell adhesion in microfluidic devices. Biomicrofluidics. 2010;4:044113. doi:10.1063/1.3523059

19.   Sharma V, Dhayal M, Govind, Shivaprasad SM, Jain SC. Surface characterization of plasma-treated and PEG-grafted PDMS for micro fluidic applications. Vacuum. 2007;81(9):1094-1100. doi:10.1016/j.vacuum.2007.02.004

20.   Sharma S, Johnson RW, Desai TA. XPS and AFM analysis of antifouling PEG interfaces for microfabricated silicon biosensors. Biosens Bioelectron. 2004;20(2):227-239. doi:10.1016/j.bios.2004.01.034

21.   Gökaltun A, Bok Kang Y, Yarmush ML, Berk Usta O, Asatekin A. Simple Surface Modification of Poly(dimethylsiloxane) via Surface Segregating Smart Polymers for Biomicrofluidics. Sci Rep. 2019;9:7377. doi:10.1038/s41598-019-43625-5

22.   Evans SD, Sharma R, Ulman A. Contact Angle Stability: Reorganization of Monolayer Surfaces? Langmuir. 1991;7(1):156-161. doi:10.1021/la00049a028

23.   Lee JH, Bang Lee H, Andrades JD. Blood Compatibility of Polyethylene Oxide Surfaces. Prog Polym Sci. 1995;20(6):1043-1079. doi:10.1016/0079-6700(95)00011-4

24. Yao M, Fang J. Hydrophilic PEO-PDMS for microfluidic applications. Journal of Micromechanics and Microengineering. 2012;22(2):025012. doi:10.1088/0960-1317/22/2/025012

25. Hoffmann P. Zwei einfache Methoden zum Nachweis von Polyethylenglykol im Holz. Deutsches Schifffahrtsarchiv. 1985;8:95-100.

26. Skoog B. Determination of Polyethylene Glycols 4000 and 6000 in Plasma Protein Preparations. Vox Sang. 1979;37(6):345-349. doi:10.1111/j.1423-0410.1979.tb02314.x

27. Schiefelbein LKJ. Sugar-Based Surfactants for Pharmaceutical Protein Formulations. Ludwig-Maximilians University; 2011.

28. Saller V, Matilainen J, Grauschopf U, Bechtold-Peters K, Mahler HC, Friess W. Particle Shedding from Peristaltic Pump Tubing in Biopharmaceutical Drug Product Manufacturing. J Pharm Sci. 2015;104(4):1440-1450. doi:10.1002/jps.24357

29. Garidel P, Hildebrand A, Neubert R, Blume A. Thermodynamic characterization of bile salt aggregation as a function of temperature and ionic strength using isothermal titration calorimetry. Langmuir. 2000;16(12):5267-5275. doi:10.1021/la9912390

30. Fuguet E, Ràfols C, Rosés M, Bosch E. Critical micelle concentration of surfactants in aqueous buffered and unbuffered systems. Anal Chim Acta. 2005;548(1-2):95-100. doi:10.1016/j.aca.2005.05.069

31. Mahler HC, Senner F, Maeder K, Mueller R. Surface activity of a monoclonal antibody. J Pharm Sci. 2009;98(12):4525-4533. doi:10.1002/jps.21776

32. Horiuchi S, Winter G. CMC determination of nonionic surfactants in protein formulations using ultrasonic resonance technology. European Journal of Pharmaceutics and Biopharmaceutics. 2015;92:8-14. doi:10.1016/j.ejpb.2015.02.005

33. Mok MM, Thiagarajan R, Flores M, Morse DC, Lodge TP. Apparent critical micelle concentrations in block copolymer/ionic liquid solutions: Remarkably weak dependence on solvophobic block molecular weight. Macromolecules. 2012;45(11):4818-4829. doi:10.1021/ma300399c

34. Kozlov MY, Melik-Nubarov NS, Batrakova E v., Kabanov A v. Relationship between pluronic block copolymer structure, critical micellization concentration and partitioning coefficients of low molecular mass solutes. Macromolecules. 2000;33(9):3305-3313. doi:10.1021/ma991634x

35. Alexandridis P, Holzwarth JF, Hatton TA. Micellization of Poly(ethylene oxide)-Poly(propylene oxide)-Poly(ethylene oxide) Triblock Copolymers in Aqueous Solutions:

Thermodynamics of Copolymer Association. Macromolecules. 1994;27(9):2414-2425. doi:10.1021/ma00087a009

36.   Kothekar SC, Ware AM, Waghmare JT, Momin SA. Comparative analysis of the properties of Tween-20, Tween-60, Tween-80, Arlacel-60, and Arlacel-80. J Dispers Sci Technol. 2007;28(3):477-484. doi:10.1080/01932690601108045

37.   Szymczyk K, Zdziennicka A, Jańczuk B. Adsorption and Aggregation Properties of Some Polysorbates at Different Temperatures. J Solution Chem. 2018;47:1824-1840. doi:10.1007/s10953-018-0823-z

38.   Mittal KL. Determination of CMC of Polysorbate 20 in Aqueous Solution by Surface Tension Method. J Pharm Sci. 1972;61(8):1334-1335. doi:10.1002/jps.2600610842

39.   Patist A, Bhagwat SS, Penfield KW, Aikens P, Shah DO. On the measurement of critical micelle concentrations of pure and technical-grade nonionic surfactants. J Surfactants Deterg. 2000;3(1):53-58. doi:10.1007/s11743-000-0113-4

40.   Lee JN, Park C, Whitesides GM. Solvent Compatibility of Poly(dimethylsiloxane)-Based Microfluidic Devices. Anal Chem. 2003;75(23):6544-6554. doi:10.1021/ac0346712

41.   5.4 Residual Solvents. In: European Pharmacopoeia. 10th ed. ; 2020.

42.   Williams SC. Elastomers Chemical Compatibility Chart. Industrial Specialties Mfg. and IS MED Specialties; 2018. Accessed October 21, 2021. https://www.industrialspec.com/images/files/elastomers-chemical-compatibility-chart-from-ism.pdf

43.   Wu Z, Hjort K. Surface modification of PDMS by gradient-induced migration of embedded Pluronic. Lab Chip. 2009;9:1500-1503. doi:10.1039/b901651a

9. Supplementary data
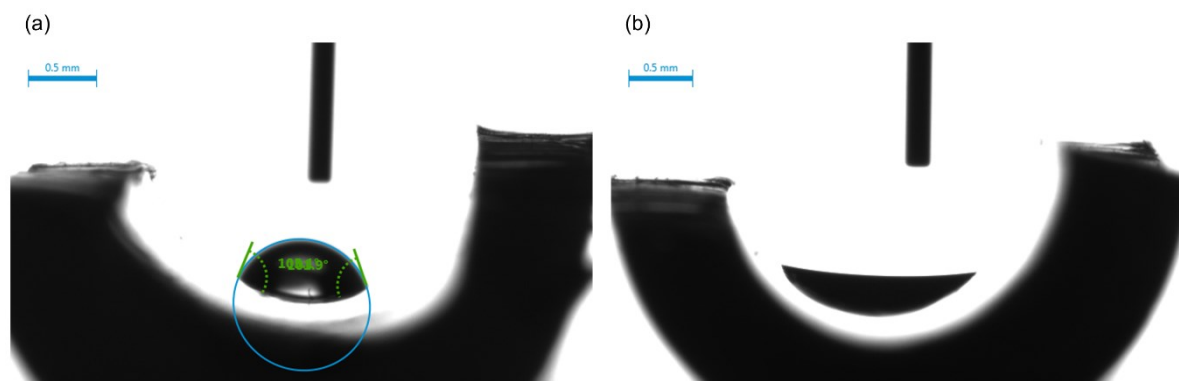
Figure S 1 Water contact angle of the inner tubing surface of the untreated silicone tubing (a) and after silanization (b). Silanization led to full wetting compared to a water contact angle of approximately 105° of the untreated silicone tubing.
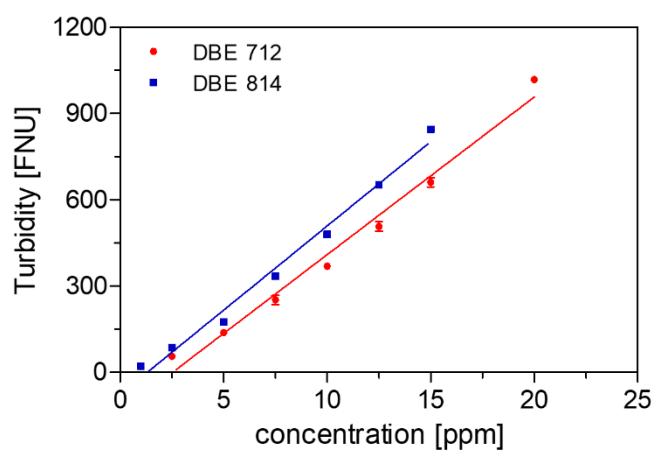
Figure S 2 Calibration curves for DBE 712 (Limit of detection (LOD): 1.2 ppm; Limit of quantification (LOQ): 3.8 ppm) and DBE 814 (LOD: 0.8 ppm; LOQ: 2.4 ppm). Both parameters were calculated based on standard deviation of the response (Sy) of the curve and the slope of the calibration curve (S). LOD and LOQ were approximated by 3.3 (Sy/S) and 10(Sy/S), respectively.

Table S 1 Conditions set for static HS-GC-MS.

Headspace sampler parameters		GC-MS parameters	
Agitator cycle	5 sec on, 2 sec off	Carrier flow rate	1.2 mL/min
Agitator speed	500 rpm	Split ratio	100 : 1
Agitator temperature	80 °C	Oven profile	40 °C for 6 min 40 to 200 °C at 50 °C/min 200 to 240 °C at 80 °C/min (hold time 1 min)
Sample incubation time	15 min	Transfer line temperature	250 °C
Syringe size	2.5 mL	Inlet temperature	250 °C
Syringe temperature	120 °C	Ion source temperature	230 °C
Injection volume	0.25 mL	Quadrupole temperature	150 °C
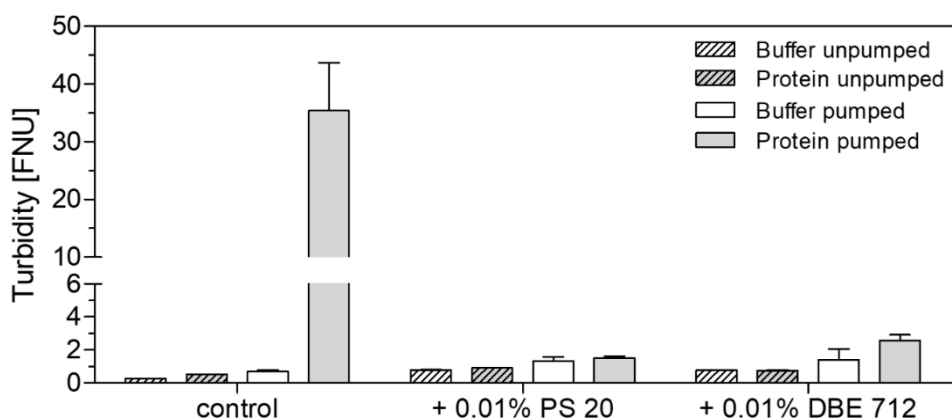
Figure S 3 Turbidity after pumping formulation buffer and 1 mg/mL mAb in 20 mM histidine pH 5.4 with and without the addition of 0.01% PS 20 or DBE 712 through silicone tubing (n=3).
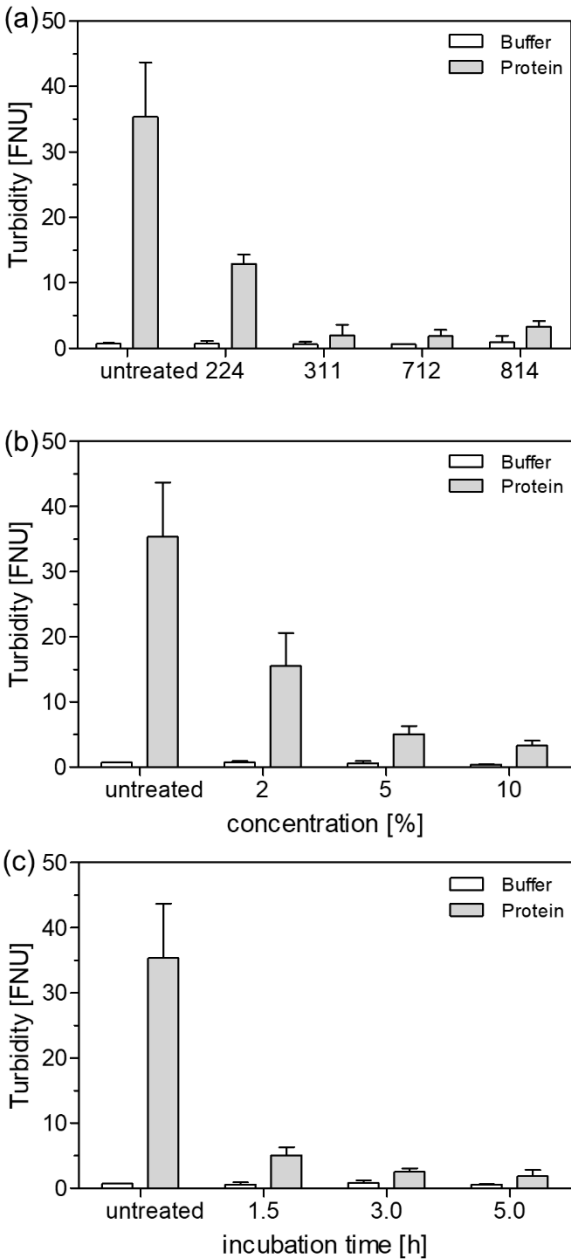
Figure S 4 Turbidity after pumping 6 mL formulation buffer and 6 mL 1 mg/mL mAb in 20 mM histidine pH 5.4 through untreated or modified silicone tubing for 1 h. Tubing (n=3) was either incubated with different PDMS-PEG copolymers at 5% (*m/v*) for 5 h (a), different concentrations of DBE 712 for 1.5 h (b) or different duration with 5% (*m/v*) DBE 712 (c).

Table S 2 Elastic modulus of PDMS-PEG untreated and modified silicone tubings (n= 3).

Copolymer	Concentration [%]	Incubation time [h]	Elastic Modulus [N/mm^2]
Untreated	0	0	4.09 ± 0.21
DBE 712	2	1.5	4.17 ± 0.08
	5	1.5	4.06 ± 0.62
	10	1.5	3.95 ± 0.77
	5	3	3.87 ± 0.63
	5	5	4.10 ± 0.21
DBE 224	5	5	4.42 ± 0.29
DBE 311	5	5	3.67 ± 0.47
DBE 814	5	5	3.96 ± 0.40
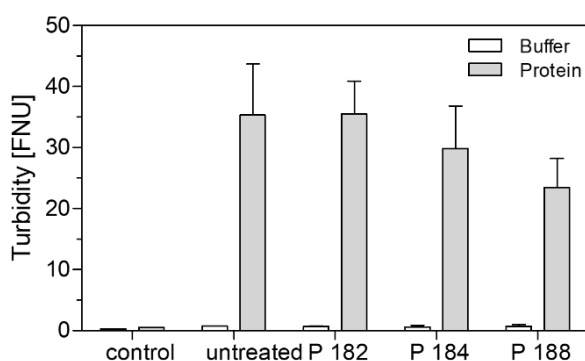
Figure S 5 Turbidity of 6 mL formulation buffer or 6 mL 1 mg/mL mAb samples pumped for 1 h in silicone tubing modified with different poloxamers. Modification conditions were 5% (*m/v*) poloxamer in toluene incubated for 5 h (n=3). Control represents an unpumped sample.

Figure S 6 Turbidity after pumping formulation buffer and 1 mg/mL HGH in 10 mM sodium phosphate pH 7.0 through DBE 712 modified silicone tubing for 1 h (n=3). Control refers to unpumped sample.
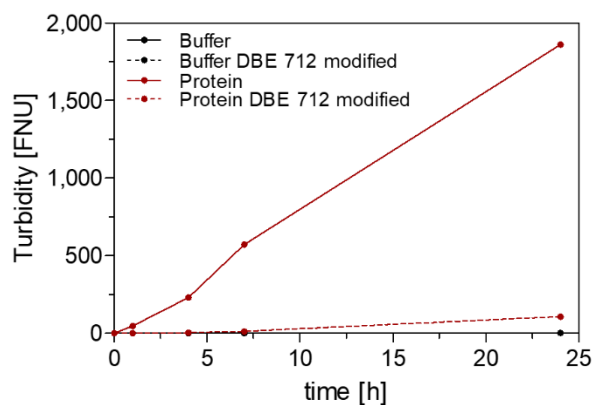
Figure S 7 Turbidity after pumping formulation buffer and 1 mg/mL mAb in 20 mM histidine pH 5.4 through DBE 712 modified silicone tubing for 24 h (n=1).
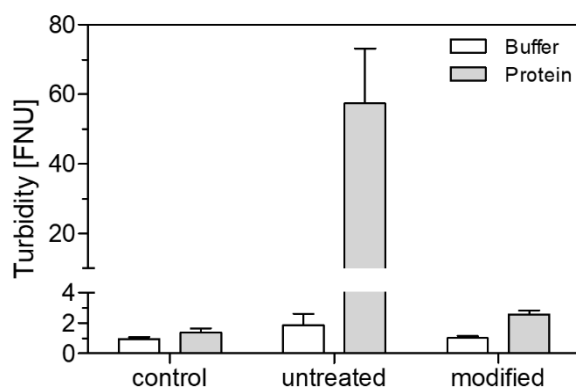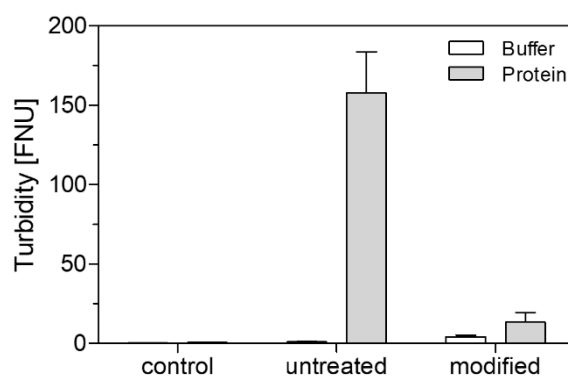

Figure S 8 Turbidity after pumping 6 mL formulation buffer and 6 mL 1 mg/mL mAb in 20 mM histidine pH 5.4 through unmodified and DBE 712 modified TPV tubing for 1 h (n=3). Control refers to unpumped sample.

Chapter IX Effect of the Tubing Material used in Peristaltic Pumping in Tangential Flow Filtration Processes of Biopharmaceutics on Particle Formation and Flux

This chapter is published as:

[1] Department of Pharmacy; Pharmaceutical Technology and Biopharmaceutics; Ludwig-Maximilians-Universität München, Munich, Germany[2]Chair for Analytical Chemistry, Technische Universität München, Munich, Germany

Author contributions:

N.D. and W.F. conceived and designed the study. I.L. prepared buffer and protein solutions and characterized samples by turbidity, subvisible particles and protein concentration. N.D. operated the TFF system. N.D. and I.L. photo documented samples. N. D. evaluated the data and wrote the original draft. W.F. revised and edited the manuscript. W.F. supervised the study.

Note from the authors:

The version included in this thesis is identical with the published article apart from minor changes.

1. Abstract

Tangential flow filtration (TFF) is a central step in manufacturing of biopharmaceutics. Membrane clogging leads to decreased permeate flux, longer process time and potentially complete failure of the process. The effect of peristaltic pumping with tubings made of three different materials on protein particle formation during TFF was monitored via micro flow imaging, turbidity and photo documentation. At low protein concentrations, pumping with a membrane pump resulted in a stable flux with low protein particle concentration. Using a peristaltic pump led to markedly higher protein particle formation dependent on tubing type. With increasing protein particle formation propensity of the tubing, the permeate flux rate became lower and the process took longer. The protein particles formed in the pump were captured in the cassette and accumulated on the membrane leading to blocking. Using tubing with a hydrophilic copolymer modification counteracted membrane clogging and flux decrease by reducing protein particle formation. In ultrafiltration mode the permeate flux decrease was governed by the viscosity increase rather than by the protein aggregation; but using modified tubing is still beneficial due to a lower particle burden of the product. In summary, using tubing material for peristaltic pumping in TFF processes which leads a less protein particle formation, especially tubing material with hydrophilic modification, is highly beneficial for membrane flux and particle burden of the product.

Keywords: protein aggregation, pumping, tubing, protein particles, tangential flow filtration, ultrafiltration, diafiltration, protein adsorption, interface, membrane fouling

Abbreviations: HPW – highly purified water; mAb – monoclonal antibody; NTU - nephelometric turbidity units; TFF – tangential flow filtration

2. Introduction

Tangential flow filtration (TFF) is an essential step in downstream processing of biopharmaceutics. This versatile process allows concentration and/or diafiltration of a few millilitres to several litres. In contrast to traditional dead-end filtration the fluid is circulated in parallel to the filter membrane and liquid as well as solutes smaller than the pore diameter are forced through the membrane into the permeate due to a transmembrane pressure. The crossflow reduces the build-up of particles and material on the membrane coming with the risk of clogging and enables a higher permeate flux. Still, since TFF is a time-consuming process, it is important to achieve a high flux for a short process to reduce operational costs. Reasons for a flux decrease include formation of a protein gel layer on the membrane surface via adsorption and concentration polarization, viscosity increase of the retentate and blocking of membrane pores by larger protein aggregates; often these effects are combined.

During operation proteins adsorb to the membrane and form a gel layer with concentration polarization.[1] Depending on the hydraulic resistance of the gel layer the permeate flux is decreased.[1] Hydraulic resistance of the protein gel layer is linked to its structure and compactness.[2] The structure of the gel layer depends on membrane material, biophysical protein characteristics, and formulation.[2–5] High cross flow rates reduce the protein convection to the membrane thereby reducing gel resistance and increasing flux.[6,7]

In the context of subcutaneous administration, high protein concentrations are desired to reach small injection volumes. During concentration via TFF, the flux decreases with increasing retentate viscosity due to permeation resistance.[8] By mature formulation development focusing on formulation components, pH and ionic strength, viscosity can be reduced.[9–11] It has to be kept in mind that an additional final compounding step makes it necessary that the concentration of the retentate after the TFF process is substantially higher than the concentration of the final drug product.

Finally, large aggregates in the retentate are deposited on the membrane in the course of the process which also reduces permeate flux ultimately clogging the pores.[12] Aggregates already present in the initial bulk have a negative impact.[13] Furthermore, aggregates may form due to pumping or stirring stress[14–16], due to the formulation change coming along with the diafiltration[17], and with the formation of the extremely concentrated gel layer phase at the membrane. The aggregate formation is affected by operation parameters like temperature, process duration, cross flow, and pressure conditions.[15,18,19] Aggregate formation the resulting decrease in flux are protein and formulation specific.[15,20,21] In addition, high particle levels in the retentate after TFF negatively impact subsequent processing, especially a following filtration step.[16,19]

Chandavarkar[14] identified peristaltic pumping as an initiator of membrane clogging due to protein aggregates formed and deposited on the membrane. A protein film is formed on the tubing surface, this film is ruptured with roller movement as the tubing gets stretched and relaxes, and protein film fragments enter the bulk.[22] Protein particle formation upon pumping can be efficiently reduced using surfactants.[22–24] However, TFF processes are commonly operated without surfactants as their concentration behaviour is unclear and protein surfactant interactions might lead to an unpredictable concentration of the surfactant in the retentate In this context, also the tubing material itself plays a major role.[23–25] Previous studies on tubing selection [23,24] mainly focused on the detection of protein particle concentrations in a single run to estimate the impact on product quality during a filling or transfer process. TFF is associated with several passages through the pump head which is linked to a higher protein particle burden. Thus, not only product quality but also membrane flux and further processability might be impacted. Consequently, a risk assessment of the peristaltic pumping and the tubing material on the membrane fouling propensity during TFF is critical.

This study aimed to understand the impact of the tubing material on protein aggregate formation caused by peristaltic pumping during TFF processes and ultimately on permeate flux. To this end three different tubing materials were used to circulate monoclonal antibody solution via a peristaltic pump. Additionally, a membrane pump was evaluated for comparison. Aggregation was monitored via turbidity, microflow imaging and photo documentation. The aggregation propensity was linked to permeate flux decrease during diafiltration operation with low viscosity. To investigate the effect of viscosity on permeate flux decrease the sample was upconcentrated from 2 mg/mL to 110 mg/mL with two tubing materials. We additionally employed tubings which were modified with DBE 712 to strongly reduce protein adsorption and film formation.

3. Materials and Methods

3.1. Materials

A model monoclonal antibody (mAb) at 30 mg/mL in 10 mM histidine pH 7.2 + 140 mM NaCl was used. The mAb had an isoelectric point of 8.2. Buffer ingredients were dissolved in highly purified (HPW) from an arium® pro DI Ultrapure Water System (Sartorius Stedim Biotech, Goettingen, Germany). The buffer was subsequently filtered using pressurized nitrogen and 0.2 µm cellulose acetate filters (47 mm ø, Sartorius Stedim Biotech). Prior to experiments, the protein sample was filtered with 0.2 µm polyethersulfone membrane syringe filters (VWR International, Ismaning, Germany). Reagents were obtained as follows: DBE–712 from Gelest (Morrisville, Pennsylvania, United States); ethanol and toluene from VWR; histidine and histidine HCl from J.T. Baker (Phillipsburg, New Jersey, United States) and NaCl from Sigma – Aldrich (Steinheim, Germany).

Tubing materials used in this study are pharmapure (Masterflex, Gelsenkirchen, Germany), silicone (Accusil, Watson-Marlow, Falmouth, United Kingdom) and santoprene (AET Lezaud, St. Wendel, Germany). All tubings had an inner diameter of approximately 3.2 mm.

3.2. Preparation of modified tubing

Surface modified silicone and santoprene tubings were manufactured as previously reported:[26] Briefly, tubing pieces were filled with 5% (w/v) DBE-712 in toluene, after 5 h of incubation the tubing was flushed with 100 mL of ethanol followed by an equal volume of HPW to remove residual free polymer. Cleaned tubings were vacuum dried at 11 mbar and 120 °C for 45 min.

3.3. Determination of protein concentration

Protein concentration was measured by UV absorption at 280 nm using a Nanodrop Micro-Volume UV-Vis spectrometer (Nano Drop 2000, Thermo Scientific, Wilmington, North Carolina, USA) based on an extinction coefficient of 1.70 mL·g^{-1}·cm^{-1}. The concentrations were not affected by turbidity as the same results were obtained when correcting samples for A350.

3.4. Sample preparation

For TFF experiments a Repligen KR2i system (Marlborough, Massachusetts, USA) equipped with a permeate and retentate scale and an auxiliary pump for buffer exchange was used. All experiments were conducted with a flat sheet cassette membrane Hystream (Low Fouling

mPES) with an area of 0.02 m^2 and a cut off 30 kDa (Repligen). Membrane functionality was checked with a water permeability test before each sample run. The system was operated at a constant transmembrane pressure (TMP) of 1.5 bar which was automatically regulated with a pressure valve based on the signals from the pressure transducers at retentate, permeate and feed outlets of the cassette holder. Feed flow rate was set constant to 100 mL/min. For the dialysis setup, 100 mL of 2 mg/mL mAb were buffer exchanged by 40x volume against formulation buffer. For ultrafiltration experiments, 2.1 l of 2 mg/ml mAb were concentrated 55x to approximately 110 mg/ml. For the different tubing setups only the 340 mm tubing piece within the pump head which had been identified as the origin of protein aggregation was exchanged. The remaining connecting was kept in pharmapure quality to minimize other potential effects of the setup. For experiments with the Simdos 10 membrane pump (KNF, Freiburg, Germany) the membrane pump was clipped into the setup for the peristaltic pump replacing the peristaltic pump as well as the inserted 340 mm tubing piece keeping the pharmapure connecting lines. For pumping experiments, the cassette was replaced by a pharmapure tubing piece resembling the holdup volume of the cassette. Depending on tubing material the duration was adapted from runs with the cassette. After runs the system was cleaned with 0.2 N NaOH followed by HPW. Each experimental setup was performed in duplicate. Flux is described as the volume passed through one m^2 membrane per hour as L/m^2/h (LMH). The starting value represents the flux after reaching a desired TMP of 1.5 bar if not stated otherwise. Formulation pH was measured after each experiment.

3.5. Photo documentation

Samples were filled in 10 R vials (Schott AG, Mühlheim, Germany) and placed in a light box with a black background. Photos were captured with a Sony alpha 6400 (Tokyo, Japan) at 135x zoom and manual focusing at fixed parameters (ISO 200, F 8.0, exposure time: 1/8).

3.6. Turbidity

Samples turbidity was analyzed in 25 mL standard vials using a Hach TL2360 Turbidimeter (Düsseldorf, Germany). Results are presented in nephelometric turbidity units (NTU).

3.7. Detection of subvisible particles

Particle size distribution and number were determined using a micro-flow imaging (MFI) system DPA4100 (Brightwell Technologies, Ottawa, Canada) equipped with a high-resolution

100 µl flow cell and the MFI View Application Software. Pre-run volume and sample volume were set to 250 µl and 650 µl, respectively. With a peristaltic pump the sample was drawn through the flow cell at a flow rate of 0.1 mL/min. To optimize illumination and provide optimal cell cleanliness the system was rinsed with HPW before and after the measurements. Highly concentrated samples were diluted in the respective formulation at least 1:5 to capture translucent particles.[27] Samples containing > 1,000,000 particles were as well diluted in the respective formulation.

3.8. Determination of apparent viscosity

The viscosity of mAb in 10 mM histidine +140 mM NaCl pH 7.2 at concentrations between 2 and 120 mg/mL were measured using an m-VROC viscosimeter (RheoSense Inc., San Ramon, California, USA) equipped with an A05 chip with 50 µm flow channel with temperature controlled at 20 °C. After equilibration of the sample filled in a 100 µl Hamilton syringe, the measurement was performed at a fixed shear rate of 1,000 s^{-1} (n=3). Data was fitted to the Ross-Minton equation:[28]

$$\eta = \eta_0 \exp \left(\frac{[\eta]c}{1 - \frac{k}{v}c[\eta]} \right)$$

with η = solution viscosity, η_0 = solvent viscosity, c = mAb concentration, $[\eta]$ = intrinsic viscosity, k = crowding factor and v = Simha shape factor.

3.9. Statistical analysis

Data is presented as two independent individual experiments and their mean ± range. A higher number of experiments was not possible due to material constraints. Although a statistical test for significance is not possible the differences seen in the study are substantial enough at low variability to allow for the conclusions on the effects associated with protein particle deposition on membranes during TFF.

4. Results

4.1. Effect of pump type on permeate flux during diafiltration

At first the effect of peristaltic pumping with pharmapure tubing vs. membrane pumping on TFF performance was evaluated in diafiltration mode against formulation buffer. The buffer system was kept in order to avoid aggregation induced by changes in pH, ionic strength, and ion environment.[17] In addition a pure formulation buffer run was performed. After approximately 5 min the TMP reached 1.5 bar in mAb runs, whereas only 1.1 bar were be reached with buffer. Peristaltic pumping of buffer resulted in a process duration of only 40 ± 1 min with a stable flux of approximately 325 LMH (Figure 1). In comparison, diafiltration took 92 ± 4 min with 2 mg/mL mAb solution with a lower initial flux of 151 ± 3 min which decreased to 114 ± 6 LMH during the experiment. Switching to a membrane pump led a comparable process duration of 91 ± 2 min at an initial flux of 138 ± 0 LMH which remained consistent at 135 ± 2 LMH. While the buffer sample appeared clear and were nearly free of particles compared to controls, the mAb solutions yielded in a substantial increase in turbidity and particle concentration after the diafiltration process. The use of the peristaltic pump resulted in more pronounced protein aggregation compared to using the membrane pump as the samples were more turbid upon visual inspection and showed higher turbidity of 7.4 vs. 4.0 NTU and concentration of particles ≥ 1 μm/mL of 340,000 vs. 65,000.
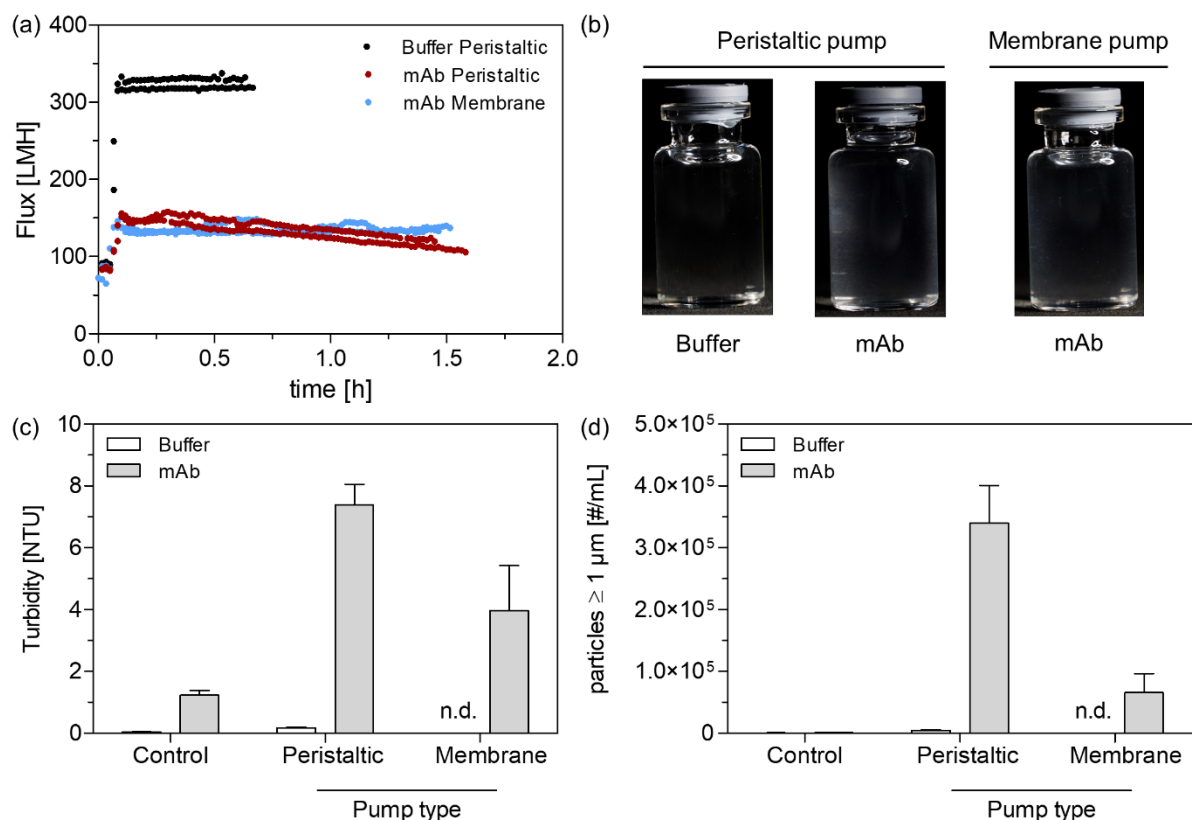
Figure 1 Diafiltration runs with buffer and 2 mg/mL mAb formulation using a peristaltic pump equipped with a pharmapure tubing and a membrane pump monitored by flux profiles (a). Final samples were characterized via photo documentation (b), turbidity (c) and particle concentration (d). Each flux profile is presented separately. A buffer sample for the membrane pump was not determined (n.d.). Control refers to an unpumped formulation. Turbidity and particle concentration is presented as mean ± range of n = 2.

4.2. Effect of tubing material on permeate flux during diafiltration

The same peristaltic pumping setup was used to evaluate the impact of silicone and santoprene tubing as alternative tubing materials as protein aggregate formation is known to be influenced by the tubing material.[23–25] Compared to diafiltration with pharmapure tubing, silicone tubing resulted in a faster process which took 81 ± 2 min at a stable flux (158 ± 3 LMH at start vs. 153 ± 1 LMH at end) (Figure 2, left column). In contrast, with santoprene tubing 126 ± 3 min process time were required and the flux strongly decreased from 134 ± 1 LMH at start to 68 ± 2 LMH at end. Turbidity and protein particle concentration were increased from silicone to pharmapure to santoprene tubing in the TFF process. Interestingly, turbidity and protein particle formation was much more drastic without the cassette, performing pumping only; this effect was least pronounced for silicone tubing.
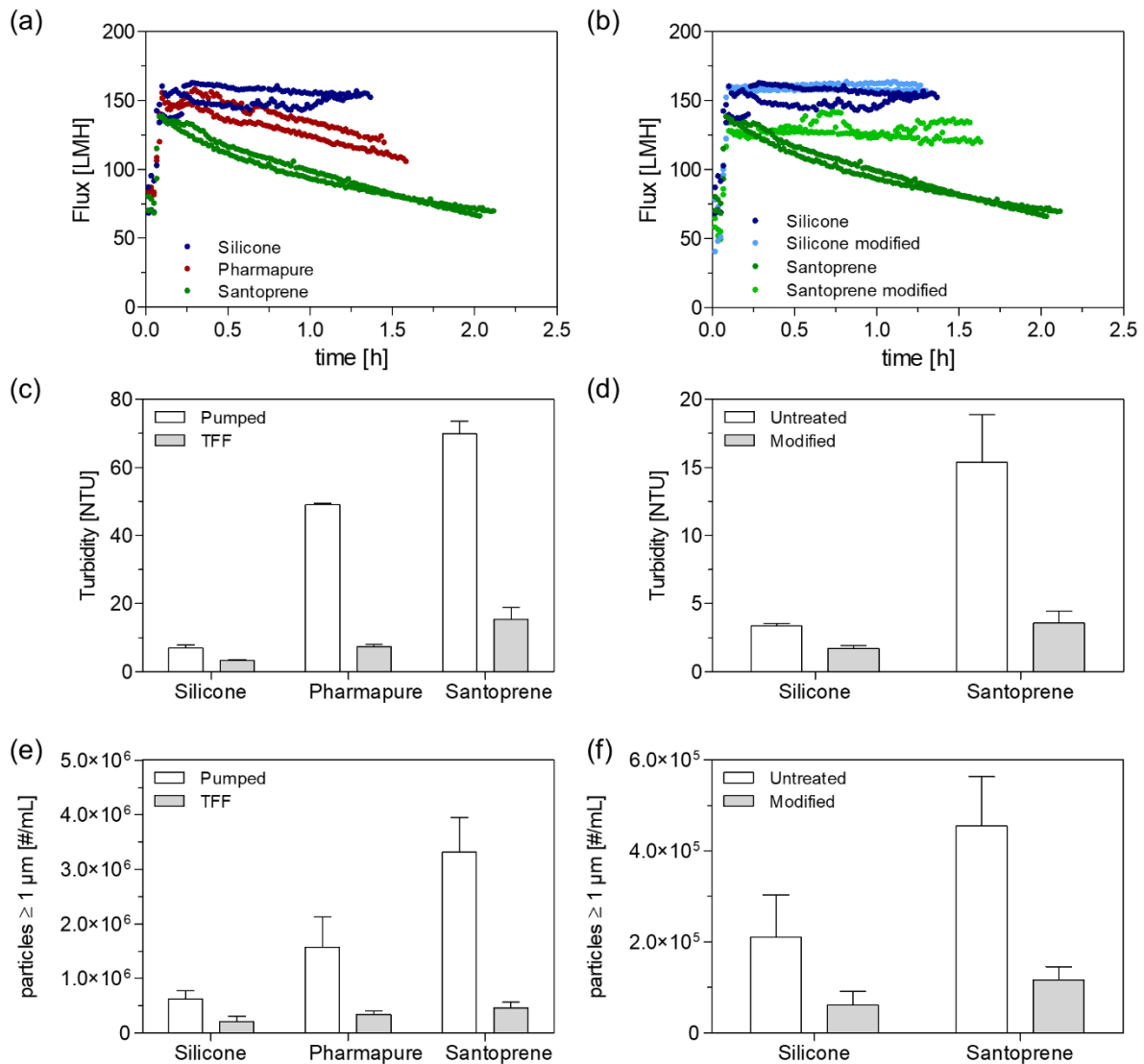
Figure 2 Diafiltration and pumping only runs with 2 mg/mL mAb formulation using a peristaltic pump equipped with untreated silicone, pharmapure and santoprene tubing (left column). Untreated silicone and santoprene tubings were compared to their DBE 712 modified analogue (right column). TFF performance was monitored by flux profiles. Each flux profile is presented separately. Final samples were characterized via turbidity and particle concentration. Turbidity and particle concentration is presented as mean ± range of n = 2.

Tubing modification with DBE 712 has been shown to reduce the protein particle formation propensity upon peristaltic pumping using silicone and santoprene tubing (Figure 2, right column).[26] The modification of silicone did not affect process duration (78 ± 1 min) and flux (start vs. end; 159 ± 1 LMH vs. 159 ± 2 LMH) compared to the untreated tubing. Nevertheless, we observed a reduction in turbidity and protein particle concentration to approximately 1.7 NTU and 61,000 particles ≥ 1 μm/mL. Modification of santoprene not only reduced turbidity and protein particle formation drastically to approximately 3.6 NTU and 116,000 particles ≥ 1 μm/mL but also led to faster and stable process of 97 ± 2 min at a stable flux 128 ± 0 LMH

at start vs. 127 ± 7 LMH at end. The protein aggregation is well reflected by the visual appearance of the samples (Figure 3). After TFF all mAb samples were markedly turbid in the rank order silicone < pharmapure < santoprene compared to the clear TFF buffer control. If only pumped without diafiltration the formulations were much cloudier. Modification of the tubing substantially reduced the visually noticeable turbidity. After pumping and diafiltration experiments, protein concentration deviated at maximum by 11% from the starting concentration. Protein loss is probably attributed to adsorption to membrane and tubing as well as the limited accuracy of dosing via the auxiliary pump.

**Figure 3** Photo documentation of buffer and mAb samples after diafiltration runs and peristaltic pumping only using different tubings.

4.3. Effect of tubing material on permeate flux during concentration

The viscosity of the retentate which is influenced by protein concentration and formulation is known to impact the flux during ultrafiltration.[8] This reduction in flux can become critical to

achieve high target concentrations and particle formulation may further slow down or stop the process. Shear rate within the pump system is difficult to estimate due to complex flow behaviour. Dreckmann et al.[29] calculated shear rates starting from approx. 1,000 s^{-1} near the tubing wall reaching up to approx. 4,000 s^{-1} in the compressed tubing during peristaltic pumping within their setup. As an estimation of viscosity increase during ultrafiltration, protein concentrations were measured at a fixed shear rate of 1,000 s^{-1}. Concentration dependent viscosity measurements (Figure 4a) revealed a strong increase in viscosity of our mAb in the buffer formulation above 80 mg/mL reaching 13 mPa·s at 120 mg/mL. During concentration, the flux decreased with both silicone and santoprene, both unmodified and modified tubing material, to approximately 10 LMH (Figure 4b).
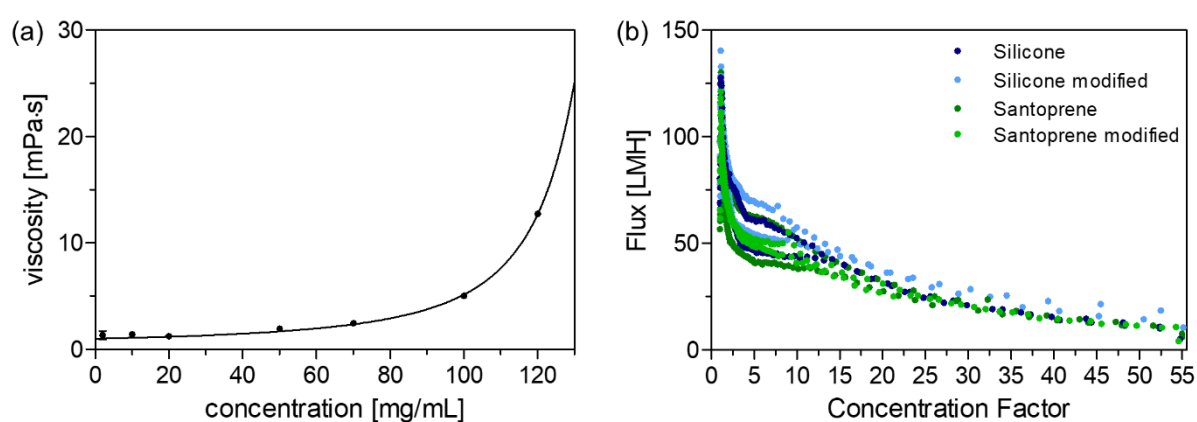
Figure 4 Viscosity of mAb in 10 mM histidine pH 7.2 + 140 mM NaCl at 2 to 120 mg/mL (a). Permeate flux in dependence of concentration factor and tubing material (b). Concentration factor is calculated based on the permeate weight. Each flux profile is presented separately.

Final concentration and total process duration were comparable between all runs (Table 1). As observed in the diafiltration setup santoprene tubing led to higher turbidity compared to the silicone tubing whereas particle concentration ≥ 1 µm was comparable. Modification with DBE 712 lowered turbidity and protein particle burden for both tubings.

Table 1 Characterization of samples processed with different tubing materials after concentration via TFF from 2 mg/mL to approx. 110 mg/mL. Data is presented as mean ± range of n =2.

Tubing	Concentration [mg/mL]	Duration [min]	Turbidity [NTU]	Particles ≥ 1 µm [#/mL]
Silicone	114 ± 7	97 ± 8	87 ± 21	2,527,856 ± 504,883
Silicone modified	103 ± 6	87 ± 6	37 ± 2	931,704 ± 737,867
Santoprene	108 ± 4	105 ± 14	200 ± 26	3,403,619 ± 595,939
Santoprene modified	104 ± 4	105 ± 2	55 ± 5	612,030 ± 56,413

5. Discussion

TFF of protein pharmaceuticals is prone to failure if formulation and process parameters are not well thought out.[15,18,19] Peristaltic pumping over longer time in absence of surfactant is typically performed. We studied the effect of the tubing material on protein aggregate formation and permeate flux. Formation of both insoluble and soluble aggregates during TFF has been observed.[18,19] As we did only see the formation of insoluble aggregates upon solely peristaltic pumping in our setup,[22,30–32] this study focused on insoluble protein aggregates. This study used a formulation pH close to the isoelectric point of the mAb and high ionic strength to simulate a worst-case scenario for protein particle formation. This choice of buffer is potentially impacted by the Donnan effect leading to high pH shifts triggering protein aggregation during TFF.[33,34] However, pH variations were below 0.1 after dia- and ultrafiltration. It seems that the high NaCl concentration counteracted the Donnan effect.[35] Cloudiness of the samples is therefore rather related to protein particle concentration induced by the TFF process and Rayleigh scattering at high concentrations.[36,37]

In a diafiltration setup without changing the formulation buffer peristaltic pumping of 2 mg/mL mAb took longer at lower initial flux compared to pure buffer. Lower initial flux in presence of mAb indicates protein layer formation on the membrane increasing its resistance. In the course of the process the flux decreased further, and protein aggregate formed already at this low mAb concentration. In previous studies, the choice of tubing material significantly affected the degree of protein particle formation.[23–25] Pharmapure and santoprene tubing led to substantially higher turbidity and protein particle concentrations after pumping only compared to silicone. Upon insertion of the cassette turbidity and protein particle concentration were lower compared to pumping only. This indicates that protein particles get caught within the cassette, deposit on the membrane and reduce the permeate flux by pore blocking.[16,20,38] Silicone tubing was associated with least protein aggregation and correspondingly the flux was not impacted. In contrast, the high protein aggregation propensity upon pumping with pharmapure and santoprene led to a decrease of the flux and the process slowed down significantly over the run time. Several studies pointed out that the type of pump influences protein particle formation during filling and TFF.[7,18,29,32] Exchanging the peristaltic pump against a membrane pump reduced the protein particle formation substantially and the flux remained stable. However, in a GMP environment single – use options for membrane pumps are limited or considerably more expensive than single – use tubings.

The protein aggregates originate from the rupture and the tear-off of the protein film formed on the tubing surface during roller movement.[22] Adsorption and therefore protein particle formation can be prevented by addition of surfactants to the formulation.[22–24,39] Callahan et al.[16]

showed that the addition of different surfactants reduced particle formation during TFF operation and led to increased filterability. Despite this highly beneficial effect of surfactants in TFF, ultra- and diafiltration runs are typically run in absence of surfactants as their retention and ultrafiltration behaviour is unclear and they are typically spiked in after the process. To overcome these limitations the tubing itself may be hydrophilized making it protein repellent. To this end we incorporated a hydrophilic co-block-polymer consisting of pure and pegylated polydimethylsiloxane blocks (DBE 712) into the tubing wall via a swelling-deswelling approach.[26] Upon contact with water DBE 712 migrates to the surface and exposes its hydrophilic blocks which increases surface hydrophilicity and inhibits protein adsorption.[40] Protein particles were successfully reduced with these modified santoprene and silicone tubings during diafiltration which was also reflected by visual appearance and turbidity. By modification of santoprene the problem of flux decrease, and extended process time could be resolved. Unmodified silicone tubing did not show this challenge and modification did not further impact its process performance. Besides beneficial effects on flux stability, lower protein particle concentration in modified tubings increase product quality and processability for e.g. sterile filtration.

When concentrating protein solutions via TFF the increasing viscosity and protein concentration lead to a flux decay.[8] In our study, the choice of tubing did not markedly affect flux and process duration. Lower turbidity and protein particle concentration for protein material processed using the modified tubings indicated a reduction in the overall protein particle formation propensity. This observation is in line with the outcome of the diafiltration studies. The lower protein particle concentrations may be of higher relevance in other ultrafiltration cases potentially being the element which keeps the TFF user from achieving the maximal concentration, extends the process time beyond what is acceptable or of brings the ultrafiltration process completely to a hold. In addition, the higher particle burden can be challenge for a subsequent filtration process and the overall bulk quality.[19] Another option to increase flux during ultrafiltration might be maximizing the pump speed. But this comes with the risk of affecting protein stability. Protein solutions show shear thinning behaviour up to a shear rate of 10,000 s^{-1}.[41] Increasing pump speed might therefore increase flux of highly concentrated protein formulations.

6. Conclusion

During manufacturing of biopharmaceutics buffer exchange and concentration by TFF is a standard unit operation. Flux reduction and potentially membrane fouling can be a results of gel layer formation on the membrane, high viscosity and protein aggregates blocking membrane pores. In the current study, we investigated the effect of tubing material and its modification on protein particle formation propensity, flux, process time and product quality. In the low viscosity TFF diafiltration process the flux decreased due to blocking of membrane pores by protein aggregates formed during pumping. The protein aggregates were caught within the cassette and subsequently deposited on the membrane. The extent of flux decrease was linked to the extent of protein particles formed with the different tubing materials. In the present setup, silicone tubing had the lowest protein particle formation propensity and did not show a decrease in flux. In contrast, santoprene and pharmapure tubing led to a decrease in flux and prolonged process duration due to high protein formation propensity. The flux decrease could be avoided by replacing the peristaltic pump against a membrane pump due to lower protein particle formation. The protein particle formation propensity of tubing material not only negatively impacts processability but also product quality. In general, protein particles should be minimal as particles smaller than 0.2 µm may not be removed via sterile filtration. Tubings can be efficiently hydrophilized by incorporation smart segregating PEG-PDMS-copolymers. This modification reduces protein particle formation by keeping the protein off the tubing surface. Thus, flux decline was prevented due by the hydrophilization due to less protein aggregation. During ultrafiltration, viscosity increase led to a comparable decrease in flux irrespective of the tubing material used. However, hydrophilized tubing reduced turbidity and protein particle formation which improves processability and product quality. Overall, protein particle formation caused by peristaltic pumping in surfactant free TFF processes has to be understood and controlled as it impacts flux, process time, and product quality. This includes investigation and selection of the optimal tubing material.

7. References

1.   Ingham KC, Busby TF, Sahlestrom Y, Castino F. Separation of Macromolecules by Ultrafiltration: Influence of Protein Adsorption, Protein-Protein Interactions, and Concentration Polarization. In: Cooper AR, ed. Ultrafiltration Membranes and Applications. Plenum Press; 1980:141-158.

2.   Huisman IH, Prádanos P, Hernández A. The effect of protein-protein and protein-membrane interactions on membrane fouling in ultrafiltration. J Memb Sci. 2000;179(1-2):79-90. doi:0.1016/S0376-7388(00)00501-9

3.   Matthiasson E. The role of macromolecular adsorption in fouling of ultrafiltration membranes. J Memb Sci. 1983;16:23-36. doi:10.1016/S0376-7388(00)81297-1

4.   McDonogh RM, Bauser H, Stroh N, Chmiel H. Concentration Polarisation and Adsorption Effects in Cross-Flow Ultrafiltration of Proteins. Desalination. 1990;79(2-3):217-231. doi:10.1016/0011-9164(90)85007-W

5.   Palecek SP, Zydney AL. Intermolecular Electrostatic Interactions and Their Effect on Flux and Protein Deposition during Protein Filtration. Biotechnol Prog. 1994;10(2):207-213. doi:10.1021/bp00026a010

6.   Fernandez-Cerezo L, M E Rayat AC, Chatel A, et al. An ultra scale-down method to investigate monoclonal antibody processing during tangential flow filtration using ultrafiltration membranes. Biotechnol Bioeng. 2019;116(3):581-590. doi:10.1002/bit.26859

7.   Fernandez-Cerezo L, Rayat ACME, Chatel A, Pollard JM, Lye GJ, Hoare M. The prediction of the operating conditions on the permeate flux and on protein aggregation during membrane processing of monoclonal antibodies. J Memb Sci. 2020;596:117606. doi:10.1016/j.memsci.2019.117606

8.   Hung JJ, Borwankar AU, Dear BJ, Truskett TM, Johnston KP. High concentration tangential flow ultrafiltration of stable monoclonal antibody solutions with low viscosities. J Memb Sci. 2016;508:113-126. doi:10.1016/j.memsci.2016.02.031

9.   Zidar M, Rozman P, Belko-Parkel K, Ravnik M. Control of viscosity in biopharmaceutical protein formulations. J Colloid Interface Sci. 2020;580:308-317. doi:10.1016/j.jcis.2020.06.105

10.   Jezek J, Rides M, Derham B, et al. Viscosity of concentrated therapeutic protein compositions. Adv Drug Deliv Rev. 2011;63(13):1107-1117. doi:10.1016/j.addr.2011.09.008

11.   Hong T, Shiraki K. Viscosity Control of Protein Solution by Small Solutes: A Review. Curr Protein Pept Sci. 2018;19:746-758. doi:10.2174/1389203719666171213114919

12.   Lucas K, Ahmad SD, Dehghani M, Gaborski T, McGrath J. Critical flux behavior of ultrathin membranes in protein-rich solutions. Sep Purif Technol. 2020;251:117342. doi:10.1016/j.seppur.2020.117342

13.   Castellanos MM, Pathak JA, Colby RH. Both protein adsorption and aggregation contribute to shear yielding and viscosity increase in protein solutions. Soft Matter. 2014;10:122-131. doi:10.1039/c3sm51994e

14.   Chandavarkar AS. Dynamics of Fouling of Microporous Membranes by Proteins. Massachusetts Institute of Technology, PhD Thesis; 1990.

15.   Yen JW. Denaturation and Aggregation of SS-Galactosidase during Tangential Flow Ultrafiltration. The Ohio State University; 1995.

16.   Callahan DJ, Stanley B, Li Y. Control of Protein Particle Formation During Ultrafiltration/Diafiltration Through Interfacial Protection. J Pharm Sci. 2014;103(3):862-869. doi:10.1002/jps.23861

17.   Ahrer K, Buchacher A, Iberer G, Jungbauer A. Effects of ultra-/diafiltration conditions on present aggregates in human immunoglobulin G preparations. J Memb Sci. 2006;274(1-2):108-115. doi:10.1016/j.memsci.2005.08.018

18.   Meireles M, Aimar P, Sanchez V. Albumin Denaturation During Ultrafiltration: Effects of Operating Conditions and Consequences on Membrane Fouling. Biotechnol Bioeng. 1991;38(5):528-534. doi:10.1002/bit.260380511

19.   Rosenberg E, Hepbildikler S, Kuhne W, Winter G. Ultrafiltration concentration of monoclonal antibody solutions: Development of an optimized method minimizing aggregation. J Memb Sci. 2009;342:50-59. doi:10.1016/j.memsci.2009.06.028

20.   Palacio L, Ho CC, Zydney AL. Application of a pore-blockage - Cake-filtration model to protein fouling during microfiltration. Biotechnol Bioeng. 2002;79(3):260-270. doi:10.1002/bit.10283

21.   Chan R, Chen V. The effects of electrolyte concentration and pH on protein aggregation and deposition: critical flux and constant flux membrane filtration. J Memb Sci. 2001;185(2):177-192. doi:10.1016/S0376-7388(00)00645-1

22.   Deiringer N, Friess W. Proteins on the Rack: Mechanistic Studies on Protein Particle Formation During Peristaltic Pumping. J Pharm Sci. 2022;111(5):1370-1378. doi:10.1016/j.xphs.2022.01.035

23.   Her C, Carpenter JF. Effects of Tubing Type, Formulation, and Postpumping Agitation on Nanoparticle and Microparticle Formation in Intravenous Immunoglobulin Solutions

Processed With a Peristaltic Filling Pump. J Pharm Sci. 2020;109(1):739-749. doi:10.1016/j.xphs.2019.05.013

24.   Her C, Tanenbaum LM, Bandi S, et al. Effects of Tubing Type, Operating Parameters, and Surfactants on Particle Formation During Peristaltic Filling Pump Processing of a mAb Formulation. J Pharm Sci. 2020;109(4):1439-1448. doi:10.1016/j.xphs.2020.01.009

25.   Deiringer N, Friess W. Reaching the breaking point: Effect of tubing characteristics on protein particle formation during peristaltic pumping. Int J Pharm. 2022;627:122216. doi:10.1016/j.ijpharm.2022.122216

26.   Deiringer N, Aleshkevich S, Mueller C, Friess W. Modification of tubings for peristaltic pumping of biopharmaceutics. J Pharm Sci. Published online 2022. doi:10.1016/j.xphs.2022.08.037

27.   Zölls S, Gregoritza M, Tantipolphan R, et al. How subvisible particles become invisible-relevance of the refractive index for protein particle analysis. J Pharm Sci. 2013;102(5):1434-1446. doi:10.1002/jps.23479

28.   Ross PD, Minton AP. Hard quasispherical Model for the Viscosity of Hemoglobin Solutions. Biochem Biophys Res Commun. 1977;76(4):971-976. doi:10.1016/0006-291x(77)90950-0

29.   Dreckmann T, Boeuf J, Ludwig IS, Lümkemann J, Huwyler J. Low volume aseptic filling: Impact of pump systems on shear stress. European Journal of Pharmaceutics and Biopharmaceutics. 2020;147:10-18. doi:10.1016/j.ejpb.2019.12.006

30.   Roffi K, Li L, Pantazis J. Adsorbed protein film on pump surfaces leads to particle formation during fill-finish manufacturing. Biotechnol Bioeng. 2021;118(8):2947-2957. doi:10.1002/bit.27801

31.   Kalonia CK, Heinrich F, Curtis JE, Raman S, Miller MA, Hudson SD. Protein Adsorption and Layer Formation at the Stainless Steel− Solution Interface Mediates Shear-Induced Particle Formation for an IgG1 Monoclonal Antibody. Mol Pharmaceutics. 2018;15(3):1319-1331. doi:10.1021/acs.molpharmaceut.7b01127

32.   Nayak A, Colandene J, Bradford V, Perkins M. Characterization of subvisible particle formation during the filling pump operation of a monoclonal antibody solution. J Pharm Sci. 2011;100(10):4198-4204. doi:10.1002/jps.22676

33.   Bolton GR, Boesch AW, Basha J, LaCasse DP, Kelley BD, Acharya H. Effect of protein and solution properties on the donnan effect during the ultrafiltration of proteins. Biotechnol Prog. 2011;27(1):140-152. doi:10.1002/btpr.523

34.   Stoner MR, Fischer N, Nixon L, et al. Protein-solute interactions affect the outcome of ultrafiltration/ diafiltration operations. J Pharm Sci. 2004;93(9):2332-2342. doi:10.1002/jps.20145

35.   Baek Y, Singh N, Arunkumar A, Borwankar A, Zydney AL. Mass Balance Model with Donnan Equilibrium Accurately Describes Unusual pH and Excipient Profiles during Diafiltration of Monoclonal Antibodies. Biotechnol J. 2019;14(7):1800517. doi:10.1002/biot.201800517

36.   Salinas BA, Sathish HA, Bishop SM, Harn N, Carpenter JF, Randolph TW. Understanding and modulating opalescence and viscosity in a monoclonal antibody formulation. J Pharm Sci. 2010;99(1):82-93. doi:10.1002/jps.21797

37.   Sukumar M, Doyle BL, Combs JL, Pekar AH. Opalescent Appearance of an IgG1 Antibody at High Concentrations and Its Relationship to Noncovalent Association. Pharm Res. 2004;21(7):1087-1093. doi:10.1023/b:pham.0000032993.98705.73

38.   Mondor M, Ippersiel D, Lamarche F, Boye JI. Effect of electro-acidification treatment and ionic environment on soy protein extract particle size distribution and ultrafiltration permeate flux. J Memb Sci. 2004;231(1-2):169-179. doi:10.1016/j.memsci.2003.11.018

39.   Deiringer N, Rüdiger D, Luxbacher T, Zahler S, Friess W. Catching Speedy Gonzales: Driving forces for Protein Film Formation on Silicone Rubber Tubing During Pumping. J Pharm Sci. 2022;111(6):1577-1586. doi:10.1016/j.xphs.2022.02.013

40.   Gökaltun A, Bok Kang Y, Yarmush ML, Berk Usta O, Asatekin A. Simple Surface Modification of Poly(dimethylsiloxane) via Surface Segregating Smart Polymers for Biomicrofluidics. Sci Rep. 2019;9:7377. doi:10.1038/s41598-019-43625-5

41.   Dharmaraj VL, Douglas Godfrin P, Liu Y, Hudson SD. Rheology of clustering protein solutions. Biomicrofluidics. 2016;10:043509. doi:10.1063/1.4955162

Chapter X Final Summary

The fill and finish process of biopharmaceutics is complex, costly and requires intensive risk mitigation to guarantee product quality and safety. **Chapter I** describes some of the major challenges with a focus on protein aggregation during manufacturing. The extensive use of pumps for transferring and filling has been identified as potential source of protein aggregates. In particular, these aggregates may reach the final drug product if formed during the final filling step. While the aggregation process in piston pumps is well described, the more versatile peristaltic pump has not been the focus of intensive research. Therefore, this thesis aims to elucidate and understand the mechanism of protein aggregation upon peristaltic pumping and to develop strategies for minimizing protein particles. This is outlined in **Chapter II**.

Potential factors that might lead to protein aggregation during peristaltic pumping are shedding of rubber particles from the tubing serving as aggregation nuclei, protein unfolding by heat generated during operation, oxidative stress by cavitation, interfacial adsorption of the protein to the tubing wall as well as the mechanical stress by deformation and stretching of the tubing. Upon operation, friction in the pump head leads to shedding of nanometre sized rubber particles from the inner tubing surface. The shed rubber particles might serve as aggregation nuclei. Due to their small size and missing marked spectral features, these particles are difficult to detect and to distinguish from and within protein particles. In **Chapter III** mixed micrometre sized protein particles containing nanometre sized silicone particles were identified and quantified using high resolution techniques. Confocal Raman microscopy allowed label free chemical component identification. Fluorescent labelling of the tubing enabled visualization and counting of the mixed particles via confocal laser scanning microscopy and via Imaging Flow Cytometry, respectively. These methods can serve as a forensic tool for identifying contaminations during processing of biopharmaceuticals. Nevertheless, silicone particles shed from tubing did not further trigger to protein aggregate formation.

The other potential key drivers for protein aggregation were thoroughly studied in **Chapter IV**. As the temperature of the pump head during operation stayed well below the melting point onset of the tested proteins, thermal unfolding is unlikely to be the root cause for protein aggregation. Neither formation of reactive hydroxyl radicals nor protein oxidation were detected ruling out cavitation as a substantial contributor to aggregation. The interfacial driven aggregation pathway was highlighted by the fact that protein aggregation was suppressed by addition of polysorbate 20 as surfactant to the formulation. The protein particles generated upon pumping result from the protein film formed on the tubing surface which gets ruptured

upon stretching during roller movement and renewed. The film fragments are released into the bulk.

Diving deeper into the driving forces for protein film formation on the tubing wall (**Chapter V**), an interplay between electrostatic and hydrophobic interactions was observed. While long-range electrostatic interaction influenced the initial adsorption speed, hydrophobic interactions became predominant upon intimate contact of the protein molecules with the tubing surface. Atomic force microscopy and streaming potential determination revealed that the process of film formation by irreversible adsorption takes place in less than a second. Adsorbed protein amount as well as particle concentration and size distribution were influenced by formulation parameters. A determining factor for adsorbed protein amount and film morphology was the Debye length which was influenced by the formulation pH and ionic strength. The adsorbed protein amount increased with decreasing Debye length which led to a higher packing density. At high ionic strength, the total number of protein particles increased and a build-up of particles larger than 25 μm was detected. The addition of polysorbate 20 inhibited protein particle formation by quickly covering up the tubing surface increasing its hydrophilicity and shielding electrostatic interactions.

The interfacial adsorption behaviour is influenced by the tubing (**Chapter IV**) as well as the protein characteristics (**Chapter V**). Higher protein particle burden of product was linked on one hand side to high surface hydrophobicity of the tubing associated with a higher protein film renewal rate and on the other hand side to low material hardness facilitating rupture of the protein film. This emphasizes the need of proper tubing selection to increase product quality. Considering the protein properties, high affinity to the tubing surface and consequently the film renewal rate was linked to high hydrophobicity, low Debye length, and low conformational stability. In this context, the initial interfacial pressure increase served as a good predictor for turbidity, protein particle concentration ≥ 1 μm, and adsorbed protein amount.

As protein film formation is reduced on more hydrophilic tubing, we modified silicone tubing using a surface segregating smart copolymer based on a polydimethylsiloxane backbone and polyethylene glycol side blocks (**Chapter VIII**). The copolymer distributes throughout the whole tubing bulk upon swelling-deswelling in polymer containing toluene. Upon contact with water, the copolymer rearranges, and the hydrophilic polyethylene glycol side blocks are exposed on to the inner tubing wall. This hydrophilization approach of the tubing led to a substantial reduction of protein particle formation as demonstrated exemplarily for two proteins and thermoplastic-based tubing. This modification is an easy and cost-effective approach to improve processability and product quality upon peristaltic pumping of protein solutions.

Admixing of the copolymer into the melt before extrusion would be the way forward to produce such smarter tubing material on larger scale.

In contrast to filling with only a single contact of a potentially surfactant containing final formulation for very short time, protein solutions without surfactant are circulated for several hours through the pump head during tangential flow filtration (TFF). The severe pumping stress triggers aggregation which can lead to decreased permeate flux and longer process time (**Chapter IX**). In low viscosity environment protein particles formed by peristaltic pumping blocked membrane pores impacting flux and process time. This effect was pronounced with tubing of high protein particle formation propensity. Using the developed smart modified tubings, the particle formation was drastically reduced, the flux remained stable, and the process was faster. Not only the TFF process itself was positively affected but also final product quality was enhanced. In ultrafiltration mode, the flux decrease was governed by the viscosity increase and not substantially impacted by the protein particle formation. But the choice of tubing material and modification greatly influenced protein particle burden which impacts product processability and quality.

In conclusion, this work contributed to the mechanistic understanding of interfacially driven aggregation during peristaltic pumping. Protein adsorption and subsequent film rupture upon stretching and relaxation of the tubing are key. The study outcomes highlight the importance of both tubing and formulation choice to minimize the risk of protein aggregation upon peristaltic pumping. New tubing materials obtained e.g. by tubing modification with surface segregating smart copolymers provide a future path to biopharmaceutics products of higher quality.

Appendix

List of publications associated with the thesis

Deiringer N[*], Haase C[*], Wieland K, Zahler S, Haisch C, Friess W. Finding the Needle in the Haystack: High-Resolution Techniques for Characterization of Mixed Protein Particles Containing Shed Silicone Rubber Particles Generated During Pumping. J Pharm Sci. **2021**;110(5):2093-2104. doi: 10.1016/j.xphs.2020.12.002

*Authors contributed equally

Deiringer N and Friess W. Proteins on the Rack: Mechanistic Studies on Protein Particle Formation During Peristaltic Pumping. J Pharm Sci. **2022**;111(5):1370-1378. doi: 10.1016/j.xphs.2022.01.035.

Deiringer N, Rüdiger D, Luxbacher T, Zahler S, Friess W. Catching Speedy Gonzales: Driving forces for Protein Film Formation on Silicone Rubber Tubing During Pumping. J Pharm Sci. **2022**;111(6):1577-1586. doi: 10.1016/j.xphs.2022.02.013.

Deiringer N and Friess W. Reaching the breaking point: Effect of tubing characteristics on protein particle formation during peristaltic pumping. Int J Pharm. **2022**; 627: 122216. doi: 10.1016/j.ijpharm.2022.122216.

Deiringer N, Aleshkevich S, Müller C, Friess W. Modification of Tubings for Peristaltic Pumping of Biopharmaceutics. J Pharm Sci. **2022**; available online. doi: 10.1016/j.xphs.2022.08.037.

Deiringer N, Leitner I, Friess W. Effect of the Tubing Material used in Peristaltic Pumping in Tangential Flow Filtration Processes of Biopharmaceutics on Particle Formation and Flux. J Pharm Sci. **2022**; available online. doi: 0.1016/j.xphs.2022.10.005.

Deiringer N, and Friess W. Afraid of the wall of death? Considerations on monoclonal antibody characteristics that trigger aggregation during peristaltic pumping. Int J Pharm. **2023**; 633: 122635. doi: 10.1016/j.ijpharm.2023.122635.

List of additional publications not directly associated with this thesis

Keil TWM*, **Deiringer N***, Friess W, Merkel OM, Evaluation of adsorption of DNA/PEI polyplexes to tubing materials. Eur. J. Pharm. Biopharm. **2022**; 179:58-64. doi: 10.1016/j.ejpb.2022.08.014.

*Authors contributed equally

Nishiumi H, **Deiringer N**, Krause N, Yoneda S, Torisu T, Menzen T, Friess W, Uchiyama S, Utility of Three Flow Imaging Microscopy Instruments for Image Analysis in Evaluating four Types of Subvisible Particle in Biopharmaceuticals, J Pharm Sci. **2022**, available online. doi: 10.1016/j.xphs.2022.08.006.

List of presentations associated with this thesis

<u>Oral presentation</u>:

Deiringer N, Friess W, Please stay my dear: Interfacial adsorption as driving force for protein particle formation during peristaltic pumping. 12th World Meeting on Pharmaceutics, Biopharmaceutics and Pharmaceutical Technology, **2021**, live online.

<u>Poster presentation</u>:

Deiringer N, Friess W, Proteins on the rack: Mechanistic studies on protein particle formation during peristaltic pumping. DPhG-DoktorandInnen-/ Postdoc-Tagung, **2021**, live online.*

*Winner of Wiley-VCH poster prize and AbbVie Mentoring Program

Deiringer N, Friess W, Protein aggregation induced by pumping of biopharmaceutics. Mentoring Retreat Chemie, Biochemie und Pharmazie Programm, **2019**, Fraueninsel, Germany.